E s c o l a d e E n g e n h a r i a • U n i v e r s i d a d e d o M i n h o

JOANNA KRAKOWIAK

ORIGIN OF THE MELT MEMORY EFFECT AND PREDICTION OF PRECURSOR STRUCTURES DIMENSIONS IN QUIESCENT AND SHEARED POLYTHYLENE MELTS: EFFECTS OF CROSSLINKING DEGREE AND CATALYST TYPE

Thesis submitted in fulfillment of the requirements for the degree of Doctor of Philosophy in Polymers Engineering

T e s e a p r e s e n t a d a p a r a o b t e n ç ã o d o g r a u d e D o u t o r e m E n g e n h a r i a d e P o l í m e r o s

F e v e r e i r o d e 2 0 0 9

ORIGIN OF THE MELT MEMORY EFFECT AND PREDICTION OF PRECURSOR STRUCTURES DIMENSIONS IN QUIESCENT AND SHEARED POLYTHYLENE MELTS: EFFECTS OF CROSSLINKING DEGREE AND CATALYST TYPE

ORIGEM DO EFEITO DE MEMÓRIA E PREVISÃO DA DIMENSÃO DAS ESTRUTURAS PRECURSORAS EM FUNDIDOS QUIESCENTES E DEFORMADOS SOB ACÇÃO DE ESFORÇOS DE CORTE: EFEITOS DO GRAU DE RETICULAÇÃO E DO TIPO DE CATALISADOR

Tese apresentada à Universidade do Minho
para obtenção do grau de Doutor em Engenharia de Polímeros
por

JOANNA KRAKOWIAK

Trabalho realizado sob a orientação do
Professor José António Martins

Fevereiro 2009

Statement of originality

I declare that the work presented in this thesis is, to the best of my knowledge and belief, original, except as acknowledged in the text, and that the material has not been submitted, in whole or in part, for a degree at this or any other institution.

I've benefited in this work of work already developed by my supervisor and co-workers. Part of this work remains unpublished. Part of the still unpublished work is reflected in the critical literature reviews of chapters 1, 2 and 3, with special relevance to chapter 2.

It is therefore appropriate to emphasize my effective contribution to this work.

The three first chapters of work are critical literature reviews. My contributions to the discussion presented in the first chapter are the critical analysis of gelation process, the inverse quenching technique, part of the analysis about spinodal decomposition, the analysis about the effect of entanglements on primary nucleation as well as the other more descriptive items on the same chapter. The critical analysis in the third chapter is of my own. As expressed in the second chapter, it results in great part from unpublished work of my supervisor. As mentioned above, in all these chapters I've benefited from existing, unpublished, work. The remaining part of the work is of my responsibility.

Acknowledgments

I would like to thank my PhD supervisor, Professor José António Martins, for supporting me during these past four years. His ideas had a major influence on this thesis. He spent a lot of time helping me, explaining and correcting. I've learned a lot during this time and I'm convinced that this knowledge will help me in the future.

I want also acknowledge Prof. Ana Vera Machado for preparing the polyethylene samples with different crosslinking degree, for carrying on density evaluations on these samples and for some FTIR experiments that were not included in this work.

I am very grateful to Weidong Zhang for his help with shear DTA instrument.

I especially thank my family for understanding and endless patience and my husband, Konrad, who has been a true and great supporter and has unconditionally loved me during my good and bad times. He had faith in me and my intellect all the time even when I didn't have faith in myself.

This thesis was supported by projects POCTI/CTM/46270/2002 and PTDC/CTM/68614/2006 funded by the Portuguese Foundation for the Science and Technology. Projects also supported by the European Community fund FEDER and project 3599/PPCDT. These funding are gratefully acknowledged.

Abstract

The aim of this work was to study the effect of melt memory in the solidification of semicrystalline polymers and to identify its origin. It contains three bibliographic critical review chapters, two additional chapters of experimental work, a proposal of future work, and an appendix with more details of experimental results. The first three chapters present the current state of the art in the understanding of the earlier crystallization stages and the effect of flow on crystallization development.

The earlier crystallization stages are discussed. Different views are presented for the earlier crystallization mechanisms, namely the nucleation resulting from a spinodal decomposition in the melt, the classical nucleation and growth, and the nucleation and crystallization development resulting from the presence of a mesophase in the molten polymer. The effect of entanglements on the crystallization and melting are also analysed. Particularly critical is a clear understanding of this last process, which requires a deep knowledge of polymer melt morphology. Its change with flow conditions will inevitably affect crystallization development. Because polymer chains in melts are considered ideal, this concept is discussed with detail. The variation with temperature and flow of parameters used to establish dimensions of chain segments in ideal chains is also analysed. Limitations of models used to describe chain dynamics are presented, discussed and their flaws identified. At the end, the study of the effect of flow on polymer melt morphology is presented.

Under the assumption that the melt memory effect is originated from thermal and mechanical history imposed to during the processing stage, its origin was studied by making the reverse experiments of those used to erase this effect and to record reproducible crystallization experiments in fully relaxed melts. It was found that pre-shearing polymer melts above their melting temperature accelerates crystallization kinetics until saturation, which is ascribed to the existence in the melt of precursor structures, consisting of chain segments aligned with flow, without crystallographic order. The melt state responsible for this saturation was identified as the steady state in shear flow. The excess in the specific free energy of melts sheared up to steady state and the strain at its onset were evaluated and expressed as a function of precursor structures surface free energies, their length and thickness. For quiescent melts their thickness was found to be maximum. Erasing the melt memory effect is ascribed to the decrease of melt excess specific free energy, which is achieved a randomization and increase in the thickness of the precursor structures existing at steady state. Application of shear fragmentises the precursors and aligns them with flow. The major conclusion of this work is that, despite the differences in the polymers studied, they show universal features concerning their flow and crystallization behaviour.

Resumo

O objectivo deste trabalho é estudar e identificar a origem do efeito da memória na solidificação de polímeros semicristalinos. O trabalho contém três capítulos de revisão bibliográfica. Há ainda dois capítulos de trabalho experimental, um capítulo com propostas de trabalho futuro e um apêndice com detalhes de resultados experimentais. Os primeiros três capítulos apresentam uma análise crítica do estado da arte no estudo dos estágios iniciais da solidificação, do efeito do fluxo no desenvolvimento da cristalização e de modelos de fluxo.

Na discussão dos estágios embrionários da cristalização são apresentadas diferentes propostas, nomeadamente o desenvolvimento dos núcleos semicristalinos como resultado da decomposição spinodal no polímero fundido, o processo clássico de nucleação e crescimento e o desenvolvimento da cristalização como resultado de uma mesofase existente no polímero fundido. O efeito dos entrelaçamentos na cristalização e fusão é também analisado. É crítico perceber-se o que lhes acontece, como e quando. Para isso é necessário perceber-se amorfologia do fundido e a sua variação com o fluxo. Admite-se que as cadeias se comportam como ideais em polímeros fundidos. Por esta razão, o conceito de idealidade é discutido com detalhe. A variação com a temperatura e fluxo dos parâmetros utilizados para estabelecer a dimensão de um segmento da cadeia ideal é também analisada. As limitações dos modelos utilizados na descrição da dinâmica de cadeias e as suas limitações são apresentados e discutidos. Finalmente é feita a análise do efeito do fluxo na morfologia do polímero fundido.

Partindo do pressuposto que a memória do fundido resulta da história térmica e mecânica imposta durante o processamento, a sua origem é estudada fazendo experiências opostas às utilizadas para apagar esse efeito e registar experiências de cristalização reprodutíveis em fundidos relaxados. Foi observado que deformando polímeros fundidos acima da sua temperatura de fusão resulta na aceleração da cristalização até à sua saturação, efeito atribuído às estruturas precursoras da cristalização. O estado do fundido responsável pela saturação foi identificado como o estado estacionário em fluxos de corte. O excesso de energia livre dos fundidos deformados até esse estado, e a deformação no seu início, foram avaliados e expressos em função das energias livres de superfície dos precursores, do seu comprimento e espessura. A espessura das estruturas precursoras é máxima em fundidos quiescentes. Apagar o efeito de memória resulta na diminuição do excesso de energia livre, o que é conseguido pela randomização e aumento de espessura das estruturas precursoras. A aplicação de um esforço de corte tem como efeito a fragmentação e orientação no sentido do fluxo das estruturas precursoras. A conclusão mais relevante deste trabalho foi a verificação da universalidade do comportamento dos polímeros em fluxo e a sua cristalização, independentemente do grau de ramificação da cadeia e das interacções intermoleculares.

Presentation of Thesis

This thesis is dived in two parts. The first part (Chapters 1 to 3) gives the theoretical and experimental background details needed for the discussion of experimental results presented in chapters 4 and 5.

Chapter 1 describes the early stages of quiescent crystallization, the primary nucleation process, theories explaining particular stages of this process and the morphology prior crystallization and during crystallization. The effect of melt memory on quiescent crystallization is also analysed and different literature explanations for this effect are presented.

The parameters used to describe the shape and dynamics of polymer chains, especially in polymer melts are described in Chapter 2. The melt morphology and its evolution with flow conditions are explained by different models, which are analyzed based on experimental results and assumptions used. Because it is assumed that Rouse model is applied to polymer melts, assumptions, limitations and claimed experimental validations of this model are analyzed with detail.

In Chapter 3 the melt morphology and its change under flow conditions are discussed, more specifically, the changes in chains' dimensions induced by shear and elongational flow. It is known that crystallization from deformed melts is accelerated when compared with that of quiescent melts, this fact being assigned to precursor structures for nucleation. A major challenge in shear-induced crystallization is to understand the formation of these structures.

A presentation of all experimental results is given in Chapters 4 and 5 and Appendix. Chapter 4 describes the effect of crosslinking degree on quiescent and shear-induced crystallization and one linear and two crosslinked polyethylenes are used. Chapter 5 presents the results obtained for Ziegler-Natta and metallocene polyethylene and the effect of different catalysers is discussed. At Appendix an additional experimental results are presented together with explanation of some procedures used in previous chapters.

The last chapter contains the proposal of future research to clarify some results obtained in this work.

Index of figures

Index of tables

Acronyms

AFM	atomic force microscope
C	crystal phase
CCR	convective constraint release
CLF	contour length fluctuations
CSR	controlled shear rate
DBS	dibenzylidene sorbitol
DSC	differential scanning calorimeter
DTA	differential thermal analysis
g	*gauche* conformation
GPC	gel permeation chromatography
M	mesomorphic phase
MFI	melt flow index
MWD	molecular weight distribution
NG	nucleation and growth
NMR	nuclear magnetic resonance
PMDS	polydimethylsiloxane
PMMA	poly(methyl methacrylate)
PTHF	polytetrahydrofuran
SAOS	small amplitude oscillatory shear
SALS	small angle light scattering
SANS	small angle neutron scattering
SAXS	small angle x-ray scattering
SCB	short chain branching
SEM	scanning electron microscope
SP	spinodal decomposition
t	*trans* conformation
TEM	transmission electron microscopy
WAXD	wide angle x-ray diffraction
WAXS	wide angle x-ray scattering
WLF	Williams-Landel-Ferry

Nomenclature

Roman letters

a	width of nucleus
a	tube diameter
a	length of the orthorhombic PE unit cell
a*	width of critical nucleus
A	constant
A	Hamaker constant
A_2	second virial coefficient
b	thickness of nucleus
b	width of the orthorhombic unit cell of PE
b	length scale of a bead-spring section
b*	thickness of critical nucleus
B	constant
c	solution concentration
c*	overlap concentration
C	constant
$\mathbf{C}^{-1/2}$	square root of the Finger tensor
C_N	characteristic ratio
C_θ	characteristic ratio of real polymer chains under ideal conditions
C_∞	characteristic ratio when N (number of chain segments) $\rightarrow \infty$
d	thickness of precursor structures
d_c	lamellae thickness
D	diffusion coefficient
D_{cm}	centre of mass diffusion coefficient
D_{eff}	effective diffusion coefficient
E_D	activation energy for transport across the nucleus surface (energy of diffusion)
E_R'	elastic component of complex modulus at the plateau region
f_g	free volume fraction at the glass transition temperature
f_i	forces arising from internal energy barriers
F_{el}	total free energy (elastic energy) of Rouse chain
G_N^0	plateau modulus
G', G'(t), G'(ω)	storage modulus
G'', G''(t), G''(ω)	loss modulus
h	Planck constant
I(q,t)	intensity of scattering
I	nucleation rate
I_0	pre-factor
k_B	Boltzmann constant
k_{sp}	spring force constant
K	constant
l	length of nucleus
l	segment length (the bond length) of the real chain
l*	length of critical nucleus
L	length of precursor structure
L_p	length of the primitive chain
L_t	test chain contour length

m	number of monomers per chain (degree of polymerization)
m_b	average molecular weight per backbone bond
m_0	average mass of the bond
M	chain molecular weight
M_{mon}	monomer molecular weight
M_n	number average molecular weight
M_w	weight average molecular weight
n	exponent
n	refractive indexes for the polymer
n_g	number of *gauche* conformations
n_0	refractive indexes for the vacuum
n_t	number of entanglement strands per cubed tube diameter
n_t	number of *trans* conformations
n_v	number of entanglement strands per unit volume
N	number of segments of the real chain
N_A	Avogadro's number
p	packing length
p	mode number
p	single-bond transition rate
q	scattering wave vector
$q_n(t)$	sum of vectors connecting the centroids of parts of the chain
Q	heat flux
Q_{Hv}	scattering invariant
Q_δ	scattering invariant for orientation fluctuation
r	radius of sphere of small solid particle
r	minimum separation distance between parallel chains
r_n, r_{n+1}	beads position vectors
r^*	radius of critical nucleus with sphere shape
R	ideal gas constant
R	thermal resistance
R_g	radius of gyration
R_{max}	extended length of a real chain
$R(q)$	density fluctuations' growth rate
$\left\langle R^2 \right\rangle_0$	average square unperturbed end-to-end chain distance
$\left\langle R_t^2 \right\rangle_0$	average square distance of the unperturbed chain for test chain
S	gel stiffness
S	average number of segments affected by a single bond transition
$S'(q,t)$	normalized intermediate scattering function
t	time
t_k	time interval
tr	trace operation
t_s	shearing time
T	temperature
T_c	crystallization temperature
T_{crit}	critical temperature
T_g	glass transition temperature
T_m	melting temperature
T_s	spinodal decomposition temperature
T_m^0	thermodynamic (equilibrium) melting temperature
u	reduced variable

$\overline{w}$	the specific work
W	characteristic Rouse relaxation rate
W	interaction potential energy of aligned chain segments in the ordered regions
W_i, W_e	Weissenberg number
V	chain volume
V_b	volume per bond
x_s	size of solvent molecules (number of lattice cells occupied)
X_B	phase B concentration
X(t)	degree of conversion to the solid phase
$\left\langle X_{CM}^2 \right\rangle$	mean square displacement of the chain centre of mass
Y_n	average number of single-bond transitions in time t
Z	number of entanglements
$\overline{Z}_N$	average number of segments displaced in time t

Greek letters

α	Isotropic swelling factor
α	Mark-Houwink constant
α_f	free volume thermal expansion coefficient
α_p	amplitude of mode p
γ	interface free energy between the solid particle and the melt
γ	Strain
γ	basal surface free energy
γ_c	critical strain
γ_0	Constant
$\dot{\gamma}$	shear rate
Γ_R	inverse correlation time
δ	Dirac delta function
δ	phase angle
ΔF_{ex}	excess of specific free energy
ΔG	variation of Gibbs free energy
ΔG_s	surface excess free energy
ΔG_v	volume excess free energy
ΔH_v	latent heat of crystallization per unit volume
ΔT	degree of supercooling
ΔE_a, E_a	activation energy
ε	static dielectric constants for the polymer
ε_o	static dielectric constants for the vacuum
ζ	friction coefficient of a Brownian particle
ζ_i	friction coefficients resulting from the internal energy barriers
ζ_o	inherent friction factor
η	viscosity
η_0	viscosity at zero shear rate
$[\eta]$	intrinsic viscosity
θ	scattering angle
θ	theta temperature
θ	valence angle between adjacent covalent bonds
κ	temperature coefficients for the unperturbed chain dimensions
λ	wavelength
λ	effective bong length along the chain axis
λ_0	crossover time to a faster dynamics

λ_i^2	eigenvalues of the Finger tensor $\mathbf{C}^{-1}$
μ	mobility of the bead (of a bead-spring section) or for concentration fluctuations
ν	number density of nuclei
ν_e	main electronic absorption frequency in the UV
v_0	Kuhn monomer volume
ν_0	intrinsic frequency of molecular vibration
Π	osmotic pressure
ρ	density
ρ	number density of molecules in each chain
σ	shear stress
σ	Lateral surface free energy
σ_{xy}	surface energy for the interface between two phases x and y
σ_e	fold surface free energy
τ	reptation time
ψ	parameter related to the Flory interaction parameter
ω	oscillation frequency

Subscripts

X_D	related to the dynamic segment
X_e	related to the chain segment between entanglements
X_k	related to the Kuhn monomer
X_R	related to Rouse model
X_s	related to the solvent

Contents

1. The quiescent crystallization of polymer melts

Understanding quiescent crystallization is crucial to analyze the effect of shear on crystallization kinetics and the final morphology developed under that crystallization process. The quiescent crystallization, *crystallization in the absence of flow*, may be divided into two processes: the primary nucleation, where active nuclei form, and the growth process, which is mainly controlled by a secondary nucleation mechanism. Since the scope of this work is the earlier crystallization stage, more specifically, understanding the origin of melt memory effect, the secondary nucleation mechanism and the overall crystallization kinetics will only be briefly presented.

The early stages of crystallization were investigated by many authors. A clear understanding of this process is still remaining, and recent contradictory experimental results on the absence, or existence, of crystallinity at the very earlier crystallization stages did not help to clarify this issue. According to the classical nucleation theory, the primary nucleation process is divided into two stages. The first is an induction period and second is a stationary nucleation process. During the induction period small nuclei (embryos), with the organization of atoms or molecules similar to those of crystals, form spontaneously by thermal fluctuations of the supercooled melt. Recent experimental results questioned whether nucleation and growth alone explain crystallization or if some other mechanism also plays a part. Many authors suggested that at very early stages of crystallization orientational fluctuation takes place. The time lag in appearance between the intense increase in the SAXS (Small Angle X-Ray Scattering) region and peaks in the WAXS (Wide Angle X-Ray Scattering) region was considered by Olmsted *et al.* [Olmsted-1998] as an evidence of spinodal decomposition following the orientational fluctuation. The supporters of classical theory [Hsiao-1995, Wang-1997] argued that this is an effect of detector sensitivity and that the initial concentration of small crystals is too low to be measured by WAXS detectors above the background of the amorphous halo, while more sensitive SAXS detectors distinguishes the crystallite signals. On the contrary, other authors assume that an intermediate mesophase is the precursor of crystallization.

Winter *et al.* [Acierno-2002, Elmoumni-2003, Pogodina-2001] observed density fluctuations occurring before orientation fluctuations with crystallinity equal to 2% or less, and concluded that the initial crystallization stages are a physical gelation process, but based on experiments of Zhang *et al.* [Zhang-2006] and Acierno *et al.* [Acierno-2003, Coppola-2006] this conclusion can be questioned. The melt memory effect described by

Ziabicki and Alfonso [Ziabicki-1994, Alfonso-1995], and Häfele *et al.* [Häfele-2005] should be reconsidered as well.

1.1. The earlier crystallization stages

1.1.1. Is the supercooled melt a physical gel?

According to Winter *et al.* [Pogodina-2001] the polymer crystallization can be viewed as a physical gelation process. It is considered that the transition from the liquid-like behaviour to the solid-like behaviour takes place at a critical gel point. This gel point is determined from the condition of the frequency independence of the loss tangent, which is equivalent to the parallelism between the $G'(\omega)$ and $G''(\omega)$ curves when plotted as a function of the $\log(\omega)$. At the critical gel point the relaxation modulus is given by

$$G(t) = S \cdot t^{n} \quad \lambda_0 < t < \infty \quad , \tag{1.1}$$

where S is the gel stiffness, n is a critical exponent lower than one, and λ_0 is a crossover time to a faster dynamics (however the physical definition of this time is not clear). The viscoelastic behaviour around the gel point could be explained in terms of the classical suspension theory: as crystallites grow in size their interaction degree increases generating a gradual increase of all mechanical properties.

Experiments performed by Winter *et al.* [Acierno-2002, Elmoumni-2003, Pogodina-2001] allowed identifying a gel point at the earlier crystallization stages from Small Amplitude Oscillatory Shear experiments (SAOS), performed during the isothermal crystallization of isotactic polypropylenes without pre-shearing. The nominal melting temperature of the polymer tested was 163 ºC and the selected crystallization temperature was 148 ºC. SAOS experiments were performed with a rheometer on supercooled melt at different times, from 1175 s up to 79500 s. The gel time was reached at around 22000 s after the start of the isothermal process. The morphology at this time, for the same crystallization temperature, was observed with a Small Angle Light Scattering (SALS) setup and with a polarized optical microscope. Both instruments were further equipped with a Linkam shearing hotstage.

At the time corresponding to the gel point evaluated with the rheometer well defined spherulites are observed in the quiescent crystallization recorded in the polarized optical microscope coupled to the hot-stage, which impinge with each other at a latter time. SALS patterns for the same crystallization temperature and crystallization time, show a diffuse

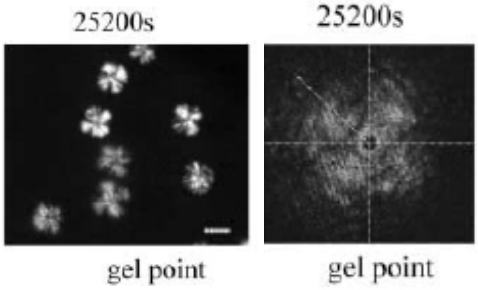

Figure 1.1. *Isothermal crystallization at 148 ºC of an iPP recorded with a hot-stage polarized microscope (left) and Small Angle Light Scattering (right) at the time corresponding to the gel point evaluated by Small Amplitude Oscillatory Shear experiments [Pogodina-2001].*

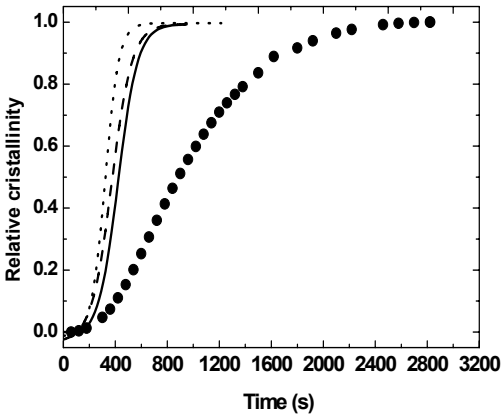

Figure 1.2. *Isothermal crystallization recorded with DSC (full circles) and parallel plate rheometer at 114 ºC. The solid, dashed and dotted lines represent the results obtained in a rheometer at frequencies of 0.1, 1, and 10 Hz, respectively [Zhang-2006].*

four-leaf pattern characteristic of spherulitic structures (Figure 1.1). Note that polarized microscopy and SALS experiments were performed without any shearing of the melt. Interestingly, quiescent DSC experiments have not detected any signal of crystallization development for crystallization times as large as 30000 s. These authors [Acierno-2002, Elmoumni-2003, Pogodina-2001] and others [Coppola-2006, Kumaraswamy-2005] considered that the crystallization process evaluated by SAOS in the rheometer, and those evaluated by SALS and optical microscopy are similar, and called them quiescent crystallization experiments. Although this is true for the optical microscopy and SALS experiments, it is not true, as shown below, for the rheometer experiments. Experiments performed after steady shearing the melt, either in the rheometer or in the Linkam shearing cell coupled to the SALS instrument were classified as shear-induced crystallization experiments.

However, the detection of gel point was done by ***Small Amplitude Oscillatory Shear*** experiments, performed at constant temperature in the viscoelastic linear regime. They allowed measuring the gel stiffness and a critical relaxation exponent. It was demonstrated that these experiments cannot be classified as quiescent experiments [Zhang-2006].

In fact, crystallization experiments performed at the same crystallization temperature with two instruments, a DSC and a rheometer, demonstrate different crystallization kinetics. Because of the different sample thermal resistance, the crystallization kinetics recorded with the DSC and polarized optical microscope coupled to the hot-stage (or SALS) is also different. As mentioned above, this result was also observed by Winter *et al.* [Pogodina-2001]: DSC experiments have not detected any signal of crystallization development at 30000 s while the gel point is observed at 22000 s. To evaluate the degree

of conversion to the solid phase of SALS experiments Winter *et al.* [Pogodina-2001] used an expression proposed by Stein *et al.* [Akpalu-1999] for the time variation of the scattering invariant Q_{Hv}, which was identified by Winter *et al.* with the scattering invariant for orientation fluctuation Q_δ. The proposed expression to evaluate the degree of conversion is:

$$X(t) = \sqrt{Q_\delta(t) / Q_\delta(\infty)} \quad . \tag{1.2}$$

The degree of conversion evaluated with eq. (1.2) agrees with evaluation made using the covered area by spherulites in Figure 1.1 (left), which is around 15 %.

To demonstrate that small amplitude shear deformations, applied in the viscoelastic linear regime, affect crystallization kinetics, and therefore that SAOS experiments cannot be considered quiescent experiments, the crystallization of a low density polyethylene was studied using the typical protocol used for DSC isothermal crystallization experiments and the results obtained with the two instruments were compared. The sample was held at 170 ºC (above the polymer melting temperature) for 60 s, cooled down to the crystallization temperature (114 ºC) at -60 ºC/min and the crystallization kinetic was recorded. Rheological experiments were performed with Small Amplitude Oscillatory Shear deformations in the viscoelastic linear regime, with a different frequencies and a constant stress of 580 Pa. A similar protocol for the temperature program was used, with the exception of the cooling rate to the crystallization temperature, where the maximum value allowed was -20 ºC/min.

As shown in Figure 1.2, small oscillatory shear deformations accelerate crystallization kinetics in comparison with that recorded in the DSC. Although for the lowest frequency tested this effect may be ascribed to the nucleating effect exerted by the different metal surfaces contacting the polymer melt, the observation that higher oscillation frequencies accelerates the crystallization kinetics in a way similar as shear deformations imposed at the molten state do demonstrate that oscillatory shear experiments, even when performed with small oscillation frequencies, cannot be considered quiescent crystallization experiments. Therefore, the information obtained from these results must be analyzed with caution.

1.1.2. Effect of melt memory on crystallization kinetics

It is commonly accepted that isothermal and non-isothermal quiescent crystallization of polymer melts is reproducible only providing that the effect ascribed to the melt memory is erased. The physical origin of this effect remains to be clarified. It is generally considered that it results from precursor structures for crystallization, which are more effective under shear flow. In part because of this, shear-induced crystallization has attracted interest of many

researchers. However, it is not known how precursor structures are created under shear flow. This subject will be further discussed in chapter 3 of this work.

To erase the effect of melt memory on crystallization kinetics, the polymer should be heated up, prior to the crystallization, at higher temperatures for short time or at lower temperatures for longer times. These temperatures should be always higher than the polymer equilibrium melting temperature. The melt memory effect was studied for the first time with detail by Ziabicki and Alfonso [Ziabicki-1994, Alfonso-1995]. Figure 1.3a shows the temperature protocol applied by these authors in a DSC. The polymer sample was first heated from 80 ºC to the temperature T_1 (above the melting temperature), kept at this temperature for varying time t_1 (from few minutes up to 400 minutes) and rapid cooled down at -100 ºC/min to crystallization temperature T_c = 127 ºC. The time required for reaching the maximum crystallization rate (crystallization peak in the heat flux curve), t_p, was plotted against the heating time, t_1, for different temperatures T_1 (see Figure 1.3b). In the authors' opinion, the time t_p reflects the number of existing nuclei: $t_p \sim \overline{N}^{-1/3}$, where $\overline{N}$ is the average number of active nuclei that survived the heat treatment at temperatures T_1. Those nuclei were considered the reason for the melt memory effect.

It must be noted that the authors' interpretation implies that at the highest temperatures, even when the treatment is performed for longer time, some embryos must always survive, which will become latter active nuclei, accelerating the crystallization process. It can also be seen that increasing the duration of annealing at high temperatures delays the crystallization rate. For higher temperatures shorter annealing time is needed to reach an asymptotic level of t_p. After a time long enough at a specific temperature no change is observed on crystallization kinetics, and it is said that the melt memory effect was erased.

At this point a remark must be made. No physical argument was present so far to

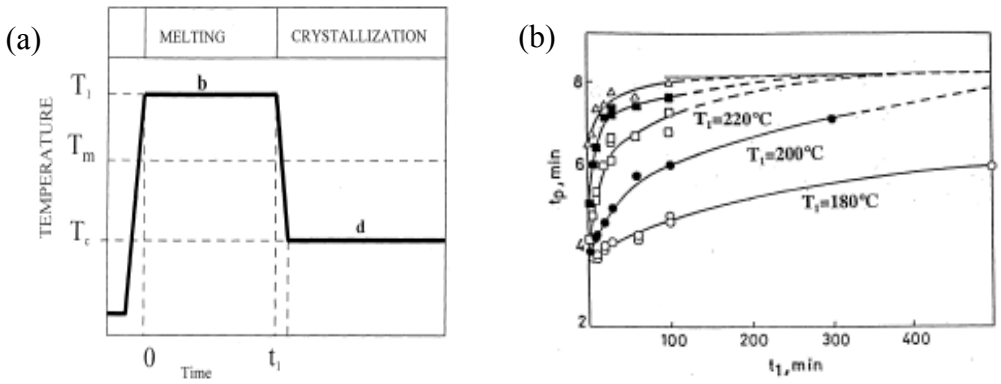

Figure 1.3. *(a) The temperature program used in the experiments of Ziabicki and Alfonso, (b) t_p as a function of the annealing time at different temperatures (○: T_1 = 180 ºC, ●: T_1 = 200 ºC, □: T_1 = 220 ºC, ■: T_1 = 240 ºC, Δ: T_1 = 260 ºC) for iPP crystallized at 127 ºC, T_m means nominal melting temperature [Alfonso-1995].*

explain why some privileged embryos survive at higher temperatures for longer times. What are the physical interactions behind this discrimination? Polymer melts used for crystallization studies have often impurities that may act as heterogeneous nuclei. Do temperature treatments promote the coalescence of these heterogeneities? Or, alternatively, since similar effects were also observed on polymers free from heterogeneities, should an alternative picture of the polymer melt morphology be considered to explain the above experimental results and others mentioned below?

The melt memory effect was also investigated by Häfele *et al.* [Häfele-2005] for the crystallization of poly(ethylene-co-octene), T_m^0 = 130 ºC. The polymer was initially annealed at 160 ºC for 10 min, cooled to the crystallization temperature (93 ºC), left until the process was completed, and then it was heated to a melt temperature T_m, annealed at the second time at this temperature for 20 minutes and cooled to the crystallization temperature T_c = 93 ºC. It can be seen in Figure 1.4 that increasing the melt temperature changes the crystallization kinetics recorded with a dilatometer, a result that is assigned to the melt memory effect. Simultaneous measurements of the 110-Bragg reflection intensity, $I_B(t)$, at the same crystallization temperature yield a perfect superposition with dilatometer experiments, which allowed concluding that the material densification recorded with the dilatometer resulted only from the crystal formation. Additionally, it was also found by SAXS experiments that lamellae thickness is independent of melt temperature. All these facts are reflected on the results of Figure 1.4 where it is found that all lines end up at the low T_m limiting value, indicating the final crystallinity independence on the melt temperature.

Based on these results it was proposed a model for explaining the melt memory effect on crystallization kinetics. It was suggested that a mesomorphic phase with liquid crystal-like properties exists in the molten state. Precursor structures were considered as objects

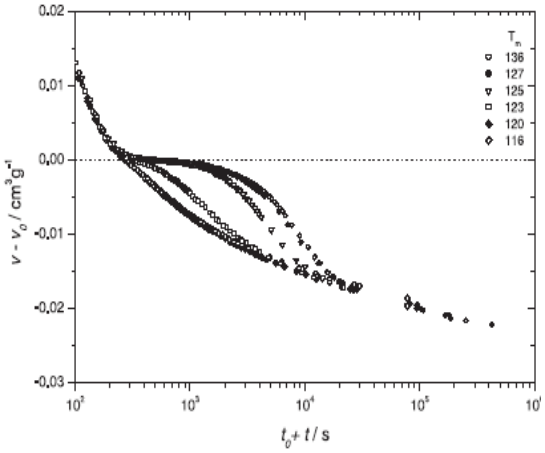

Figure 1.4. *Volume changes observed in a dilatometer as a function of time for poly(ethylene-co-octene) annealed at different temperatures (from 116 ºC to 136 ºC) and crystallized at 93 ºC [Häfele-2005)].*

containing crystallites. During crystallization its volume grows with time. At high melt temperatures, where the memory effect was erased, the objects are void from crystallites, while at lower melt temperatures they are being progressively filled with crystallites. In the conceptual explanation of this model the authors consider the same volume occupied by objects of the precursor phase, regardless the melt temperature.

It was also recognized in this work that no direct signals from the objects of precursor structure in their initial form, *i.e.* prior to their filling with crystallites, were detected. Despite this, their existence was postulated from the following arguments: 1. their function as a container which offers a crystal nucleation rate much higher than that of the free melt, and 2. the generation of an orientational texture of the crystallites within one object. This last argument results from the need to explain the formation of crystalline folded chain lamellae in the primary nuclei as an aggregation of existing crystallites.

This work presented an alternative picture for the melt morphology. Still, it is not clear what precursor structures are. Their function as a container for infilling of crystals is difficult to support with experimental arguments. It is known that the radius of gyration of polymer chains is approximately the same at the molten and solid states and that one chain participates in several lamellae [Ballard-1980]. This result does not fit to the assumption of a "container" free from crystallites at high temperatures. From the above considerations, it seems plausible to consider ordered regions at the molten state, with a size varying with the melt temperature, as the source for the effects observed. This aspect will be discussed further in this work and more details for the model of crystallization from a mesophase will be presented below.

To add further complexity to the understanding of the origin of precursor structures, NMR experiments of Saalwächter *et al.* [Maus-2007] on syndiotactic polypropylene indicate similar melt structures for melts with and without memory: static ^{1}H and ^{13}C spectra are similar; also the area of peaks associated to *tggt* and *gttg* sequences are similar for both melt types. This result was considered by the authors as the first experimental proof for the existence of "dormant" nuclei [Janeschitz-Kriegl-2005] that are sporadically activated on the same time scale as the crystallite growth.

It must be noted that the existence of ordered regions considered in the above paragraph is not inconsistent with the results of Saalwächter *et al.* The population of different conformational states at a specific melt temperature, in the absence of flow, is determined only by the Boltzmann distribution. Therefore, it is not a surprise the observation of similar melt structures for melts with and without memory.

1.1.3. The inverse quenching technique

The measurements of rheological properties at a fixed degree of crystallization may provide information concerning the evolution of the structure during the early crystallization stages. An innovative experimental protocol, called "the inverse quenching", allowed stopping the crystallization process and producing a stable crystalline-amorphous system [Acierno-2003, Coppola-2006]. An isotactic poly(1-butene) sample (melting temperature around 134 ºC) was annealed at 160 ºC during 10 minutes and rapidly cooled to the crystallization temperature T_c = 94 ºC. After different crystallization times, t_c, the temperature was raised to a value, T_{iq}, still lower than melting temperature, slowing down the crystallization kinetics. This method is based on the crystallization rate temperature dependency. A suitable choice of T_c and T_{iq} should stabilize a system composed of a melt phase and a crystalline fraction produced at a lower temperature. The *G*' evolution was recorded during the whole experiment (Figure 1.5).

The recording of the storage and complex moduli evolution was done using a multiple wave dynamic test, which is equivalent to a dynamic frequency sweep but requires much shorter experimental time. In this *Multiwave* testing mode several frequencies, which are higher order harmonics of a fundamental frequency ω_f, are simultaneously applied. At each discrete frequency the storage and loss moduli are obtained by means of a discrete Fourier transformation of the stress response to the compound strain. In this way a frequency range of three decades is swept in a fraction of the time required for a dynamic frequency sweep, allowing therefore an accurate determination of the gel time at lower temperatures.

The *Multiwave* tests covered a frequency from 5×10^{-4} to 10 rad/s and the total strain applied was less than 5 %. The gel time evaluated with a fundamental frequency of 0.06 rad/s at the crystallization temperature of 94 ºC corresponds of a degree of conversion to the solid phase of 1.29%, indicating that the gelation process occurs at very low degrees of phase

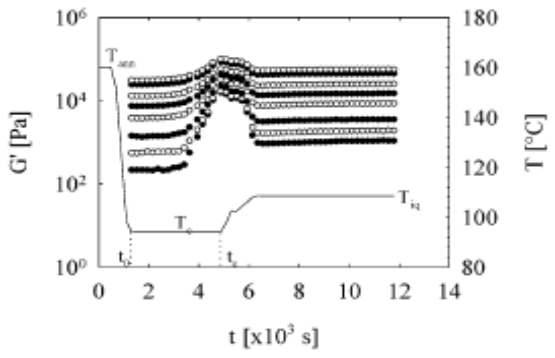

Figure 1.5. *Storage modulus as a function of time during the inverse quenching experiment (for frequencies from top to bottom equal 12, 6, 2.4, 1.2, 0.6, 0.24, 0.12, 0.06 rad/s) The solid line represents the thermal protocol applied to the sample [Coppola-2006].*

conversion [Coppola-2006]. It should be noted that this value is much lower than that estimated from Figure 1.1 (left), for e quiescent crystallization Coppola *et al.* evaluated the degree of conversion to the solid phase from the time variation of G' at T = 94 ºC for the oscillation frequency of 0.06 rad/s using

$$X(t) = \frac{G'(t) - G'(0)}{G'(\infty) - G'(0)} \quad , \tag{1.3}$$

where $G'(0)$, $G'(t)$ and $G'(\infty)$ are the elastic modulus values at the start of crystallization, at time t during the crystallization process and at its end, respectively.

Results obtained with the inverse quenching technique for different frequencies used by the *Multiwave* test are shown in Figure 1.5. After an induction time the modulus increases indicating the beginning of crystallization, but it stops growing when the temperature is raised. Optical microscopy images taken at different time after reaching the quenched temperature T_{iq} also didn't show any changes in spherulite size or number [Acierno-2003].

Multiwave tests performed at 109 ºC (the selected inverse quenched temperature) on samples crystallized with different degrees of conversion at 98 ºC are presented in Figure 1.6. The figure shows also the storage modulus variation of the pure melt and the fully crystallized sample. According to the authors, all results indicated in Figure 1.6 were obtained at 109 ºC, but they represent the image of constant crystallinity states obtained at 94 ºC. Especially relevant for the authors are the results for the degree of conversion of 0.58 %. For this value of phase transformation the storage modulus increases and stabilizes in a plateau value. Its variation allowed identifying a slower relaxation process with a relaxation time around 1000 s, indicating for the first time that slow relaxation processes take place at very low degrees of conversion [Coppola-2006].

The authors tried also to explain the viscoelastic behaviour around the gel point and

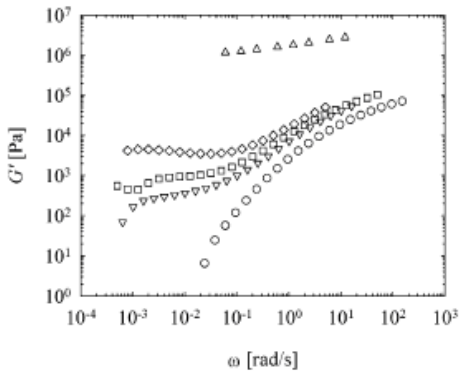

Figure 1.6. *Storage modulus as a function of frequency of poly(1-butene) at 109 ºC for result obtained after crystallization at 94 ºC (○ – melt, ∇ - 0.58 %, □ – 1.29 %, ◊ - 2.8 %, Δ – 100 %) [Coppola-2006].*

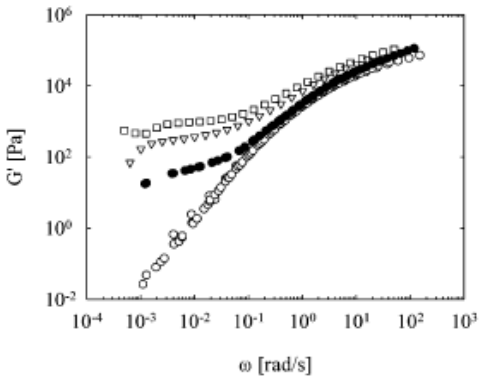

Figure 1.7. *Storage modulus of poly(1-butene) at 109 ºC (symbols as in Figure 1.6) and from simulation of molten sample filled with glass beads (filled symbols) [Coppola-2006].*

tested the assumption of Winter *et al.* [Pogodina-2001] that gel point results from the increased interaction between spherulites originated by chains belonging to several spherulites. Based on the evaluation of the typical nucleation density at 94 ºC the average distance between nuclei centres was evaluated. The value obtained was around 129 μm, which is also the average distance between spherulites, assuming that all nuclei grow at the same time. Since this distance is many orders of magnitude larger than the coil size, around 100 Å, it was concluded that the bridging between spherulites is an extremely unlikely event.

To confirm further this conclusion, glass beads with an average diameter of 60 μm were immersed in the same PB1 molten sample (volume fraction 12 %) and subjected to a similar protocol. After this addition, the sample's equivalent degree of conversion was around 24 %. The result obtained, indicated by filled symbols in Figure 1.7, shows that the presence of an amount one order of magnitude larger of a noninteracting filler has much less effect in enhancing the polymer low-frequency elasticity.

Based on these results Copolla *et al.* questioned the existence of a critical gel transition and the indication of a critical gel state by the frequency-independent loss tangent at intermediate frequencies. Instead, they suggested that the strong change in the viscoelastic properties at very low crystallinity levels might be attributed to the presence of "dormant nuclei", which are, according to Janeschitz-Kriegl *et al.* [Janeschitz-Kriegl-2005], stable nuclei that form in the melt at any given temperature below the melting point.

1.2. Primary nucleation

1.2.1. Classical nucleation theory

Primary nucleation may be classified as homogeneous or heterogeneous. Homogenous nucleation is defined by the spontaneous aggregation of molecules and occurs at high supercooling in pure polymers, while in heterogeneous nucleation aggregations appears at relatively low supercooling when a foreign body is present in the melt (the free energy barrier for nucleation is smaller). The nucleation from polymer melts is usually a type of heterogeneous nucleation [Nishi-1999].

According to the classical nucleation theory, clusters of molecules existing in the supercooled melt join each other to create embryos that further grow in size originating a nucleus with a critical size. Nuclei with this size are stable and grow into crystalline structures with a nucleation rate that is crystallization temperature dependent (see Figure 1.8).

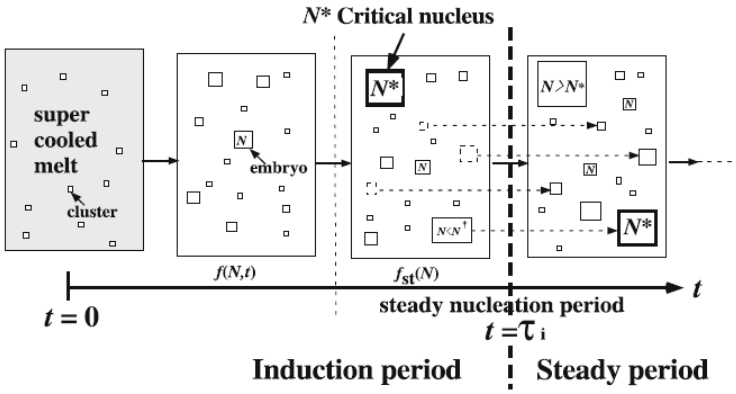

Figure 1.8. *The induction and steady periods during the nucleation process; N is the size of nucleus, N* - size of critical nucleus, defined as number of atoms or repeating units within the nucleus and* τ_i *is the induction time [Hikosaka-2005].*

The time between the start of the isothermal process and the formation of nuclei with critical size is called *the induction time*. Since the estimation of nuclei critical size is difficult and, as it will be seen below, for polymers the predicted dimensions of critical nuclei are orders of magnitude larger than the known dimensions of the crystalline folded chain lamellae, the definition of induction time is dependent on the instruments' sensitivity used to follow the crystallization process. For example, recording the time for nuclei detection with an optical microscope is not a good measurement for the induction time, since the instrument resolution does not allow the detection of structures with the size estimated for critical nuclei. The same argument may be extended to other experimental techniques.

The formation of solid structures in a supercooled melt is accompanied by a reduction in the Gibbs free energy. The overall excess free energy, ΔG, between a small solid particle with radius of sphere *r* and the solute in solution is equal to the sum of the surface excess free energy and the volume excess free energy:

$$\Delta G = \Delta G_s + \Delta G_V = 4\pi r^2 \gamma + \frac{4}{3}\pi r^3 \Delta G_v \quad . \tag{1.4}$$

The surface excess free energy, ΔG_s, is the excess free energy between the surface of the particle and its bulk, while the volume excess free energy, ΔG_V, is the excess free energy between a very large particle ($r = \infty$) and the solute in solution. ΔG_V is a negative number and γ is the interface free energy between the solid particle and the melt. For a small sphere the ratio between its area and volume is large; ΔG initially increases with *r* and passes a maximum before becoming negative (see Figure 1.9). ΔG^* is the energy barrier that has to be overcome by the thermal motion of molecules to create a stable nucleus and is molecular weight independent.

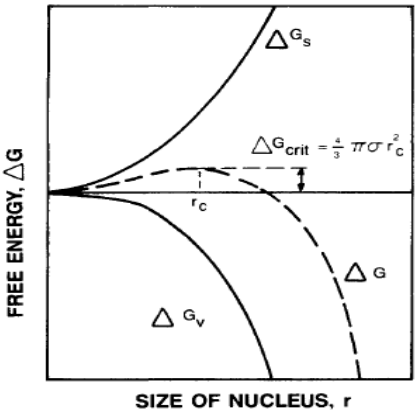

Figure 1.9 *Free energy as a function of nucleus size [Mullin-1961].*

The concept of critical nucleus is the major result of classical nucleation theory. At a temperature below the equilibrium melting temperature a nucleus with a critical size exists. Nuclei with smaller size are unstable and their probability of decrease is higher than the probability of growth. If the critical size is overstepped, the nucleus is stable. Such a nucleus is called active or supercritical. Assuming as in eq. (1.4) that the critical nuclei have spherical shape, its radius and the critical free energy for formation are given by eqs. (1.5) and (1.6), respectively:

$$r^* = -\frac{2\gamma}{\Delta G_v} = -\frac{2\gamma T_m^0}{\Delta H_v \Delta T} \quad , \tag{1.5}$$

$$\Delta G^* = \frac{16\pi\gamma^3}{3(\Delta G_v)^2} = \frac{16\pi\gamma^3 (T_m^0)^2}{3\Delta H_v^2 \Delta T^2} \quad , \tag{1.6}$$

where ΔH_v is latent heat of crystallization per unit volume (negative quantity). Since $\Delta T = T_m^0 - T$, it is clear that both, the radius of critical nucleus and the critical energy barrier, should decrease with temperature.

Classical nucleation theory may also be applied to polymers, but the strong anisotropy

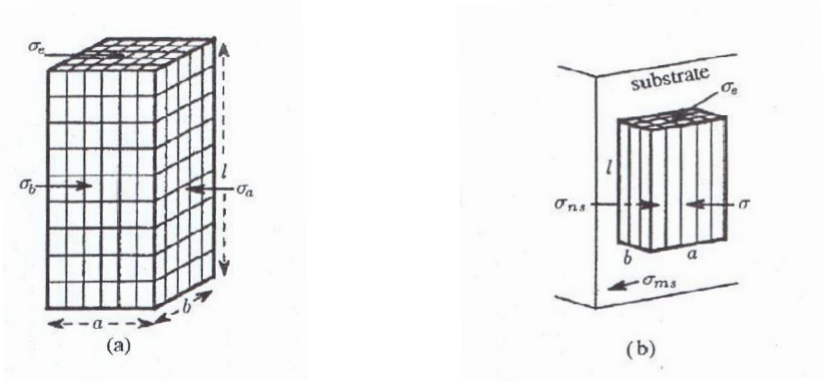

Figure 1.10. *Two types of primary nucleation: (a) homogeneous and (b) heterogeneous.*

of polymer crystals has to be considered. Because of that, polymer nuclei are assumed as constituted by the packing of parallelepipedic units or blocks containing chain segments aligned in the transversal direction. In this case nuclei are defined by three geometrical parameters: width *a*, thickness *b*, length in the chain direction *l* and three surface energies: lateral σ_a (face *bl*) and σ_b (face *al*), and fold σ_e (face *ab*) [Hoffman-1961]. For **homogenous nucleation**, Figure 1.10a, the free energy of nuclei formation is:

$$\Delta G(a,b,l) = -abl\Delta g + 2bl\sigma_a + 2al\sigma_b + 2ab\sigma_e \quad . \tag{1.7}$$

Equalling to zero the partial derivatives with aspect to *a*, *b* and *l*, the nuclei critical dimensions and critical free energy are:

$$a^* = \frac{4\sigma_a}{\Delta g};\ b^* = \frac{4\sigma_b}{\Delta g};\ l^* = \frac{4\sigma_e}{\Delta g} \quad , \tag{1.8}$$

$$\Delta G^* = \Delta G(a^*,b^*,l^*) = \frac{32\sigma_a\sigma_b\sigma_e}{(\Delta g)^2} \quad . \tag{1.9}$$

The free energy of formation for a nucleus in contact with a plane substrate (**heterogeneous nucleation**) - Figure 1.10b - can be written as [Binsbergen-1973]:

$$\Delta G = -abl\Delta g + al\sigma + 2bl\sigma + 2ab\sigma_e \quad , \tag{1.10}$$

with $\sigma_a = \sigma_b = \sigma$ and $\Delta\sigma = \sigma + \sigma_{ns} - \sigma_{ms}$. $\Delta\sigma$ = 0 when nucleus and the substrate are of the same nature. σ_{ns} is surface energy for the interface between the nucleus *n* and the substrate ($\sigma_{ns} = 0$ if the substrate is the polymer crystal) and σ_{ms} is surface energy corresponding to the interface between the substrate *s* and polymer *m* (when the substrate is the polymer crystal itself $\sigma_{ms} = \sigma$). The critical nucleus dimensions and the critical free energy are:

$$a^* = \frac{4\sigma}{\Delta g};\ b^* = \frac{2\Delta\sigma}{\Delta g};\ l^* = \frac{4\sigma_e}{\Delta g} \quad , \tag{1.11}$$

$$\Delta G^* = \frac{16\sigma\sigma_e\Delta\sigma}{(\Delta g)^2} \quad . \tag{1.12}$$

As long as $\Delta\sigma$ is less than 2σ, the nucleation on a substrate is more probable than the homogenous nucleation.

The above equations for the critical dimensions and free energy of formation of the critical nucleus were derived under the assumption that this nucleus is a single crystal with length a^*, width b^* and thickness l^*. Most probably, the critical nucleus in semicrystalline polymers crystallized from melts is intrinsically semicrystalline, with folded chain lamellae

separated by amorphous interlamellar regions. However, fully crystalline nuclei may be created in polymers crystallized from solution, and lamellae having a thickness around 1 μm may be created in the crystallization of PE under pressure [Gedde-1995].

Reliable estimations for the size and free energy of formation of critical nucleus are not known. Because of temperature dependence of driving force for crystallization, this size depends on the supercooling degree, $\Delta g = \Delta h \cdot \Delta T / T_m^0$, and the maximum allowed value would occur for the smallest allowed supercooling. It may be evaluated from non-isothermal crystallization experiments at different cooling rates by extrapolating the onset of crystallization, detected by the instrument at different cooling rates, to zero cooling rate [Martins-1999], but so far this procedure was not applied to polymer crystallization.

Since the fold surface free energy σ_e is larger than σ, the ratio between the two being between 2 and 10, depending on the polymer, it may be concluded that for the same supercooling the critical nucleus thickness is 2 to 10 times larger than its width. For example, for a PE crystal, the equilibrium ratio between the thickness and the width is around 7, a value that is ***three*** to ***four*** orders of magnitude greater than the values obtained experimentally [Gedde-1995]. This anomaly between calculated results and experimental observations was understood as the result of an unfavourable thickness-to-width ratio leading to the crystal rearrangement after thermal stimulation.

The validity of this apparently unanimous conclusion may be questioned by experimental results of lamellae thickness obtained with Small Angle X-ray Scattering. The lamellar thickness is constant since the earlier crystallization stages and its value depends only on the supercooling degree [Strobl-2006]. It is still controversial if this supercooling should be defined with respect to the equilibrium melting point or to another temperature above it. Some experimental results seems to support the last view and they are part of the support over which is constructed a thermodynamic scheme for explaining the polymer crystallization [Strobl-2006], that will be briefly explained below.

Predictions for this size were also presented by Hikosaka *et al.* [Hikosaka-2005]. Their predictions started from an expression for the radius of gyration for a thin parallelepipedic nucleus. The following expression was proposed, without derivation, for the radius of gyration of a thin parallelepipedic nucleus:

$$R_g = \left\{ \left(l^2 + b^2 + a^2 \right) / 12 \right\}^{1/2} \quad . \tag{1.13}$$

Nucleating agents were added to polyethylene to increase its nucleation density and the intensity of the signal was observed by SAXS. The dependence of the integrated scattering intensity on the scattering vector q is given by the Guinier's law,

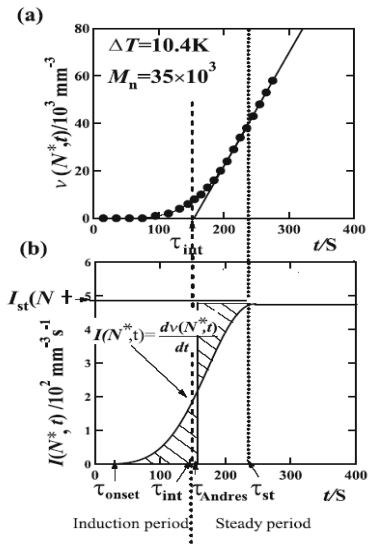

Figure 1.11. *(a) Number density of nuclei and (b) nucleation rate as a function of time observed by optical microscopy for polyethylene, T_c = 129.1 ºC, ΔT = 10.4 K [Hikosaka-2005].*

$$I_x(q,t) \propto \exp\left\{-\left[R_g(t)\right]^2 q^2/3\right\} \tag{1.14}$$

and it allows evaluating the radius of gyration at different crystallization times. Using a small supercooling of only 10.4 K the integrated scattering intensity was measured at different times. Optical microscopy experiments allowed evaluating under those conditions an induction period of 2.5 min (see Figure 1.11). Results of measurements after 3 min allowed the evaluation of the radius of gyration from the above equation. The value obtained was 162 Å and the primary nuclei predicted thickness was 560 Å, close to value obtained from eq. (1.11) with $\Delta g = 6.8 \times 10^5\ \Delta T$ J/m^3 and $\sigma_e = 88 \times 10^{-3}$ J/m^2. However, some aspects of the work of Hikosaka *et al.* are not clear, particularly those related with eq. (1.13) and some non-coincident values used for the driving force for crystallization and surface energies in different works, apparently for the same polymer [Hikosaka-2005, Okada-2007]. The differences between these values are of several orders of magnitude. Also, it should be noted that the radius of gyration of any solid body is evaluated from its moment of inertia, which is defined with reference to an axis of rotation. Therefore, the correct expression for R_g should be expressed as a function of two dimensions only instead of the three dimensions considered in eq. (1.13).

1.2.2. Nucleation as the result of spinodal decomposition?

Phase transformations may occur by nucleation and growth when the free energy of mixing has a positive curvature $\left(\partial^2 \Delta G/\partial X^2\right) > 0$ or by spinodal decomposition when the curvature is negative $\left(\partial^2 \Delta G/\partial X^2\right) < 0$ (see Figure 1.12). The limits of composition within which a single phase is not stable are defined by the points at which a line is tangential to

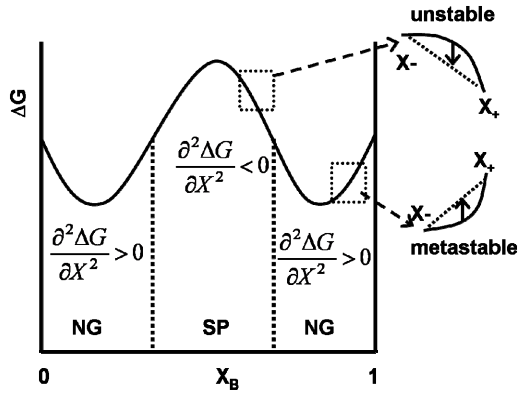

Figure 1.12. *Variation of molar Gibbs free energy of mixing with phase B concentration. Vertical dotted lines indicate the limits of spinodal decomposition (SP) which occurs when the free energy has negative curvature (system unstable). Otherwise, nucleation and growth (NG) occurs.*

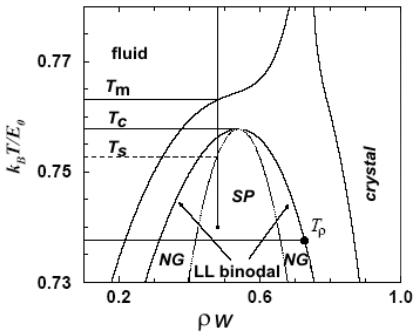

Figure 1.13. *Calculated generic phase diagram for a polymer melt. T_m and T_s are the melting and spinodal temperatures encountered along the (constant density) quench path (dotted line). T_c is the temperature at which the liquid-liquid phase has a critical point and T_ρ is the temperature, below the spinodal T_s, at which the energy barrier to crystallization is zero (it is expected that this energy barrier should decrease with increasing the quenching depth below T_s). Adapted from [Olmsted-1998].*

the free energy curve in two places (two free energy minima). These two points define the *binodal* region that contains the region of spinodal decomposition. The loci of spinodal points are at the concentrations at which $\left(\partial^2 \Delta G / \partial X^2\right) = 0$.

The binodal and spinodal meet at the critical point. To reach the spinodal region of the phase diagram, a transition must take the material through the binodal region or the critical point (Figure 1.13). The spinodal decomposition is observed when a very fast transition, often called a *quench*, takes the material through the binodal region or the critical point, moving from the stable to the spinodally unstable region of the phase diagram. Because in spinodal phase transformations the system is unstable for a specific concentration of the two phases, the decrease in free energy proceeds by the spontaneous growth of perturbation and small changes in composition lead to a separation into two phases, X_+ and X_-. The region where these events occur is the spinodal region and the phase separation process is known as spinodal decomposition (see Figure 1.12).

By contrast to spinodal decomposition where no energy barrier is required for the phase transformation to occur, in transformations by nucleation and growth an energy barrier needs to be surmounted to achieve the global free energy minimum. The system is metastable to small concentration fluctuations and large changes in composition are needed for the phase change. A key difference between these two phase transformation processes is that for nucleation, by contrast to phase separation by spinodal decomposition, the new phase must initiate with a composition that is *not* near that of the parent phase. Nucleation is a phase transition that is large in degree (composition change) but small in extent (size), whereas spinodal decomposition is small in degree but large in extent. In resume, ***metastable*** mixtures

transform by nucleation and growth while ***unstable*** mixtures transform by spinodal decomposition. A quench into the spinodal regime leads to spontaneous decomposition into two phases while a quench into the nucleation and growth regime (NG) will only lead to phase separated structures in the presence of nuclei for phase growth.

Two possibilities were considered for the application of the above ideas to polymer melts. One considers the two phases as isotropic liquids, with one rich in conformational states more appropriate for crystallization and denser, while the other is depleted of those conformational states and is thus less dense. The other considers the occurrence of a transition to a metastable or unstable liquid crystalline phase which has associated a spatial density modulation [Heely-2003].

It was demonstrated that a conformation-density coupling can induce a liquid-liquid phase transition. In another words, it was shown that the spinodal decomposition can occur in polymer melts quenched to a specific temperature, T_s - see Figure 1.13 - if polymer chain segments adopt the appropriate chain conformation to crystallize, which for PE is the *trans* chain conformation, while for iPP is the helical conformation. These changes on conformations are followed by changes in density (ordered chain segments packing more densely than those with random conformation), originating therefore small concentration fluctuations [Olmsted-1998].

Experimental results supporting this view were obtained from the quiescent and shear-induced crystallization of polymers. However, pre-nucleation density fluctuations, leading to a metastable phase, were also found in different classes of crystallization besides the homopolymer crystallization, including the crystallization of inorganic substances such as the formation of calcium carbonate from aqueous solutions of sodium carbonate and calcium nitrate [Heely-2002, page 359]. These observations led the authors to the suggestion that pre-nucleation density fluctuations might be a universal phenomenon, not restricted to the crystallization of polymers.

These density fluctuations were also observed by Imai *et al.* [Imai-1994], who investigated the cold crystallization of poly(ethylene terephthalate) (PET) using SAXS and WAXS. It was concluded that spinodal decomposition occurs in quenched samples from the melt at temperatures five degrees above T_g and that this occurrence resulted from density fluctuations originated by the different densities of rotational isomeric states frozen during the quenching process. The model proposed considers that polymer annealing at a temperature above the glass transition causes the transformation of frozen *gauche* conformations in the amorphous state to *trans* conformations.

According to Imai *et al.* [Imai-1994] the annealing at five degree above T_g increases the length of ordered domains, which was experimentally confirmed by SAXS experiments. They increase from an initial value of 60 Å up to 85 Å after annealing during 100 min. Obviously, the density of parallel ordered domains is higher than that of the surrounding disordered regions. Since their length increases with the annealing time, it was considered that when a critical length is reached, longitudinal adjustment occurs, yielding still more efficient packing at the formation of critical nuclei with a thickness of around ¼ the length of ordered domains (≈ 20 Å). The authors did not explain what happens to the other ¾ of these aligned ordered domains. It is implicit in their reasoning that they are destroyed after the formation of primary nuclei. The need for ordered domains of larger size was explained as the result of entanglements that obstruct the polymer chain's diffusion to the critical nuclei.

The lag between the intensity in the SAXS region and the appearance of peaks in the WAXS region was considered as the main experimental evidence of spinodal decomposition at the earlier crystallization stages. An additional support for the occurrence of spinodal decomposition during crystallization was the validity test for the Cahn-Hilliard equation [Cahn-1958], which was found to hold in the description of spinodal phase transformations in metal alloys. To perform a Cahn-Hilliard analysis of Small Angle Light (or X-ray) Scattering, a series of scattering patterns as a function of time are taken. The intensity of scattering I, is plotted against the scattering vector q, $q = (4\pi/\lambda)\sin(\theta/2)$, where θ is the scattering angle and λ is the radiation wavelength. Those analyses are performed in a regime where only SAXS is observed, while no signal of WAXS, related to the development of crystalline order, is detected. The slope of plot gives the density fluctuations' growth rate $R(q)$ at a given scattering vector:

$$I(q,t) = I(q,0)\exp[2R(q)t] \quad . \tag{1.15}$$

This density fluctuations growth rate may be expressed as

$$R(q) = \mu\, q^2\left[a(T_s - T) - \frac{1}{2}gq^2\right] = q^2 D_{eff}\left[1 - \frac{1}{2}\left(\frac{q^2}{q_m^2}\right)\right] \quad , \tag{1.16}$$

where μ is the mobility for concentration fluctuations. D_{eff} is an effective diffusion coefficient, $D_{eff} = -\mu\, a(T_s - T)$ and it is negative below the spinodal temperature, signifying therefore unstable growth. The growth rate is maximum at a finite $q = q_m = \{[a(T_s - T)]/g\}^{1/2}$ due to the competition between slow growth at long wavelengths and high energy cost at small wavelengths; g is related to a gradient free energy term and penalizes composition gradients.

The representation of $R(q)/q^2$ versus q^2 can be taken as a measure of the dynamic driving force for the concentration fluctuation's growth. According to the Cahn-Hilliard

model its linearity indicates the presence of spinodal decomposition. Figure 1.14 illustrates the SAXS data obtained at different crystallization times for the iPP isothermal crystallization at 140 ºC. From these curves the growth rate $R(q)$ is obtained and the Cahn-Hilliard plot constructed – Figure 1.15. The maximum in $R(q)$ is visible in the inset, and the extrapolation to $q^2 = 0$ of the linear fit to the plot allows the evaluation of $D_{eff.}$ – see eq. (1.16) Effective diffusion coefficients may be evaluated in this way for different crystallization temperatures.

Plotting the D_{eff} values as function of temperature allows the evaluation of the spinodal decomposition temperature, which marks the lower limit of melt stability, *i.e.* the temperature below which the melt spontaneously separates into two phases. The value of spinodal decomposition temperature, T_s, is evaluated by extrapolating to $D_{eff} = 0$ in the plot of effective diffusion coefficient D_{eff} versus temperature.

As mentioned above, the appearance of SAXS signals before WAXS and the Cahn-Hilliard plots were used as the main support for the spinodal decomposition. As discussed below, this interpretation has been questioned by other authors that performed similar experiments. They argued that the higher sensitivity of detectors used for SAXS experiments in comparison with those used for WAXS experiments is the reason for the earlier detection of SAXS signals. Conflicting results were also obtained from molecular dynamics simulations, some supporting the spinodal decomposition while others favour the nucleation and growth.

Because the above objections, the group supporting the spinodal decomposition performed experiments with a new WAXS detector with a 10^4 improvement factor in the count rate capability over previous detectors. Again, the appearance of a SAXS peak versus the scattering wave vector q at an early time of crystallization was observed before the appearance of any WAXS signal. Further, this delay was observed much beyond the limits

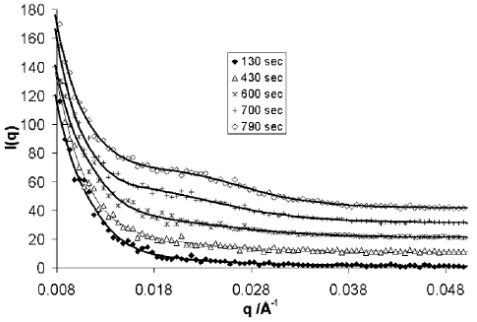

Figure 1.14. *SAXS data obtained for the isothermal crystallization of iPP at 140 ºC. The intensity data at different times is offset for clarity [Heeley-2003].*

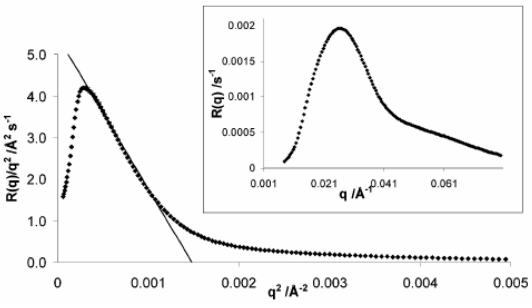

Figure 1.15. *Analysis of the scattered intensity according to linearized Cahn – Hilliard theory. The inset shows the maximum in R(q) at q_m. The intersection of the line with q = 0 allows the evaluation of D_{eff} [Heeley-2003].*

of systematic experimental error. It was therefore concluded that the emergence of Bragg peaks indicates the end of induction period, SAXS patterns visible during induction period indicate the evolution of noncrystalline structures, and that density fluctuation takes place before crystallization process [Heeley-2003].

Additional shear-induced crystallization experiments with iPP showed that the lag in appearance between SAXS and WAXS patterns is observed only at small supercoolings while at large supercoolings both signals grow together [Heeley-2002]. The SAXS pattern with a length scale between 50 Å to 200 Å was observed prior to the development of crystals and changed its shape to that typical of lamellar crystals when WAXS indicate the beginning of crystallization (its intensity at the early stages was around 100 times weaker than the diffraction ring after crystallization started). The value obtained for the spinodal decomposition temperature, T_s, was 419 ± 3 K, which is 18 K below the measured melting point for crystals with long spacing 175 Å and 40 K below the equilibrium melting point $T_m^0 = 459$ K.

To get deeper insight into the earlier crystallization stages, Gee *et al.* [Gee-2006] performed computer simulations using clusters of more than 2000 2.4 GHz processors. The simulations were performed with polar and apolar polymers. Between 6000 and 20000 chains were used to simulate a polymer melt. The united atom model was used. Therefore, for PE the hydrogen atoms were lumped to the backbone carbon atoms to which they are attached. The force field parameters consisted of both valence (stretch, bending, and torsion terms) and nonbonded potential terms (van der Waals and Coulomb). The initial starting polymer configurations were generated using a Monte Carlo method. The monomers were allowed to "polymerize" in a head-to-tail manner with no monomer reversals. The initial atomic positions of the amorphous melt structures were generated using a random distribution of torsional angles, which was generated using a Monte Carlo method that assigns random values to all rotatable torsions in the polymer chain. The resulting amorphous structure was then relaxed by energy minimization. The total time of simulations was ~ 50 ns, which took $\sim 1 \times 10^6$ processor hours for each polymer melt.

Two polyethylene melts with chains having 240 and 768 beads (above the critical molecular weight) were simulated at 600 K. The melt was allowed to relax for 5 ns, cooled in increments of 50 K under constant particle number and pressure and equilibrated for a minimum of 5 ns at 550 K and 500 K. The simulation showed a microphase separation from the melt into many liquid crystalline domains (see Figure 1.16 – panels **a** to **c**). They coalesce, grow and form oriented domains (chain-folded domains that resemble the lamellae of polymer crystals). It was concluded that cooling from melt leads to primary phase separation of

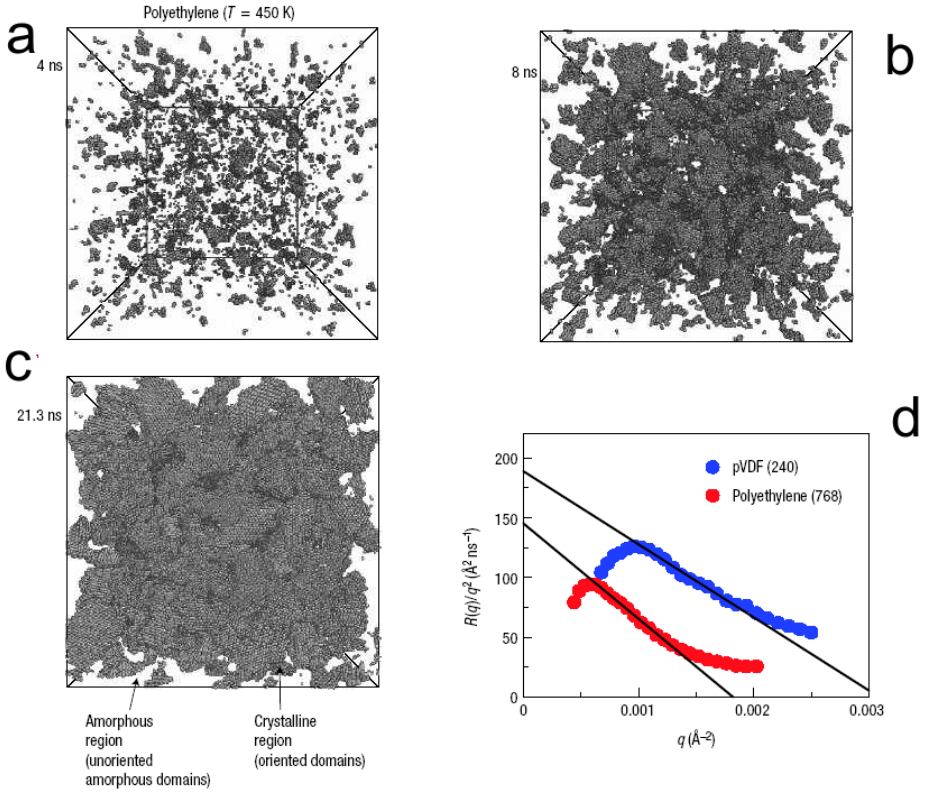

Figure 1.16. *Molecular dynamics simulations for the evolution of crystallization process in polyethylene at 450 K during the first 21.3 ns (panels* **a** *to* **c***). White colour indicates the unoriented amorphous domains. Panel* **d** *shows the Cahn-Hilliard plot obtained from molecular dynamics simulations for polyethylene and poly(vinylidene fluoride). Adapted from [Gee-2006].*

nematic ordered domains and isotropic unordered domains. At the same time a secondary phase separation occurs between smectic liquid-crystal phase (characterized by close packing of rod-like segments) and amorphous phase. The smectic regions thicken by nucleation and growth mechanism and have a fringed-micelle-like morphology. From molecular dynamics simulations, a Cahn-Hilliard plot was obtained (panel **d**) and the linear nature at the earlier stages demonstrated the presence of spinodal decomposition.

Contrary to the experimental, theoretical and computational results supporting spinodal decomposition as the process occurring at the earlier crystallization stages, an equal amount of experimental results, theories and molecular dynamics simulations exists that denies this process. Some of them are related with specific morphological features and will be discussed in the paragraph below. Among the experimental results denying the spinodal decomposition are those of Panine *et al.* [Panine-2008] and Xiao *et al.* [Xiao-2007]. Xiao *et al.* performed similar experiments as those mentioned above but with Small Angle Light Scattering. No peaks were detected and also no maximum in $R(q)$ was observed. Since the wavelength used in these experiments (visible light) is much smaller than the dimension estimated for the ordered structures at the earlier crystallization stages, these results will not be discussed further.

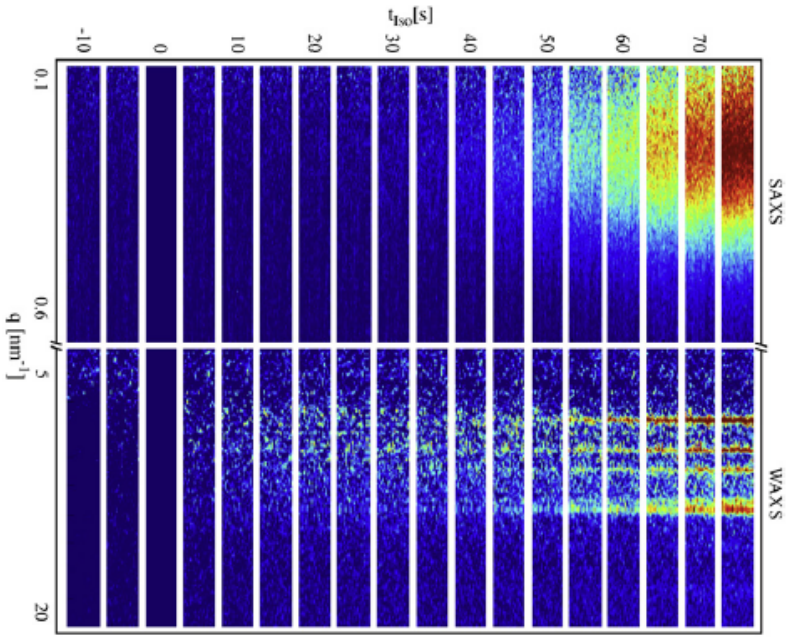

Figure 1.17. *Azimuthal sectors of SAXS and WAXS patterns recorded during rapid temperature quenched to crystallization temperature 145 ºC, t_{Iso} is the isothermal crystallization time [Panine-2008].*

Panine *et al.* [Panine-2008] used high brilliance SAXS and WAXS techniques during the isothermal crystallization of iPP at 145 ºC. Although these authors have some wrong statements in their work, namely those related to the existence of a smectic phase at the earlier crystallization stages, which was recognized to be the result of additives present in the polymer [de Jeu-2006], their experiments concerning SAXS and WAXS seems to be trustable. The key results of these experiments are in Figure 1.17. The WAXS signals are detected prior to SAXS signals. No signal of long-range density fluctuation supporting the spinodal decomposition was found and authors argued that the early stages of isothermal crystallization in iPP should be described by a nucleation and growth mechanism.

Muthukumar *et al.* [Muthukumar-2000, Muthukumar-2003] performed molecular dynamics simulations similar to those performed by Gee *et al.* [Gee-2006]. Similar force fields and the united atom model were used. The main differences are not negligible. Muthukumar used Langevin dynamics simulation of a single polyethylene chain crystallizing from solution. A maximum ensemble of *four* separated, non-interacting, chains were considered. In the simulation a polymer chain of $N = 2000$ beads (each bead corresponding to one methylene unit) was equilibrated above the melting point and quenched. Aggregations with local orientational order, called "baby nuclei", connected by flexible chains were observed, see Figure 1.18.

In agreement with experimental results of SANS [Ballard-1980], it was found that one chain participates in many nuclei and that it is reeled with time leading to fast merging of nuclei. Curiously, this argument was also used by the supporters of the spinodal

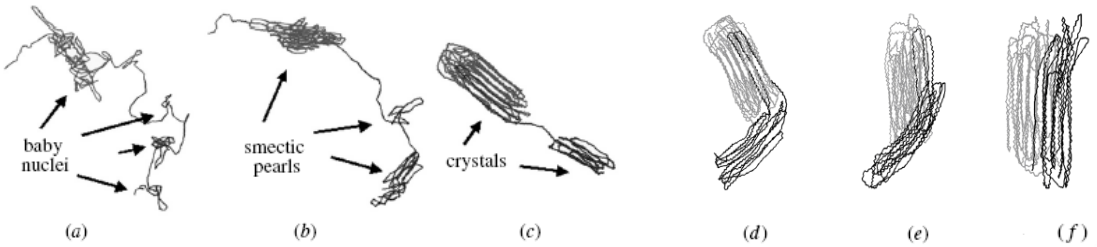

Figure 1.18. *Growth (a-c) and merging (d-f) of smectic pearls for N = 2000: (a) t = 50 s, (b) t = 500 s, (c) t = 7400 s, (d) t = 10300 s, (e) t = 12850 s, (f) t = 13350 s [Muthukumar-2000].*

decomposition. However, since strands had possibility to stretch and some nuclei may dissolve, the average distance between baby nuclei may not change immediately after quenching. It was considered that the merging of nuclei and formation of lamellae requires a highly cooperative mechanism involving all lamella stems (Figure 1.18). This explanation fits within the nucleation process, the only difference being that one chain participates in several nuclei.

Based on their simulation results and theoretical arguments, Muthukumar *et al.* argued that the mechanism of polymer crystallization, even in the early stages, including the induction period, is nucleation and growth and the assumption that $R(q)/q^2$ versus q^2 rising sharply, reaching a maximum and decreasing at higher q values, is wrong. According to Muthukumar *et al.* if the mechanism was simple spinodal decomposition into two phases, $R(q)/q^2$ should show a monotonic linear decrease from a positive value at $q \rightarrow 0$ and its slope should be independent of quench depth. As an additional argument in his favour is the fitting of scattering data shown in Figure 1.15. The fitting to spinodal decomposition theory is only superficial.

1.2.3. Crystallization as an effect of a mesophase

The nucleation process may also be understood as a phase transformation in a small region that requires additional energy to overcome a nucleation barrier between a melt and a non-crystallographic ordered phase [Strobl-2000, Strobl-2005, Sirota-2007]. If this barrier is sufficiently high, an additional intermediate phase (mesophase) is formed. The energy barrier for its formation is lower than the energy barrier for the formation of nuclei with crystallographic order, and its free energy is intermediate between that of the melt and the stable phase. This intermediate phase between liquid and crystalline states should be characterized by long-range order, *i.e.* parallel arrangement of chain axes (like in a solid), and positional disorder (like in liquid).

It is considered that crystals nucleating via a mesophase follow the Ostwald's rule of stages: "***a crystallizing system progresses from the supersaturated state to equilibrium in***

stages, each stage representing the smallest possible change in free energy". Another way of expressing this rule is stating that a substance capable of crystallizing in several forms, will select first the least stable form, which is followed by forms of increasing stability [Threlfall-2003].

For polymers, the most known mesophase is the hexagonal phase of polyethylene, which receives this classification because the unit cell parameters correspond to a hexagonal crystal class, even though the cell symmetry is not precisely hexagonal [Philips-2005]. This phase has many gauche conformational states, and from an entropic point of view it seems to be more similar to liquid than crystal: atoms are not fixed in the hexagonal lattice, but they are entropically stabilized and the packing density is lower than the crystal phase.

The transition from the normal pressure PE orthorhombic unit cell to the hexagonal phase was observed at very high pressures [Rastogi-1991, Heeley-2002]. This phase transition was studied with proton NMR [Sozzani-2005] and DSC instrument by de Langen *et al.* [de Langen-1999, de Langen-2000]. Figure 1.19 shows the phase diagram where it is clear the similarity of results obtained with both instruments: hexagonal phase appears as a stable phase above 490 K and 3000 bar.

Keller *et al.* [Keller-1994] showed that the hexagonal phase can exist as a mesophase at much lower pressure and temperature than those reported earlier. At normal pressure the mesomorphic phase can be observed in polyethylene when chains are chemically modified by irradiation or if a mechanical field is applied to ultrahigh molar mass polyethylene fibres. All these studies drew attention to the possibility that the formation of crystals should require the presence of a mobile phase under all circumstances, in the case of crystalline polymers in general and of polyethylene in particular.

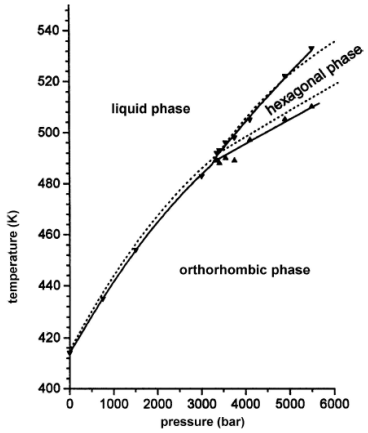

Figure 1.19. *Polyethylene phase-diagram: solid lines – NMR data compared with DSC data - dotted lines [de Langen-1999].*

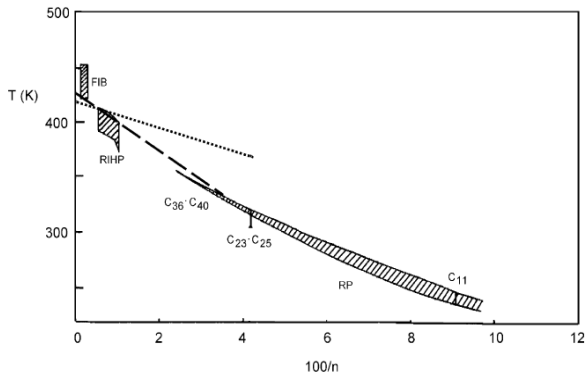

Figure 1.20. *The stability range of the mesomorphic phase for n-alkanes (RP), irradiated polyethylene (RIHP) and ultrahigh molar mass PE fibre (FIB); n is the number of carbons in the crystal stem [Ungar-1986].*

The intermediate phase between the crystalline state and the melt was also found in *n*-alkanes for chains with less than around 40 carbon atoms. This mesophase was more crystal than liquid-like and it was observed under normal conditions [Strobl-2006]. It was also called "*the rotator phase*" because chain reorientation about the long axis constituted the main aspect of disorder. Those results were confirmed by Sirota *et al.* [Sirota-1999] who observed that n-$C_{16}H_{34}$ nucleates into the metastable rotator-phase before converting into the stable triclinic crystal modification. Ungar [Ungar-1986] examined the transitions between molten and hexagonal phases of different *n*-alkanes and polyethylenes and found that there is a continuous change in the conformational statistics when going from short chain *n*-alkanes to polyethylene (see Figure 1.20). The upper line in Figure 1.20 gives the transition between the melt and mesomorphic phase, and the lower line that between the mesomorphic and the crystalline state.

The experimental verification of a mesophase and the observation of a granular lamellar structure provided by the widths of the Bragg reflection in WAXS patterns, TEM and AFM images (see Figure 1.21) has lead Strobl [Strobl-2000, Strobl-2005, Strobl-2006] to propose a new crystallization mechanism (see Figure 1.22) and a thermodynamic scheme described below. According to this mechanism, the formation and growing of lamellae takes place through intermediate states, *i.e.* following the Ostwald rule of stages. A mesomorphic phase is first created, then a granular crystalline structure is developed, and finally the lamellar crystal is formed by the merging of granular blocks. The chain sequences are first attached onto the growth face of a mesomorphic layer with minimum thickness (enough to keep them stable). The layer thickens until a critical thickness is reached and it solidifies by formation of block-like crystallites. Stabilization of crystallites with time (merging of blocks) leads to further decrease of Gibbs free energy. The stabilization degree is different for different parts of the sample, and some regions may even remain as granular crystals.

The direct connection between the granular block structure and the transient mesomorphic phase was made by Sirota [Sirota-2007]. Using arguments similar to those of

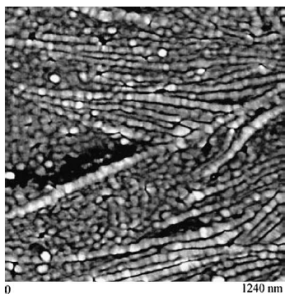

Figure 1.21. *AFM image obtained for sPP isothermally crystallized at 135 ºC [Hugel-1999].*

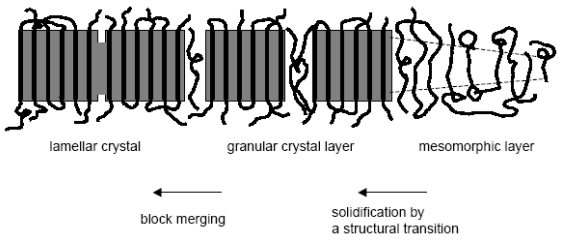

Figure 1.22. *The mechanism of growing of polymer crystallites through granular structures [Strobl-2000].*

Strobl, he was led to the conclusion that the granular substructure observed in polymer crystals is a fingerprint of the transition from the transient intermediate state from which the crystal derived. He considered further that it is the lateral density differences between mesophases and stable crystal phases that originates the block structure when the lattice contracts. The average density in the lamellae is set in by the mesophase, but because after crystallization is completed there is still stress to be relaxed, the crystal breaks up into blocks. This stress is caused by the lattice contraction due to the ends of crystalline stems which are kinetically tethered to positions in the amorphous melt set by the original mesophase packing density.

Two possible relaxation paths postulated by Sirota are presented in Figure 1.23: ***a*** **-** the packaging of stems forming the crystalline block structure is held fixed and the amorphous region relaxes to accommodate that stem packing; further stabilization yields the block structure making harder additional stem diffusion and merging; ***b*** – diffusion and chain motion during annealing makes possible the coarsening of crystalline domains while rearrangements occurring at the amorphous region accommodate the coarsening process. For both cases the free energy of the crystal phase will decrease with respect to that of the mesophase, the decrease being higher for path ***b***.

A thermodynamic multiphase scheme to explain the evolution of the above processes and the formation of stable crystals was proposed by Strobl [Strobl-2000, Strobl-2005, Strobl-2006] and considers four different phases: the amorphous melt (***a***), the mesomorphic layers (***m***), the native crystals (c_n) and the stabilized crystals (c_s).

It is assumed that crystalline lamellae may exist both in an initial "*native*" and in a final "*stabilized*" form. The scheme in Figure 1.24 shows the stability ranges and transition lines for these phases. Temperature is plotted against the crystal size. The inverse of the lamellae thickness is the size parameter. Following the nomenclature of Strobl, the lamellae thickness (d_c) is equal to the number of structure units in a stem (***n***) multiplied by the stem

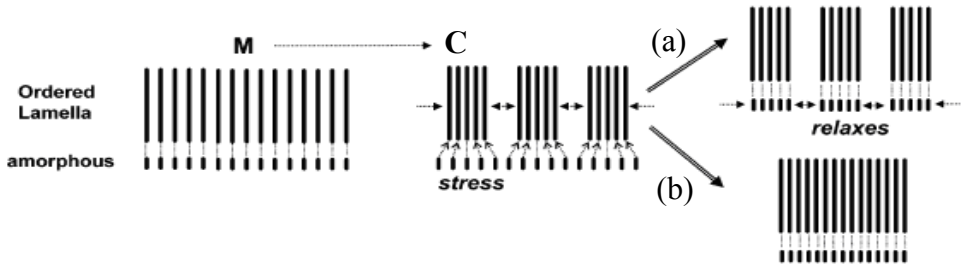

Figure 1.23. *Scheme showing the stress and relaxation of the lateral density of the ordered lamellae and amorphous region during the transition from the mesomorphic phase (***M***) to the crystal phase (***C***) together with two possible paths of relaxation: (a) relaxation driven by the stress, and (b) diffusion–driven relaxation [Sirota-2007].*

length increment per structure unit (Δz): $d_c = n \cdot \Delta z$. Five transition lines, all functions of n^{-1} are considered: $\boldsymbol{T_{am}}$ is the transition line from the amorphous melt to the mesomorphic state; $\boldsymbol{T_{acs}}$ is the transition line from the amorphous melt to the final stabilized crystal; $\boldsymbol{T_{mcs}}$ is the transition line from the mesomorphic layer to the stabilized crystal; $\boldsymbol{T_{acn}}$ is the transition line from the amorphous melt to the initial native crystal and $\boldsymbol{T_{mcn}}$ is the transition line from the mesomorphic layer to the native crystal.

The extrapolation of the different lines to $n^{-1} = 0$ (infinite thickness) yields different T^{∞} temperatures: T_{ac}^{∞} is the equilibrium melting temperature of a stabilized crystal with infinite thickness, the other is related to a native crystal with infinite thickness T_{mc}^{∞} and the last one to a mesomorphic layer with infinite thickness, T_{am}^{∞}. This last temperature does not have physical meaning because mesomorphic layers do not have crystallographic order.

Two crossing points involving the T_{am} line are crucial in the Strobl thermodynamic scheme. The crossing points X_n and X_s mark the amorphous melt ↔ metastable phase transition. The position of these two points controls what happens during an isothermal crystallization followed by heating. X_n is the stability limit of native crystals and X_s corresponds to the point at which stabilized crystals melt.

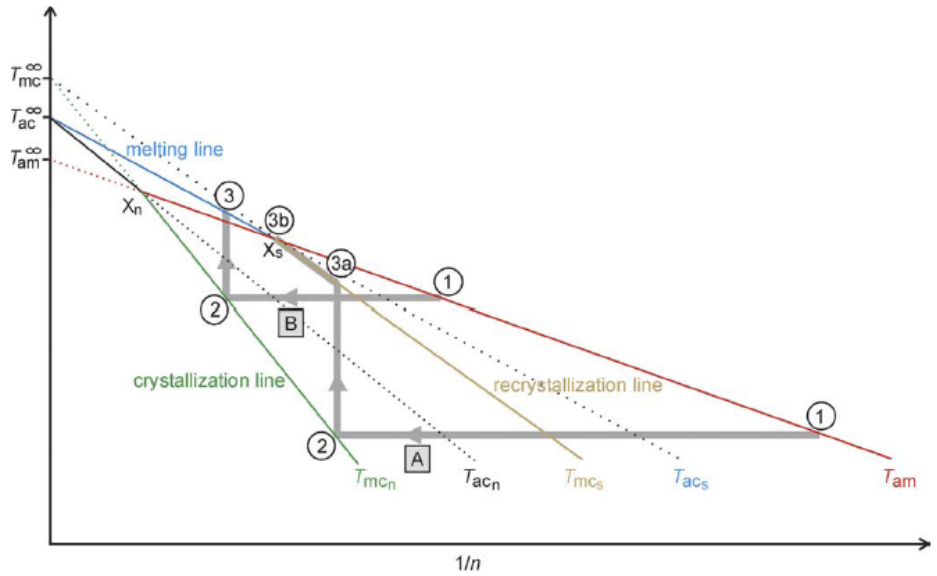

Figure 1.24. *Temperature versus n^{-1} phase diagram for polymer layers in a melt ("**a**") dealing with 3 phases: mesomorphic "**m**", native crystalline "**cn**" and stabilized crystalline "**cs**". Two pathways for an isothermal crystallization followed by heating, **A** (low crystallization temperatures) and **B** (high crystallization temperatures) are indicated: (1) chain attachment onto a mesomorphic layer with a thickness determined by the transition line $\boldsymbol{T_{am}}$; (1) – (2) spontaneous layer thickening; (2) formation of native crystals when the thickness reaches the transition line $\boldsymbol{T_{mcn}}$. The following stabilization of crystallites causes a change of the related transition lines and a shift of the crossing point from $\boldsymbol{X_n}$ to $\boldsymbol{X_s}$. **Pathway A during heating**: upon reaching the transition line $\boldsymbol{T_{mcs}}$ (3a) onset of continuous recrystallization processes up to the melting at $\boldsymbol{X_s}$ (3b). **Pathway B during heating**: the crystallites melt when $\boldsymbol{T_{acs}}$ is reached (3). The experimental "crystallization line" is identical with $\boldsymbol{T_{mcn}}$, the "melting line" is identical with $\boldsymbol{T_{acs}}$, the "recrystallization line" is to be identified with $\boldsymbol{T_{mcs}}$ [Strobl-2005].*

Further details of the Strobl thermodynamic scheme are shown in Figure 1.24. Pathways A and B refer to two different scenarios for the isothermal crystallization. It may be a low temperature crystallization proceeding from the glassy state (pathway A) or it may be high temperature crystallization from the melt (pathway B). The main distinction between these two crystallization processes occurs at point "2". In the crystallization from the melt (pathway B) it is considered that the thickened native crystals stabilize further at the same point into a lower free energy state. Otherwise they would transform immediately into the mesomorphic state on heating. The crystal stabilization implies that the crossing point with a transition line is shifted to X_s. This means that crystallites remain stable until the next transition line is reached, which in this case is a direct transition to the melt without interference of a mesomorphic phase.

1.2.4. Nucleation kinetics and the effect of entanglements on primary nucleation

As mentioned previously the classical nucleation theory divides the primary nucleation into two periods depending on the nucleation rate behaviour: induction period, where nucleation rate increases with time, and steady (stationary) nucleation period, where I saturates at constant rate I_{st} (see Figure 1.11).

According to the classical nucleation theory I is a product of the probability of diffusion and that of formation of a critical nucleus [Becker-1935],

$$I = I_0 \exp\left(-\frac{E_D}{k_B T} - \frac{\Delta G^*}{k_B T}\right) = I_0 \exp\left(-\frac{E_D}{k_B T} - \frac{C}{\Delta T^2}\right) \tag{1.17}$$

where E_D is the activation energy for transport across the nucleus surface (energy of diffusion), I_0 is a pre-factor dependent on temperature and molecular weight, k_B is the Boltzmann constant, ΔT is the degree of supercooling, and C is a constant expressed as: $C = 16\sigma\Delta\sigma\sigma_e / kT_m^0\Delta h$.

The nucleation rate depends, among other factors such as the supercooling degree and the presence or absence of nucleating agents, on the polymer molecular weight, and therefore on the number of chain entanglements. The effective role played by entanglements on polymer crystallization is still to be clarified, and some contributions pretending to clarify this aspect will be presented below.

The effect of polymer molecular weight on the nucleation rate, as well as in the lamellae growth rate, was studied with detail by Mandelkern *et al.* [Ergoz-1972]. The nucleation rate increases with molecular weight up to a maximum at around 10^5 g/mol and from this point on it decreases with the molecular weight increase. Figure 1.25 illustrates

the behaviour for linear polyethylene. These results, which date back to 1972, indicate that nucleation rate decreases with the number of entanglements for polymers with very high molecular weight. The effect of molecular weight on the diffusion term of eq. (1.17) was analysed by Hoffman *et al.* [Hoffman-1982] who attempted to describe the effect of reptation in the diffusion term of secondary nucleation process (spherulite growth rate).

Rastogi *et al.* [Rastogi-2005, Lippits-2006a, Lippits-2006b, Rastogi-2007, Lippits-2007] analyzed the problem of the distribution of entanglements along a chain during the crystallization and melting processes. Entanglements are topological constraints to the chain's diffusion. Therefore, it is considered that they are confined to the amorphous regions, whereas crystalline regions are void of them. It is also considered that this heterogeneous distribution of entanglements is lost on melting and that after this process they are uniformly distributed along the chain, the average spacing between them being equal to the average tube diameter (see §2.3).

Beside the above conjectures, it is not clear if during crystallization all entanglements migrate to the amorphous interlamellar regions, if only a part of them migrates while the other is destroyed by chain disentanglement, the factors that qualify and quantify this migration, if chain diffusion is the controlling factor for migration or if nucleation also plays a part, and what is the kinetics for the homogeneous redistribution of entanglements along the tube after melting. We must note that tube model, briefly described in chapter 2, considers that the number of entanglements is constant. Following this important assumption, and in agreement with an analysis of Flory and Yoon [Flory-1978], it is implicit that during crystallization all entanglements would migrate to the amorphous region, which would

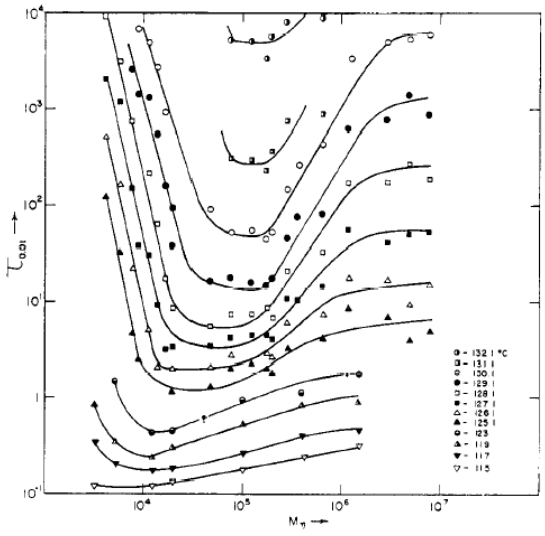

Figure 1.25. *Variation of nucleation rate (expressed as the time required for 1 % of the absolute amount of crystallinity to develop) with molecular weight at different temperatures for linear polyethylene [Ergoz-1972].*

increase significantly the number of interactions in this region at the solid state. This conclusion was questioned in part by Di Marzio *et al.* [Di Marzio-1979] who estimate the time to reel in a polymer molecule from the melt onto the growing crystal surface, which according to their evaluations was around three orders of magnitude smaller than the characteristic time estimated by Flory and Yoon [Flory-1978], 10^{-3} s against 1 s for the Flory and Yoon estimate. This difference results from different theories used in the evaluation of these values. Flory and Yoon used an expression for the relaxation time derived from the Rouse theory, which, as can be seen in chapter 2, is clearly wrong, not only for the theory itself but also for the situation where it was applied. Di Marzio *et al.* considered that the time in question should be the one needed by a chain to reptate a distance proportional to its end-to-end length. The subject behind the discussion at that time was which model for the semicrystalline morphology should be favoured, if the switchboard model of Flory and Yoon or the regular chain folding model. However, the discussion did not clarified what happens to entanglements existing in the melt during and after crystallization.

In the experiments of Rastogi *et al.* two different ultra-high molecular weight polyethylenes (UHMW-PE) were used [Rastogi-2005]. One was obtained from highly active heterogeneous Ziegler-Natta catalysts and high polymerization temperatures and the other was obtained from single site catalysts and low polymerization temperatures. The crystalline lamellae and the amorphous interlamellar region of the former are composed of several different PE chains (Figure 1.26a). After melting, regardless the melting conditions, low or high heating rates, it yields always a ***homogeneous melt*** where entanglements are regularly distributed along the chain. On the other hand, the metallocene UHMW-PE powders yields single crystals formed from single chains. The melting behaviour of these nascent UHMW-PE powders is different from the Ziegler-Natta PE's. The difference between the onset, or peak temperatures, is around 0.5 ºC, being higher for the metallocene PE (around 140 ºC).

Oscillatory shear experiments performed at constant oscillation frequency and temperature, 10 rad·s^{-1} and 180 ºC, respectively, allowed detecting variations of the modulus with time as a function of different heating rates, Figure 1.27a. Samples were heated from 120 ºC to 140 ºC at heating rates from 0.25 ºC/min to 10 ºC/min, heated further from 140 ºC to 180 ºC at 30 ºC/min. After a residence time of 15 min at 180 ºC the above mentioned rheological experiments were performed. Contradictory information about this residence time appears in the main paper [Rastogi-2005] and in its supplemental information, 15 min and 12 h, respectively. The output of these experiments is a complex modulus variation with time. The authors represented the plateau modulus variation with time, which presumably is

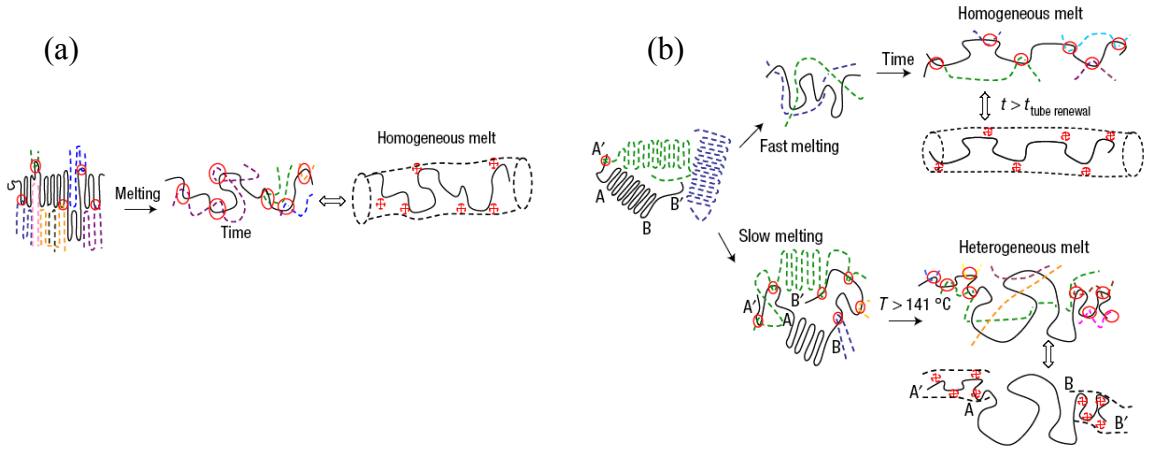

Figure 1.26. *(a) Heterogeneity defined by distribution of entanglements in the crystalline and amorphous regions is lost during melting, (b) Disentangled regions obtained by controlled synthesis during fast and slow melting result in homogeneous and heterogeneous melts [Rastogi2005].*

the time variation of the complex modulus. A representative sample of the results obtained is illustrated in Figure 1.27a.

For the same heating rate (0.25 ºC/min), results of Figure 1.27a indicate significant differences for the Ziegler-Natta and metallocene PE's rheological behaviour. It is considered that a homogeneous melt is responsible for the behaviour observed for Ziegler-Natta PE, while the metallocene PE behaviour results from a heterogeneous melt. The folded chain single crystals retain their shape after slow heating to the melt temperature and a residence time of 15 min at 180 ºC. The topological interactions are reduced to small sections at the chain ends, while sections of folded chains participating in the single crystals remain free from entanglements (Figure 1.26b and Figure 1.27a). However, after a fast melting (10 ºC/min) between 120 ºC and 140 ºC, curiously the melting temperature range for these polymers, the nascent metallocene PE powders show similar behaviour to that of

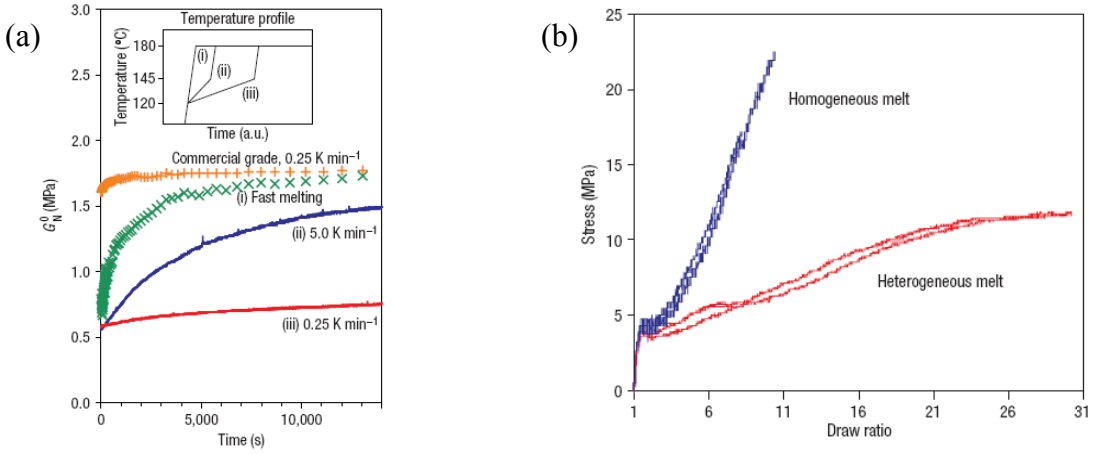

Figure 1.27. *The plateau modulus as a function of time for metallocene and commercial Ziegler-Natta samples (a) and the stress-strain curves of the crystals formed from heterogeneous and homogenous melts (b) [Rastogi-2005].*

Ziegler-Natta PE – an homogeneous melt. Even at slow heating rate, the ultimate behaviour, for very long time, is always that of homogeneous melt. The difference between homogeneous and heterogeneous melts appears to depend only on the rate of heating within the melt temperature range, which imparts to the disentangling process a kinetic character.

The surprising result and interpretation obtained from this work was the uniaxial drawing of samples crystallized from the two different melt states. No details were provided for the sample's preparation procedure for uniaxial tests. *Polymer powders should have been melted, compressed, and cooled down to yield the test specimens with appropriate shape for uniaxial tests*. The results obtained, indicated in Figure 1.27b, refer to the uniaxial drawing *at an unspecified drawing rate, at 120 ºC, where both polymers are still solid*. Assuming a similar drawing rate for both samples, it is visible that the Ziegler-Natta PE (sample labelled as homogeneous melt) shows much lower drawing ratio than the metallocene PE (heterogeneous melt).

The authors concluded that the homogeneous distribution of entanglements in the first prevent chain segments between entanglements to be deformed to lower entropic states, while the single folded chains without topological interactions with neighbouring chains may be stretched to much higher draw ratios.

No information was provided by the authors concerning the degree of crystallinity for both samples, neither the sample weight nor scanning rate used was provided for the DSC experiments. It is reasonable to assume that the metallocene PE's samples have higher crystallinity degree. The drawing in Figure 1.26 and the area of DSC scans presented (assuming similar sample weight and scanning rate) support this assumption. Objectively, *since the drawing experiments were performed at the solid state, the authors' conclusion implies that topological interactions are stronger than van der Waals interactions between adjacent chain segments in the single chain folded crystal*.

In more recent works of Rastogi *et al.* it was reported an acceleration of crystallization kinetics when crystallization proceeds from disentangled melts in comparison with the crystallization kinetics from entangled melts. According to the authors this result suggests that homogeneous nucleation occurs faster than the heterogeneous nucleation [Lippits-2007], which is a strange statement because it is not known any dependence of nucleation type (homogeneous or heterogeneous) on an intrinsic feature of a polymer melt, its number of entanglements.

1.3. Secondary crystallization and overall crystallization kinetics

The statement made at the paragraphs §1.1 and §1.2 illustrates only a few of the existing problems in the description of polymer crystallization in quiescence. The description of polymer crystallization under shear flow presents additional complications, some of which will be mentioned in chapter 3.

Once the primary nuclei are created it is known that their growth proceeds by a process of secondary nucleation: chain stems are nucleated at the surface of stable nuclei. The growth rate of chain lamellae may be recorded with an optical microscope coupled to a hot-stage. The lamella splaying generates semicrystalline structures, the spherulites. At a specific crystallization temperature, the growth rate of spherulites is considered to be the same as the growth rate of the crystalline lamellae.

Studies on the temperature variation of this growth rate allowed identifying temperature windows with distinct growth kinetics, which were assigned by some authors to different regimes of secondary crystallization: regime I, II and III. It was considered that the lamellae growth front shows different roughness in these regimes. It is flat in regime I and its growth occurs only after the infilling of lamellae growth front by chain stems. It shows regularly spaced protrusions, and chain stems are deposited to fill the space between protrusions in regime II. In regime III the lamellae growth front is highly irregular and chain stems are deposited randomly at the growth front. This theory, due to Lauritzen and Hoffman [Hoffman-1976, Hoffman-1982], although widely accepted, is not the unique description of secondary crystallization process, and is far from being consensual. Other alternative descriptions exist [Point-1979a, Point-1979b]. An example of literature review in this area of crystallization is ref. [Goldbeck-Wood-1992].

The step after the description of the lamellae and spherulite growth is the description of their growth kinetics and impingement at specific crystallization temperatures or cooling rates. This is the field of overall crystallization kinetics theories. There are theories considering a single mechanism approach, and theories considering two different mechanisms simultaneously concurrent and consecutive, besides other commonly used fitting procedures that adopt somewhat arbitrary coupling of single mechanism equations in parallel and series. Other semi-empirical equations are also applied in the description of the quiescent overall crystallization kinetics. Reviews and different perspectives for dealing with this another area of crystallization kinetics may be found at the following references: [Eder-1990, Piorkowska-2006, Cruz-Pinto-1994].

1.4. Brief summary of the chapter

A general theory of crystallization kinetics does not exist in part probably because of the earlier crystallization stages poor understanding, which is the source of any order established further on. Unless this specific point is clarified, it would be impossible to develop a general crystallization kinetics theory. To help further in this point it is primordial to understand the source of melt memory effect on polymer crystallization, and to have a clear, and uncontroversial picture of melt morphology either for quiescent and sheared melts.

In chapter 2 features of melt morphology and chain dynamics are discussed, and in chapter 3 the effect of shear flow on melt morphology, chain dynamics and shear-induced crystallization are analyzed. At the end, it is expected that the picture of melt morphology that will emerge will help to clarify the origin of melt memory effect, which seems to be the key point to understand the earlier crystallization stages and the subsequent steps of crystallization kinetics.

1.5. References

Acierno-2002 — Acierno S, Grizzuti N, Winter HH (2002) *Effects of molecular weight on the isothermal crystallization of poly(1-butene)*. Macromolecules 35:5043-5048.

Acierno-2003 — Acierno S, Grizzuti N (2003) *Measurements of the rheological behavior of a crystallizing polymer by an "inverse quenching" technique*. J Rheol 47:563-576.

Akpalu-1999 — Akpalu Y, Kielhorn L, Hsiao BS, Stein RS, Russell TP, van Egmond J, Muthukumar M (1999) *An investigation of the early stages of structure development during isothermal melt crystallization of homogeneous copolymers of ethylene and 1-octene: Time-resolved synchrotron X-ray and SALS*. Macromolecules 32:765-770.

Alfonso-1995 — Alfonso GC, Ziabicki A (1995) *Memory effects in isothermal crystallization. II. Isotactic polypropylene*. Colloid Polym Sci 273:317-323.

Ballard-1980 — Ballard DGH, Burgess AN, Nevin A, Cheshire P, Longman GW, Schelten J (1980) *Small Angle Neutron Scattering studies on polypropylene*. Macromolecules 13:677-681.

Becker-1935 — Becker R, Döring W (1935) *The kinetic treatment of nuclear formation in supersaturated vapors*. Ann Phys 24:719-754.

Binsbergen-1973 — Binsbergen FL (1973) *Heterogeneous nucleation in the crystallization of polyolefins. III. Theory and mechanism*. J Polym Sci: Polym Phys Ed 11:117-135.

Cahn-1958 Cahn JW, Hilliard JE (1958) *Free energy of a nonuniform system. I. Interfacial free energy*. J Chem Phys 28:258-267.

Coppola-2006 Coppola S, Acierno S, Grizzuti N, Vlassopoulos D (2006) *Viscoelastic behavior of semicrystalline thermoplastic polymers during the early stages of crystallization*. Macromolecules 39:1507-1514.

Cruz-Pinto-1994 Cruz-Pinto JJC, Martins JA, Oliveira MJ (1994) *The isothermal crystallization of engineering polymers – POM and PEEK*. Colloid and Polymer Sci 272:1-16.

de Jeu-2006 de Jeu WH, Séréro Y, Al-Hussein M (2006) *Liquid crystallinity in block copolymer films for controlling polymeric nanopatterns*. Adv Polym Sci 200:71-90.

Di Marzio-1979 Di Marzio EA, Guttman CM, Hoffman JD (1979) *Is crystallization from the melt controlled by melt viscosity and entanglement effects?* Faraday Discuss Chem Soc 68:210-217.

Eder-1990 Eder G, Janeschitz-Kriegl H., Liedauer S (1990) *Crystallization processes in quiescent and moving polymer melts under heat transfer conditions*. Polym Prog Sci 15:629-714.

Elmoumni-2003 Elmoumni A, Winter HH, Waddon AJ, Fruitwala H (2003) *Correlation of material and processing time scales with structure development in isotactic polypropylene crystallization*. Macromolecules 36:6453-6461.

Ergoz-1972 Ergoz E, Fatou JC, Mandelkern L (1972) *Molecular weight dependence of the crystallization kinetics of linear polyethylene: I. Experimental results*. Macromolecules 5:147-157.

Flory-1978 Flory PJ, Yoon DY (1978) *Molecular morphology in semicrystalline polymers.* Nature 272:226-229.

Gedde-1995 Gedde ULF (1995) *Polymer physics.* Chapman & Hall: London.

Gee-2006 Gee RH, Lacevic N, Fried LE (2006) *Atomistic simulations of spinodal phase separation preceding polymer crystallization*. Nature materials 5:39-43.

Goldbeck-Wood-1992 Armitstead K, Goldbeck-Wood G (1992) *Polymer crystallization theories.* Adv Polymer Sci 100:219-312.

Häfele-2005 Häfele A, Heck B, Hippler T, Kawai T, Kohn P, Strobl G (2005) *Crystallization of poly(ethylene-co-octene). II Melt memory effects on first order kinetics*. Eur Phys J E 16:217-224.

Heeley-2002 Heeley EL, Poh CK, Li W, Maidens A, Bras W, Dolbnya IP, Gleeson AJ, Terrill NJ, Fairclough JPA, Olmsted PD, Ristic RI, Hounslow MJ, Ryan AJ (2002) *Are metastable, precrystallisation, density-fluctuations a universal phenomena?* Faraday Discuss 122:343-361.

Heeley-2003 Heeley EL, Maidens AV, Olmsted PD, Bras W, Dolbnya IP, Fairclough JPA, Terrill NJ, Ryan AJ (2003) *Early stages of crystallization in isotactic polypropylene*. Macromolecules 36:3656-3665.

Hikosaka-2005 Hikosaka M, Watanabe K, Okada K, Yamazaki S (2005) *Topological mechanism of polymer nucleation and growth – the role of chain sliding diffusion and entanglement*. Adv Polym Sci 191:137-186.

Hoffman-1961 Hoffman JD, Lauritzen JI (1961) *Crystallization of bulk polymers with chain folding: theory of growth of lamellar spherulites*. J Res Natl Bur Stand 65A:297-336.

Hoffman-1976 Hoffman JD, Davis GT, Lauritzen JI (1976) *The rate of crystallization of linear polymers with chain folding* in *Treatise on solid state chemistry* 3:467-614, NB Hannay, Plenum Press.

Hoffman-1982 Hoffman JD (1982) *Role of reptation in the rate of crystallization of polyethylene fraction from the melt*. Polymer 23:656-670.

Hsiao-1995 Hsiao BS, Sauer BB, Verma RK, Zachman GH, Seifert S, Chu B, Harney P (1995) *New insight of isothermal melt crystallization in poly(aryl ether ether ketone) via time-resolved simultaneous Small-Angle X-ray-Scattering Wide-Angle X-ray-Diffraction measurements*. Macromolecules 28:6931-6936.

Hugel-1999 Hugel T, Strobl G, Thomann R (1999) *Building lamellae from blocks: the pathway followed in the formation of crystallites of syndiotactic polypropylene*. Acta Polym 50:214-217.

Imai-1994 Imai M, Kaji K, Kanaya T (1994) *Structural formation of poly(ethy1ene terephthalate) during the induction period of crystallization. 3. Evolution of density fluctuations to lamellar crystal*. Macromolecules 27:7103-7108.

Janeschitz-Kriegl-2005 Janeschitz-Kriegl H, Ratajski E (2005) *Kinetics of polymer crystallization under processing conditions: transformation of dormant nuclei by the action of flow*. Polymer 46:38563870.

Keller-1994 Keller A, Hikosaka M, Rastogi S, Toda A, Barham P, Goldbeck-Wood G (1994) *An approach to the formation and growth of new phases with application to polymer crystallization: effect of finite size, metastability, and Ostwald's rule of stages*. J Mater Sci 29:2579-604.

Kumaraswamy-2005 Kumaraswamy G (2005) *Crystallization of polymers from stressed melts*. J Macromol Sci, Part C: Polymer Reviews 45:375-397.

de Langen-1999 de Langen M, Prins KO (1999) *Mobility of polyethylene chains in the orthorhombic and hexagonal phases investigated by NMR*. Chem Phys Lett 299:195-200.

de Langen-2000 de Langen M, Prins KO (2000) *NMR investigation of phase transitions in polyethylene in the vicinity of the hexagonal high pressure phase*. Polymer 41:1175-1182.

Lippits-2006a Lippits DR, Rastogi S, Höhne GWH (2006) *Melting kinetics in polymers*. Phys Rev Lett 96:218303-218700.

Lippits-2006b Lippits DR, Rastogi S, Talebi S, Bailly C (2006) *Formation of entanglements in initially disentangled polymer melts*. Macromolecules 39:8882-8885.

Lippits-2007 Lippits DR, Rastogi S, Höhne GWH, Mezari B, Magusin PCMM (2007) *Heterogeneous distribution of entanglements in polymer melts and its influence in crystallization*. Macomolecules 40:1004-1010.

Martins-1999 Martins JA, Cruz Pinto JJC (1999) *The temperature calibration on cooling of differential scanning calorimeters.* Thermochim Acta 332:179-188.

Maus-2007 Maus A, Hempel E, Thurn-Albrecht T, Saalwächter K (2007) *Memory effect in isothermal crystallization of syndiotactic polypropylene – role of melt structure and dynamics?* Eur Phys J 23:91-101.

Mullin-1961 Mullin JW (1961) *Crystallization*, Butterworths (2nd edition published in 1972).

Muthukumar-2000 Muthukumar M, Welch P. (2000) *Modelling polymer crystallization from solutions*. Polymer 41:8833-8837.

Muthukumar-2003 Muthukumar M (2003) *Molecular modelling of nucleation in polymers*. Phil Trans R Soc Lond A 361:539-556.

Nishi-1999 Nishi M, Hikosaka M, Ghosh SK, Toda, A, Yamada K (1999) *Molecular weight dependence of primary nucleation rate of polyethylene. I. An extended chain single crystal*. Polym J 31:749-758.

Okada-2007 Okada K, Watanabe K, Wataoka I, Toda A, Sasaki S, Inoue K, Hikosaka M (2007) *Size distribution and shape of nano-nucleus of polyethylene simultaneously determined by SAXS.* Polymer 5:382-392.

Olmsted-1998 Olmsted P, Poon W, McLeish T, Terrill T, Ryan A (1998) *Spinodal assisted crystallization in polymer melts*. Phys Rev Lett 81:373-376.

Panine-2008 Panine P, Di Cola E, Sztucki M, Narayanan T (2008) *Early stages of polymer melt crystallization*. Polymer 49:676-680.

Philips-2005 Phillips TL, Hanna S (2005) *Simulations of the mobile phase of polypropylene*. Polymer 46:11035-11050.

Piorkowska-2006 Piorkowska E, Galeski A, Haudin J-M (2006) *Critical assessment of overall crystallization kinetics theories and predictions*. Prog Polym Sci 31:549-575.

Pogodina-2001 Pogodina NV, Lavrenko VP, Srinivas S, Winter HH (2001) *Rheology and structure of isotactic polypropylene near the gel point: quiescent and shear-induced crystallization*. Polymer 42:9031-9043.

Point-1979a Point JJ (1979) *A new theoretical approach to the secondary nucleation at high supercooling*. Macromolecules 12:770-775.

Point-1979b Point JJ (1979) *Reconsideration of kinetic theories of polymer crystal-growth with chain folding*. Faraday Disc 68:167-176.

Rastogi-1991 Rastogi S, Hikosaka M, Kawabata H, Keller A (1991) *Role of mobile phases in the crystallization of polyethylene. 1. Metastability and lateral growth*. Macromolecules 24:6384-6391.

Rastogi-2005 Rastogi S, Lippits DR, Peters GWM, Graf R, Yao Y, Spiess HW (2005) *Heterogeneity in polymer melts from melting of polymer crystals*. Nature materials 4:635-641.

Rastogi-2007 Rastogi S, Lippits DR, Höhne GWH, Mezari B, Magusin PCMM (2007) *The role of amorphous phase in melting of linear UHMW-PE; implications for chain dynamics*. J Phys: Cond Matter 19:205122-205143.

Sirota-1999 Sirota EB, Herhold A (1999) *Transient phase-induced nucleation*. Science 283:529-532.

Sirota-2007 Sirota EB (2007) *Polymer crystallization: metastable mesophases and morphology*. Macromolecules 40:1043-1048.

Sozzani-2005 Sozzani P, Bracco S, Comotti A,·Simonutti R (2005) *Motional phase disorder of polymer chains as crystallized to hexagonal lattices*. Adv Polym Sci 181:153-177.

Strobl-2000 Strobl G (2000) *From the melt via mesomorphic and granular crystalline layers to lamellar crystallites: a major route followed in polymer crystallization?* Eur Phys J E 3:165-183.

Strobl-2005 Strobl G (2005) *A thermodynamic multiphase scheme treating polymer crystallization and melting*. Eur Phys J E 18:295-309.

Strobl-2006 Strobl G (2006) *Crystallization and melting of bulk polymers: New observations, conclusions and a thermodynamic scheme*. Prog Polym Sci 31:398-443.

Threlfall-2003 Threlfall T (2003) *Structural and thermodynamic explanations of Ostwald's rule*. Org Process Res Dev 7:1017-1027.

Ungar-1986 Ungar G (1986) *From plastic-crystal paraffins to liquid-crystal polyethylene: continuity of the mesophase in hydrocarbons*. Macromolecules 19:1317-1324.

Wang-1997 Wang W, Schultz JM, Hsiao BS (1997) *Dynamic study of crystallization- and melting-induced phase separation in PEEK/PEKK blends*. Macromolecules 30:4544-4550.

Xiao-2007 Xiao Z, Akpalu YA (2007) *New insights into the characteristics of early stage crystallization of a polyethylene*. Polymer 48:5388-5397.

Zhang-2006 Zhang W, Martins JA (2006) *Evaluation of the effect of melt memory on shear-induced crystallization of low-density polyethylene*. Macromol Rapid Commun 27:1067-1072.

Ziabicki-1994 Ziabicki A, Alfonso GC (1994) *Memory effects in isothermal crystallization. I. Theory*. Colloid Polym Sci 272:1027-1042.

2. Melt rheology and polymer chain dynamics

The purpose of this chapter is to make a critical analysis of parameters used to describe the shape and dynamics of polymer chains, especially in polymer melts. As will be seen, experimental results supporting the validity of specific models for chain conformation and dynamics, and therefore allowing to draw a picture of melt morphology and their evolution with flow conditions, are highly questionable. The questioning is based on raw experimental results, without filtering by any theoretical model, being therefore free from their assumptions. Some assumptions of models for polymer chain dynamics will also be highlighted. The analysis performed in this chapter is based on an unpublished work developed by Martins [Martins-2008]. This analysis will also justify the interpretation of experimental results made latter on in this work.

Since polymer chains have a large number of repeated units (molecules connected by covalent bonds), which can occupy different conformational states, the description of their spatial shape, interactions of chains segments with segments of the same chain or of other chains, and change of chain's shape with deformations and temperature (because the occupation of different conformational states also changes with temperature) is a complicated problem. To handle these problems, several models were proposed to describe the spatial shape of polymer chains at the molten state, as well as for solutions under special conditions (theta conditions). The results of these models were further tested against experiments. A brief summary of different models may be found in a textbook of polymer science [Sperling-2001].

There are two schools of though. One, in great majority, supports the Flory random coil model mainly because the Gaussian formulation of chains conformations allows a mathematical description of their dynamical behaviour and viscoelastic properties. The other school considers the existence of short-range order in polymer melts (and also in amorphous polymers at the solid state). The number of recent publications on this topic is scarce. One of the latest reviews dealing with this aspect was published in 1994 [Gabrys-1994]. This current started to gain impetus around 1975 with electron microscopy observations of ordered clusters in solid amorphous polymers [Geil-1975], which were considered latter to suffer from experimental errors [Flory-1979, Uhlmann-1979]. However, the arguments presented by Uhlmann [Uhlmann-1979] were contested by Geil [Geil-1979]. Difficulties of formulating a mathematical model for melt morphology hampered the development of this school. Despite this, order in polymer melts is still an important issue because there are still open questions in polymer physics. One of them is the physical nature

of topological constraints. Also, "*one cannot help wondering: if the presence of short-range order in amorphous polymers became generally accepted, how many papers appearing in this field would have to change?*" [Gabrys-1994].

As stated by Sperling, "*the model that seems to be close to the truth for most polymers of interest is the random coil model. However, the subject is not yet settled*" [Sperling-2001]. In this model a polymer chain with N covalent bonds, each with length l, is described as a tri-dimensional random walk of N_k monomers each with length l_k. Each monomer with length l_k is called Kuhn monomer, or statistical monomer. The length l_k may be evaluated from measurements of unperturbed chains dimensions – chains in theta solvents at a specific temperature. The quantity measured that allows evaluating l_k is the chain's radius of gyration, usually measured from scattering experiments of light, X-rays or neutrons at low angles. From these experiments, a quantity called characteristic ratio is evaluated and later used to estimate values of l_k.

This estimation is not unequivocal. First, for similar temperature and different solvents, quite different values are obtained for the characteristic ratio. A typical example is atactic polystyrene where differences of around 50% in values for the characteristic ratio are obtained. Obviously this result questions l_k as an indicator of the minimum value for the random walk step length, because the precise value is unknown. Secondly, analysis of the unperturbed radius of gyration of PS indicate that the asymptotic Gaussian behaviour is approached only for around 100 Kuhn monomers, which precludes the use of the statistical monomer concept for chain segments with lower length. However, molecular dynamics simulations have shown that for chains with 10 random steps (10 Kuhn monomers), the probability function for the chain dimension is similar to a Gaussian distribution. Importantly, both the experiments and the molecular dynamics simulations confirm that the Kuhn monomer, which contains around 5 monomers of the real chain, in which constraints resulting from bond angle and conformational states exist, cannot be treated as an entropic spring.

To cope with this problem, it was proposed recently the concept of dynamic bead size. It was suggested that this parameter, together with the molecular weight between entanglements and the Kuhn monomer length, should be considered by theoretical models to characterize chain statistics and determine the molecular weight dependence of some physical properties.

All above points would have little importance if they would restrict to a simple estimation of polymer chains dimensions. However, theories dealing with polymer chain dynamics consider the Kuhn monomer length as the base unit of polymer chain. Problems

seems start to appear when the elastic constant of an entropic spring is assigned to the Kuhn monomer and the length of a segment in the Rouse chain (average length between two beads) is identified with the Kuhn monomer length. In the Rouse original bead-spring theory it was always considered that the length of a chain segment between two beads should be large enough for Gaussian properties to prevail, around 100 monomers. Also, in a critical analysis of the Rouse model made by de Gennes [de Gennes-1976], where several deficiencies were identified, it was also considered that the number of monomers in the chain segment between beads should have Gaussian behaviour, which is clearly not the case for a single Kuhn monomer. This seems to be an important problem because claims for the short-term dynamics limited validity of Rouse model were carried out under the above assumption. This point, as well as other points related with the Rouse model applicability to the description of local chain dynamics and the physical interpretation of Rouse modes will be discussed below. The reason for this discussion is that because the assumption of Rouse model validity in polymer melts, and the assumed existence of fast Rouse modes, which are assigned to differences in phase between adjacent Kuhn monomers, it is considered that ordered regions in polymer melts involving several Kuhn monomers are forbidden by this theory and therefore inexistent.

Also, based on the identification between Rouse segment and Kuhn monomer a relationship between different relaxation times is established. The reptation time is related to the Rouse relaxation time of the chain, a Rouse relaxation time of chain segments between entanglements is defined on the same grounds as the Rouse relaxation time of the chain (which is surprising because the boundary conditions for solving the diffusion equation are not the same for the Rouse chain and the chain segment between entanglements – the chain ends are considered in the first case), and all above relaxation times are related to the Kuhn relaxation time, which is assigned to relaxation processes occurring at the glass transition region.

The main reason of the above identity (Rouse segment and Kuhn monomer) made by many theoretical groups results from the fractal nature of the Gaussian chain, or the self-similarity of chain segments in that chain: any segment of a Gaussian chain, and any division of that segment, is also Gaussian. Theoretically this is a valid argument, but experiments demonstrate that around 100 Kuhn monomers (approximately 500 real monomers) are needed in a PS chain for the Gaussian behaviour to be observed. For PE it is 10 Kuhn monomers or around 50 real monomers.

This chapter begins with an analysis of ideal chains, which includes a discussion about the characteristic ratio, the definition of Kuhn monomer and the evaluation of dynamic bead

size. In the following part a critical analysis of Rouse model will be made, with emphasis on the definition of a Rouse chain segment, the meaning of friction coefficient and Rouse modes. Experimental results claiming the validity of Rouse model in polymer melts will also be analysed. The definition of Rouse relaxation time for chain segments between entanglements will be discussed. At the end, the tube model and reptation will be presented and the contribution of contour length fluctuations for explaining the zero shear rate viscosity dependence on the 3.4 exponent of the molecular weight will also be briefly presented.

2.1. Ideal chains

Ideal chains are real chains under theta conditions. Under these conditions energetic interactions between segments of the same or different chains are inexistent, and changes on chains' free energy result only from entropic variations originated by changes of chain conformations. In ideal chain models, polymer chains consist of immaterial links, each one joined to two nearest neighbours, having no interactions with solvent molecules or with other links of the same or another chain [Grosberg-1994, Flory-1989]. There are several models of ideal chains. A common feature to all is the absence of volume interactions. They assume that polymer segments can be overlapped with each other as in a phantom chain. Because two segments cannot occupy the same space at the same time, due to their finite van der Waals volume, the interaction between segments is called excluded volume interaction, and it must be considered to explain the polymer behaviour in good and bad solvents.

It was verified experimentally that chains in polymer melts behave as real chains in a solvent at a specific temperature called theta temperature. This assumption was based on the verification that the radius of gyration was the same in a melt and in a theta solvent. Because elastic neutron scattering experimental data shown in Figure 3.4a can be fitted with an ideal chain statistics model, it was concluded that the model of polymer chain in theta conditions and at the molten state should be the random coil model. However, R_g values equalling those of the unperturbed chains can also be explained with other models of molten state, namely those considering that the melt contains ordered regions with folded chain conformations [Privalko-1974].

The question of order or disorder at the molten state is an important issue. It determines our understanding of this state, the models developed for explaining melt morphology, the development of solid state morphology and polymer properties in general. This issue is addressed in textbooks on polymer science. For example, Sperling

[Sperling-2001] discusses the subject in a chapter entitled "*The amorphous state*". Here, arguments favouring the existence of order are presented together with others that favour the existence of disorder. As stated by this author "*the issue of the conformation of polymer chains ... remains an area of current research. The vast bulk of research to date suggests that the random coil should be at least close to the truth for many polymers of interest*". The main problem with models suggesting the existence of order if that they have not reached the state of development as the random coil model which, by considering Gaussian chain statistics, allows predictions of polymer properties and fitting of experimental data obtained with a wide range of techniques.

A full discussion of this subject is difficult and beyond the scope of this work. There is an extensive amount of literature, which is not easy to read. Some basic assumptions used to construct the ideal chain model and to evaluate the chain segment's dimensions are not clearly highlighted. Also, results obtained by different experimental techniques, mainly Small Angle Scattering, are not easy to interpret, and some of them are based on applications of models which are themselves based on other strong assumptions that often are not mentioned by their authors. Despite the contributions of de Gennes for the understanding of Small Angle Scattering by polymer molecules, the following statement illustrates his opinion about these techniques: "*I am worried about all small angle scattering studies. There are too many effects to be considered*" [de Gennes-2003].

Below the conditions for evaluating chains' dimensions are discussed together with the definition of random chain segment. This definition is important because it is the basis for theoretical developments and validation of experimental results obtained with different techniques. It is also the starting point for developing models such as the Rouse model and chain reptation inside a tube.

As mentioned above, ideal chain dimensions are evaluated in polymer melts and in solvents under theta conditions. Under these conditions, interactions between the real chain and its environment exactly compensate intrachain excluded volume interactions, and the real chain behaves as ideal, adopting its "unperturbed" dimensions. Physically, the theta temperature is the value that cancels the second order corrections in the virial expansion of the osmotic pressure concentration dependence:

$$\frac{\Pi}{cRT} = \frac{1}{M_n} + A_2 c + \dots \quad , \tag{2.1}$$

where Π is the osmotic pressure, c the solution concentration, R and T are the ideal gas constant and temperature, respectively, and A_2 the second virial coefficient [Rubinstein-2003, Teraoka-2002]. Formally, A_2 accounts for the effect of energetic interactions between

different molecules. The theta temperature is different for each combination of polymer-solvent and separates the regimes of good and poor solvents. For good solvents the individual coils are swollen, different coils tend to keep apart causing mixing of polymer and solvent, while for poor solvent individual coils are compressed and chains stick together.

2.1.1. The characteristic ratio

An ideal chain may be described as a random walk of Kuhn monomers obeying Gaussian statistics. Defining the Kuhn segment length as l_k, and the number of Kuhn monomers as N_k, the average square distance between chain ends is

$$\left\langle R^2 \right\rangle_0 = N_k l_k^2 = C_\infty N l^2 \quad , \tag{2.2}$$

where N and l are the number of segments and segment length (*the bond length*) of the real chain, respectively, and C_∞ is the characteristic ratio. This may be *an experimental value* or *a model dependent value*. For both cases it accounts for the different restriction effects on the average end-to-end chain distance, enabling the real chain to be represented by a chain of randomly joined segments. The N_k and l_k of this ideal chain are related to N and l of the real chain by the characteristic ratio. Further details about this relationship are presented below. In the ideal chain there is no correlation between adjacent chain segments: each segment is freely joined to its neighbouring segments. The subscript zero in the average square distance between chain ends expresses the ideality of conditions mentioned above. The overall chain conformational shape is unperturbed by the presence of solvent molecules or by the presence of other chains.

At this point, it is important to define precisely the ***characteristic ratio***. According to **IUPAC** Compendium of Chemical Terminology, 2nd edition (1997), it is the ratio of the mean square end-to-end distance $<R^2>$ of a linear polymer chain in a theta state to Nl^2, where N is the number of rigid sections in the main chain, each of length l. In simple single strand chains, the bonds are taken as the rigid sections. The recommended symbol is C_N (C_∞ when $N \to \infty$). This definition is imprecise because it does not reflect the effect of intramolecular interactions (valence angle and torsion angles) on the characteristic ratio value, and considers this value as the result of experimental measurements only.

Perhaps, a clearer definition is the following:

"*the dimensionless characteristic ratio is defined as the ratio of the mean square unperturbed end-to-end distance for a real chain (or a model of a chain) and the value expected for a freely joined chain with the same number of bonds, of the same mean square length;*

$$C_\infty = \frac{\left\langle R^2 \right\rangle_0}{Nl^2} \quad , \tag{2.3}$$

for any chain with any flexibility whatsoever, the characteristic ratio approaches a limiting value as ***N*** *becomes large; this limit is determined by extrapolation of the characteristic ratio versus 1/N to zero*" [Mattice-1999].

The above definition implies that the experimental value for the characteristic ratio of a polymer melt, or a solution at theta conditions, equals C_θ, which is the experimental factor that accounts for all restriction effects on the average value for the end-to-end distance of a polymer chain. Ideally C_∞, evaluated theoretically with the rotational isomeric state model, should be as similar as possible to C_θ. Note that we distinguish C_θ from C_∞. The first is evaluated experimentally while the second results from the restriction effects of ideal chain models, being one for a chain of freely joined segments, and increasing in value with the number of restrictions considered and values assigned to *trans* and *gauche* conformational energies. From the above definition it results also that the characteristic ratio of ***any*** freely joined chain is one.

However, the above definition of characteristic ratio is not universal. Some reference textbooks [Strobl-1996, Doi-1996] use a different definition that is not consistent with the one presented above. Strobl and Doi, for example, define the characteristic ratio ***only*** in the limit of very long chains. Although the equation used in this definition

$$\left\langle R^2 \right\rangle_0 = C_\infty Nl^2 = N_k l_k^2 \quad , \tag{2.4}$$

is formally similar to eq. (2.3), the characteristic ratio definition of Strobl and Doi is the reciprocal of (2.3) – the variables at the numerator are specific of the equivalent chain while those at the denominator, N and l, refer to the number of monomers and length of the backbone bond of one monomer unit in the real chain. The real chain is viewed as released of all restrictions between chain segments, that is, it is considered, as in eq. (2.3), a freely joined chain.

This characteristic ratio definition is then

$$C_\infty = \frac{N_k l_k^2}{Nl^2} = \frac{l_k^2}{l^2} \quad . \tag{2.5}$$

The second equality is justified in [Strobl-1996] and [Doi-1996] by the scaling dependence of the average square end-to-end distance on the "degree of polymerization" which, in limit of very long chains, is assumed to be the same for the equivalent and real chains (therefore the ratio $N_k/N = 1$).

Other definitions of characteristic ratio are also common in the literature. For example, Ding and Solkolov [Ding-2004b] and Grosberg and Khokhlov [Grosberg-1994] define the characteristic ratio as

$$C_\infty = \frac{l_k}{l} \quad . \tag{2.6}$$

The differences between the definitions (2.3), (2.5) and (2.6) are evident, and they have important consequences, since they are propagated in theories and experimental results that are fitted with theoretical models. However, regardless the polymer molecular weight, the value evaluated experimentally for the characteristic ratio (C_θ) is the same for definitions (2.3) and (2.5) because all constraints on the chain spatial shape are implicitly included in the l_k and N_k values. Limitations of the definition C_∞ with eq. (2.5) will become clear below.

The definition adopted in this work is that of eq. (2.3). The characteristic ratio of real polymer chains, evaluated from polymer solutions at theta conditions, or in polymer melts, is designated by C_θ. Different theta temperatures exist for different solvents yielding therefore different values for C_θ and consequently different values for the Kuhn segment length (Table 2.1) [Mays-1985]. The unperturbed chain dimensions at the molten state, and therefore the characteristic ratio, also change with temperature, generally decreasing with it. To express this dependence, a temperature coefficient for unperturbed chain dimensions is defined as

$$\kappa = \frac{\partial \ln C_\theta}{\partial T} = \frac{1}{\left\langle R^2 \right\rangle_0} \frac{\partial \ln\left(6\left\langle R_g^2 \right\rangle\right)}{\partial T} \quad , \tag{2.7}$$

Table 2.1. *Characteristic ratio values in different solvents and theta temperatures for atactic polystyrene and parameters of the equivalent chain. Average values for characteristic ratio at the molten state are also indicated [Mays-1985, Krishnamoorti-2002, Boothroyd-1991]. Data for melts of PS and PE was evaluated by Small Angle Neutron Scattering. Data in the last column at the right is the number of real monomers in one statistical monomer.*

Polymer and solvent (or melt)	Theta temperature (ºC)	C_θ	M_k (g/mol)	l_k (Å)	n
PS-1-chloro-n-decane	8.5	10.4	811.69	19.61	7.80
PS-cycloheptane	19.0	10.5	819.50	19.80	7.87
PS-cyclooctane	20.5	10.5	819.50	19.80	7.87
PS-cyclopentane	20.5	10.7	835.11	20.18	8.02
PS-cyclohexane	34.5	10.7	835.11	20.18	8.02
PS-Butanone/2-propanol (87/13 vol)	67	12.5	975.59	23.57	9.37
PS-ethylcyclohexane	70	9.25	721.94	17.44	6.93
PS-methylcyclohexane	70.5	8.8	686.82	16.59	6.60
PS-melt	120 - 240	9.3	725.84	17.54	6.97
PE-diphenilmethane	142.2	7.0	147.47	13.20	5.25
PE-diphenil ether	163.9	6.8	143.26	12.82	5.10
PE-melt	110	7.9	166.43	14.90	5.92
PE-melt	140	7.5	158.01	14.14	5.62
PE-melt	190	7.0	147.47	13.20	5.25

Table 2.2. *Temperature coefficients for the unperturbed chain dimensions in solution and at the molten state [Mays-1985, Boothroyd-1991, Yamakawa-1982].*

Polymer and solvent (or melt)	Temperature range (ºC)	$\kappa \times 10^3$ (ºC^{-1})
PS-cyclohexanes	34.5 - 75	-1.2
PS-diesters	34.5 - 67	-0.6
aPS-solid and melt	20 - 154	-0.1
PE	140	-1.1
PE-melt	110 - 190	-1.25

where R_g is the radius of gyration measured at theta conditions or at the molten state.

Changes with temperature of unperturbed chain dimensions for PS and PE in different solvents and at the molten state are indicated in Table 2.2. It is clear the different behaviour in solution and at the molten state. The differences are usually assigned to specific solvent effects, more specifically to the "*capacity of some θ solvents to induce a conformer population different from what is favoured in the melt state*" [Krishnamoorti-2002]. However, as shown in Figure 2.1, the differences may not be limited only to a change in value, but also to a change in signal. For example, for poly(ethylene-ethylene) the temperature coefficients for chain dimensions are negative in solution and positive in the melt [Krishnamoorti-2002]. It is not clear if this different temperature dependence results from a solvent interaction effect or from chain tacticity. Some results where negative temperature coefficients were evaluated were obtained from solution viscometry. On the other hand, results also obtained from solution viscometry have shown negative temperature coefficient for isotactic PMMA, constant κ for aPMMA and positive κ for sPMMA [Yamakawa-1982]. These different results between theta solutions and melts raise the question about the reasonability of Flory conclusion (also confirmed by de Gennes using a self-consistent field approximation) that chain dimensions are unperturbed, having ideal behaviour, in theta solutions and polymer melts [Flory-1949, de Gennes-1979].

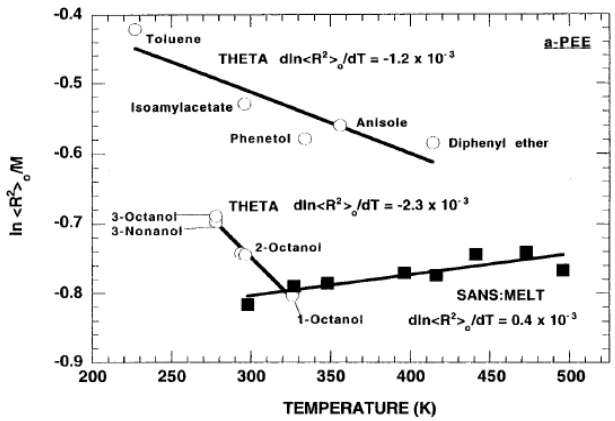

Figure 2.1. *Theta-condition and melt-based chain dimension data as a function of temperature for atactic poly(etyleneethylene) (a-PEE). Note the different slopes in solution and at the molten state [Krishnamoorti-2002].*

In conclusion, for a specific polymer, the *characteristic ratio* is a measurement of the coil size. It increases with polymer molecular weight up to a limiting value for chains with high molecular weight. This value depends on the solvent used and its temperature. Polymers with similar characteristic ratio do not have necessarily the same unperturbed coil size because, according to the definition in eq. (2.3), it depends on the number of chain segments (polymer molecular weight) and preferred conformations adopted by adjacent chain segments. An example that proves this statement is poly(ethylene), -$[CH_2CH_2]_n$-, C_∞ = 6.81, poly(isobutylene), -$[CH_2(CH_3)_2C]_n$-, C_∞ = 6.61 and poly(dimethylsiloxane), -$[Si(CH_3)_2O]_n$-, C_∞ = 6.29 [Mattice-2003].

2.1.2. The Kuhn monomer

The Kuhn segment length and the number of Kuhn monomers of one chain are evaluated considering that a real chain of unperturbed mean square end-to-end distance $\langle R^2 \rangle_o$ and extended length R_{max} may be described by a statistically equivalent chain of randomly joined segments in number N_k, each having a length of l_k, under the conditions that the mean square end-to-end distance and extended length of the equivalent chain are the same as those of the real chain. The first condition requires that

$$\left\langle R^2 \right\rangle_0 = N_k l_k^2 = C_\theta N l^2 \quad , \tag{2.8}$$

while the second condition requires that

$$R_{\max} = N_k l_k = N l \sin(\theta/2) \quad , \tag{2.9}$$

where θ is the valence angle between adjacent covalent bonds.

From these two conditions the length of a chain segment of the equivalent chain and their number (also called Kuhn monomer segment length and number of Kuhn monomers in the chain) are evaluated. They are, respectively,

$$l_k = \frac{\left\langle R^2 \right\rangle_0}{R_{\max}} = \frac{C_{\theta.} \cdot l}{\sin(\theta/2)} \quad , \tag{2.10}$$

and

$$N_k = \frac{R_{\max}^2}{\left\langle R^2 \right\rangle_0} = \frac{N \cdot \sin^2(\theta/2)}{C_{\theta.}} \quad . \tag{2.11}$$

All above equations were expressed as a function of the characteristic ratio of the real chain under ideal conditions, C_θ. The Kuhn monomer molecular weight may also be evaluated, and it gives us information about the number of monomers in the real chain that are incorporated into one statistical monomer. For this evaluation, the number of segments in

the real chain must be calculated from the polymer molecular weight (M), the monomer molecular weight (M_{mon}) and the number of carbon atoms in one monomer. For vinylic polymers $N = 2M/M_{mon}$ and the molecular weight of the Kuhn monomer is

$$M_k = \frac{M_{mon} C_{\theta.}}{2\sin^2(\theta/2)} \quad . \tag{2.12}$$

Table 2.1 indicates for different characteristic ratio values, values evaluated for Kuhn monomer segment length, its molecular weight and the number of real monomers in one statistical monomer. It is clear that different C_θ values yield different values for the Kuhn monomer length, Kuhn monomer molecular weight and chain end-to-end distance. Furthermore, for polymer melts the number of gauche conformational states increases with temperature affecting the average chain end-to-end distance, which must be temperature dependent as illustrated by the temperature coefficient values for the unperturbed chain dimensions (Table 2.2). The length, number and weight of the Kuhn monomer must also be temperature dependent, although their precise dependence is still unknown and not considered by theoretical models. However, as mentioned below and detailed in the next chapter, the radius of gyration for polymer chains do not change significantly at the molten and solid state. This may result from the relatively low temperature dependence of the temperature coefficient κ.

There are three important points to note about the statistically equivalent chain. The first is that segments of this chain, due to their uncorrelation, are energetically indistinguishable, while in the real chain each segment can be only at well defined low energy states (*trans* or *gauche* conformation). Their relative population is given by the Boltzmann distribution. Once known the height of energy barrier between conformational states and the energy difference between them, the rate of transition between states and their relative population may be evaluated. The second is the nature of the random coil model of chains in quiescent polymer melts, which is based on the verification that a real chain in a theta solvent (or in a polymer melt) may be represented by a chain of freely joined segments. The third is the spatial dimensions of the real chain in ideal conditions. Since for the same polymer different C_θ values may be evaluated for different solvents, the natural question is: which one should be selected to describe the chain conformation in a polymer melt? This is an important question since the length of the Kuhn monomer represents the minimum segment length value where correlations between adjacent segments are lost.

Another important point to note about the Kuhn monomer is the implicit assumption of eq. (2.9). It is considered that the chain is completely stretched inside of a single Kuhn monomer, which is a strong assumption, hardly fulfilled for most polymers. This assumption

also explains why the Kuhn segment cannot be treated as an entropic spring and the reason why the Gaussian behaviour is observed only for chain segments containing around 100 real monomers [Ding-2004a, Ding-2004b].

2.1.3. The dynamic bead size

Because of the above limitations with the Kuhn segment length definition, the concept of dynamic bead size was proposed. Eq. (2.8) is now expressed in terms of the number of dynamic segments of the chain (N_D) and their average length (l_D)

$$\left\langle R^2 \right\rangle_0 = N_D l_D^2 = C_\theta n l^2 \quad , \tag{2.13}$$

which may be expressed as a function of the mass of the dynamic segment (m_D) and the average mass of the bond (m_0), which for a vinylic polymer is $m_0 = M_{mon}/2$,

$$\left\langle R^2 \right\rangle_0 = \frac{M}{m_D} l_D^2 = C_\theta \frac{M}{m_0} l^2 \quad , \tag{2.14}$$

from which a relationship between l_D and l is obtained

$$l_D^2 = C_\theta \frac{m_D}{m_0} l^2 \quad . \tag{2.15}$$

The main problem with the above definition is that the evaluation of m_D requires the knowledge of l_D besides that of C_θ, l and m_0. The evaluation of these values, which were assumed to correspond to the length of a Rouse bead-spring chain segment, was performed by Small Angle Neutron Scattering data [Nicholson-1981] and dynamic birefringence measurements [Inoue-2002]. Both evaluations are biased since they started from assumptions on the validity of specific theoretical models, the Rouse and Zimm model in the first case [Nicholson-1981], and a modified stress optical law in the second [Inoue-2002]. In this last case it was considered that the complex modulus frequency dependence may be splitted into two independent components, one describing the behaviour at the glassy region and another describing the behaviour at the rubbery region [Inoue-1991]. Assuming further that contributions to the modulus at the rubbery plateau region are purely entropic, the molecular weight of a bead and spring chain segment was evaluated from

$$m_D = \frac{3\rho RT}{E'_R} \quad , \tag{2.16}$$

where E'_R is the value of the elastic component of the plateau modulus, ρ is the polymer density (which may be replaced by the polymer concentration when solutions are considered), R is the ideal gas constant, T is the temperature, and the factor 3 arises from the relationship

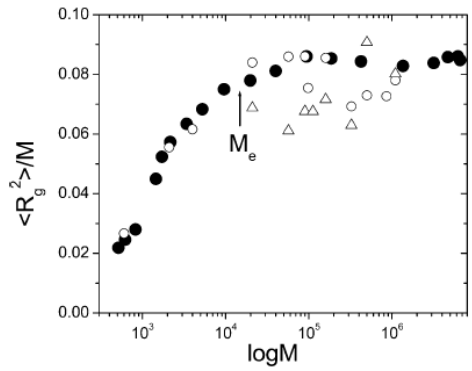

Figure 2.2. *Molecular weight dependence of the ratio* $< R_g^2 > / M$ *in polystyrene.* M_e *is the molecular weight between entanglements [Ding-2004a].*

of E'_R with the corresponding shear modulus assuming an incompressible behaviour of the polymer at the plateau region.

As shown, both procedures, to evaluate l_D in the first case and m_D in the second case, are questionable because assumptions are used for their evaluation. From these works one important conclusion can be drawn, and it is not dependent on theoretical considerations. It is illustrated in Figure 2.2, and shows that, for example for PS, the Gaussian behaviour is reached for molecular weights of around 100000 g/mol, around 140 Kuhn monomers, each with a molecular weight of 720 g/mol containing 6.9 real monomers. This figure also shows that PS chains become entangled before achieving a Gaussian coil. This is a result of key importance. It demonstrates that a chain segment between entanglements cannot be treated as Gaussian coil, as it is done in some theoretical applications of tube model.

2.1.4. Conclusions about ideal chains

Two different arguments were presented to prove that polymer chains in melts have ideal behaviour. The first was due to Flory [Flory-1949] and the second was due to de Gennes [de Gennes-1979] using a self-consistent field argument.

Flory analysed the interaction of a polymer chain with a solvent molecule as a swelling phenomena [Flory-1949]. He considered that there exists a close parallel between the expansion of a polymer chain in a good solvent and the swelling of a macroscopic three-dimensional network. As the polymer molecule is swollen by the osmotic action of the solvent, the chain molecule is spread to a less probable configuration. There is then the development of an elastic reaction which is similar to that induced on the rubber stretching, or in the isotropic swelling of a gel.

In this analysis a lattice model was used to evaluate the free energy of mixing, which was expressed as a function of the entropy of dilution of a system of polymer segments combined in a single continuous structure, the entropy of the elastic deformation of

the polymer molecule, and the heat of mixing of polymer and solvent. The final expression obtained for the free energy of mixing was expressed as a function of the size of solvent molecules - number of lattice cells occupied - (x_s), the number of random segments of polymer chain (N_k) or the chain molecular weight (M), an isotropic swelling factor (α), and a chemical potential accounting for the effect of energetic interactions (or the parameter ψ which is related to the Flory interaction parameter) [Flory-1949, Flory-1953]. The equilibrium conditions were obtained by finding the derivative of the free energy of mixing and equalling it to zero. The result obtained is

$$\alpha^5 - \alpha^3 = 2C_M \psi \cdot (1 - \theta/T)\sqrt{M} \quad , \tag{2.17}$$

or

$$\alpha^5 - \alpha^3 \propto (C/x_s)\psi \cdot (1 - \theta/T)\sqrt{M} \quad , \tag{2.18}$$

where $C_M \propto C/x_s$, θ is the theta temperature and C is a constant with a value around unit.

When the term at the right-hand side is zero the isotropic swelling factor is one, and the chain is unperturbed. This happens when T equals the θ temperature or when the solvent molecule is itself polymeric such that x_s is very large. It was concluded therefore that "*a polymer molecule situated in a medium consisting of other polymer molecules of the same kind, or in a medium of unlike polymer molecules with which it mixes athermally, will occupy spatial configurations coinciding with those calculated in the random flight approximation, undistorted by interference effects*". This assumption was the support for the Gaussian treatment of the rubber elasticity.

The alternative procedure of de Gennes considers a self-consistent field argument [de Gennes-1979]. We may start with an initial guess about the repulsive potential experienced by a monomer of a test chain and assume that by successive interactions a self-consistent condition is achieved. Since the concentration of the test chain monomers is peaked around its centre of gravity, monomers of the test chain at this region will experience maximum repulsion. On the slopes of this peak there is a force pointing outward. Due to the smaller concentration of monomers of other chains at the same region (because density fluctuations in a molten polymer are weak), they experience an inward force. Since the total potential is constant in space ($\partial U_{tot}/\partial \vec{r} \equiv 0$), this force exactly equals the force caused by monomers of the test chain, and therefore the test chain experiences no force and remains ideal [de Gennes-1979, p. 54].

The argument of de Gennes on the ideality of polymer chains at the molten state is more general than that of Flory. It does not consider any model, or preferred spatial arrangement, of polymer chains, while Flory's arguments start from a random-flight of chain

segments on a lattice. That is, it may equally well be applied to chains with random coil conformation, or to the regular folded chain model of Privalko and Lipatov [Privalko-1974], or still to any other spatial arrangement intermediate between these two.

On the part of experiments, it is known that the radius of gyration of semicrystalline polymer chains in approximately the same at the molten and solid state and that shear flow changes the radius of gyration up to 1.3 times the chain radius of gyration in quiescent conditions. These two experimental results will be discussed with more detail in the following chapter together with their relevance for establishing the polymer morphology at the molten state, its change with flow and during the solidification process.

2.2. Unentangled chain dynamics – the Rouse model

The application of Rouse model to the description of polymer chain dynamics is filled with assumptions that go far beyond those originally established by the author [Rouse-1953] and reanalysed latter on [Rouse-1998]. Other limitations of this model were identified [de Gennes-1979, pages 165-172]. For example, it is found in the literature that "*Rouse devised a treatment of polymer chains in a melt*" [Strobl-1996], while the title of Rouse's paper is "*a theory of the linear viscoelastic properties of dilute solutions of coiling polymers*" [Rouse-1953].

The Rouse model is a model for the dynamics of a single chain. Because this model was developed in the free-draining limit (the position of different chain molecules are not affected by the flow of solvent), the model seems to be clearly wrong for the situation for which it was developed. The motion of isolated polymer chains in a solvent is affected by hydrodynamic interactions, or "backflow" effects, that drive other chain segments into motion [de Gennes-1979, Strobl-1996, Doi-1996, Teraoka-2002]. In the original Rouse work (page 1274 of [Rouse-1953]), he presented experimental arguments supporting the free-draining assumption validity. However, the model did not fit experimental results and it was modified by Zimm to include the hydrodynamic interaction effect. The correction was made through the introduction of Oseen tensor to account for perturbation effects of one monomer in other monomers of the chain. In a more recent work of Rouse [Rouse-1998], he came back to this point and considered that the use of hydrodynamic interactions in a molecular theory of the viscosity of polymer solutions is inappropriate because it treats a fluid as a structureless continuum.

Rouse reanalyzed the original theory and he claims to have corrected it to take into account additional relaxation processes different from the configurational diffusion initially considered. Among the new processes is the "*formation of relatively persistent local van der Waals association between segments of the polymer molecule*", which were called by Rouse "*cryptocrystallites*". In this last work, no new equations were formulated. Rouse invoked a general symmetry principle of physics, the Curie symmetry principle, according to which, coupling producing interferences between processes of vectorial nature and processes of scalar nature can be disregarded, to cancel three irreversible processes occurring concurrently. Those irreversible processes are: one vectorial process, the configurational relaxation of polymer molecules as a consequence of rotations around chemical bonds taking place as a result of flow, and two scalar processes, the relaxation of strains affecting the lengths and angles of chemical bonds and the formation of intermolecular van der Waals interactions between segments of a polymer molecule. To our knowledge, no further confirmation of these arguments was provided.

Despite the above mentioned limitations and model conjectures, it is considered that the model "*seems to be correct in a melt because the Rouse model works quite satisfactorily*" [Strobl-1996]. Neutron scattering studies of Richter *et al.* [Richter-1989, Richter-1990, Paul-1998] are used to support this view. It is considered also that in a melt, or concentrated solutions, hydrodynamic interactions are screened out and therefore the Rouse model is valid [Higgins-1994]. No further justifications were presented for its validity.

Because the melt used in the claimed experimental validation of Rouse model had a molecular weight larger than the molecular weight between entanglements, it seems strange the validity of Rouse model in this situation because entanglement effects are not considered in the model formulation. It is a single chain dynamics model. As recognized by de Gennes [de Gennes-1979], one model assumption is that of "phantom" chain behaviour, which means "*to neglect any effect of knots along the chain*". In theta solvents or polymer melts "*coils tend to be knotted*" [de Gennes-1979].

Therefore, the conditions under which the claimed validity of Rouse model was established by Richter *et al.* must be carefully analyzed. This analysis will lead us to works of another co-author, Paul *et al*. [Paul-1997, Smith-1997] that studied the validity of Rouse model by molecular dynamics simulations using the bead-spring, the united atom and the explicit atom models. It will be seen at the end that the key questions are: i) what is the minimum number of chain segments (real monomers) in a chain for verification of Gaussian statistics and ii) may the Kuhn monomer be treated as a Gaussian spring. These two points were analysed in the previous section of this work.

2.2.1. The Rouse model and Rouse modes

There are several different derivations of Rouse model [Rouse-1953, Doi-1996, de Gennes-1979, Strobl-1996]. The simplest one was done by de Gennes and the main steps are described below.

In the Rouse model a polymer chain is divided into subsections of beads and springs. Each subsection must be sufficiently large to obey Gaussian statistics. For PE, this means that it should contain, at least, 10 statistical monomers (Kuhn monomers) or around 50 real monomers [Kopf-1997, Paul-1997]. However, as mentioned in the introduction, because of the self-similarity of Gaussian chain segments, theories identify Rouse segment with Kuhn monomer [Doi-1996, Teraoka-2002].

Each subsection is represented by a spring of no volume, average length $<b_R>$, spring force constant $k_{sp} = 3k_BT / < b_R^2 >$ and a rigid bead of infinite modulus. The chain contains N_R sections of N_R springs and (N_R + 1) beads. Since sections are freely-joined, the characteristic ratio of Rouse chain is one.

The assumption of ideality, implicit in the requirement of complying with Gaussian statistics, is one of Rouse model first assumptions. The total free energy (elastic energy) of Rouse chain is purely entropic, and it is the sum of free energy of different subsections between beads n and n+1, with position vectors $\mathbf{r}_n$ and $\mathbf{r}_{n+1}$,

$$F_{el} = \sum_{n=0}^{N_R-1} F_{n,n+1} = k_{sp} \sum_{n=0}^{N_R-1} (\mathbf{r}_{n+1} - \mathbf{r}_n)^2 = k_{sp} \sum_{n=0}^{N_R-1} \mathbf{b}_{R,n}^2 \quad . \tag{2.19}$$

Each bead, with the exception of the first and last one, experiences a force f_n from its two neighbours, and the velocity of bead n is a linear function of forces applied to n and its neighbours. The force f_n is

$$\mathbf{f}_n = \frac{\partial F_{el}}{\partial r_n} = 2k_{sp}\left[(\mathbf{r}_{n+1} - \mathbf{r}_n) + (\mathbf{r}_{n-1} - \mathbf{r}_n)\right] = 2k_{sp}(\mathbf{r}_{n+1} - 2\mathbf{r}_n + \mathbf{r}_{n-1}) \quad , \tag{2.20}$$

and the velocity is

$$\frac{\partial \mathbf{r}_n}{\partial t} = \mu \cdot \mathbf{f}_n = \frac{2k_{sp}}{\zeta_R}(\mathbf{r}_{n+1} - 2\mathbf{r}_n + \mathbf{r}_{n-1}) \quad , \tag{2.21}$$

$$\frac{\partial \mathbf{r}_n}{\partial t} \cong \frac{2k_{sp}}{\zeta_R} \frac{\partial^2 \mathbf{r}_n}{\partial n^2} \quad . \tag{2.22}$$

In eq. (2.21) μ has the dimension of a mobility. The velocity of bead n should have been written as $(\partial \mathbf{r}_n / \partial t) = \sum_m \mu_{mn} \mathbf{f}_n$. The locality of response was assumed, so that μ is nonzero only when $m = n$. Therefore μ is the bead mobility and its reciprocal ζ_R is the bead friction

coefficient. The subscript R is used to distinguish this friction coefficient related to Rouse model from the generic friction coefficient of a Brownian particle ζ. The same was done above for N_R and b_R. Further discussion on the physical meaning of ζ_R will be made below. Other formulations of Rouse theory consider in eq. (2.21) an additional random force term on each bead due to random fluctuations of solvent molecules with beads, $\mathbf{f}_{r,n}(t)$. The average value of this random force is zero and it looses its memory instantaneously, so that its autocorrelation function is

$$\left\langle \mathbf{f}_{r,n}(t) \cdot \mathbf{f}_{r,n}(t') \right\rangle = 6k_B T \zeta_R \delta(t-t') \quad , \tag{2.23}$$

where δ is the Dirac delta function [Teraoka-2002]. In the transition from (2.21) to (2.22) it was considered that the n dependence on $\mathbf{r}_n$ is very small on the length scale of a segment and it was used the Taylor series expansion

$$\mathbf{r}_{n\pm1} = \mathbf{r}_n \pm \frac{\partial \mathbf{r}_n}{\partial t} + \frac{1}{2}\frac{\partial^2 \mathbf{r}_n}{\partial n^2} \pm \ldots \quad , \tag{2.24}$$

to express (2.21) as a second order linear partial differential equation. This was the procedure followed by de Gennes (and also by Kawakatsu [Kawakatsu-2004]) which allows, after establishing appropriate boundary conditions for the first and last beads, resolving eq. (2.22) in terms of eigenmodes.

An alternative, more complicated, procedure for solving Rouse model implies expressing the (N_R + 1) differential eqs. (2.21), with the random force term included, in terms on (N_R + 1) normal coordinates, one for each bead. The advantage of this procedure is that it allows an easier perception of the physical meaning for the different normal modes. Each normal coordinate is defined as a linear combination of the beads position' vectors $\mathbf{r}_n(t)$:

$$\mathbf{q}_i(t) = \frac{1}{N_R}\sum_{n=1}^{N_R} \cos\frac{in\pi}{N_R}\mathbf{r}_n(t) \qquad (i = 0,\ 1,\ 2,\ldots) \quad . \tag{2.25}$$

Increasing the mode number, more detail will be obtained for the chain motion. The 0th normal mode is the centre-of-mass position of the N_R beads,

$$\mathbf{q}_0(t) = \frac{1}{N_R}\sum_{n=1}^{N_R} \mathbf{r}_n(t) \equiv \mathbf{r}_{CM}(t) \quad . \tag{2.26}$$

In normal mode 1,

$$\mathbf{q}_1(t) = \frac{1}{N_R}\sum_{n=1}^{N} \cos\frac{n\pi}{N_R}\mathbf{r}_n(t) \quad , \tag{2.27}$$

the chain is divided in two halves, and the $\mathbf{q}_1(t)$ vector connects the centroids of the halves. Changes in $\mathbf{q}_1(t)$ are associated with rotation of the chain as a whole. *This is the reason why Rouse mode 1 is also called rotation mode*. For mode 2 the chain is divided in four halves;

a vector 1 connects the second quadrant to the first and a vector 2 connects the third to the fourth quadrant. The $\mathbf{q}_2(t)$ is the sum of vectors 1 and 2 and it is more sensitive to conformational changes than $\mathbf{q}_1(t)$.

Supplementing eq. (2.22) with the following boundary conditions (due to forces acting on the first and last beads)

$$\left.\frac{\partial \mathbf{r}_n}{\partial t}\right|_0 = \left.\frac{\partial \mathbf{r}_n}{\partial t}\right|_N = 0 \quad , \tag{2.28}$$

a solution of (2.22) is

$$\mathbf{r}_{n,p} = \alpha_p \cos\left(\frac{\pi p n}{N_R}\right) \cdot e^{-t/\tau_p} \quad , \tag{2.29}$$

where p = 1, 2, …, N_R is the mode number, α_p is the corresponding amplitude and the cosine was chosen to match the boundary conditions defined by eq. (2.28).

The relaxation time of p mode is

$$\tau_p = \frac{\zeta_R N_R{}^2 \left\langle b_R^2 \right\rangle}{3\pi^2 k_B T} \frac{1}{p^2} \quad . \tag{2.30}$$

The relaxation time of mode zero is infinite. The relaxation time of the first mode is a rotational relaxation time and it is usually considered as the Rouse relaxation time of the chain. Note, that the above equation was expressed on purposed as a function of variables specific to Rouse chain: N_R, $\langle b_R \rangle$ and ζ_R.

2.2.2. Critique of Rouse model and uses made of this model

As mentioned above, Rouse model was formulated to explain the dynamic behaviour of polymers in diluted solutions. Phantom chains are considered and chain interactions are disregarded. Locality of response is assumed and the mobility (or friction coefficient) of a single bead is considered in the equation describing the movement of a chain section.

De Gennes made a discussion about the microscopic origin of bead friction coefficient [de Gennes-1979]. In the solution considered by Rouse it would be associated with the hydrodynamic friction of a bead on the solvent. For Gaussian chains $N_R \to \infty$ and ζ_R does not contain any information on the effect of internal barriers because they are not seen by the first modes. A proof of this assessment was made invoking the Kuhn theorem. In the Rouse model the overall friction coefficient is the sum of the friction coefficients for all beads, $\zeta_{R,chain} \approx N_R \zeta_R$ (as it will be shown below). Therefore, a chain with very high conformational energy barriers floating in a solvent will have mobility in the solvent that will depend on the solvent viscosity only, and not on the chain internal energy barriers. Using the de Gennes

example, a rigid twisted wire floating in a solvent may have translational movement. Also, solvent friction forces (f_s) and forces arising from internal energy barriers (f_i) exist in a chain when one extremity is fixed at the origin and the other is deformed with constant velocity. The ratio between the two forces is

$$\left(f_i/f_s\right) \cong \left(\zeta_i/\zeta_s {N_R}^2\right) \ , \tag{2.31}$$

where ζ_i and ζ_s are the friction coefficients resulting from the internal energy barriers and solvent, respectively. This equation is the Kuhn theorem and it shows that for very long chains, when N_R is larger than $\left(\zeta_i/\zeta_s\right)^{1/2}$, the internal friction is negligible.

On the other hand, a similar reasoning made for a chain inserted on a solid state matrix, moving trough vacancy diffusion in the solid, indicates two types of barriers: one for vacancy formation and the other for internal barriers resulting from changes in chain conformation for going from one state to another. Considering that Brownian motion of polymer chains results from Markoff random transitions between their rotational isomeric states [Iwata-1971], an equation similar to that of Rouse model was derived. In this equation the friction coefficient depends strongly on conformational barriers. It must be noted that the assumption of Markoff random transitions implies that each of the chain conformations at a specific time is independent of previous conformations. Also, this assumption corresponds to neglecting entanglements and backflow effects and it considered that other chains behave as solvent molecules. Besides the work of Iwata *et al.*, other modifications of Rouse model, dealing specifically with the friction coefficient, were also presented. An example is the generalized Rouse model of Hess [Hess-1988]. This generalization considers, besides the random force, a dynamic friction function term in eq. (2.21) that should consider the entanglement effects in the dynamics of polymeric liquids. An entanglement friction function is therefore introduced as a kernel of memory function acting on the velocity of each bead,

$$\sum_n \int_0^t \Delta\zeta_{R,mn}(t-\tau)\frac{\partial r_n(\tau)}{\partial \tau} d\tau \quad . \tag{2.32}$$

Still another analysis about the ambiguity, and lack of clearness, in the definition of friction coefficient may be found in the original Rouse work [Rouse-1953] and also in Strobl book [Strobl-1996]. Initially, Rouse considers that μ is the mobility of the end of a submolecule (*bead* of a bead-spring section). Later on in the discussion, Rouse considers that because the mobility should depend on the viscous forces exerted by the medium along the entire length of the chain, μ should be inversely proportional to the chain length included in the submolecule.

This requirement results from an analysis of eq. (2.30). It shows that the Rouse relaxation time of a chain depends on the size of the section considered $\langle b_R^2 \rangle$, besides its dependence on the square of the number of sections (springs). This relaxation time is therefore arbitrary because of the dependence on $\langle b_R^2 \rangle$. Expressing eq. (2.30) as

$$\tau_R = \frac{\left(\zeta_R / \langle b_R^2 \rangle\right)}{3\pi^2 k_B T} \langle R_o^4 \rangle \quad , \tag{2.33}$$

where only mode one was considered and $\langle R_o^2 \rangle$ is the average of the square distance between the ends of the Rouse chain, the friction coefficient has to be proportional to the number of statistical monomers in each spring. It is clear, that this is a basic requirement for the validity of Rouse model [Strobl-1996]. However, the spring considered in this model has no volume and it is therefore difficult the experimental evaluation of a friction coefficient for this situation. That is the reason why experiments claiming the validity of Rouse model yield $\zeta_R / \langle b_R^2 \rangle$ as a fitting parameter to the experimental results.

2.2.3. The Rouse relaxation time of an entanglement strand

In practice Rouse model is also applied to chain segments between entanglements. Each chain segment is treated as a Rouse chain with N_e sections of springs and N_e +1 beads. The argument for this procedure is, as mentioned above, the self-similarity of Gaussian chains. An equation similar to (2.30) is used for the Rouse relaxation time of a chain segment between entanglements, τ_e,

$$\tau_e \approx \frac{\zeta_e \langle b_e^2 \rangle}{k_B T} N_e^2 \quad , \tag{2.34}$$

where ζ_e should now be the friction coefficient of a bead-spring section in the chain segment between entanglements.

It must be noted that since entanglements are regarded as topological constraints to chain motion, their nature must be considered to establish suitable boundary conditions to replace eq. (2.28). However, because their physical nature is unknown, an *ad-hoc* replacement is made in eq. (2.30) of N_R by N_e. Further, using self-similarity arguments the averages of the square end-to-end distance of the springs (on the Rouse chain and in the chain segment between entanglements) are equalled to the square of the Kuhn segment [Rubinstein-2002],

$$l_k^2 = \langle b_e^2 \rangle = \langle b_R^2 \rangle \quad , \tag{2.35}$$

and this relationship is used to relate the two relaxation times, the Rouse relaxation time of the chain and the Rouse relaxation time of the chain segment between entanglements,

$$\tau_R = \tau_e \left(\frac{N_R}{N_e} \right)^2 = \tau_k {N_R}^2 \quad , \tag{2.36}$$

where τ_k is the relaxation time of a Kuhn monomer defined as

$$\tau_k = \frac{\zeta_k {l_k}^2}{3\pi^2 k_B T} \quad , \tag{2.37}$$

and ζ_k is the Kuhn monomer friction coefficient.

According to Martins [Martins-2008], it is also implicitly considered, without any justification, that

$$\zeta_k = \zeta_e = \zeta_R \quad . \tag{2.38}$$

The last equality is physically unacceptable. The physical dimensions of friction coefficient ($\mathbf{kg \cdot s^{-1}}$) or ((energy x time)/area) imply different values for the above friction coefficients. In a concentrated solution, or polymer melt, friction results from physical interactions of one chain segment with neighbouring segments of the same or different chains. This fact was demonstrated experimentally by Cerf [Cerf-1958]. It was assigned to internal friction effects which may result from chain deformation or changes in chain conformations [de Gennes-1979]. The numbers of (real) monomer-monomer contacts are necessarily different in a Kuhn monomer (around 5 real monomers), in a chain segment between entanglements (7 Kuhn monomers for PE, 32 for PP, 23 for PS) and the number of monomers of a Rouse (unentangled) chain, between two and four times the number of monomers of a chain segment between entanglements.

For this reason, the equalities in eq. (2.35) and (2.38) are wrong which invalidates the relationship between the different relaxation times in eq. (2.36) [Martins-2008]. Also since Kuhn monomer was defined in §2.1.2 as the minimum chain segment length for monomers of real chain loosing their correlation, it results in that, it cannot be equalled to average values because sections of segments with length lower than the average are correlated, and therefore not statistical. Also, a Kuhn monomer contains around 5 monomers of the real chain, far below the minimum number required for verification of Gaussian properties. Likewise, the *ad-hoc* definition of Rouse relaxation time of a chain segment between entanglements is wrong because it suffers of all above mentioned limitations of Rouse model, and in addition the absence of proper boundary conditions definitions.

2.2.4. The temperature dependence of friction coefficient

Because of the equality in eq. (2.35) and the relationship between the different relaxation times in eq. (2.36), the friction coefficient in these last equations is considered to be the Kuhn monomer friction coefficient. It was shown above that the Kuhn monomer cannot be considered as a Gaussian spring in any type of bead-spring model.

So far, to our knowledge, it is inexistent a derivation of monomeric friction coefficient from first principles. Different approaches are used for this evaluation. A list of empirical approaches based on free volume models may be found in a classical work of Berry and Fox [Berry-1968]. For $T > T_g$ the friction factor per atom is defined as

$$\zeta = \zeta_0 \exp\left[\frac{1}{f_g + \alpha_f (T - T_g)}\right] \quad , \tag{2.39}$$

where ζ_0 is the inherent friction factor, presumed constant, independent of molecular weight and temperature, f_g is the free volume fraction at the glass transition temperature (T_g), equal to $2.3RT_g/E_a$, and α_f is the free volume thermal expansion coefficient, equal to $2.3R/E_a$, where R is the ideal gas constant and E_a the flow activation energy [Rojo-2004, Berry-1968].

Other approaches for this evaluation are described for example by Ferry [Ferry-1980] and van Meerveld [van Meerveld-2004]. Van Meerveld discusses two procedures. One is based on fitting experimental curves of $G'(\omega)$ and $G''(\omega)$ with theoretical models to evaluate the Rouse relaxation time of a chain segment between entanglements, eq. (2.34), and from this the Kuhn monomer friction coefficient (ζ_k) is evaluated. The value obtained for this parameter is model dependent. The other procedure is similar to that used by Ferry [Ferry-1980], where fitting to the relaxation spectra is used to estimate a value for ζ_k. In any case, the evaluation is for a specific temperature, and extrapolations to other temperatures are made using equations of WLF, Vogel or Arrhenius. Typical values for the monomeric friction coefficient are indicated in Table 2.3.

2.2.5. The diffusion coefficient of the Rouse chain

The diffusion coefficient of the Rouse chain is evaluated from the Einstein relation for the relationship between the diffusion coefficient and the particle friction with the solvent

$$D = \frac{k_B T}{\zeta} \quad . \tag{2.40}$$

Considering a random walk of N_k steps each with length l_k and that each step is executed in a time interval t_k, the mean square displacement after N_k steps at time $t = N_k t_k$ is

$$\left\langle [\mathbf{r}(t) - \mathbf{r}(0)]^2 \right\rangle = N l_k^2 \quad . \tag{2.41}$$

Table 2.3. *Flow activation energy, Kuhn monomer friction coefficient, its length and molecular weight for three polyolefins with chain of increasing bulkiness. The last row indicates the number of real monomers in one Kuhn monomer. The value evaluated for ζ_k refers to 463.15 K. Information obtained from [Martins-2008], [van Meerveld-2004] and [Ferry-1980]. Values for Kuhn monomer are for T = 413 K.*

	PE	PP	PS
E_{flow} (kJ/mol)	26.6 33	44.6	95.5
ζ_k (kg/s)	4.74×10^{-13}	1.04×10^{-12}	1.12×10^{-10}
l_k (Å)	14	11	18
Molecular weight of Kuhn monomer (g/mol)	150	180	720
Number of monomers in one Kuhn chain segment	5.40	4.27	6.90

The ratio of the mean square displacement to the time, divided by six, for a random walk in three dimensions, is the particle diffusion coefficient

$$D = \frac{\left\langle [\mathbf{r}(t) - \mathbf{r}(0)]^2 \right\rangle}{6t} \quad , \tag{2.42}$$

which for a random walker in a cubic lattice is $l_k^2 / 6t_k$ (independent of time).

In diluted solutions the isolated chain is treated as a Brownian particle and the centre of mass diffusion of this Brownian particle is evaluated. Since it is subjected to a random fluctuating force imposed by solvent molecules, its equation of motion

$$\zeta_{R,chain} \frac{\partial \mathbf{r}_{CM}(t)}{\partial t} = \mathbf{f}_{r,CM}(t) \tag{2.43}$$

is similar to eq. (2.21) where the potential term due to interactions between adjacent springs was neglected (because we are treating the centre of mass motion of the chain) and the random fluctuating force term was included because the chain is treated as a Brownian particle and this fluctuating force acts on the whole chain. The friction factor in eq. (2.43) refers to the Rouse chain. Therefore, considering the discussion made in §2.2.2, it is equal to $\zeta_{R,chain} = N_R \zeta_R$, where N_R is the number of springs in the Rouse chain. The above equation may be recognized as the Langevin equation with the inertial and potential terms neglected.

The solution of eq. (2.43) is

$$\mathbf{r}_{CM}(t) = \mathbf{r}_{CM}(0) + \frac{1}{\zeta_{R,chain}} \int_0^t \mathbf{f}_{r,CM}(t) dt \quad . \tag{2.44}$$

The mean square displacement of the chain centre of mass is

$$\left\langle [\mathbf{r}_{CM}(t) - \mathbf{r}_{CM}(0)]^2 \right\rangle = \frac{1}{\zeta_{R,chain}^2} \int_0^t dt \int_0^t \left\langle \mathbf{f}_{r,CM}(t) \cdot \mathbf{f}_{r,CM}(t') \right\rangle dt' \quad , \tag{2.45}$$

which following eq. (2.23), modified for the random force acting on the chain centre of mass, yields

$$\left\langle [\mathbf{r}_{CM}(t) - \mathbf{r}_{CM}(0)]^2 \right\rangle = \frac{6 k_B T \zeta_{R,chain}}{\zeta_{R,chain}^2} t \quad . \tag{2.46}$$

Note that $\int_0^t \delta(t-t')dt' = 1$.

From eqs. (2.42) and (2.46) it follows that the diffusion coefficient of the centre of mass of Rouse chain is

$$D_{R,CM} = \frac{k_B T}{\zeta_{R,chain}} = \frac{k_B T}{N_R \zeta_R} \quad . \tag{2.47}$$

2.2.6. Rouse model predictions and fitting with experimental results

As mentioned above, Rouse model was formulated to describe the linear viscoelastic behaviour of polymers in diluted solutions. The shear relaxation modulus for this model may be evaluated by application of fluctuation-dissipation theorem (or alternatively by application of stress optical law) [Stobl-1996]. The result is

$$G(t) = \frac{cN_A}{M} k_B T \sum_{p=1}^{N_R} \exp\left(-\frac{t}{\tau_p/2}\right) \quad , \tag{2.48}$$

where cN_A/M represents the number of polymer chains per unit volume and the relaxation times involved in the mechanical relaxation are half those of the normal modes [Strobl-1996, Doi-1996]. If the polymer volume fraction is kept constant, then $G(t)$ is inversely proportional to the chain length: $G(t) \propto N_R^{-1}$.

Because the viscosity at zero shear rate is

$$\eta_0 = \int_0^\infty G(t)dt = \frac{cN_A}{M} \frac{k_B T}{2} \tau_R \sum_{p=1}^{N_R} \frac{1}{p^2} \quad , \tag{2.49}$$

the zero shear rate viscosity for Rouse model increases linearly with the polymer molecular weight, or $\eta_0 \propto N$.

Other results of this model are the prediction for the chain relaxation time on the square of chain molecular weight, $\tau_R \propto N^2$ (see eq. (2.30)), and the dependence for the centre of mass chain diffusion of $D_{R,CM} \propto N^{-1}$ - eq. (2.47). In summary,

$$\textit{Rouse model (ideal chains):} \qquad \eta_0 \propto N; \quad \tau \propto N^2; \quad D \propto N^{-1} \quad . \tag{2.50}$$

In the above relationships the subscript R in N_R was dropped and N_R was replaced by N, the number of random segments in the chain. It must be noted, however, that for non-gaussian chains this value is dependent on the model/approximation considered.

Experimental results obtained for polymer chains in theta conditions are

$$\eta_0 \propto N^{1/2}; \quad \tau \propto N^{3/2}; \quad D \propto N^{-1/2} \quad . \tag{2.51}$$

The dependencies measured experimentally for good solvents are

$$[\eta] \propto N^{3(\nu-1)}; \quad \tau \propto N^{3\nu}; \quad D \propto N^{-\nu} \ , \tag{2.52}$$

where $[\eta]$ is the intrinsic viscosity and $\nu = 3/5$ [Doi-1996].

It is clear the disagreement between the Rouse model predictions and experimental results. A better agreement is obtained when hydrodynamic interactions are considered. Since the purpose of this discussion is to illustrate failures of Rouse model, model corrections resulting from hydrodynamic interactions will not be discussed further.

Because it is assumed that for polymer melts hydrodynamic interactions are shielded, it was considered that Rouse model could explain the dynamical behaviour of these polymers with a molecular weight below the critical molecular weight (unentangled polymer melts), and that it also explains the short term dynamics of higher molecular weight polymers. This is the main reason for incorporation of Rouse model features into more complicated models for the description of entangled polymer melts dynamics. The analysis here is restricted to unentangled polymer melts and the results shown below demonstrate the model failure for entangled polymers.

In the literature searched few references were found with experimental results for the molecular weight dependencies of η_0, τ and D for unentangled polymers. One of the first works with this information was performed by Pearson *et al.* [Pearson-1987] using attenuation of NMR spin echoes in a pulsed field gradient and polyethylenes with molecular weight from 500 g/mol up to 100 000 g/mol. Large discrepancies exist in the literature for the molecular weight between entanglements of PE, between 900 g/mol up 1300 g/mol and the critical molecular weight is between 2 to 4 times this value. Pearson *et al*. found that the molecular weight dependence on viscosity at 175 ºC can be described by two power law regions, $\eta_0 \propto M^{1.8}$ below 5000 g/mol and $\eta_0 \propto M^{3.6}$ above 5000 g/mol. Following the results of Pearson *et al.*, the critical molecular weight of PE should be around 5000 g/mol. Further, they found that the diffusion coefficient can be characterized by a single power law in all molecular weight range studied, $D \propto M^{-2}$. It must be noted that the zero shear rate power law relationship obtained by Pearson *et al.* for the low molecular weight region is in disagreement with commonly accepted values. Berry and Fox [Berry-1968], based on a large set of experimental results on fractions of different molecular weight of concentrated solutions, found the following dependence: $\eta_0 \propto N$ for $M < M_c$ and $\eta_0 \propto N^{3.4}$ for $M > M_c$. In this evaluation it was considered the viscosity correction for constant friction coefficient for $M < M_c$. According to Berry and Fox this correction is important for polymers with $M < M_c$ because the friction factor per chain atom is dependent on density for polymers within this range of molecular weight. The correction is not needed for polymers with $M > M_c$.

Apparently, Pearson *et al.* have not performed this correction. Relationships similar to those obtained by Berry and Fox were obtained for polymer melts by Colby *et al.* [Colby-1987].

The experimental results of Pearson *et al.* suggest the invalidity of Rouse model for unentangled polymers (see eq. (2.50)), while those of Berry and Fox [Berry-1968] and Colby *et al.* [Colby1987] suggest that its validity would be limited to polymers with molecular weight below the critical molecular weight (because of the zero shear rate molecular weight dependence). However, Pearson *et al.* [Pearson-1987] found that the product $\eta_0 D$ verifies Rouse model. The reason indicated was "*the elimination of local friction factor so that the comparison with theory requires no unknown parameters*". In a latter work similar results were obtained for polybutadiene [Pearson-1994].

Other experimental results used to support the validity of Rouse model were obtained first by Higgins *et al.* [Higgins-1985] and latter on by Richter *et al*. [Richter-1989, Richter-1990, Richter-1993, Richter-1994]. These authors used neutron spin-echo spectroscopy to investigate the dynamic structure factors for single chain relaxation in polymer melts of varying molecular weight. The results were presented in the form of a normalized intermediate scattering function $S(q,t)/S(q,0)$ as a function of time. This function describes the decay of the density fluctuations **at one value** of the wavevector ***q*** and it is caused by the change in the positions of segments due to diffusive motion. If the segments do not move, the intermediate scattering function will not decay. The experimental values for this normalized intermediate scattering function are compared with model predictions for the same intermediate scattering function.

This expression for Rouse model was derived by de Gennes [de Gennes-1967]. Three length scales were considered: the length scale of the radius of gyration R_g, the length scale of the tube diameter a (average distance between topological constraints of a chain in an entangled melt or concentrated solution) and the length scale of a bead-spring section in the Rouse model b_R (σ in the original de Gennes work). To each length scale is associated a wave vector region (or a scattering angle regime).

For low scattering wave vectors (or small angle regime), when $q << R_g^{-1}$, where diffusion regime prevails, the normalized intermediate scattering function is

$$S'(q,t) = S(q,t)/S(q,0) = \exp(-\Omega_{cm} t) \ , \tag{2.53}$$

where $\Omega_{cm} = D_{cm} q^2$ and D_{cm} is the centre of mass diffusion [de Gennes-1967, Doi-1986, Higgins-1994].

When $q > R_g^{-1}$ (or large angle regime) two different length scales must be considered: the length scale between R_g and the tube diameter (a), and the length scale between a and

the average end-to-end distance of a bead-spring section (b_R). Only the last length scale is of interest here. Because for $t > \tau_R$, $S'(q,t) \to 0$, only the time region lower than the Rouse relaxation time of the chain will be considered ($t < \tau_R$). The normalized intermediate scattering function obtained for Rouse model with the above assumptions is

$$S'(q,t) = S(q,t) \Big/ S(q,0) = \int_0^\infty \exp\left\{ -u - \left(\Gamma_R\, t\right)^{1/2} g\left[\frac{u}{\left(\Gamma_R\, t\right)^{1/2}} \right] \right\} du \ , \tag{2.54}$$

with

$$g(y) = \frac{2}{\pi} \int_0^\infty \frac{1 - \exp\left(-x^2\right)}{x^2} \cos(xy)\, dx \ , \tag{2.55}$$

and the inverse correlation time Γ_R is given by

$$\Gamma_R = \frac{1}{3\pi} \frac{k_B T\, b_R^2}{\zeta_R} q^4 \ . \tag{2.56}$$

For a time much larger than the inverse correlation time ($t >> \Gamma^{-1}$), the behaviour of Rouse chain is

$$S'(q,t) \cong \exp\left[- \left(\Gamma_R\, t\right)^{1/2} \right] . \tag{2.57a}$$

A detailed description of these derivations may be found in Teraoka [Teraoka-2002, pages 243-256]. This limiting time is only reached at times of order $10\Gamma^{-1}$ which is beyond the range explored in experiments. Therefore, the parameter Γ_R may be obtained by a direct fitting of eq. (2.57a) to experimental results or by taking the initial slope of the normalized intermediate scattering function, which is

$$\Omega_R = -\lim_{t \to 0} \frac{d}{dt} S'(q,t) = \frac{\pi}{4} \Gamma_R = \frac{1}{12} \frac{k_B T\, b_R^2}{\zeta_R} q^4 \ . \tag{2.58}$$

Eq. (2.57a) may also be written as

$$S'(q,t) \cong S'(q,t) = \exp\left[-q^2 \left(\frac{1}{3\pi} \frac{k_B T\, b_R^2}{\zeta_R} t \right)^{1/2} \right] = \exp\left[-q^2 \left(\frac{W}{9\pi}\, b_R^4\, t \right)^{1/2} \right] = \exp\left[-\frac{u}{3\sqrt{\pi}} \right] , \tag{2.57b}$$

with $W = 3k_B T / \zeta_R\, b_R^2$ and $u = q^2 \left(W\, b_R^4\, t \right)^{1/2}$. Eq. (2.54) was used by Higgins *et al.* and eq. (2.57b) - by Richter *et al.*. For both cases the adjustable parameter is the ratio ζ / b_R^2. Two other important relationships are those involving Rouse relaxation time for the chain and W (or Γ):

$$\tau_R = \frac{{N_R}^2}{\pi^2} \frac{1}{W} = \frac{{N_R}^2 b_R^4 q^4}{9\pi^3} \frac{1}{\Gamma_R} = \frac{\left\langle R_0^4 \right\rangle q^4}{9\pi^3} \frac{1}{\Gamma_R} \ . \tag{2.59}$$

These equalities assign to W and Γ the role of a relaxation rate. Particularly W is usually interpreted as a *"characteristic Rouse relaxation rate*" [Richter-1989]. As shown in the above relationship there is an important, unknown, proportionality factor, the number of bead-spring sections in the chain.

It is both the fitting quality of eqs. (2.54) or (2.57a,b) to experimental data and the comparison of the ratio ζ_R / b_R^2 with known values for the ratio between the Kuhn monomer friction coefficient (**not the friction coefficient of a bead-spring section of the Rouse chain, because it is unknown**) and the Kuhn monomer length (**l_k, not b_R because it is also unknown, but may be estimated**), that are used to ascertain the partial model validity. Another complementary, yet partial, test of Rouse model validity is the verification of the q^4 dependence of Ω_R [Richter-1989].

The experimental results obtained by Higgins *et al.* and Richter *et al.* and their fitting with the above equations are shown in Figures 2.3 and 2.4. Results in Figure 2.3 refer to a mixture of high molecular weight polytetrahydrofuran (PTHF) in a high molecular weight deuterated PTHF matrix (H/H) and in a low molecular weight deuterated PTHF matrix (H/L). The scattering vector is the same for both curves, q = 0.09 Å^{-1}. The value estimated for the tube diameter is 30 Å. According to Higgins and Benoit [Higgins-1994], it seems unlikely that the neutron spin-echo scattering experiments, for which the lowest q value is around 0.02 Å^{-1} would show effects of entanglement constraints in polymer motion. However, the lower curve for the H/L mixture is clearly different from the upper curve for the H/H mixture. The first was fitted with eq. (2.54) and the fitting allowed to evaluate Ω_R and inverse correlation time Γ_R = 5.5 × 10^7 s^{-1}. The scattering experiments were performed at 418 K. The value evaluated for the ratio ζ_R / b_R^2 is 7.3 × 10^6 N·s/m^3. The upper curve was fitted with

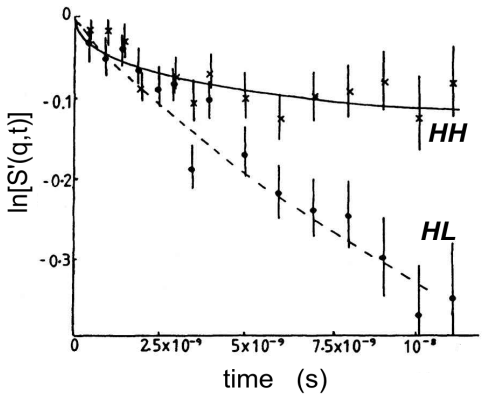

Figure 2.3. *Logarithm of $S'(q,t)$ as a function of time for a mixture of a high molecular weight polytetrahydrofuran (PTHF) in:* (□) *a high molecular weight deuterated PTHF matrix and* (,) *a low molecular weight PTHF matrix. Γ_R = 5.5 × 10^7 s^{-1} and q = 0.09 Å^{-1}. The lower curve for the mixture with the low molecular weight was fitted with eq. (2.48) [Higgins-1985].*

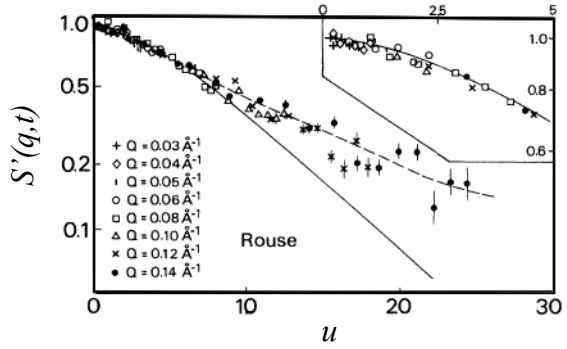

Figure 2.4. *Neutron spin-echo results for PMDS at 200 ºC. The prediction from Rouse model, eq. (2.57b) is indicated with a solid line. The dashed line is a guide to the eye. The inset shows the relaxation function at small values of the scaling variable [Richter-1989].*

a modified reptation model [Higgins-1985].

Other results obtained for a polydimethylsiloxane (PMDS) melt by Richter *et al.* [Richter-1989] are in Figure 2.4. The figure shows neutron spin-echo results at 200 ºC. The logarithm of the normalized intermediate structure function is plotted against a reduced variable $u = q^2 \left(W\ b_R^4\ t \right)^{1/2}$ - see eq. (2.57b). The model validity would imply the superposition of all data points for different scattering vectors in a single line. At small u (short times) the curves approach Rouse dynamics. At longer times the curves deviate from Rouse behaviour. The deviations increase with time and this fact was assigned to entanglement effects that were neglected in the model formulation. Similar results were obtained for other polymers [Richter-1990].

Fitting the results of Figure 2.4 with eq. (2.57b) yields for the parameter ζ_R / b_R^2 the value of 8.9×10^6 N·s/m^3. The Kuhn monomer length evaluated for PMDS at 200 ºC is $l_k = 6.2$ Å and the Kuhn monomer friction coefficient evaluated at the same temperature is $\zeta_k = 2.81 \times 10^{-12}$ kg/s. The ratio ζ_k / l_k^2 is 7.32×10^6 N·s/m^3. It was based on the agreement between these two values that Richter *et al.* [Richter-1989], and other authors [Strobl-1996, Kawakatsu-2004] consider the Rouse model valid for polymer melts.

Still another result of Richter *et al.* [Richter-1990] used to support the scattering experiments (or better, the direct observation of the entanglement distance in a polymer melt and the transition from Rouse regime to reptation) is the variation of tube diameter with the melt temperature. The results were obtained for a poly(ethylene-co-propylene). The normalized intermediate scattering function, when plotted as a function of the dimensionless variable *u,* yields curves similar to those of Figure 2.4. For long times the curves level-off instead of tending to zero as predicted by Rouse model. According to Strobl [Strobl-1996], this behaviour is indicative of chain confinement, "*at least a temporary one*". From values of the intermediate scattering function at long times the tube diameter was

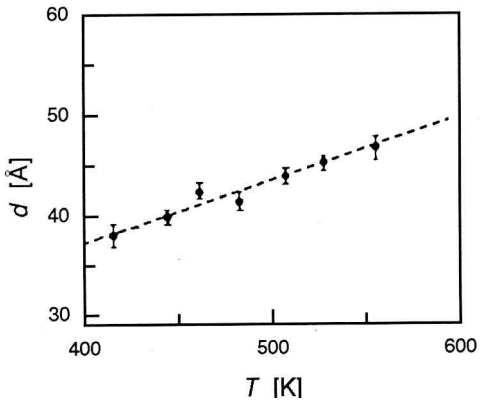

Figure 2.5. *Variation of tube diameter with temperature. The tube diameter was evaluated from the intermediate scattering function at long time [Strobl-1996].*

evaluated. The result of [Richter-1990] is plotted in Figure 6.9 of [Strobl-1996] reproduced below – Figure 2.5.

The figure shows an increase of tube diameter with melt temperature, a result that was interpreted differently by the authors [Richter-1990] and Strobl [Strobl-1996, page 281]. Richter *et al.* found that the result obtained was opposite to the expected. However they found that the tube diameter evaluated from scattering experiments and that evaluated from plateau modulus value, obtained by rheological experiments, agree, indicating an increase of tube diameter with temperature. After this discussion the result obtained was accepted as valid. Strobl considers normal the variation shown in Figure 2.5 and the result is interpreted in the following way: "*the motional constraints get weaker with increasing temperature*".

However, as shown in §2.1.1 and Table 2.2 the coefficient for thermal expansion of unperturbed chain dimensions is negative for polyethylene. In a work of Richter *et al.* [Zirkel-1992] for poly(ethylene-co-polypropylene), the same polymer used to construct the result of Figure 2.5, it is shown that $\kappa = -0.8 \times 10^{-3}$ K^{-1} at T = 200 ºC. Results in a wider temperature range are also shown in Figure 3 of [Zirkel-1992]. These results were obtained by Small Angle Neutron Scattering (SANS) while the results used to construct Figure 2.5 were obtained by neutron spin-echo spectroscopy. Since the tube diameter is the average distance of chain section between entanglements with N_e monomers each of length l_k, then

$$a = \sqrt{N_e} l_k \ . \tag{2.60}$$

Because κ is negative, a must decrease with temperature. Therefore, it is clear the disagreement between the two different sets of results. It questions the validity of the interpretation made in [Butera-1991] and [Strobl-1996] for the normalized intermediate scattering function at long times.

The discussion about the validity of Rouse model by Richter *et al.* continued. In [Paul-1998] it was made a critical test to Rouse model by molecular dynamics simulations

and neutron spin echo spectroscopy. The chain motion of an unentangled PE melt was studied. Computer simulations have shown systematic deviations from Rouse behaviour [Paul-1997, Kopf-1997]. Computer simulations and experiments were performed on a dense PE melt of n-$C_{100}H_{202}$ at 509 K. These chains are shorter than the entanglement length ($N_e \approx 136$) and the dynamic behaviour should be that of an unentangled melt. It was concluded that for chains which should be ideal Rouse chains, the model is capable of describing the behaviour only in time scales of the order of the Rouse time for the chain relaxation (or larger) and in length scales of the order of R_g or larger. The regime where Rouse model works for unentangled chains is that where they show Fickian diffusion. The deviations were assigned to interchain interactions.

This result demonstrates the invalidity of Rouse model (and Rouse modes) for unentangled chains. However, it must be noted that the chain length used in the simulations and experiments is in around the lower limit for Gaussian behaviour. Chains with at least 10 statistical segments are required before they can be described as Gaussian coils, which means for PE around 54 monomers (around 110 carbon atoms) [Paul-1997].

In the most recent work of Richter *et al.* [Smith-2001] the non-Gaussianity of chain motion in unentangled polymer melts was recognized, and it was concluded that intermolecular correlations account for deviations of Rouse predictions. Further, it was concluded that Rouse-type analytical models fail to account for this non-Gaussianity leading to large deviations between the experimental dynamic structure factor and model predictions.

2.3. Entangled chain dynamics

For concentrated solutions or polymer melts it is considered that chains interact with neighbouring chains. These interactions are considered as topological constraints to chain motion (or entanglements). The physical nature of entanglements is not known. One recent review paper [Wang-2007] discussed different views and models of entanglements. The following quotation describes, although not unanimously, the current view: "*the concept of localized entanglement coupling at a relatively small number of points, which lay at the hearth of classical theory, must give way to the view where the effect of entanglements is one that pervades the length of a molecule: the net result is one of topological constraints on chain motion of molecules. For sufficiently high molecular weight curvilinear motion alone is allowed*." [Klein-1978]. This view describes the effect, its spreading through the length of the chain constraining its motion to a tube. However, as pointed out by Martins

[Martins-2008], other constraints, not only of topological nature, may also explain the confinement of chain motion to a tube.

Even though the physical nature of entanglements is unknown, at least some of their effects on entangled polymer melts viscoelastic properties are identified. It is known from experiments that the molecular weight dependencies of zero shear rate viscosity, longest relaxation time and diffusion coefficient for entangled melts are

$$entangled\ melts: \quad \eta_0 \propto N^{3.4}; \quad \tau \propto N^{3.4}; \quad D \propto N^{-2.3} \quad . \tag{2.61}$$

The above dependencies clearly indicate that the dynamical behaviour of entangled polymers cannot be explained by Rouse model.

Although the theoretical framework used to explain viscoelastic linear and nonlinear behaviours of entangled polymer melts, which is based on reptation model and tube concept, had suffered several modifications to explain certain flow features that were not explained by the initial versions of reptation and tube model, it is clear that failures still exist in the current, and more sophisticated, theoretical formulations. Some of these failures will be mentioned below.

However, it seems clear (at least in part) the experimental evidence of reptation and confinement of chain motion to a tube. This is mainly because some predictions of reptation model were found to be close to the experimentally observed values. Some of theoretical modifications made on the initial model allowed also to explain other flow features. For example the 3.4 dependence on molecular weight of zero shear rate viscosity was explained by considering the effects of chain-end fluctuations. Although relevant and interesting, a detailed critical analysis of several modifications to reptation and tube models will be postponed to a future work. A superficial analysis of some aspects of these models that do not fit with experimental results was already presented [Martins-2006].

2.3.1. Reptation

Accounting for all interactions in the physical description of polymer melts (or concentrated solutions) flow is a complicated many-body problem that was simplified by Doi-Edwards with the introduction of ***tube*** model. Latter, de Gennes proposed the ***reptation*** theory to describe the movement of a chain inside the tube.

A simplified description of these two concepts may be the following. From the set of highly entangled chains a ***test chain*** is selected. The test chain interacts with neighbouring chains and a tube-like region is imagined that surrounds the test chain confining its movement into a tube-like region. The tube model assumes the following:

***i*)** The test chain is winding inside the tube. This assumption has to be considered because of the random coil model of polymer chains, which implies that the test chain has N independent (statistical) monomers each with length l. So far it is not required any assumption on the type of independent monomers of the test chain. They may be a monomer of the equivalent chain or of the Rouse chain.

***ii*)** The diameter of the tube involving the test chain changes along the tube and also in time.

***iii*)** These changes result from small movements of monomers in the test chain that occur within a short period of time.

***iv*)** For longer time scales the test chain can move along the tube and movements beyond the imposed constraints are forbidden.

***v*)** The head portion of the test chain is free to explore the next direction. As it moves out of the existing tube, a new section is added to it and at the same time the tail vacates a portion of the existing tube. Therefore, the overall change in the length of the tube with time is small.

The test chain contour length is L_t and the average square distance of the unperturbed chain is $\left\langle R_t^2 \right\rangle_0 = N_k l_k^2$. This test chain was described with the parameters of the equivalent chain. Often the test chain is described with the Rouse chain parameters, and identified with the equivalent chain, because of the self-similarity of Gaussian chains. It was shown above that this identification is wrong.

Since the *test chain* is constrained by other chains at the tube surface, and the physical nature of constraints is unknown, one has to consider another chain, *free from constraints*, moving inside the tube and sharing properties with the test chain. This new chain is the ***primitive chain***, also called ***primitive path***. It is also an ideal chain, with the same average square end-to-end distance as the test chain, $\left\langle R_p^2 \right\rangle_0 = \left\langle R_t^2 \right\rangle_0 = N_k l_k^2$, but, as it will be seen, with a different length, $L_p < L_t$. The primitive chain is a coarse grain view of the test chain. All small scale motions in the test chain are averaged to form the primitive chain – see Figure 2.6. Because this primitive chain is free from constraints it is treated as a Rouse chain and reptation is the unidimensional diffusion of this primitive chain inside the tube.

The primitive chain has Z sections ($Z \equiv$ number of entanglements in the chain $= N_k / N_e$) each with an average length a ($a \equiv$ tube diameter). The average square end-to-end distance of the primitive chain is

$$\left\langle R_p^2 \right\rangle = Za^2 = \left\langle R_t^2 \right\rangle = N_k l_k^2 \quad , \tag{2.62}$$

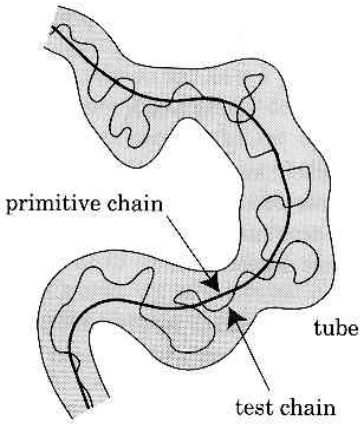

Figure 2.6. *Tube model with the test chain and the primitive chain.*

from which a relationship is obtained between the tube diameter and the Kuhn monomer segment length

$$a = \sqrt{N_e} l_k \quad , \tag{2.60}$$

where N_e is the number of random segments (each with the length of a Kuhn monomer) in a chain segment between entanglements.

The length of the primitive chain is

$$L_p = Za = \frac{N_k l_k^2}{a} = \frac{l_k}{a} L_t \quad . \tag{2.63}$$

For real chains the ratio (l_k/a) is between $0.1\,L_t$ and $0.4\,L_t$, but because chains are considered Gaussian, the difference between the two lengths is neglected.

The reptation time is defined as the time needed for the primitive chain to renew its encasing tube

$$\tau \approx \frac{\langle L_p^2 \rangle}{D_c} = \frac{\langle L_p^2 \rangle \zeta_{chain}}{k_B T} \quad , \tag{2.64}$$

or

$$\tau \cong \frac{(Z^2 a^2) Z \zeta_a}{k_B T} = \frac{Z^3 a^2 \zeta_a}{k_B T} \quad . \tag{2.65}$$

This reptation time was expressed only as a function of primitive chain parameters. Because Z is proportional to the number of chain segments (or polymer molecular weight), it is found that reptation time depends on the cube of polymer molecular weight.

As the primitive chain is an ideal chain free from constraints, the curvilinear diffusion coefficient is identified with the diffusion coefficient of the Rouse chain, eq. (2.47). Also, when the test chain is considered a Rouse chain, the average length of the primitive chain is related to the length of a Rouse (test) chain by

$$L_p = Za = \frac{N_R b_R^2}{a} = \frac{b_R}{a} L_t \quad . \tag{2.66}$$

Therefore the reptation time may also be expressed as a function of parameters of the Rouse chain as

$$\tau \approx \frac{\left\langle L_p^2 \right\rangle}{D_t} = \frac{N_R^3 \zeta_R}{k_B T} \frac{b_R^4}{a^2} \quad . \tag{2.67}$$

Because, as mentioned above, b_R is identified with the Kuhn monomer and the friction coefficient of a bead-spring section ζ_R is identified with ζ_k, the above equation is generally expressed as

$$\tau \cong \frac{l_k^2 \zeta_k}{k_B T} N_e^2 \left(\frac{N_k}{N_e} \right)^3 \quad , \tag{2.68}$$

and this relaxation time is related with the other relaxation times, τ_R, τ_e and τ_k. The relationships are the following [Rubinstein-2002]:

$$\tau = \tau_R Z = \tau_e \left(\frac{N}{N_e} \right)^3 = \tau_k N_e^2 \left(\frac{N}{N_e} \right)^3 \quad . \tag{2.69}$$

As mentioned above, this relationship relies on the (wrong) assumption that the number and length of Kuhn monomers in one chain are exactly the same as the number and length of Rouse "monomers" in the same chain.

An equation similar to (2.30), despite a numeric constant, might have been derived in a way similar to that used in the derivation of eq. (2.68) if the average square end-to-end distance was used instead of the average square length of the primitive chain length. This is the reason for the different dependence on the polymer chain molecular weight of eq. (2.30) for the Rouse relaxation time of the chain – in N^2 - and eq. (2.68) for the reptation time - in N^3. For the same reason, the prediction of reptation model for the molecular weight dependence of diffusion coefficient is $D \propto M^{-2}$. The experimental results for the molecular weight dependence of reptation time and diffusion coefficient were indicated in eq. (2.61).

An evident problem with the above definition of reptation time and other relaxation times is their temperature dependence. By assuming an Einstein relation for the diffusion coefficient, it is implicit a direct temperature dependence of relaxation time on the reciprocal of the temperature

$$\tau \propto \frac{\zeta}{T} \quad , \tag{2.70a}$$

and an indirect temperature dependence through the temperature dependence of ζ, which was already discussed in §2.2.4. Assuming, as it is considered in literature, that the temperature

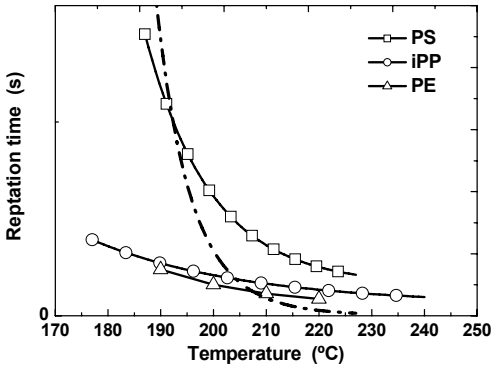

Figure 2.7. *Temperature variation of reptation time for PE, iPP and PS. Data from [Zhang-2006] and [Martins-2006]. The solid-dot line is the fit of eq. (2.70b) to reptation time data of iPP.*

dependence of ζ is given by eq. (2.39), or $\zeta = \zeta_0 \exp(-E_a/RT)$, where E_a is the flow activation energy and ζ_o the inherent friction factor, eq. (2.70a) may be fitted to experimental data in the form

$$\tau \propto \frac{\zeta_0}{T} e^{-E_a/RT} \quad . \tag{2.70b}$$

Experimental results for the temperature variation of reptation time are scarce. It is commonly accepted that the shift factors of reptation time at different temperatures with respect to a reference temperature follows an Arrhenius law. Therefore, attempts to account for their temperature dependence have been mainly restricted to applications of Arrhenius equations or to the temperature dependence of the monomeric friction coefficient on free volume, such as those mentioned in section §2.2.4. The temperature variation of reptation time for three different polymers is indicated in Figure 2.7. This time is evaluated experimentally from oscillatory shear experiments performed at the viscoelastic linear regime. The reptation time is defined at the reciprocal of the frequency at which the elastic and dissipative components of shear modulus intersect. The experimental data for iPP was fitted with eq. (2.70b), with E_a = 44 kJ/mol, the flow activation energy evaluated for iPP [Martins-2006]. The value obtained for the parameter ζ_o was 5.0×10^{-10} kg.s.

2.3.2. Reptation by changes in chains conformations

An alternative explanation of reptation process considers that reptation proceeds by conformational transitions, instead of a curvilinear diffusion of Rouse chain sections. In this description it is considered that the origin of sliding diffusion is caused by bond rotation and rearrangement of neighbouring units. A single-bond transition is shown in Figure 2.8 [Canpolat-1995].

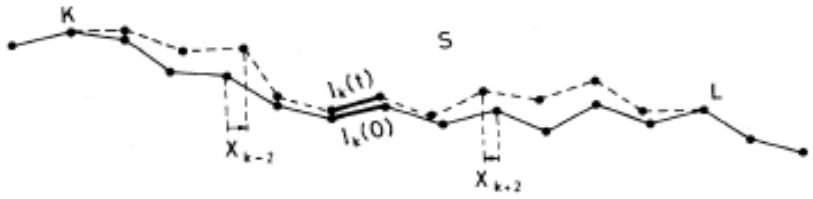

Figure 2.8. *The single-bond (I_k) transition and conformation change of the chain between points K and L. x_{k-2} and x_{k+2} are the displacement vectors of I_{k-2} and I_{k+2} bonds [Canpolat-1995].*

It is considered that the effective activation energy is molecular weight independent for long chains and that the conformational transition rate is described by a single energy barrier. A single-bond transition rate is expressed by

$$p = \nu_0 e^{-E/k_B T} \quad , \tag{2.71}$$

with v_o as intrinsic frequency of molecular vibration. The transition rate multiplied by time t and number of segments in the chain N gives Y_N, the *average number of single-bond transitions* in time t,

$$Y_N = tN\nu_0 e^{-E/k_B T} \quad . \tag{2.72}$$

The number of these transitions is considered small in comparison with the number of chain segments. Therefore, it is assumed that displacements caused by these transitions are confined to non-overlapping contours. If the average number of segments affected by a single bond transition is S, then the average number of segments displaced in time t is

$$\overline{Z}_N = Y_N S = tSN\nu_0 e^{-E/k_B T} \quad . \tag{2.73}$$

It is now considered that the displacement of a segment x_k is random and that the mean square displacement of the chain centre of mass $\left\langle X_{CM}^2 \right\rangle$ is described in terms of parameters of the equivalent (or any other) random chain. To be clear with the nomenclature, the expression obtained for $\left\langle X_{CM}^2 \right\rangle$ is

$$\left\langle X_{CM}^2 \right\rangle = \frac{1}{N^2}\left\langle \sum_{k=1}^{Z_N}\sum_{l=1}^{Z_N} x_k x_l \right\rangle = \frac{b^2}{N^2}\overline{Z}_N \tag{2.74}$$

where $N = M/m$ and $\left\langle x_k x_l \right\rangle = b^2\delta_{kl}$.

The mean square value of the displacement of the centre of mass along the contour, is related to the chain diffusion coefficient by Fick's law (see eq. 4.8 in [Canpolat-1995]), from which the relaxation time (reptation time) obtained as:

$$\tau_r = \frac{N^3 a^2}{b^2 \nu_0 S} e^{E/k_B T} \quad . \tag{2.75}$$

Similarly to eqs. (2.65) and (2.67), this relaxation time shows the dependence on molecular mass of N^3. In addition it shows a temperature dependence on the energy barrier for

conformational transition $e^{E_a/RT}$. This equation gives a qualitative better fit to experimental results of Figure 2.7 than eqs. (2.65) or (2.67), because the diffusion coefficient was evaluated from the Fick's law of diffusion, instead of using the Einstein relation for this coefficient, which is the reason for the (1/T) factor in these equation. A more detailed discussion of this alternative procedure for evaluation the reptation time will be postponed to a future work.

2.3.3. Other modifications of tube model and reptation

The sections above in this work illustrate the complexity and difficulties in the modelling of chain conformations in polymer melts and its change with flow. Although it seems clear that experimental evidences exist for the chain confinement to a tube, and in part also for reptation, there are many unclear aspects of reptation model some of which were presented above.

Some flow features were not explained by the tube model and reptation. Among them are the 3.4 dependence of zero shear rate viscosity on molecular weight. Also, reptation time values predicted by tube model are larger than the values measured with experiments and reptation theory does not explain many feature of the nonlinear viscoelastic flow behaviour of polymer melts. Several relaxation mechanisms were therefore considered to explain these failures. Among these mechanisms are the *contour length fluctuations*, the quick *extension of the chain* due to an external force and *chain retraction*, the *constraint release* caused by disentanglement due to reptation motion. A scheme with the different mechanisms is shown in Figure 2.9.

The inset in this figure illustrates three physical processes of polymer dynamics in a constraining tube. Under reptation the whole chain diffuses randomly along the tube (solid line). Under contour length fluctuations (CLF) the chain ends explore new tube configurations. This relaxation process occurs without the chain centre of mass motion (reptation) and by means of longitudinal fluctuations of the total entangled tube length. Therefore, as a result of this relaxation process the tube length fluctuations $\left\langle \Delta L^2 \right\rangle^{1/2}$ should be subtracted from $\left\langle L^2 \right\rangle$ to yield a corrected reptation time

$$\tau \approx \frac{\left\langle L_p - \Delta L_p \right\rangle^2}{D_t} \propto Z^3 \left(1 - \frac{1.5}{\sqrt{Z}} \right)^2 \quad . \tag{2.76}$$

A plot of the right-hand side of the above equation for $10 \le Z \le 100$ is in Figure 2.10. The constant 1.5 is evaluated from detailed calculations [Doi-1996, Watanabe-1999]. It can be seen that this correction explains the 3.4 dependence of reptation time (and also of zero shear rate viscosity) on polymer molecular weight.

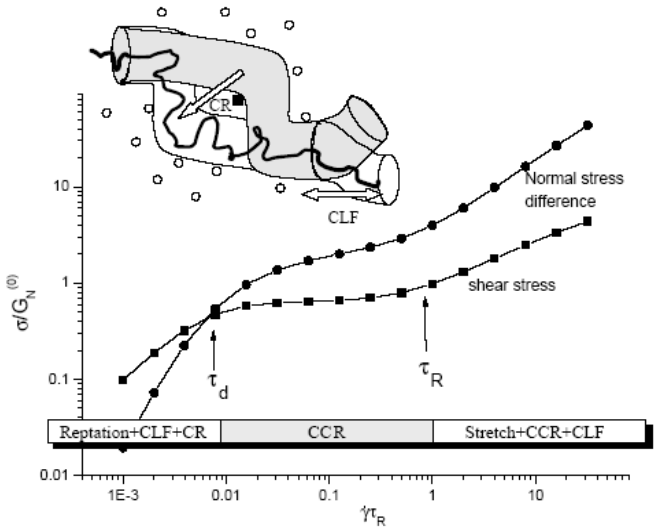

Figure 2.9. *Illustration of the shear rate regions at which different tube-dynamic processes dominate. The shear stress and the first normal stress difference are plotted as a function of shear rate. Reptation moderated by contour length fluctuations (CLF) dominates the pseudo-newtonian regime at low shear rates. When shear rates are faster than the reciprocal of reptation time, the mechanism of convective constraint release (CCR) causes the shear stress to level off at a plateau. At high shear rates, faster than the slowest contour length fluctuation mode (CLF), the chains start to stretch and the shear stress rises again. Inset: Tube before relaxation (shaded); tube after relaxation (white) [Bent-2003].*

The other mechanism indicated in the inset is constraint release (CR), which may be thermal and convective. Under thermal constraint release an entanglement with a neighbouring chain, shown in the figure by a solid square, may disappear, allowing relaxation of that part of the tube without reptation.

Different theoretical approaches exist to explain the above mechanisms, and to each one a different physical description is associated. Watabane [Watanabe-1999] gives a detailed review. A more updated analysis of existing problems with reptation theory and different versions of tube model were provided by McLeish *et al.* [MacLeish-2002, Graham-2006]. A fuller account of these developments is outside the scope of this work. Some failures of the above models and mechanisms were already presented [McLeish-2003, Wang-2003a,

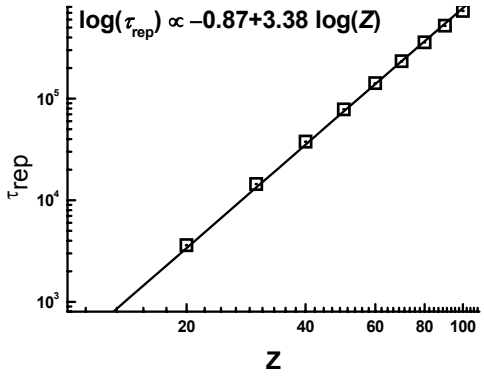

Figure 2.10. *Plot of eq. (2.76) for the variation of reptation time with the number of sections in the tube (or polymer molecular weight) after accounting for contour length fluctuations.*

Wang-2003b, Wang-2007, Martins-2006].

As shown in ref. [Watanabe-1999], all above mechanisms contribute for a decrease of the reptation time evaluated from the Doi-Edwards original theory. Regardless the mechanism, or association of mechanisms considered by the different versions of tube model, it is always implicitly assumed that the number of constraints imposed by the surrounding chains to the test chain is constant. Exceptions are formulations of tube models considering that topological constraints act as slip-links. For some relaxation processes, such as the chain stretch, it is also considered an increase in the number of constraints with the primitive path length of the test chain.

Experimental results obtained by different research groups [Tapadia-2004, Martins-2006], indicate that the number of constraints to the flow is not constant. It decreases when the melt is sheared up to steady-state. This decrease was quantified and it is between 2/3 and 1/2 of the initial constraints. These results question one basic assumption of tube models. Other problems with the different relaxation mechanisms considered were also discussed [Martins-2006].

The Doi-Edwards theory for the reological properties of entangled polymer melts predicts with good agreement the response to large step-shear, but fails the description of nonlinear shear properties [Mead-1998, Mhetar-1999] for a range of shear rate $\dot{\gamma}$ above $1/\tau_d$. The experiments demonstrate that shear stress is almost constant for highly entangled melts or increases slowly with $\dot{\gamma}$. DE theory predicts a maximum in shear stress and an asymptotic decreases with $\dot{\gamma}$ as $\dot{\gamma}^{-0.5}$. Also experimental curves of shear viscosity vs. $\dot{\gamma}$ for different M_w merge in the high-shear-rate nearly into a single curve (which shows weak dependence of $\eta(\dot{\gamma})$ on M_w), while DE predicts a decrease of viscosity with increasing of M_w. Most of the

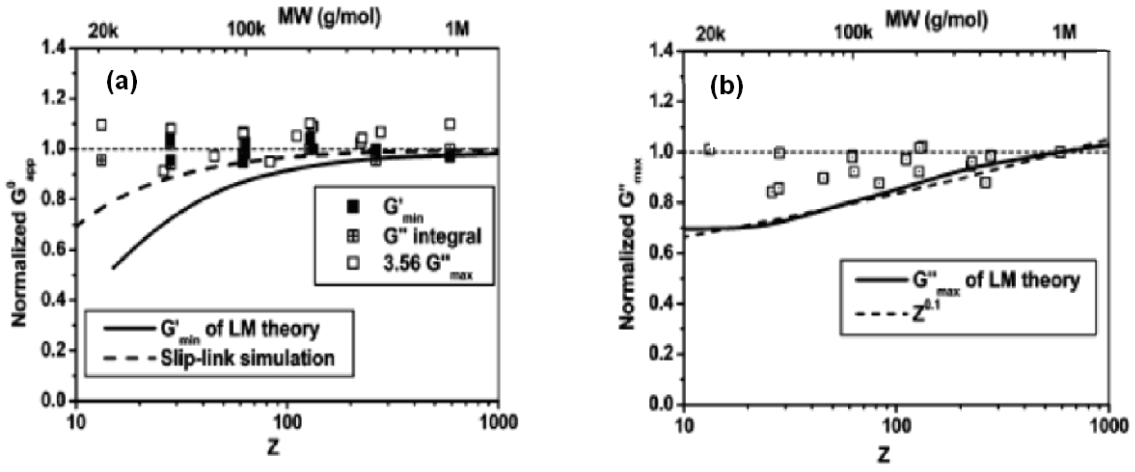

Figure 2.11. *(a) Normalized G^0_{app} (by G_N^0 = 1.15 MPa) and (b) G''_{max} (by G_N^0 = 0.35 MPa) vs. number of entanglements and molecular weight. The dashed line corresponds to the slope $Z^{0.1}$ and solid – LM theory [Liu-2006b].*

failings occur because the theory predicts that in fast flow there is orientation of tube into the flow direction.

A recent analysis of the different modifications of tube model was done by the group of Baily and Keunings *et al.* [Liu-2006a, Liu-2006b]. As shown in Figure 2.11, the molecular weight and number of entanglements Z dependence of G_N^0 and G'' (normalized by G_N^0 = 1.15 MPa, according to [Fetters-1994]) is very weak $G_{N,\exp}^0 \sim Z^{0.01\text{-}0.015}$, and lower than predictions of different versions of tube-based models such as the Likhtman-McLeish model [Likhtman-2000]. It was considered that the main reason for this discrepancy is the overestimation of CLF effect which should be less important for chains with low number of entanglements.

2.4. Conclusions

The discussion made above raises a question that was advanced by many researchers working in this area, which is if a new physics [McLeish-2003] or another tube model [Likhtman-2000] should be needed to describe flow dynamics of polymer melts. It seems that the answer lies on if the random coil model and topological constraints are an adequate description of polymer melt morphology.

2.5. Appendix

The above sections intend to illustrate the complexity and difficulties of modelling chain conformations in polymer melts, its change with flow, as well as the degree of complexity and limitations of current flow models. Part of these difficulties resulted from different formulations and nomenclature adopted by different authors. An attempt to correct some common mistakes and standardize the nomenclature was made in a recent work [Larson-2003], which followed the nomenclature of Rubinstein and Colby [Rubinstein-2003].

Three topics will be presented in this appendix without the discussion made previously. They are evaluation of plateau modulus, the concept of packing length and the number of entanglement strands per cubed tube diameter.

2.5.1 Determination of plateau modulus

A key parameter to all flow models is the plateau modulus (G_N^0), which allows the evaluation of chain molecular weight between entanglements, and therefore the tube diameter. A critical review of different methodologies and equations used for its evaluation was presented recently [Fetters-2005, Liu-2006a].

Generally, G_N^0 is determined by measuring linear viscoelastic properties in oscillatory shear experiments. From these experiments, the plateau modulus may be evaluated by one of the methods presented below.

1 – It may be determined from the values of G' at a frequency where G'' reaches a minimum, ω_{min} (see Figure 2.12a) [Watanabe-1999, Ferry-1980]. Because the slope of G' in the plateau region increases with increasing polydispersity, and the negative slope of G'' at the high-frequency side of the terminal peak is decreasing, ω_{min} is poorly defined, influencing therefore the corresponding evaluation of G'. By this reason, this method was modified [Wu-1987, Wu-1992, Wu-1989, Eckstein-1998], and G_N^0 was obtained from the storage modulus, where tan δ reaches minimum in the plateau zone (see Figure 2.12b): $G_N^0 = (G')_{\tan\delta \to \min}$.

2 – The second method is similar to the first one, but a Van Gurp-Palmen plot is constructed instead [Van Gurp-1998]. In this plot the phase angle, δ, is plotted against the absolute value of the complex modulus $|G^*(\omega)|$. The minimum in the plot defines the plateau modulus value (Figure 2.12c).

3 – The third method involves the numerical integration of the loss modulus G'' in the terminal zone,

$$G_N^0 = \left(\frac{2}{\pi}\right)\int_{-\infty}^{\infty} G''(\omega) g \ln(\omega) \quad . \tag{2.77}$$

Determination of plateau modulus by this method is unaffected by MWD, but it requires a molecular weight of at least 50 times M_e to separate the terminal zone from the high frequency motion [Ferry-1980, Sanders-1969]. Since for polydisperse polymers the terminal relaxation spectrum is broad, and some authors argued that the loss modulus peak should be symmetric, a simplification was proposed, where twice the area of the peak up to the frequency of the maximum is taken [Onogi-1970, Wu-1985]:

$$G_N^0 = \frac{4}{\pi}\int_{-\infty}^{\omega_{\max}} G''(\omega) g \ln(\omega) \quad . \tag{2.78}$$

This equation gives a value lower than that obtained with (2.77) because the true peak is always skewed towards high frequencies, but it can be used especially in some cases where there is not enough experimental data at high frequencies.

4 –The method of Raju–Rachapudy-Graessley [Raju-1979] is based on an empirical "universal" terminal spectrum inferred from observations of different monodisperse polymer species (Figure 2.12d). The area under the loss modulus peak divided by the maximum of the G'' terminal peak yields a universal proportionality constant *K*:

$$\frac{G_N^0}{G''_{\max}} = 2.303\left[\frac{2}{\pi}\int_{-\infty}^{+\infty}\frac{G''(\omega/\omega_{\max})}{G''_{\max}}d\log(\omega/\omega_{\max})\right] = K \quad . \tag{2.79}$$

For polymers with monodisperse molecular weight distribution the constant *K* is equal to 3.56 and the plateau modulus is determined from

$$G_N^0 = 3.56G''_{(\max)} \quad . \tag{2.80}$$

5 – Another method was developed by Wu [Wu-1989]. The crossover parameter in the terminal zone ($G_x = G' = G''$) is correlated with the sample molecular weight in terms of MWD. For MWD ≤ 3 the relation is

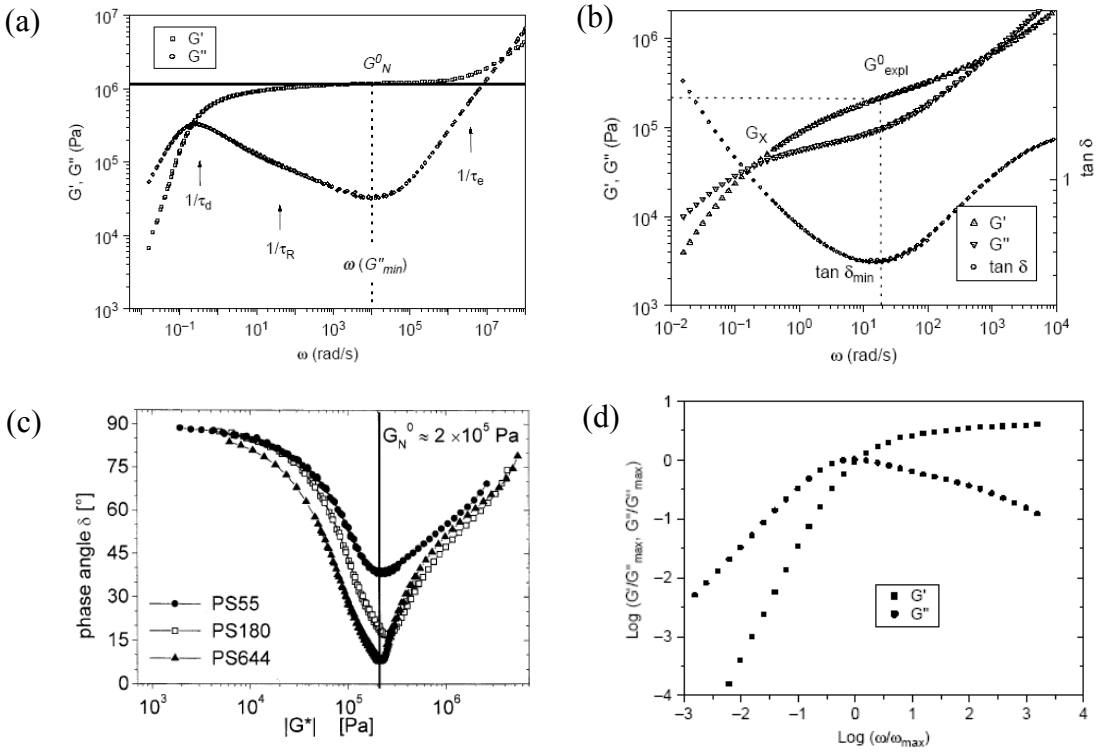

Figure 2.12. *Master curves of the storage and loss modulus for (a) polybutadiene with M_w = 410 kg/mol [Wang-2003b] and (b) polyisobutylene with M_v = 85 kg/mol [Liu-2006a]. (c) The van Gurp-Palmen plot of three polystyrene samples with different molecular weight (numbers following "PS" denotes M_w in kg/mol) [Trinkle-2001]. (d) Universal terminal relaxation spectrum for monodisperse polymers [Raju-1981]*

$$\log\left(\frac{G_N^0}{G_x}\right) = 0.38 + \frac{2.63\log\dfrac{M_w}{M_n}}{1+2.45\log\dfrac{M_w}{M_n}} \quad . \tag{2.81}$$

This method was proposed especially for polymers for which above equations did not work because the minimum and maximum of G'' are indistinct or G'' have very limited dynamic window.

For long-chain monodisperse polymer samples, methods 1, 3 and 4 show excellent agreement with an error of 5-10 % which is close to the experimental uncertainty.

2.5.2. The packing length

Witten *et al.* [Witten-1989] introduced the concept of packing length, p, defined as the ratio of the chain volume, V, and the squared unperturbed end-to-end chain distance $\left\langle R^2\right\rangle_0$:

$$p = \left[\frac{V}{\left\langle R^2\right\rangle_0}\right] = \left[\frac{M}{\left\langle R^2\right\rangle_0 \rho N_A}\right] = \left[\frac{V_e M}{\left\langle R^2\right\rangle_0 M_e}\right] = \left[\frac{V_b M_e}{\left\langle R^2\right\rangle_0 m_b}\right] \quad , \tag{2.82}$$

where N_A is Avogadro's number, V_b is volume per bond, m_b is average molecular weight per backbone bond and ρ is the density [Fetters-1999].

Fetters *et al.* [Fetters-1994] established the relationships between the packing length and the molecular weight between entanglements, plateau modulus (see Figure 2.13a) and the tube diameter. These relationships are:

$$M_e = \frac{p^3 \rho N_A}{B^2} \quad , \tag{2.83}$$

$$G_N^0 = \frac{4}{5}\frac{B^2 kT}{p^3} \quad , \tag{2.84}$$

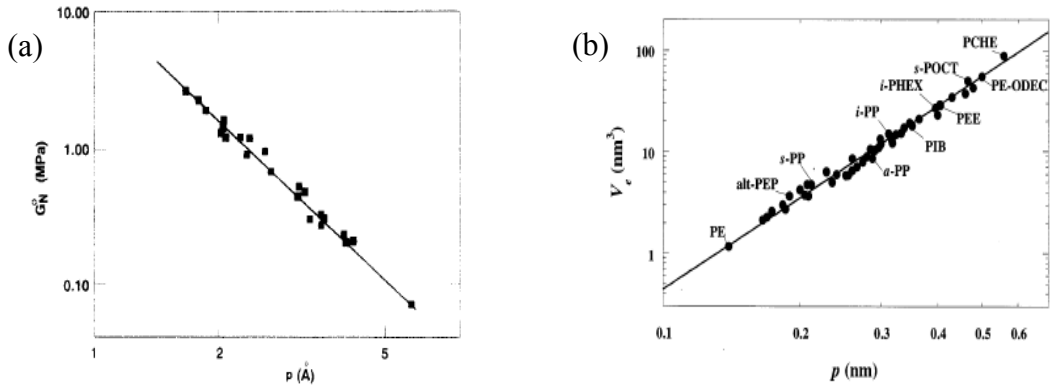

Figure 2.13. *The dependence of plateau modulus (a) and volume of a chain segment between entanglements (b) versus packing length for different polymers at 413 K [Fetters-2002].*

$$a = \frac{p}{B} \quad , \tag{2.85}$$

where $B = 2A/\sqrt{6^3}$, and A is a constant of order unity. Since A is dependent on temperature ($A = \left[5\left(6^3 G_N^0 p^3\right)/kT\right]^{1/2}$, evaluated by least-squares linear regression of G_N^0 vs p^{-3} for 26 polymers with SANS-measured chain dimensions) it gives information that there is a contribution from unknown dynamical events, which is against the model.

Also, the volume of a chain segment between entanglements can be expressed as a function of the packing length (see Figure 2.13b):

$$V_e = \nu_0 N_e = a^2 p \quad , \tag{2.86}$$

where N_e is the number of Kuhn monomers in an entanglement strand, a is the tube diameter and v_0 is the Kuhn monomer volume. From the Figure 2.13b and eq. (2.86) it was concluded that that tube diameter is the same for all polymers indicated (the slope is constant and equal to a^2). This way the chemical structure of polymer is related to their basic physical properties by packing length, where degree of entanglements is predicted basing on their chain dimension and density.

$$G_N^0 = \frac{kT}{V_e} = \frac{kT}{a^2 p} \quad . \tag{2.87}$$

2.5.3. The number of entanglement strands per cubed tube diameter

The number of entanglement strands per unit volume is defined as:

$$n_v = \rho N_A / M_e \quad . \tag{2.88}$$

It shows the relationship between the size of polymer coils and the degree to which they are entangled with each other; the larger is the chain, the greater number of the other chains it will

Table 2.4. *Experimental values of parameters described above for typical polymers at different temperatures [Fetters-1996].*

polymer	T	ρ	G_N^0	$\langle R^2\rangle_0/M$	ν_0	p	M_e	a	N_e	V_e	n_t
	K	g cm^{-3}	MPa	Å^2	Å^3	Å	kg/mol	Å	-	nm^3	calc
PE	298	0.851	3.5	1.40	329	1.39	602	29.0	3.58	1.18	21.4
	413	0.785	2.6	1.25	318	1.69	1,040	36.0	6.89	2.28	21.3
a-PP	298	0.852	0.48	0.678	358	2.88	4,390	54.6	23.9	8.57	18.6
	348	0.825	0.48	0.678	369	2.97	4,970	58.1	27.1	-	-
	413	0.791	0.47	0.678	385	3.10	5,780	62.6	31.5	12.1	19.9
	463	0.765	0.42	0.678	398	3.20	7,010	68.9	38.2	15.2	21.1
i-PP	463	0.766	0.43	0.694	407	3.12	6,850	69.0	36.5	14.9	22.1
s-PP	463	0.766	1.35	1.03	604	2.10	2,180	47.4	7.83	2.74	22.6

encounter and with it might entangle [Fetters-1994, Fetters-1999].

The number of entanglement strands per cubed tube diameter, n_t, is obtained by multiplying the number of entanglement strands per unit volume by the cube of the tube diameter. This dimensionless quantity should therefore be a universal constant for all polymers providing that tube diameter is determined only by the number of chain segments between constraints. A relationship between n_t and the packing length was established and n_t was calculated by Lin [Lin-1987] for different polymers.

$$n_t = n_v a^3 = \frac{\rho N}{M_e}\left[C_\infty \frac{M_e}{m} b^2\right]^{3/2} = \left[\frac{M_e \left\langle R^2 \right\rangle_0}{M}\right]^{1/2} p^{-1} = \left[\frac{kT}{p^3 G_N^0}\right]^{1/2} \quad . \tag{2.89}$$

G_N^0 and V_e expressed in term of p and n_t are equal:

$$G_N^0 = \frac{\rho RT}{M_e} = \left[\frac{kT}{n_t^3 p^3}\right] \cong 0.032 T p^{-3} \quad , \tag{2.90}$$

$$V_e = \frac{M_e}{\rho N_a} = \frac{kT}{G_N^0} = n_t^2 p^3 \quad . \tag{2.91}$$

Values obtained shown in Table 2.4 indicate that n_t is approximately equal to 22, confirming that apparently a universal constant may be established for polymer chains that relates the entanglement density and the volume of a tube section between constraints.

2.6. References

Bent-2003 Bent J, Hutchings LR, Richards RW, Gough T, Spares R, Coates PD, Grillo I, Harlen OG, Read DJ, Graham RS, Likhtman AE, Groves DJ, Nicholson TM, McLeish TCB (2003) *Neutron-mapping polymer flow: scattering, flow visualisation and molecular theory*. Science 301:1691-1695.

Berry-1968 Berry GC, Fox TG (1968) *The viscosity of polymers and their concentrated solutions.* Adv Polym Sci 5:261-357.

Boothroyd-1991 Boothroyd AT, Rennie AR, Boothroyd CB (1991) *Direct measurement of the temperature dependence of the unperturbed dimensions of a polymer.* Europhys Lett 15:715-719.

Butera-1991 Butera R, Fetters LJ, Huang JS, Richter D, Pyckhout-Hintzen W, Zirkel A, Farago B, Ewen B (1991) *Microscopic and macroscopic evaluation of fundamental facets of the entanglement concept*. Phys Rev Lett 66:2088-2091.

Canpolat-1995 Canpolat M, Erzan A, Peckan Ö (1995) *Reptation of polymer chain by conformal transition in the entangled regime*. Physical review E 52:6904-6907.

Cerf-1958 Cerf R (1958) *Statistical mechanics of chain macromolecules in a velocity field*. J de Phys Radium 19:122-134.

Colby-1987 Colby RH, Fetters LJ, Graessley WW (1987) *Melt-viscosity molecular weight relationships for linear polymers*. Macromolecules 20:2226-2237.

Ding-2004a Ding Y, Kisliuk A, Sokolov AP (2004) *When does a molecule become a polymer?* Macromolecules 37:161-166.

Ding-2004b Ding Y, Sokolov AP (2004) *Comment on the dynamic bead size and Kuhn segment length in polymers: example of polystyrene*. J Polym Sci, Polym Phys 42:3505-3511.

Doi-1986 Doi M, Edwards SF (1986) *The theory of polymer dynamics*. Oxford University Press. New York.

Doi-1996 Doi M (1996) *Introduction to polymer physics.* Clarendon Press. Oxford.

Eckstein-1998 Eckstein A, Suhm J, Frederich C, Maier RD, Sassmannshausen J, Bochmann M, Mülhaupt R (1998) *Determination of plateau moduli and entanglement molecular weights of isotactic, syndiotactic, and atactic polypropylenes synthesized with metallocene catalysts.* Macromolecules 31:1335-1340.

Ferry-1980 Ferry JD (1980) *Viscoelastic properties of polymers*. Wiley. New York.

Fetters-1994 Fetters LJ, Lohse DJ, Richter D, Witten TA, Zirkel A (1994) *Connection between polymer molecular weight, density, chain dimensions, and melt viscoelastic properties*. Macromolecules 27:4639-4647.

Fetters-1996 Fetters LJ, Lohse DJ, Colby RH (1996) *Chain dimensions and entanglement spacings.* Physical Properties of Polymers Handbook 2E. AIP Press New York.

Fetters-1999 Fetters LJ, Lohse DJ, Milner ST (1999) *Packing length influence in linear polymer melts on the entanglement, critical, and reptation molecular weights*. Macromolecules 32:6847-6851.

Fetters-2002 Fetters LJ, Lohse DJ, García-Franco CA, Brant P, Richter D (2002) *Prediction of melt state poly(α-olefin) rheological properties: the unsuspected role of the average molecular weight per backbone bond*. Macromolecules 35:10096-10101.

Fetters-2005 Fetters LJ, Lee JH, Mathers RT, Hustad PD, Coates GW, Archer LA, Rucker SP, Lohse DJ (2005) *Influence of syndiotactic propylene units on the rheological parameters of poly(ethylene-propylene) copolymers*. Macromolecules 38:10061-10066.

Flory-1949 Flory PJ (1949) *The configuration of real polymer chains*. J Chem Phys 17:303-310.

Flory-1953 Flory PJ (1953) *Principles of polymer chemistry*. Cornell University Press.

Flory-1979 Flory PF (1979) *Introductory lecture: levels of order in amorphous polymers*. Faraday Discuss. Chem. Soc. 68:14-25.

Flory-1989 Flory PJ (1989) *Statistical mechanics of chain molecules*. Hanser. Munich.

Gabrys-1994 Gabrys B (1994) *Long history of short-range order in polymers*. TRIP 2:2-4.

Geil-1975 Geil PH (1975) *Morphology of amorphous polymers*. Ind Eng Chem. Prod Res Dev 14:59-71.

Geil-1979 Geil PH (1979) *Additional remark*. Faraday Discuss Chem Soc 68:141-144.

de Gennes-1967 de Gennes PG (1967) *Quasi-elastic scattering of neutrons by dilute polymer solutions: I. Free-draining limit.* Physics 3:37-45.

de Gennes-1976 de Gennes PG (1976) *Dynamics of entangled polymer solutions. I. The Rouse model.* Macromolecules 9:587-893.

de Gennes-1979 de Gennes PG (1979) *Scaling concepts in polymer physics*. Cornell University Press.

de Gennes-2003 de Gennes PG (2003) *Simple views on condensed matter*, 3rd edition, Series in Modern Condensed Matter Physics 12, World Scientific Publishing Co. Singapore.

Graham-2006 Graham RS, Bent J, Hutchings LR, Richards RW, Groves DJ, Embery J, Nicholson TM, McLeish TCB, Likhtman AE, Harlen OG, Read DJ, Gough T, Spares R, Coates PD, Grillo I (2006) *Measuring and predicting the dynamics of linear monodisperse entangled polymers in rapid flow through an abrupt contraction. A Small Angle Neutron Scattering Study*. Macromolecules 38:2700-2709.

Grosberg-1994 Grosberg AY, Kholkhlov AR (1994) S*tatistical physics of macromolecules*. NY American Institute of Physics Press.

Van Gurp-1998 Van Gurp M, Palmen J (1998) *Time-temperature superposition for polymeric blends*. Rheol Bull 67:5-8.

Hess-1988 Hess W (1988) *Generalized Rouse theory for entangled polymeric liquids*. Macromolecules 21:2620-2632.

Higgins-1985 Higgins JS, Roots JE (1985) *Effects of entanglements on the single motion of polymer molecules in melt samples observed by neutron scattering*. J Chem Soc. Faraday Trans 81:757-787.

Higgins-1994 Higgins JS, Benoit HC (2002) *Polymers and neutron scattering*. Oxford University Press. New York.

Inoue-1991 Inoue T, Okamoto H, Osaki K (1991) *Birefringence of amorphous polymers. A. Dynamic measurement on polystyrene*. Macromolecules 24:5670-5675.

Inoue-2002 Inoue T, Uematsu T, Osaki K (2002) *The significance of the Rouse segment: its concentration dependence*. Macromolecules 35:820-826.

Iwata-1971 Iwata K (1971) *Irreversible statistical mechanics of polymer chains. I. Fokker-Planck diffusion equation.* J Chem Phys 54:12-26.

Kawakatsu-2004 Kawakatsu T (2004) *Statistical physics of polymers: an introduction*. Springer-Verlag Berlin Heidelberg.

Klein-1978 Klein J (1978) *Evidence for reptation in an entangled polymer melt*. Nature 271:143-145.

Kopf-1997 — Kopf A, Dunweg B, Paul W (1997) *Dynamics of polymer "isotope" mixtures: molecular dynamics simulations and Rouse model analysis*. J Chem Phys 107:6945-6955.

Krishnamoorti-2002 — Krishnamoorti R, Graessley WW, Zirkel A, Richter D, Hadjichristidis N, Fetters LJ, Lohse DJ (2002) *Melt-state polymer chain dimensions as a function of temperature.* J Polym Sci. Part B. Polym Phys 40:1768-1776.

Larson-2003 — Larson RG, Sridhar T, Leal LG, McKinley GH, Likhtman AE, McLeish TCB (2003) *Definitions of entanglement spacing and time constants in the tube model*. J Rheol 47:809-818.

Likhtman-2000 — Likhtman AE, Milner ST, McLeish TCB (2000) *Microscopic theory for the fast flow of polymer melts*. Phys rev lett 85:4550-4553.

Lin-1987 — Lin Y-H (1987) *Number of entanglement strands per cubed tube diameter, a fundamental aspect of topological universality in polymer viscoelasticity*. Macromolecules 20:3080-3083.

Liu-2006a — Liu C, He J, van Ruymbeke E, Keunings R, Bailly C (2006) *Evaluation of different methods for the determination of the plateau modulus and the entanglement molecular weight*. Polymer 47:4461-4479.

Liu-2006b — Liu C, He J, Keunings R, Bailly C (2006) *Do tube models yield consistent predictions for the relaxation time and apparent plateau modulus of entangled linear polymers?* Macromolecules 39:3093-3097.

MacLeish-2002 — McLeish TCB (2002) *Tube theory of entangled polymer dynamics*. Adv Phys 51:1379-1527.

McLeish-2003 — McLeish TCB (2003) *Present puzzles of entangled polymers*. Rheology Reviews 8:197-233.

Martins-2006 — Martins JA, Zhang W, Brito AM (2006) *Saturation of shear-induced isothermal crystallization of polymers at the steady state and the entanglement-disentanglement transition*. Macromolecules 39:7626-7634.

Martins-2008 — Martins JA (2008) *Discussions on the validity of random coil model for polymer melts and demonstration of failures in Rouse model description of polymer chain dynamics at the molten state*. To be submitted.

Mattice-1999 — http://gozips.uakron.edu/~mattice/ps674/c.html webpage of Mattice WL

Mattice WL, Suter UL (1994) *Conformational theory of large molecules – the rotational isomeric state model in macromolecular systems*. John Wiley & Sons.

Mattice-2003 — Mattice WL, Helfer CA, Sokolov AP (2003) *On the relationship between the characteristic ratio of a finite chain, C_n, and the asymptotic limit, C_∞.* Macromolecules 36:9924-9928.

Mays-1985 — Mays JW, Hadjichristidis N, Fetters LJ (1985) *Solvent and temperature influences on polystyrene unperturbed dimensions*. Macromolecules 18:2231-2236.

Mead-1998 — Mead DW, Larson RG, Doi M (1998) *A molecular theory for fast flows of entangled polymers*. Macromolecules 31:7895-7914.

van Meerveld-2004 van Meerveld J (2004) *Modified constraint release in molecular based reptation models for fast flows*. J Non-Newtonian Fluid Mech 122:263–272.

Mhetar-1999 Mhetar V, Archer LA (1999) *Nonlinear viscoelasticity of entangled polymeric liquids*. J Non-Newtonian Fluid Mech 81:71-81.

Nicholson-1981 Nicholson LK, Higgins JS, Hayter JB (1981) *Dynamics of dilute polymer solutions*. Macromolecules 14:836-843.

Onogi-1970 Onogi S, Masuda T, Kitagawa K (1970) *Rheological properties of anionic polystyrenes. I. Dynamic viscoelasticity of narrow-distribution polystyrenes*. Macromolecules 3:109-116.

Paul-1997 Paul W, Smith GD, Yoon DY (1997) *Static and dynamic properties of a n-$C_{100}H_{202}$ melt from molecular dynamics simulations*. Macromolecules 30:7772-7780.

Paul-1998 *Paul W, Smith GD, Yoon DY, Farago B, Rathgeber S, Zirkel A, Willner L, Richter D (1998)* Chain motion in an unentangled polyethylene melt: a critical test of the Rouse model by molecular dynamics simulations and neutron spin echo spectroscopy. *Phys Rev Lett 80:2346-2349.*

Pearson-1987 *Pearson DS, Ver Stratae G, von Meerwall E, Schilling FC (1987)* Viscosity and self-diffusion coefficient of linear polyethylene. *Macromolecules 20:1133-1141.*

Pearson-1994 *Pearson DS, Fetters LJ, Graessley WW, Ver StrataeG, von Meerwall E (1994)* Viscosity and self-diffusion coefficient of hydrogenated polybutadiene. *Macromolecules 27:711-719.*

Privalko-1974 *Privalko VP, Lipatov YS (1974)* "Entanglement" concept and chain conformation in bulk amorphous polymers. *Makromol Chem 175:641-652.*

Raju-1979 Raju VR, Rachapudy H, Graessley WW (1979) *Properties of amorphous and crystallizable hydrocarbon polymers. IV. Melt rheology of linear and star-branched hydrogenated polybutadiene.* J Polym Sci: Polym Phys Ed 17:1223-1235.

Raju-1981 Raju VR, Menezes EV, Marin G, Graessley WW, Fetters LJ (1981) *Concentration and molecular weight dependence of visco- elastic properties in linear and star polymers.* Macromolecules 14:1668-1676.

Richter-1989 *Richter D, Ewen B, Farago B, Wagner T (1989)* Microscopic dynamics and topological constraints in polymer melts: a neutron spin-echo study. *Phys Rev Lett 61:2140-2143.*

Richter-1990 *Richter D, Farago B, Fetters LJ, Huang JS, Ewen B, Lartigue C (1990)* Direct microscopic observation of entanglement distance in a polymer melt. *Phys Rev Lett 64:1389-1392.*

Richter-1993 *Richter D, Willner L, Zirkel A, Farago B, Fetters LJ, Huang JS (1993)* Onset of topological constraints on polymer melts: a mode analysis by neutron spin echo spectroscopy. *Phys Rev Lett 71:4158-4161.*

Richter-1994 Richter D, Willner L, Zirkel A, Farago B, Fetters LJ, Huang JS (1994) *Polymer motion at the crossover from Rouse to reptation dynamics*. Macromolecules 27:7437-7446.

Rojo-2004 Rojo E, Muñoz ME, Santamaría A, Peña B (2004) *Correlation between conformational parameters and rheological properties of molten syndiotactic polypropylenes*. Macromol Rapid Commun 25:1314-1318.

Rouse-1953 Rouse PE (1953) *A theory of the linear viscoelastic properties of dilute solutions of coiling polymers*. J Chem Phys 21:1272-1280.

Rouse-1998 Rouse PE (1998) *A theory of the linear viscoelastic properties of dilute solutions of coiling polymers. II. A first order mechanical thermodynamic property*. J Chem Phys 108:4628-4633.

Rubinstein-2002 Rubinstein M, Panyukov S (2002) *Elasticity of polymer networks*. Macromolecules 35:6670-6686.

Rubinstein-2003 Rubinstein M, Colby RH (2003) *Polymer physics*. Oxford University Press, New York.

Sanders-1969 Sanders JF, Ferry JD (1969) *Polymer entanglement spacings estimated from integration of the loss compliance.* Macromolecules 2:440-442.

Smith-1997 Smith GD, Paul W, Yoon DY, Zirkel A, Hendricks J, Richter D, Schober H (1997) *Local dynamics in a long-chain alkane melt from molecular dynamics simulations and neutron scattering experiments*. J Chem Phys 107:4751-4755.

Smith-2001 Smith GD, Paul W, Monkenbusch M, Richer D (2001) *On the non-gaussianity of chain motion in unentangled polymer melts.* J Chem Phys 114:4285-4288.

Sperling-2001 Sperling LH (2001) *Introduction to physical polymer science*. 3rd edition. J Wiley & Sons, New York.

Strobl-1996 Strobl G (1996) *The physics of polymers – concepts for understanding their structures and behaviour*. Springer-Verlag Berlin Heidelberg.

Tapadia-2004 Tapadia P, Wang S-Q (2004) *Nonlinear flow behaviour of entangled polymer solutions: yieldlike entanglement-disentanglement transition*. Macromolecules 37:9083-9095.

Teraoka-2002 Teraoka I (2002) *Polymer solutions – an introduction to physical properties*. J Wiley & Sons. New York.

Trinkle-2001 Trinkle S, Friedrich C, *Van Gurp-Palmen plot: a way to characterize polydispersity of linear polymers*. Rheol Acta 40:322-328.

Uhlmann-1979 Uhlmann DR (1979) *Electron microscopy and SAXS studies of amorphous polymers*. Faraday Discuss Chem Soc 68:87-95.

Wang-2003a Wang S-Q (2003) *Chain dynamics in entangled polymers: diffusion versus rheology and their comparison.* J Polym Sci. Part B: Polym Phys 41:1589-1604.

Wang-2003b Wang S, Wang S-Q, Halasa A, Hsu W-L (2003) *Relaxation dynamics in mixtures of long and short chains: tube dilation and impeded curvilinear diffusion*. Macromolecules 36:5355-5371.

Wang-2007 Wang SQ, Ravindranath S, Wang Y, Boukany P (2007) *New theoretical considerations in polymer rheology: elastic breakdown of chain entanglement network.* J Chem Phys 127:64903.

Watanabe-1999 Watanabe H (1999) *Viscoelasticity and dynamics of entangled polymers*. Prog Polym Sci 24:1253-1403.

Witten-1989 Witten TA, Milner ST, Wang Z-G (1989) *Multiphase macromolecular systems*. ed. Culbertson BM, Plenum New York.

Wu-1985 Wu S (1985) *Dynamic rheology and molecular weight distribution of insoluble polymers: tetrafluoroethylene-hexafluoropropylene copolymers.* Macromolecules 18:2023-2030.

Wu-1987 Wu S (1987) *Entanglement, friction, and free volume between dissimilar chains in compatible polymer blends*. J Polym Sci, Polym Phys Ed 25:11-2529.

Wu-1989 Wu S (1989) *Chain structure and entanglement.* J Polym Sci, Polym Phys 27:723-741.

Wu-1992 Wu S, Beckerbauer R (1992) *Chain entanglement in homopolymers, copolymers and terpolymers of methyl methacrylate, styrene and N-phenylmaleimide.* Polymer 33:509-515.

Yamakawa-1982 Yamakawa H, Yoshizaki T (1982) *Temperature coefficients of unperturbed chain dimensions. Helical wormlike chains*. Macromolecules 15:1444-1445.

Zirkel-1992 Zirkel A, Richter D, Pyckhout-Hintzen W, Fetters LJ (1992) *Temperature dependence of the unperturbed dimensions of alternating poly(ethylene-propylene).* Macromolecules 25:954-960.

Zhang-2006 Zhang W, Martins JA (2006) *Evaluation of the effect of melt memory on shear-induced crystallization of low-density polyethylene*. Macromol Rapid Commun 27:1067–1072.

3. The shear-induced crystallization

To understand polymer crystallization, either in quiescent, and by major reasons in shear, it is imperative the knowledge of the melt morphology and its change with the flow conditions. More specifically, it must be known the effect of deformations induced by shear and elongational flows on polymer chains, namely the changes in chains' dimensions. Depending on the flow deformation duration and intensity, chains' dimensions may change up to a limiting value. During cooling they relax to higher entropic conformational states, characteristic of quiescent melts. It is known that crystallization from deformed melts is accelerated when compared with that of quiescent melts. The reason for this acceleration is assigned to precursor structures of nucleation. A major challenge in shear-induced crystallization is to understand the formation of these structures, because it is assumed that they are absent in quiescent crystallization and that shear flow activates their formation. To cope with this problem, several model polymers were studied, including mixtures of short and long chains of the same polymer. Also, some experiments were carried out to test the rheological properties of supercooled polymer melts at the very earlier stages of crystallization. Several shear-induced crystallization experiments were performed in different instruments under controlled conditions to understand what processing variables affect flow deformation. Besides temperature, the shear stress and strain were the elected parameters in those experiments. Conditions needed to establish a skin oriented layer and a core spherulitic structure were identified. Another challenge of crystallization from oriented melts is to understand how, from highly deformed melts, the shish-kebab structures are created. Only recently a light was shed onto this problem. The above different aspects and problems of polymer crystallization from oriented melts will be presented below. Due to their relevance for this work, emphasis will be given to works and results focused on the formation of precursor structures.

3.1. Melt morphology

3.1.1. Effect of flow deformations on the melt morphology

Experiments performed with stiff DNA chains demonstrated that for shear flow the maximum chain alignment with the flow direction is around 50% of the contour chain length [Smith-1999], while for elongational flow it is around 90% of L [Perkins-1997]. The amount of chain extension is mainly a function of the applied shear flow strength

expressed by the Weissenberg number (W_i or W_e). It is the product of the chain relaxation time and the flow process deformation rate ($W_e = \dot{\gamma}\tau$). The relaxation time for constant temperature is constant and W_e reflects the strength of the flow. Its increase implies the chain extension increase, up to limiting values, both in shear and elongational flows - see Figure 3.1.

The above results are easily understood because while elongational flow has only a single elongational component, shear flow has a rotational and an elongational component. The resulting deformation depends on their relative magnitude. A coiled state exists when the rotational component dominates and the maximum extension is reached when the two components are similar in magnitude. Contrary to a prediction of de Gennes [de Gennes-1974] a fully stretched state cannot exist in shear flow. Under the action of a flow field, chain molecules may adopt conformations parallel or perpendicular to it. Wirtz *et al.* [LeDuc-1999] showed that for DNA molecules the average number of chain conformations aligned with flow increases with shear rate (Figure 3.2). Since due to the rotational component a fully stretched state does not exist, the average number of conformations aligned with flow changes with time, and the time to change orientation from one conformation to another decreases with shear rate.

Based on the above description, the morphology of a sheared polymer melt may be briefly characterized by the coexistence in a dynamic melt of coiled and partially stretched chains, the polymer chains continuously undergoing small extensions and tumbling motion. It is important now to analyse changes in chains dimensions from a quiescent to a sheared melt. As seen in the previous chapter, the random coil model describes the morphology of a chain in a quiescent melt as a random walk of Kuhn monomers. Shear flow does not affect significantly the chain dimensions. Figure 3.3 shows the dimensionless radius of gyration

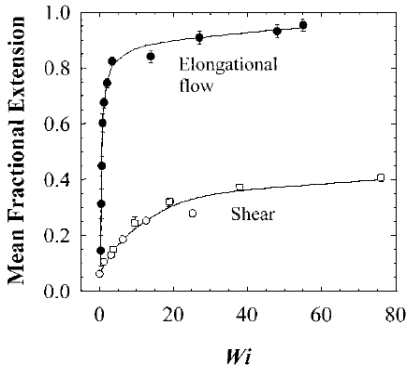

Figure 3.1. *The mean fractional extension as a function of Weissenberg number for elongational (filled circles) and shear (open circles) flow of DNA chains [Smith-1999].*

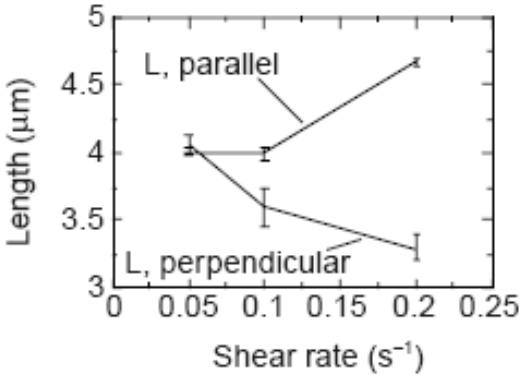

Figure 3.2. *Time-averaged parallel and perpendicular lengths to the flow direction of DNA molecules as a function of shear rate [LeDuc-1999].*

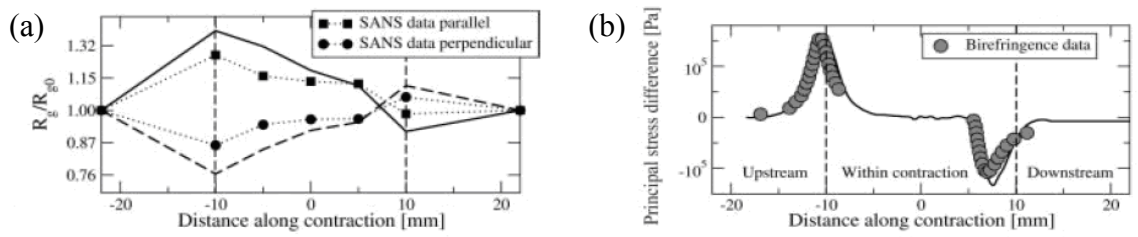

Figure 3.3. *Anisotropy of the radii of gyration (R_g/R_{g0}) by SANS (a) and entanglement strands by birefringence (b) as a function of distance along the slot die during flow of polystyrene: points show experimental data and curves show theoretical predictions. The parallel and perpendicular SANS data indicate the averages of the scattering intensity S(q) in the directions parallel and perpendicular to the flow [Bent-2003].*

deformed by the flow (a) and principal stress difference (b) inside a die [Bent-2003]. It is visible that even at the die entrance, where chains experience maximum deformation, R_g/R_{g0} does not increase more than 1.3.

3.1.2. Effect of temperature on the chain's configuration

This effect was illustrated in section §2.1.1 (Table 2.2. and Figure 2.1), where the temperature coefficient for the unperturbed chain dimension of some polymers was indicated. Since for most polymers the *gauche* state is at a higher energy level than the *trans* state, and the occupation of these states follows the Boltzmann distribution, the increase of temperature increases the population of the higher energetic states. It is assumed that polymer chains at the molten state adopt a random coil conformation. Their spatial arrangement is determined only by short-range interactions, the chain having ideal behaviour, just like a polymer chain under *theta* conditions. Elastic neutron scattering experiments, among others, are used to support the above assumption. They demonstrate that the scattering intensity of labelled PMMA dispersed in a melt of the same unlabelled polymer is fitted with a Gaussian distribution of chains conformations (see Figure 3.4a).

However, as shown in Figure 2.1, the effect of temperature on the chain's dimensions is not so obvious. The decrease in coil dimension with temperature found for polyethylene results from the population increase of high-energy *gauche* states at high temperatures causing a decrease in the chain end-to-end distance. For other polymers, such as the one shown in Figure 2.1 and syndiotactic PMMA, coils expand with temperature increase. It any case, for polymer melts, this variation seems to be not significant.

For understanding the crystallization from sheared melts, it is important to know the chain dimensions in crystallized and molten states, more precisely, the effect of order on polymer chain morphology. It was verified experimentally that the dimension of coiled polymer chains, evaluated through radius of gyration measurements do not change significantly at the molten and solid state. In fact, the radius of gyration may be considered

to be approximately the same at these two states. The conformational, crystalline ordering, and changing of temperature (cooling from a temperature above the equilibrium melt temperature to the crystallization temperature) don't change the spatial shape of very long chains during crystallization [Pratt-1978]. It was concluded therefore that crystallization does not require the macromolecule to fold into a single lamella. Rather the conformation adopted by a polymer chain at the solid state should consist of a three-dimensional array of stems arranged around the chain centre of mass. Their estimated length evaluated by SAXS experiments is around twice the lamellar thickness [Ballard-1980]. Each crystalline lamella consists therefore of stems derived from many polymer chains.

Another piece for this puzzle is the result shown above for the variation of the radius of gyration of quenched iPP samples with different molecular weight. The validity of random coil model would imply a linear dependence of R_g on $M^{1/2}$. Figure 3.4b shows that a non-linear dependence exists, which is especially evident for chains with low molecular weight [Li-2005a]. While the Gaussian character of chains' conformation seems to be confirmed at both the molten and solid states for chains with high molecular weight, the results obtained for chains with low molecular weight, but much larger than the critical molecular weight, seem to question the general validity of this model.

During crystallization process molecules tend to move towards the lowest conformational energy states [Blundell-1996]. For some polymers, as polyethylene, the chains stems at the lamellae have only the extended *trans* conformation (lower energy conformation) while chain segments at the amorphous interlamellar region can be either at *trans* or *gauche* conformations [Earl-1979]. Chains of other polymers, such as polypropylene, adopt the helical *trans-gauche* conformation, with 3 monomers per helix turn.

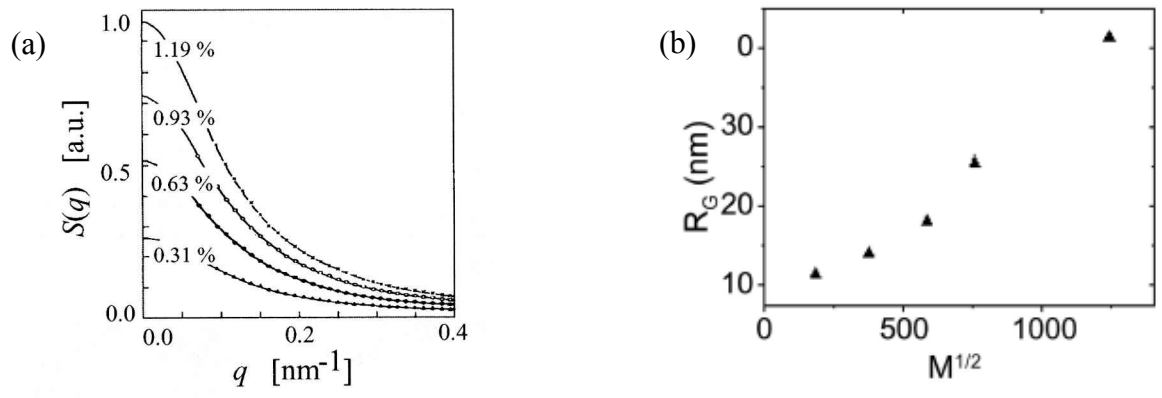

Figure 3.4. *Elastic neutron scattering experiments on labelled PMMA samples dispersed in a melt of unlabeled PMMA (a) [Kriste-1975] and variation of the radius of gyration for quenched iPP as a function of $M^{1/2}$(b) [Li-2005a]. Validity of the random coil model for polymer chains at the molten (a) and solid (b) phases. The validity in (b) is restricted to chains of high molecular weight [Li-2005a]. In (a) the continuous curve is the theoretical prediction using ideal chain statistics. Numbers in (a) show the density of the labelled PMMA.*

In conclusion, restraining the analysis to high molecular weight chains, these results indicate that polymer chains conformation in the quiescent melt and solid semi-crystalline may be considered as Gaussian, and the results above (§3.1.1) indicate that shear flow increases the radius of gyration value obtained for a quiescent melt to a maximum of 1.3 R_g. Further it was shown that the number of conformations aligned with shear flow increases with flow intensity, and it will be suggested below that ordered regions, which may have a dynamic character, may exist in sheared and quiescent melts, coexisting with other chains in tumbling motion. The possibility of a crystal, in this case an ordered region without crystallographic order, coexisting with its melt was confirmed by non-equilibrium molecular dynamics simulations of particles sheared between two parallel plates (one amorphous and another crystalline) [Butler-2002]. The simulations revealed stationary states corresponding to coexistence between the strained crystal and its shearing melt. The coexistence is explained by a balancing of effects between the crystal growth rate and the rate of surface erosion by the shearing melt. The non-equilibrium liquid-crystal interface includes a band of shearing whose thickness increases rapidly with the shear stress.

3.2. The precursor structures

It is commonly accepted that crystallization enhancement in deformed polymer melts results from the formation of precursor structures, which are at the origin of primary nuclei. According to many investigators [Somani-2002a] precursors of primary nuclei consist of aggregates of ordered chain segments without crystallographic order. Its existence implies the existence of order at the molten state, the enhancement of (positional) order by the action of flow and the coexistence of ordered structures with a dynamic melt, as described in §3.1. Therefore, understanding and controlling their origin remains still a challenge.

It was shown in Chapter 1 that quiescent polymer melts retain the memory of previous deformations. This memory affects crystallization kinetics and it may be erased by heating the quiescent melt for long time, always at temperatures higher than the equilibrium melting temperature, or by heating the melt at higher temperatures for shorter time. It seems reasonable to assume that precursor structures are related to the effect of melt memory observed during the crystallization of quiescent polymer melts. Therefore a procedure to study their origin is to analyse the effect of melt memory on the solidification of sheared polymer melts. These studies were performed with a shear DTA instrument and they will be briefly presented below and in Chapters 4 and 5 of this work.

Several experiments were performed to understand the formation of precursor structures and their effect on shear-induced crystallization. Among them are the gelation experiments of Winter *et al.* [Elmoumni-2003, Acierno-2003, Pogodina-2001], the crystallization experiments of Kornfield *et al.* [Kornfield-2002, Kumaraswamy-2002, Kumaraswamy-1999] using the short-term shearing protocol of Janeschitz-Kriegl *et al.* [Liedauer-1993, Jerschow-1997, Janeschitz-Kriegl-2003a, Janeschitz-Kriegl-2003b, Janeschitz-Kriegl-2007], the results for the saturation of anisotropy in melts sheared above the equilibrium melting temperature in Linkam hot-stage of Mitchell *et al.* [Nogales-2003], the SAXS-WAXS experiments in sheared melts of Somani *et al.* [Somani-2002a, Somani-2005], and the X-ray information on fast quenched extruded melts of Ryan *et al.* [Ryan-1999]. A brief description of these results will be presented below.

3.2.1. Melt memory experiments

3.2.1.1. Isothermal crystallization

Experiments performed by Martins and Zhang [Martins-2006, Zhang-2006] allowed establishing a clear link between melt morphology and crystallization kinetics. The polymer was heated up to different temperatures, always above the polymer melting temperature. The melt was then sheared at those temperatures under controlled conditions, and further cooled to the crystallization temperature, without application of any additional shear deformation during cooling or at the crystallization temperature (Figure 3.5). By this way, it was ensured that any recorded effect on crystallization resulted only from applied flow memory retained by the polymer melt.

It was observed an acceleration of crystallization with the increase of shear rate or shearing time and a saturation of crystallization kinetics at a constant strain. It was further found that the strain needed to saturate crystallization decreases with the sheared melt temperature increase. This effect suggested that a well defined melt state should be

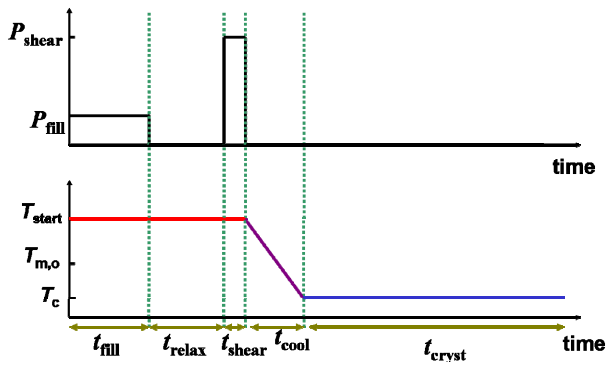

Figure 3.5. *Scheme of the protocol used by Martins et al. [Martins-2006, Zhang-2006].*

responsible for the saturation of crystallization. The search for this state was done by performing rheological experiments at well defined temperatures. In these experiments the viscosity of the melt was recorded as function of time at constant shear rate (Figure 3.6a). They are known as shear-stress growth experiments, because it is also possible to record the variation of shear stress as a function of shearing time, and to observe its increase up to a maximum value, followed by the decrease and further stabilization at a constant value. These experiments showed that the critical strain necessary to stabilize the viscosity measured with the parallel plate configuration is similar to the one that saturates the crystallization kinetics measured with the shear DTA. Both strains have the same temperature variation: an exponential decrease with the increase of sheared melt temperature (Figure 3.6b).

3.2.1.2. Non-isothermal crystallization

Chai *et al.* performed one of the first experiments where the effect of melt memory on the non-isothermal shear induced crystallization kinetics was studied [Chai-2003]. A Ziegler-Natta catalyzed iPP was pre-sheared during different times at 170 ºC with two shear rates, 3 s^{-1} and 9 s^{-1}, yielding different strains applied to the molten polymer. After a waiting time of 2 s the molten polymer was cooled with a constant cooling rate of -20 ºC/min. Values obtained for the ratio $R(\dot{\gamma})/R_o$ are plotted in Figure 3.7. $R(\dot{\gamma})$ is the final radius of the spherulites, evaluated on solid samples, for samples sheared with two different shear rates, and R_o is the final spherulite radius for samples crystallized under quiescent conditions. Results shown in this figure indicate a saturation of the spherulite radius with the applied strain. For strains larger than 1000 s.u. no further change in the spherulite radius is observed.

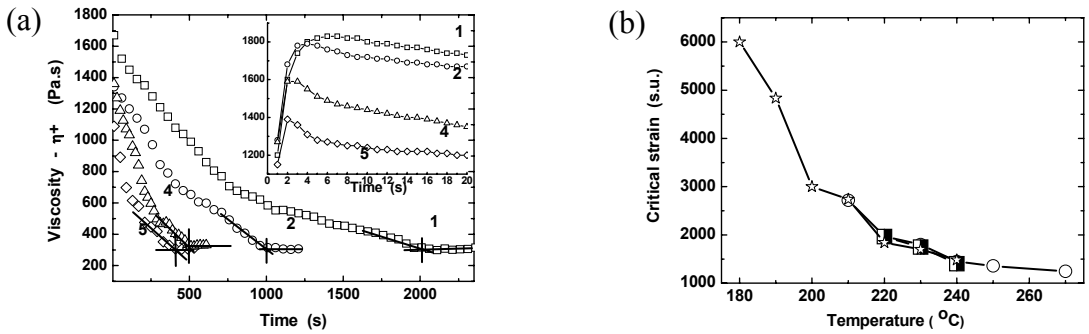

Figure 3.6. *Results of stress growth in shear for isotactic polypropylene. (a) Transient viscosity measured at 220 ºC with the parallel plate configuration at the shear rates indicated. The solid lines show the evaluation of the critical strain (indicated by the vertical lines) at the onset of the steady-state. The inset in (a) shows the behaviour recorded for short shearing times. The average critical strain is ≈1970 s.u. and the measurement error in the strain values is ± 10%. (b) Temperature variation of the critical strain measured with the shear DTA (open symbols) and a parallel plate rheometer (half-filled symbols) [Martins-2006].*

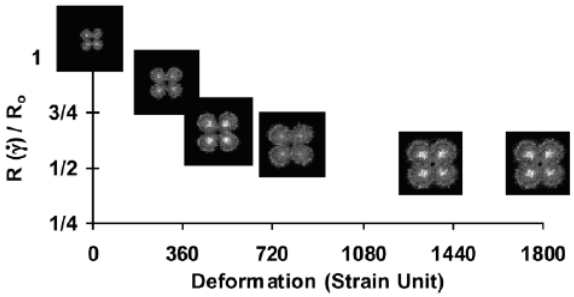

Figure 3.7. *Normalized spherulite radius as a function of the total strain and corresponding SALS patterns evaluated in the solidified polymer after a controlled cooling at -20 ºC/min (T_s = 170 ºC, t_w = 2 s) [Chai-2003].*

These researchers were the first to suggest the need for a "*critical strain*" to saturate the morphology developed after pre-shearing a melt.

Martins and Zhang [Zhang-2007] analyzed the effect of melt memory on shear-induced non-isothermal crystallization of low-density polyethylene and polypropylene. Conceptually, these experiments are similar to those of Chai *et al.* [Chai-2003] mentioned above. The main difference, besides different strains, is that the sheared polymer melts were cooled with different cooling rates. The remaining experimental procedure is similar to that mentioned in §3.2.1.1.

Results of these experiments are similar to those of the effect of melt memory on shear-induced isothermal crystallization. Both, isothermal and non-isothermal, experiments require the establishment of a steady-state in shear flow to saturate the crystallization kinetics. Saturation occurs at the same strain values that decrease with the melt temperature increase and are independent of cooling rate, depending only on the melt temperature.

3.2.2. The gelation experiments

Discussion about the validity of gelation process was made in Chapter 1. However, despite the criticism made, some experiments performed by Pogodina, Winter *et al.* [Elmoumni-2003, Acierno-2003, Pogodina-2001] gave new information for the morphology at the early crystallization stages. A brief description of the experimental protocol and equipment used is presented below. A new rheo-optical device was used. The typical assembling consisted of a Small Angle Light Scattering (SALS) setup (laser beam, polarizer, analyser and CCD camera) and a rotational rheometer coupled to a Linkam shearing hot-stage. This setup was complemented by the inclusion of a half-wave plate, whose rotation, driven by a motor, allowed performing intensity measurements with either the polarizers crossed (H_v) or in parallel (V_v).

Experiments performed by Winter *et al.* involved the determination of a gel point. Its determination requires testing the sample during the quiescent crystallization with Small

Amplitude Oscillatory Shear deformations. It is implicitly assumed, although not stated in none of the published works, that these Small Amplitude Oscillatory Shear deformations applied at the viscoelastic linear regime do not have any effect on the overall crystallization kinetics. As explained in Chapter 1, this assumption is wrong, since any measurable deformation applied at the viscoelastic linear regime by small oscillations, results in an acceleration of crystallization kinetics [Zhang-2006].

The isotactic polypropylene sample was annealed at 200 ºC, the temperature maintained for 3 min, and the sample pressed to the final thickness (≈ 0.2 mm). It was then cooled at -30 ºC/min to the crystallization temperature (148 ºC), where immediately a short-term shearing with constant shear rate was applied and crystallization recorded by Small Amplitude Oscillatory Shear at constant frequency. This experimental protocol is similar to the short-term shearing protocol of Janeschitz-Kriegl *et al.* (Figure 3.17). Also, similarly to this protocol, the shearing time is lower than 60 s, and much shorter than the crystallization time, to minimize the crystallization during shear. At this relatively high temperature the crystallization kinetics is slow. The estimated crystallization time for a truly quiescent experiment is around 24 h.

Results obtained from the monitoring of crystallization are indicated in Figure 3.8 by the SALS invariants Q_η and Q_δ. These invariants are integrated intensities along the scattering vector, Q_η is the density fluctuation invariant and Q_δ is the orientation fluctuation invariant, related therefore to the optical anisotropy. They indicate that density fluctuations start to occur earlier than orientation fluctuations, pass through a maximum, and decrease at later stages when the crystalline phase becomes dominant [Elmoumni-2003]. The orientation fluctuations due to optical anisotropy of crystals develop at much later stages and show sigmoidal growth. With the increase of shear, expressed by the W_e number, both invariants are

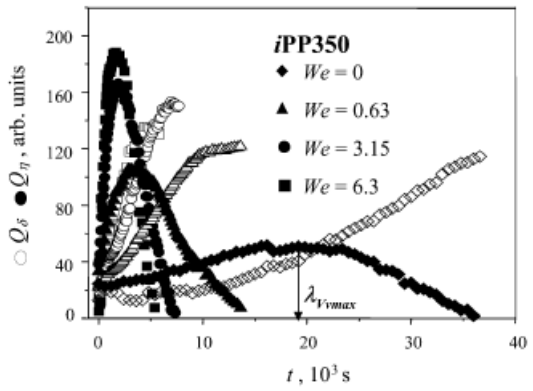

Figure 3.8. *SALS invariants Q_η (full symbols) and Q_δ (open symbols) versus time for iPP samples with increasing W_e values (increasing shear rate) [Elmoumni-2003].*

shifted to shorter times.

3.2.3. The shear-induced structures generated with the short-term shearing protocol

The application of the short-term shearing protocol of Janeschitz-Kriegl *et al.* (Figure 3.17) by Kornfield *et al.* [Kornfield-2002, Kumaraswamy-2002, Kumaraswamy-1999] gave further insight into effect of shear flow on the formation and development of precursor structures for crystallization. They used a compact version of the system developed by Janeschitz-Kriegl which was initially applied to an extruder, requiring therefore a large amount of material and being limited on the experimental techniques used to follow the crystallization development. The idea behind this protocol was to impose to a melt well-defined flow and thermal histories by applying controlled shear pulses during short shearing times, always at the crystallization temperature (or at temperatures below the polymer equilibrium melting temperature). A more detailed description of this protocol will be presented below (§3.3.2.3.). The version developed by Kornfield *et al.* added a few additional possibilities to facilitate *in-situ* structural characterization and the ability to work with a small amount of material.

Isotactic polypropylene was used in these experiments, as well as in most experiments on shear-induced crystallization. Shear pulses were applied at the crystallization temperature (T_c = 141 ºC, σ_w = 0.06 MPa, $T_{reservoir}$ = 180 ºC) to make the flow of polymer melt from a reservoir to a duct [Kumaraswamy-1999]. The half-crystallization time at this temperature was larger than one hour. It must be noted that in this protocol the application of shear pulses implies injection of material at the reservoir temperature to the duct (at the crystallization temperature) and, therefore, the disturbance of the material temperature at the duct. It is assumed that, due to the long crystallization time at this temperature, the resulting temperature increase is conveniently relaxed before the crystallization detection.

Birefringence measurements along the duct showed that the birefringence relaxes to zero for shear pulses applied at T_c with duration lower than 5 s. For longer shear pulses (the maximum attained with this instrument is 12 s) a significant increase in the birefringence is detected. Further, measurements of the time for the transmitted light intensity $I_{tot}(t)$ were made and it was found to decrease to half of its initial value $I_{tot}(t = 0)$ - $I(t = t_{1/2})$ - indicating a saturation of $t_{1/2}$ for shearing times greater than 5 s.

This information was further related to the solid-state morphology developed, resulting from the time duration of the applied shear-pulse. It was found that pulses with duration lower than 5 s yielded no observable oriented structures, while longer shear pulses yielded an oriented ***skin*** layer and a ***core*** spherulitic structure. As expected, the measured

diameter of these spherulitic structures was much lower than that observed for the quiescent crystallization at the same temperature.

Since the stress at the wall was maintained constant (0.06 MPa), the "*critical*" shear stress at the boundary between the oriented skin and core layer was found to be 0.047 MPa. This evaluation was done on a solidified sample by considering a linear variation of the shear stress at the wall (0.06 MPa) to its centre, where it is zero. This stress was considered to be the critical stress needed for the development of the "*shear-induced structure*" described below, being the formation of these structures correlated with the formation of the skin-core morphology. These conditions were used by Kornfield *et al*. [Kimata-2007] in another work to generate shish-kebab structures at the oriented skin layer and to explain with more detail their formation (see §3.5).

The most important aspect of these works was the observation of birefringence variation with the shear pulse time duration at temperatures from 135 ºC up to 175 ºC, above the nominal melting temperature measured in a DSC (≈ 170 ºC). Results of these "***melt shearing***" experiments are indicated in Figure 3.9, where it is plotted the variation of birefringence with the shearing time. An upturn in the birefringence is observed. This upturn was understood by the authors as the result of the formation of an oriented structure that they called "shear-induced structure". It must be stressed that during all these experiments, the reservoir where the molten polymer was pumped from to the duct was maintained at 180 ºC. The key result is that the "*shear-induced structure*" appears at shorter times for higher temperatures.

Upon cessation of shearing it was found that the "shear-induced structure", or better, the birefringence, decays to zero for temperatures of 170 ºC and above (because of the low strain applied to the molten polymer), while it decays to non-zero values for temperatures below 170 ºC (see Figure 3.10). These results indicate clearly that the formation of "shear-induced structures" is controlled by the relaxation dynamics of the melt. From these results the authors concluded that under shear flow the formation of line nuclei proceeds via a kinetic, rheologically controlled, pathway [Kumaraswamy-2005]. They concluded also that the activation energy barrier that controls the formation of nuclei in quiescent crystallization is here eliminated [Kumaraswamy-2002]. The validity of these conclusions will be discussed below.

The shift factor to superimpose all curves in Figure 3.9 was also evaluated, plotted against temperature and found to have similar temperature variation as the rheological shift factor for isotactic and atactic polypropylene (which was evaluated by the authors with a WLF equation). Also interesting, and not mentioned by the authors, is the activation energy

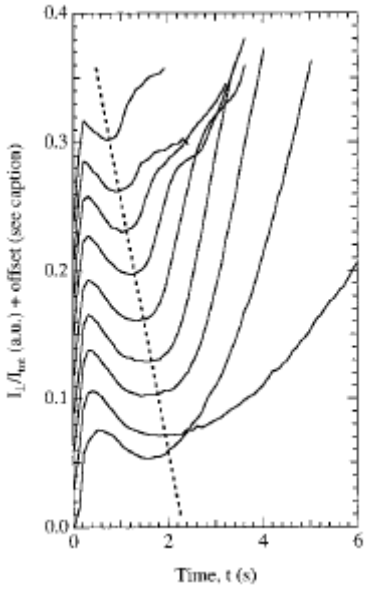

Figure 3.9. *Melt-shearing experiments showing the temperature dependence of birefringence traces at 135, 140, 145, 150, 155, 160, 165, 170, and 175 °C, starting from the bottom. Figure 3.17 shows the thermo-mechanical protocol (σ_w = 0.06 MPa, t_s < 12 s) [Kumaraswamy-1999].*

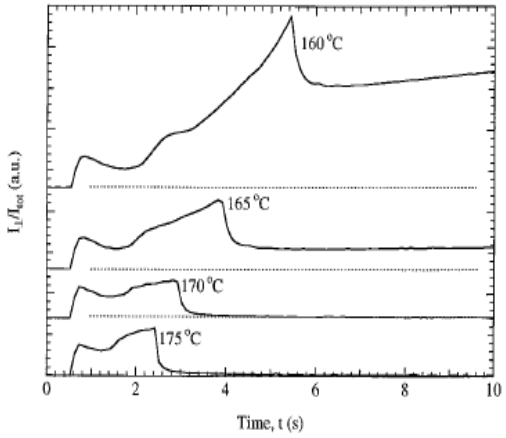

Figure 3.10. *The birefringence observed during and after cessation of flow (σ_w = 0.06 MPa) as a function of the measurement time for Ziegler-Natta polypropylene [Kumaraswamy-1999].*

evaluated from this shift factor. It is exactly the same as the flow activation energy of isotactic polypropylene (≈ 44 kJ/mol), a result that is not surprising considering that these experiments are melt-shearing experiments [Martins-2008]. Therefore, the denominated shear-induced structure results only, and exclusively, from shear-deformations imposed to the molten polymer. The time for upturn of birefringence is then the time needed to orientate chains in the sheared melt, with a morphology described in §3.1, with the flow direction, this being one of the reasons why the oriented structures appear at shorter times at higher temperatures [Martins-2006, Martins-2008].

The relevance of the above conclusion will appear shortly. The correlation between the shear-induced structure and the skin-core morphology made by Kornfield *et al.* [Kumaraswamy-1999] is not straightforward. The origin of these two effects is different. As mentioned previously, the shear induced structure is observed when the polymer at 180 ºC is sheared to the flow channel at a lower temperature (between 135 ºC and 175 ºC). It is a flow effect that generates melt anisotropy which is detected by the birefringence upturn. When this anisotropic melt contacts the cooler walls of the flow channel, the orientation is frozen and the skin-core morphology is generated. Therefore, while the shear-induced structure is intrinsically a flow effect (because it is also observed at temperatures above the polymer nominal melting temperature), the skin-core morphology is a thermal effect induced by flow. This is the reason why a critical stress is needed to observe the skin-core

morphology: anisotropy must be generated in the melt and it must be frozen by the temperature gradients in the flow channel [Martins-2008].

3.2.4. Scattering experiments

The *in situ* scattering measurements provide insight into the morphological features of structures induced by flow before crystallization. Despite the difficulties in detecting the weak signals from the small volume fraction of structures developing at early crystallization stages, some studies showed the clear existence of precursor structures. Imai *et al.* [Imai-1992, Imai-1994] in their quiescent crystallization experiments observed SAXS peak before WAXS and explained their results by melt density fluctuations and a spinodal decomposition mechanism [Heeley-2002], being this the primary nucleation process controlling factor. Others [Hsiao-1995, Wang-1997] claimed that the above observation results from smaller detector sensitivity of WAXS comparing to SAXS (more details were given in section §1.2.2).

Although the exact nature of precursor structures is not clear yet, it is obvious that large-scale structures exist before the formation of crystals in the polymer melt. The main question, besides their dimension, is if the structure has, or not, crystalline order. One of the first known experiments for the detection of precursor structures after shear was done by Ryan *et al.* [Ryan-1999], and it allowed answering some of the above questions. A SAXS pattern with length scale from 50 to 200 Å was identified in solidified isotactic polypropylene collected from an extruder working at steady state, the extrudate being cooled in a column of chilled nitrogen. The corresponding WAXS didn't show any Bragg peaks. A straightforward correspondence between the structure observed on the solidified sample and that existing at steady state is prone to mistakes since die-swell, draw ratio and contraction during solidification may change the structure dimension. A conclusion from this work is that precursor structures don't have crystalline order. This seems to be a reasonable result because it is conceptually difficult to accept the existence of structures with crystallographic order in sheared polymer melts.

The existing confusion concerning the possible structure of precursors results also from different experimental protocols adopted by different researchers. An example of this is the μWAXS experiments of Gutiérrez *et al.* [Gutiérrez-2004]. They found a crystallinity level less than 1 % on different positions of iPS samples. Since these experiments were performed on samples quenched in air to room temperature before shearing at 260 ºC (equilibrium melting temperature of iPS is 243 ºC according to Petermann *et al.* [Petermann-1977]) and not

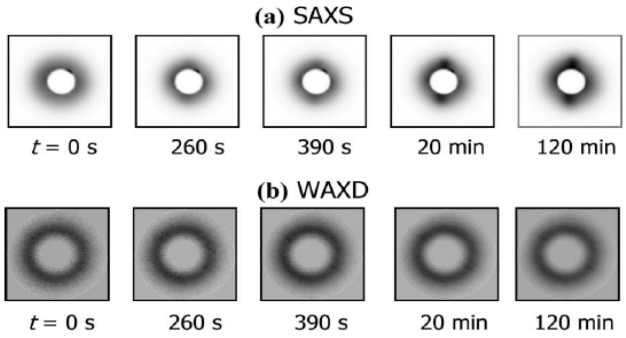

Figure 3.11. *SAXS (a) and WAXD (b) patterns of a Ziegler-Natta iPP melt at 175 ºC (protocol of Figure 3.17, strain equal 1428 %, $\dot{\gamma} = 57\ s^{-1}$, $t_s = 0.25$) [Somani-2002a].*

at the molten state, they don't provide a clear indication for the order of precursor structures, even though the slow crystallizing rate of this polymer.

Information on the morphology and lifetime of precursor structures was obtained by Somani *et al.* [Somani-2002a]. An isotactic polypropylene was sheared at 175 ºC with shear rate of 57 s^{-1} and total strain of 1428 %. SAXS patterns, obtained after shearing, showed the formation of structures stable for up to two hours after cessation of shear with a layer-like superstructure - the assemblies of precursors of primary nuclei (the "layer") separated by unoriented chains - while, also in this case, the corresponding WAXD patterns showed absence of crystal reflections (Figure 3.11). The average spacing between "layers" was around 430 Å.

More detailed measurements of precursor structures' dimension was made by Nogales *et al.* [Nogales-2003]. Polyethylene with a nucleating agent - dibenzylidene sorbitol (DBS) - was sheared at 170 ºC with different shearing rates, while the anisotropy of the structure was monitored by SAXS. It was found that it increases with the applied strain, up to saturation. Structures with around 500 Å in the flow direction and 100 Å in transverse direction were measured at the saturation. Since at 170 ºC the nucleating agent is ineffective, the observed structures result only from the intrinsic polymer melt anisotropy. Separation between troughs parallel to the flow direction was around 10 μm and saturation of anisotropy was observed at $\approx 10^3$ strain units (see Figure 3.12).

Based on their own results and results of others, Somani *et al.* proposed a model for the formation of precursor structures at the early crystallization stages after shear, Figure 3.13 [Somani-2002a]. It must be noted that according to this model, and the commonly accepted view, it is implicitly assumed that shear flow creates precursor structures, and that they are absent before shear and in quiescent crystallization processes.

The application of a step shear to the amorphous melt with molecules in random-coil conformation orientates chains. After cessation of flow, only the chains above a critical chain

length will remain in oriented state [Keller-1997]. The aggregation of oriented chain segments results in clusters with different extent of molecular orientation. These clusters are considered as the precursors of primary nuclei. Their stability depends on the relaxation behaviour of ordered chains and interactions between aligned chain segments in the clusters. At temperatures below the polymer melting temperature the precursors develop crystalline structures. A physical support to this model is inexistent. For example, the authors have not evaluated the contribution of interaction between aligned chain segments in the clusters for their stability.

The experiments of Nogales *et al.* indicate that anisotropic clusters develop under the application of shear. As mentioned above, since DBS is ineffective as nucleating agent at the temperatures where shear was performed, one would expect that shearing the melt without DBS at the same large strains ($\approx 10^3$ s.u.) would lead also to a saturation of anisotropy. Clusters with aligned chain segments, should then be intrinsic to polymer melt morphology, the only result of shear being their fragmentation and alignment with the flow direction [Martins-2008].

3.3. The shear-induced isothermal crystallization kinetics

Crystallization kinetics is accelerated when shear or elongational flows are applied to polymer melts and morphologies different from those obtained under quiescent conditions are observed. For very high shear strain shish-kebab structures develop (in shear flow they are observed only near the capillaries or mould's walls, in the skin-core morphology), while

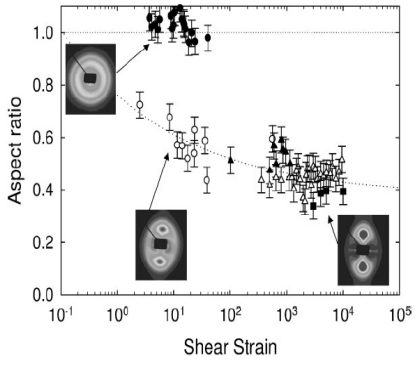

Figure 3.12. *Aspect ratio of oriented structures in PE with 1% DBS evaluated by SAXS as a function of the applied strain: 0.01 s^{-1} (●), 0.1 s^{-1} (○), 1 s^{-1} (▲), 5 s^{-1} (Δ) and 20 s^{-1} (■). The curved line is an eye-guide and the horizontal line represents the level for PE melt without DBS [Nogales-2003].*

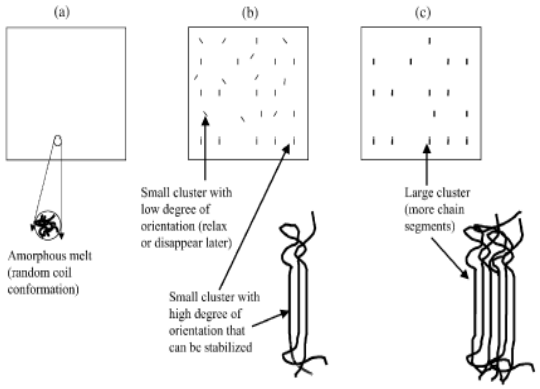

Figure 3.13. *Proposed scheme for the origin of shear-induced precursors of primary nuclei for i-PP: before shear (a), short time after shear (b) and final stable precursors (c) [Somani-2002a].*

spherulites, smaller in size than under quiescent conditions, are observed for lower strain (the core structure).

Increasing shear rate or shearing time accelerates crystallization kinetics and its saturation occurs at a strain value that depends only on the melt temperature and polymer chemical structure, regardless the crystallization mode, isothermal or non-isothermal. The enhancement of crystallization is promoted for higher molecular weight polymers. Below, the effects of molecular weight, polydispersity and chain branching on crystallization kinetics are described. Also other factors controlling shear-induced crystallization, when shear pulses are applied differently at the melt or crystallization temperatures, are analysed and discussed.

3.3.1. Effects of chain length and branching

There are not systematic results for the effects of molecular weight, molecular weight distribution and chain branching on the shear-induced crystallization kinetics. Most published works have acknowledged an important effect of high molecular weight chains on flow induced crystallization and on the formation of shish-kebab structures. As for the effect of chain branching on shear induced crystallization, it is not well studied.

Literature results will be presented below on: 1. the effect of molecular weight distribution on the ability of a melt to store shear deformations at the molten state and their effect of the structures developed after crystallization; 2. the effect of molecular weight and molecular weight distribution on shear-induced crystallization kinetics and 3. effect of branching.

3.3.1.1. Melt memory effect of molecular weight distribution

From experiments of Chai *et al.* [Chai-2003], who worked with two polymers of similar molecular weight but different molecular weight distribution it was concluded that the melt memory is retained only for the sample with a larger proportion of long chains and broader molecular weight distribution. The fundaments for this conclusion will be presented and criticized below. Two different polyethylenes, a linear metallocene, PE1, $M_w = 9.5 \times 10^4$ g/mol, MWD = 2.4, and a Ziegler-Natta catalyzed sample, PE3, $M_w = 10^5$ g/mol, MWD = 3.1, where pre-sheared using different shear rates at 190 ºC with a constant strain of 360 s.u.. After pre-shearing, the samples were hold at different waiting times, from 2 s up to 480 s at the sheared melt temperature. Then the molten polymer was cooled with a constant cooling rate of -20 ºC/min. The mean radius of the spherulites at the end of crystallization was measured. R_0 is the average spherulite radius of a sample

crystallized at quiescent conditions: cooling from 190 ºC to room temperature at -20 ºC/min. $R(\dot{\gamma})$ is the spherulite radius for sheared sample.

Result of the ratio $R(\dot{\gamma})/R_o$ for samples sheared with different shear rates and different waiting times is plotted in Figure 3.14. These results pretended to evaluate the effect of melt memory of the final spherulite size. It was found that while for the metallocene polymer the shear rate does not affect the final spherulite dimension, being independent on the waiting time after shear, for the Ziegler-Natta polymer both, shear rate and waiting time, affect the final spherulite size. After a long waiting time (480 s) no change in the final spherulite size was observed. These results were interpreted in terms of the melts' longest relaxation time effect. Values evaluated for this time were: 2.8 s for PE1 and 27.3 s for PE3. Results in Figure 3.14 indicate that the authors' interpretation based on the melt relaxation time should also hold for PE3 and the waiting time of 120 s. For all shear rates tested, the spherulite radius after this waiting time should be the same as for the quiescent crystallized sample.

Despite this failure in the results interpretation, it can be concluded that the melt memory effect on the crystallization development is more pronounced for polymers with broader molecular weight distribution. Also, when the strain applied to the molten polymer (≈ 360 s.u.) is compared with the values of strain needed to saturate crystallization [Zhang-2006, Martins-2006] and melt anisotropy [Nogales-2003], which are around 10^3 s.u., it is evident that hardly any permanent effect will be observed for long waiting times.

3.3.1.2. Effect on shear-induced crystallization of molecular weight and molecular weight distribution

Compared with molecular weight, the molecular weight distribution has a second order effect on crystallization under shear flow [Duplay-2000]. Partial information about

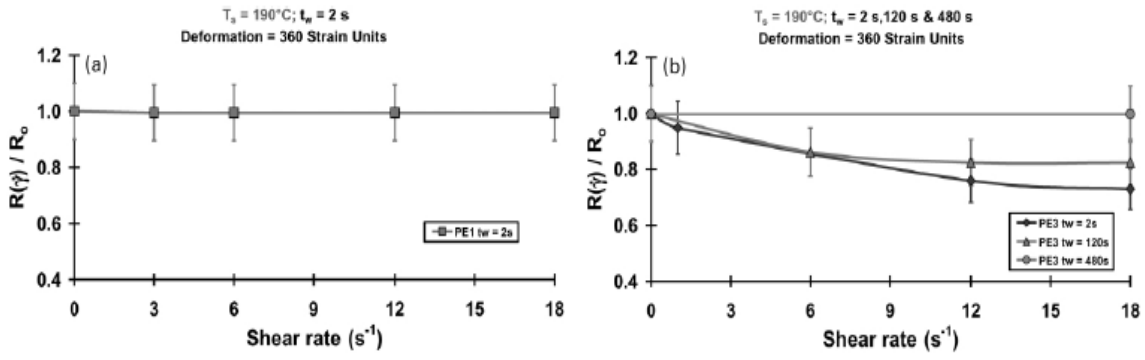

Figure 3.14. *Spherulite radius as a function of shear rate and different waiting times, (a) for linear metallocene hexane-copolymer (labelled as PE1) and (b) Ziegler-Natta catalysed low-density polyethylene (labelled as PE3) [Chai-2003].*

the effects of these two parameters on shear induced crystallization was obtained for iPP of different molecular weight and polydispersity. Samples at the melt temperature were previously pre-sheared with a constant shear rate of 5 s^{-1} and a shearing time of 100 s. They were further cooled to the crystallization temperature T_c = 138 ºC and the course of crystallization was recorded with oscillatory shear measurements ($\omega = 10\ s^{-1}$). Relative crystallization kinetics was evaluated by the shear modulus elastic component increase.

During the course of these experiments the imposed shear deformation accelerates crystallization. But because it was the same for all materials tested, it is possible to conclude the following: i) the higher molecular weight sample crystallizes faster and ii) the increase of molecular weight distribution delays the crystallization kinetics [Vleeshouwers-1996].

Besides accelerating crystallization, high molecular weight chains have also an important role in the morphology development. Somani *et al.* [Nogales-2001, Somani 2006] and Yang *et al.* [Yang-2004] found that shish-kebab structures are formed earlier for blends with higher amount of high molecular weight species. Samples containing larger amount of long chain species exhibits higher degree of crystal orientation, higher amount of the oriented crystal fraction and faster crystallization kinetics expressed by lower values of crystallization half-time.

To elucidate further the effect of long chains on shear-induced crystallization, polymer chains with high molecular weight and lower polydispersity (fractionated iPP) were mixed with a lower molecular weight metallocene iPP. The concentration of fractionated chains varied from zero up to values larger than the overlap concentration (*c**), which is the concentration at which the coiled chains of the fractionated polymer overlap each other. Assuming that the volume of a coiled chain, expressed through its radius of gyration, is

$$V = \frac{4}{3}\pi\left\langle R_g^2\right\rangle^{3/2} \quad , \tag{3.1}$$

and that it may be expressed as $V = \overline{M}_w / N_A\, c^*$, the overlap concentration in g/cm^3 is given by

$$c^* = \frac{3\overline{M}_w}{4\pi\, N_A \left\langle R_g^2\right\rangle^{3/2}} \quad . \tag{3.2}$$

For $\overline{M}_w$ = 923.2 kg/mol, using the molecular weight for the Kuhn monomer equal to 180 g/mol and the Kuhn monomer length equal to 11 Å, the value obtained for the overlap concentration is 1.1 × 10^{-2} g/cm^3, while the value used by the authors was 7 × 10^{-3} g/cm^3. Concentrations as large as twice the overlap concentrations were studied [Seki-2002]. The short-term shearing protocol was used in all experiments described above. No pre-shearing at the melt temperature was performed. Deformations were applied at

the crystallization temperature. They orientate chains segments with flow and crystallization development freezes the imposed orientation, which is higher near the channel's walls.

Several conclusions were drawn, some based on experimental results and others on conjectures. They were based mainly on morphological analysis of samples sheared below and above a critical stress to generate the shear-induced structure (§3.2.3). It was assumed that different nuclei are at the origin of the core spherulitic structure and the oriented skin layer. The first are point-like precursors while the last are threadlike precursors. The mechanism for formation of these precursors is unknown, and conjectures were made for their formation and orientation with flow. It was conjectured, for example, that threads are elaborated from point-like nuclei, but the elaboration mechanism was not explained.

Basically, the main conclusions are that shear-induced crystallization was affected by addition of long polymer chains while the effect was absent in quiescent crystallization. Also, the addition of long chains does not affect too much the formation of point-like precursors, but it affects significantly the formation of threadlike precursors. It was found that the critical stress needed to generate the oriented layer decreases with the increase in the concentration of long chains. It decreases around 10% as c increases to $0.5c^*$ but it is almost unchanged with further increase to $2c^*$. The formation of threads was found to saturate at a long chain concentration equal to the overlap concentration: "*increase of concentration from* c^* *to* $2c^*$ *produces little further enhancement on the formation of threads*" [Seki-2002]. In conclusion, threads may be created with application of a critical stress and concentration equal to half the overlap concentration and saturate at the same critical stress and concentration equal to the overlap concentration.

The results expressed above demonstrate that the role of long chains on the formation of the oriented skin structure is not the one assigned by the authors. As mentioned at §3.2.3, the skin-core morphology is a thermal effect induced by flow. That is, for formation of an oriented skin layer, chain segments must be orientated with flow direction and the maximum orientation is around 0.4 the average contour chain length. What can be concluded from the results of Seki *et al.* [Seki-2002] is that the development of this orientation is accelerated when the high molecular weight chains concentration increases because inter-chain interactions are promoted. If the high molecular weight chains had any triggering effect on the threads formation, the orientation effects should be observed only at the overlap concentration. However, even in the melt without any high molecular weight chains, the oriented skin layer is observed, but at higher stresses.

Additional information on the role played by the high molecular weight chains in the formation of oriented structures under shear flow was obtained by Azzuri *et al.*

[Azzurri-2005]. They showed that at 130 ºC the highest molecular weight sample of isotactic poly(1-butene) (M_w = 850000 g/mol) relaxes after several hours, while the lowest M_w sample (M_w = 116000 g/mol) relaxes in less than one second. These results demonstrate the long life of structures oriented with flow. Conciliating oriented structures with a dynamic entangled melt is a difficult task that must be accomplished to understand their molecular origin.

Another aspect that also needs to be clarified is the effect of high molecular weight chains on the amount ("concentration") of chains oriented with the flow. Earlier views considered that it depends on shear rate. Keller *et al.* [Hill-1983, Lieberwirth-2000, Keller-1997, Pope-1978] postulated that higher shear rate increases the amount of oriented chains. It was found that for a given shear rate only molecules above a critical molecular weight can be oriented (M^* - the critical orientation molecular weight). The higher molecular weight samples needed smaller critical shear rate to achieve orientation [Somani-2000, Nogales-2001]. The critical orientation molecular weight shear rate dependence evaluated from experimental results was $M^* \propto \dot{\gamma}^{-0.15}$ [Somani-2000]. The fraction of oriented crystallites was determined from the ratio of the scattered intensity due to the oriented (anisotropic) component to the total scattered intensity.

Considering the current model of polymer chains in the molten state, where topological constraints hinder chain's movement increasing its relaxation time, the above results indicate that chains of higher molecular weight, containing therefore more constraints and relaxing slower, are oriented with the flow at a lower critical shear rate. The orientation with flow should imply the attainment of a steady-state, and the above experimental result means that this state is reached at lower shear rates (and therefore lower strain) for samples with higher molecular weight.

3.3.1.3. Effect of branching

The effect of branching on crystallization kinetics and morphology is apparently less

Table 3.1. *Composition and molecular weights of LCB-iPP polymers, LCB 01 indicate the linear iPP [Agarwal-2003].*

sample	diene level (ppm)	Molecular weight			
		M_n	M_w	M_z	M_{z+1}
LCB 01	0	51000	150000	249000	356000
LCB 05	170	52000	203000	460000	845000
LCB 07	250	66000	229000	527000	949000
LCB 13	375	112000	276000	634000	118000

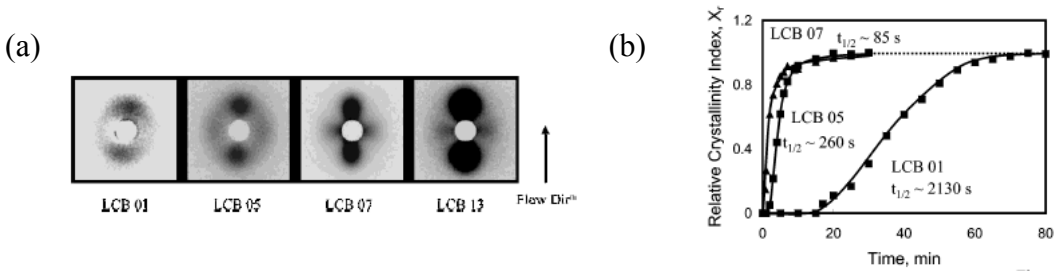

Figure 3.15. *SAXS patterns 30 min after shear (a) and half-time of crystallization (b) of long chain branched polypropylenes ($T_{experiment}$ = 140 ºC, $\dot{\gamma}$ = 60 s^{-1} and t_s = 0.25 s) [Agarwal-2003].*

important than that of molecular weight. A series of long chain branched isotactic polypropylene with four different molecular weights were prepared by adding diene to the reactor during iPP synthesis. The composition of branched isotactic polypropylenes is shown in Table 3.1. All molecular weight components increase significantly with the diene level. Agarwal *et al.* [Agarwal-2003] used a protocol similar to that of Kornfield *et al.* to analyse the effect of branching on shear-induced crystallization. The polymer sample was annealed during 5 min at 200 ºC, cooled at -30 ºC/min to 140 ºC and subjected to a shear rate of 60 s^{-1} for 0.25 s (corresponding strain ≈ 1430 %).

In-situ SAXS measurements made 30 min after shear showed that SAXS intensities along the equator and the meridian increase with the branching level. The meridional maxima are attributed to the evolution of kebab-like lamellar structures oriented perpendicular to the flow direction. Under identical shear conditions, the oriented structures fraction is larger in LCB 13 than in linear polypropylene (Figure 3.15a). From WAXD pattern presented in the work of Agarwal *et al.*, but not shown here, it was concluded that also crystal orientation is stronger in LCB-iPP polymers compared to linear iPP. The effects of LCB on the melt crystallization kinetics under shear can be clearly seen in Figure 3.15b where it is visible that the LCB-iPP polymers crystallize much faster than the linear polymer (the $t_{1/2}$ value for LCB-iPP is about one order of magnitude smaller than that of linear iPP). Agarwal *et al.* attribute the increase in the kinetics to an increase of crystal nuclei due to orientation of polymer molecules and formation of stable crystallization precursor structures in the sheared melt. However, since the alignment of polymer chains with flow should be more difficult for branched polymer chains, we may consider also the possibility of different chains participating in the formation of primary nuclei.

3.3.2. Factors controlling the saturation of crystallization kinetics

3.3.2.1. The nucleation density

The crystallization kinetics from sheared (or unsheared) polymer melts saturates because of the limited nucleation density: the material has finite volume and primary nuclei

must reach critical dimensions to be stable and grow. Therefore, a crystalline solid with the maximum density of nuclei would be formed by tiny crystals, all having the size of critical nuclei. This size may be estimated by measuring the crystallization temperature onset at different cooling rates and extrapolating it to zero cooling rate [Martins-1999].

As mentioned in Chapter 1, the maximum nucleation density measured so far for the quiescent crystallization of polymers was 10^{17} nuceli/m^3 for PE crystallized at 85 ºC [Janeschitz-Kriegl-2003b]. Galeski *et al.* [Nowicki-2004] evaluated the nucleation density in the quiescent crystallization of isotactic polypropylene-montmorillonite nanocomposites. The nuclei density evaluated for an iPP sample with 3% of nanocomposite under quiescent conditions at T_c = 132 ºC was between 10^{12} to 10^{13} nuclei/m^3. This specific sample had better exfoliation. For the pure iPP, the highest nucleation density measured was 10^{16} nuclei/m^3 [Janeschitz-Kriegl-2003b]. All high values for nucleation density in PE and iPP were obtained for low crystallization temperatures. The factor controlling the saturation of crystallization in the quiescent crystallization is therefore the degree of supercooling.

Shear flow accelerates crystallization and nucleation density is expected to increase to larger values. For the iPP nanocomposite mentioned above, at the same crystallization temperature, the observed increase was between 10^3 to 10^4 orders of magnitude (overall nucleation density around of 10^{17} nuclei/m^3). In these experiments, the nanocomposite thin films, obtained by compression molding, were placed between two heated parallel glass plates. Shear flow was applied at the crystallization temperature by moving the lower plate with a constant speed. For this specific case a shear rate of 0.68 s^{-1} was applied during 3 min, ensuring a total strain of ~200 s.u..

To estimate the highest nucleation density resulting from the combined effects of shear flow and supercooling, Janeschitz-Kriegl [Janeschitz-Kriegl-2003b] considered that the rate for formation of primary nuclei is proportional to the specific work, which may be expressed as

$$\overline{w} = \int_0^{t_{shear}} \eta\left[\dot{\gamma}(t)\right]\,\dot{\gamma}^2(t)dt \tag{3.3a}$$

where η is the shear rate dependent viscosity and the integration is over the entire time of shearing [Mykhaylyk-2008]. The Cox-Merz rule is generally used to evaluate the viscosity at a specific shear rate from the complex viscosity at a specific oscillation frequency. For a constant shear rate the above equation reduces to

$$\overline{w} = \eta\gamma^2 / t_{shear} \quad . \tag{3.3b}$$

Figure 3.16 shows estimated values of nucleation density for different supercooling degrees and values of specific work evaluated following the procedure described above. They refer to the shear-induced crystallization of iPP. Lines connecting data points for the same specific work have negative slope, which decreases with the increase of specific work. Application of mechanical work allows observing significant nucleation density at relatively low supercoolings, around 60 ºC. Similar nucleation density may be observed under quiescent conditions but at much larger supercoolings. Extrapolation of different lines converges to a value of nucleation density between 10^{18} and 10^{19} nuclei/m^3, which would correspond to cooling a quiescent melt with a supercooling of around 140 ºC. One may therefore consider the above values as the maximum allowable nucleation density in polymer crystallization.

It is implicit in the above results that Janeschitz-Kriegl considers the mechanical work performed on the supercooled melt the factor controlling the nucleation density increase. On the other hand, as mentioned above, Kornfield *et al.* considers the stress as the factor controlling the transition from the skin oriented layer to a core spherulitic structure. To understand which factor is controlling the nucleation density increase, the different contributions to the final nucleation density value must be evaluated separately. At first, and most importantly, is the degree of supercooling. The second factor is the deformation imposed on the supercooled melt. At last one has to consider the melt memory effect contribution to the overall nucleation density.

The typical nucleation density for the quiescent crystallization of iPP at a supercooling

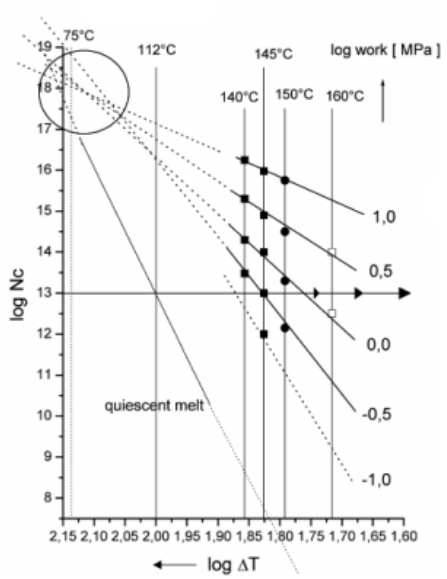

Figure 3.16. *Double-logarithmic plot for the density of nuclei as a function of supercooling degree. The course of line for quiescent melt considers the evaluated nucleation density at different supercoolings (note that the slope of the log of the work for a quiescent melt is infinite). Lines connecting symbols data points refer to the same value of specific work [Janeschitz-Kriegl-2003b].*

of around 90 ºC is ~10^{10} nuclei/m^3. The effect of melt memory in the nucleation density increase at the same crystallization temperature was estimated to be, at maximum, around 10^2 nuclei/m^3. It remains therefore that the additional contribution of shear deformations applied on the supercooled melt is around 10^7 nuclei/m^3 [Zhang-2007].

3.3.2.2. Effect of shear deformations applied above the nominal melt temperature

As mentioned above, studies on the melt memory effect on shear induced crystallization identified the strain applied to the molten polymer as the factor controlling both shear-induced isothermal and non-isothermal crystallization. The melt state responsible for this saturation was also identified as the steady-state. It was also shown that at this state the number of topological constraints is significantly lower than for an unsheared polymer melt. For iPP around 2/3 of topological constraints are destroyed during the transition to steady state [Zhang-2006, Martins-2006]. A large number of experiments with different polymers, including ionomers, slightly crosslinked polyethylenes, Ziegler-Natta and metallocene catalyzed polyethylenes, that will be presented in Chapters 4 and 5 of this work confirmed these results.

From the results presented in §3.1 for melt morphology and in §3.2 for precursor structures, information can be obtained for the melt morphology at steady state, which is important to understand the role of precursor structures in shear-induced crystallization. As mentioned above, the key question is to understand how in entangled polymers oriented structures with the flow direction can coexist with a dynamic melt, in which it is known that in shear flow the maximum extension is around 40% the full chain length. Further, a fully stretched chain segment between constraints, evaluated from the molecular weight between entanglements, is around 110 Å for PE and ~350 Å for iPP. Further discussion on these issues will be done in Chapter 4 of this work.

3.3.2.3. Effect of shear deformations applied at the crystallization temperature

Contrary to the experiments of Martins *et al.* [Martins-2006, Zhang-2006] where shear was applied at the processing temperature, Janeschitz-Kriegl *et al.* [Janeschitz-Kriegl-1999, Janeschitz-Kriegl-2003a, Liedauer-1993] and Kornfield *et al.* [Kumaraswamy-1999, Kumaraswamy-2000, Kumaraswamy-2002, Seki-2002] used the short-term shearing protocol. The objective of this protocol was to separate the effects of primary nucleation resulting from shear deformation, which was assumed to occur mainly during shear, from the growth of crystals. Results obtained with this protocol were described as well as the different factors

contributing to the overall nucleation density. Shear deformation applied at the crystallization temperature is just one of the three factors above identified.

The thermo-mechanical protocol used by Janeschitz-Kriegl *et al.* is indicated in Figure 3.17. Polymer sample is initially held during a time t_{relax} at a temperature higher than thermodynamic melting temperature to erase the memory of filling process and cooled to crystallization temperature, which is between 140 ºC and 160 ºC. When the nominal isothermal temperature is reached, the polymer melt is subjected to flow (t_s in range 0.1 to 1 s, shear rate in the range 300 to 1000 s^{-1}). Importantly, during this stage, the polymer at an accumulator, which is at a temperature much higher than the polymer at the duct, is pumped to the duct, disturbing therefore the initially established isothermal conditions. However, since the isothermal crystallization temperatures used in these experiments are relatively high, and the crystallization time long, the process may be assumed as nearly isothermal.

The time, at which the retardation reaches half the wavelength, was measured and plotted as a function of shearing time for different shear rates at the wall (Figure 3.18). From this plot it was then concluded that crystallization rate is a product of the fourth power of shearing rate and second power of shearing time: $\dot{\gamma}^4 t_s^2$. The second power of shearing time was evaluated from the slope of solid lines fitting the data at constant shear rate, while the fourth power of shearing rate was evaluated from distances between adjacent lines (*i*, *i-1*) corresponding to $4\log(\dot{\gamma}_{w,i-1}/\dot{\gamma}_{w,i})$. The number of nuclei increases with the increase of supercooling degree and mechanical work (longer shearing time and higher shear rate) [Liedauer-1993].

In the experimental protocol of Kornfield *et al.* the reservoir was filled with polymer melt and held at 225 ºC (above the equilibrium melting temperature of polymer equal 208 ºC) for 5 min. Then the polymer melt was cooled to different crystallization temperatures T_c and

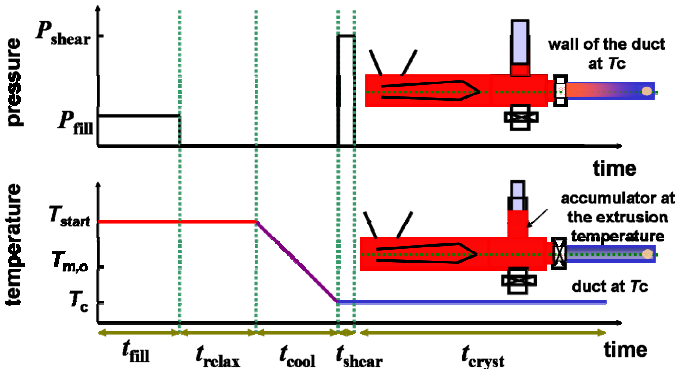

Figure 3.17. *The protocol of short-term shearing experiment performed by Janeschitz-Kriegl et al. [Janeschitz-Kriegl-1999, Janeschitz-Kriegl-2003a, Liedauer-1993] and later by Kornfield et al. [Kumaraswamy-2000, Kumaraswamy-2002, Seki-2002].*

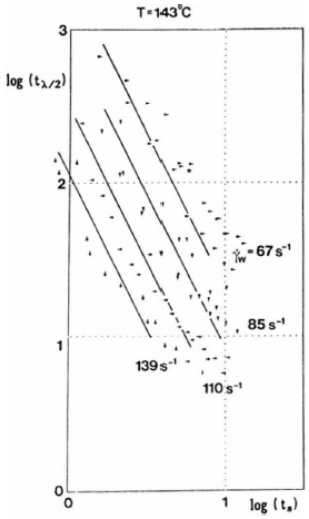

Figure 3.18. *Double logarithmic plot of time at which half the wave length of retardation is reached against the shearing time for polypropylene at 143 ºC, the shear rate at the wall $\dot{\gamma}_w$ is used as parameter [Liedauer-1993].*

subjected to flow with shear stress at the wall, σ_w, of 0.03 and 0.06 MPa during different shearing times t_s. The polymer was then allowed to crystallize. The turbidity and birefringence variation were monitored as a function of crystallization time. It was found that crystallization time decreased with increasing shearing time and saturated (reached a plateau after shearing time of 5 s, and longer duration of shear didn't reduce further $t_{1/2}$). The enhancement in crystallization kinetics was expressed by the change of $t_{1/2}$ with shearing time, where the half-time, $t_{1/2}$, is the time taken for the transmitted intensity to decrease to half of its initial value. It must be noted that this half-time is different from the crystallization half-time measured with a thermal analysis instrument, because crystallization of material near the windows is enough to reduce the transmitted intensity to half of its initial value.

3.4. Shear-induced non-isothermal crystallization

Despite its importance in the processing of semicrystalline polymers, only a few works reported results on shear-induced non-isothermal crystallization. Included in this classification are works where shear deformation was applied during the cooling process, following a protocol similar to the short-term shearing protocol. Previously, in §3.2.1, the effects of shear deformations applied at the molten state and cooling the melt with different rates were discussed.

One work on shear-induced non-isothermal crystallization presented results obtained with a parallel plate rheometer, which incorporates a differential thermal analysis setup [Nagatake-2000]. Another analyzed the effect of pre-shear treatments on the shear induced

non-isothermal crystallization of isotactic polypropylene (iPP), and Small Angle X-ray Scattering (SAXS) was used to follow the crystallization kinetics [Li-2005b]. Only low shear rates were used, and both works concluded that shear flow accelerates the crystallization kinetics.

The effects of shear rate, pressure and molecular weight on the non-isothermal crystallization of iPP were also analyzed with a dilatometer [Van der Beck-2006]. In this work the shear rate was applied at different temperatures during the cooling process and cooling rates were about -1.4 to -2 ºC/min. Shear rates and shear duration were controlled for ensuring a constant strain. The main conclusions are similar to those reported above. Increasing the temperature at which shear is applied resulted in an increase of the liquid to solid onset transition temperature and less oriented samples. It was also stated in this work that application of shear at high temperatures resulted in a remelting of "*flow-induced crystalline structure*" and relaxation of oriented chains.

3.5. The solid state morphology

3.5.1. Skin-core morphology

As mentioned before, crystallization kinetics after shear is always accelerated compared to quiescent crystallization. Under certain conditions, an oriented skin layer and a core spherulitic structure are observed [Kumaraswamy-1999, Kornfield-2002, Seki-2002, Yang-2004]. Between the skin and core layers, a "fine-grained" layer exists, which due to rotational component of shear flow, contains crystals aligned in a direction transverse to the flow [Jerschow-1996]. The optical micrographs in Figure 3.19 show crystallites with

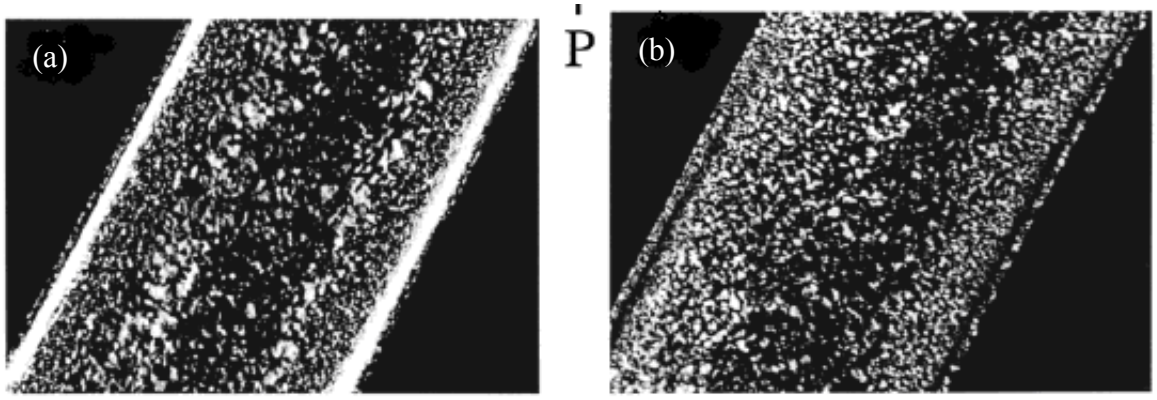

Figure 3.19. *Micrograph of PP crystallized at 141 ºC after shearing at a wall shear stress of 0.06 MPa for12 s; characteristic skin-core morphology is formed. Bright region represents oriented skin when is viewed down the neutral direction (a) and dark when is viewed down the flow direction (b) [Kumaraswamy-1999].*

cylindrical geometry oriented along the flow direction in the skin region. In the centre sperulitic structures are observed, which are much smaller than those observed during quiescent crystallization in the same conditions. Based on the above observations a schematic model showing the evolution of those structures with shearing time was proposed by Kumaraswamy *et al.* (Figure 3.20). Immediately after 1 s of shearing the nucleation density near the wall is much higher when compared with that at the core. Long threadlike precursors are formed at 2 s of shearing. They proliferate with time, and after 4 s saturation of the density of threadlike precursors is observed. The nonlinear dependence of the nucleation density with distance from the wall suggests that nuclei are transformed the action of flow. A "*critical*" shear stress at the boundary between the skin (containing the threadlike precursors) and "*fine-grained*" layer (containing the core spherulites structures) was calculated by authors to be 0.047 MPa [Kumaraswamy-1999]. Shearing the polymer melt with shear stress lower than critical value (0.03 MPa) with a strain similar to that used to generate the skin-core morphology, enhances crystallization but doesn't cause the formation of skin-core structure. Isayev *et al.* [Isayev-1995] found that at higher temperatures, higher shear strains are needed to develop an oriented skin layer.

3.5.2. The shish-kebab

The skin layer observed above critical value of stress was found to be composed from structures reminding shish-kebabs observed in injection-molded strips. Those structures were observed for the first time in polyethylene's solutions by Pennings *et al.* [Pennings1965] in 1965. They argued that central core fibrils (shish) are formed from fully stretched/extended chains and lamellae (kebabs) are formed from folded-chain lamellar structures. The chain alignment in the kebabs was believed to be parallel to the central core.

Presently it is known that the chains in the shish part are extended out in the direction

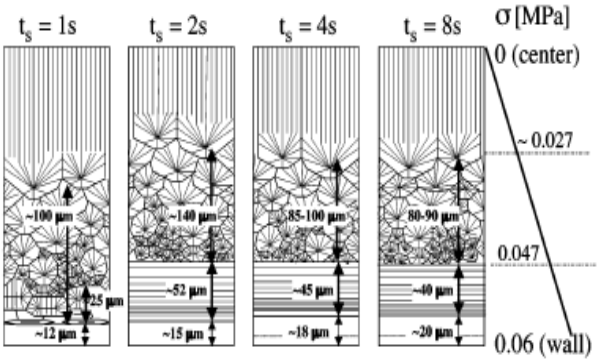

Figure 3.20. *Diagram of evolution of the final semicrystalline microstructure with increasing shear duration at 141 ºC [Kumaraswamy-2004].*

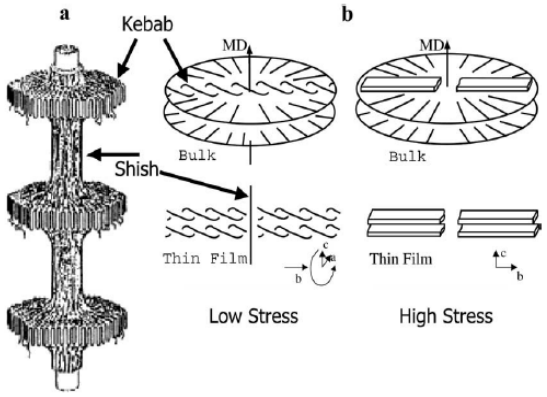

Figure 3.21. *Schematic model of shish-kebab structures depending on shear stress in polyethylene [Keller-1997].*

of the flow filed. When flow is stopped and the sample supercooled, polymer crystallizes, the chain relaxation is inhibited and fibril structures, the "shish", are created [Holt-2002]. The shish structures may be crystalline or mesomorphic (with small crystalline fraction) but both have similar linear connectivity along the flow direction. The kebabs (shish-induced layered crystalline lamellae) are perpendicular to the flow direction, have poor lateral connectivity and grow out epitaxially and radially from the line nuclei through a secondary nucleation process [Nogales-2001, Somani-2005]. The shish-kebab structures are observed in strong elongational flows and in shear flow close to the slit wall where the shear stress can be very large [Eder-1997].

Because the presence of long chains enhances the formation of shish, Kimata *et al.* [Kimata-2007] hypothesized that shish propagate by a local mechanism that is active at the long chain ends. The longer chains in the melt accelerate this propagation after being adsorbrd to the tip of a shish, and by recruiting neighbouring chains to join them.

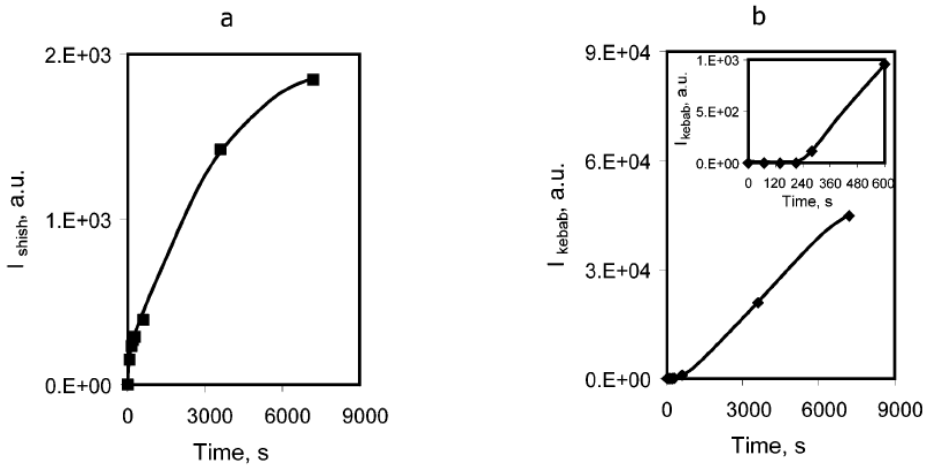

Figure 3.22. *The SAXS intensities of shish (a) and kebab (b) as a function of time for Ziegler-Natta iPP ($\dot{\gamma}$ = 60 s^{-1}, t_s = 5 s, T = 165 ºC) [Somani-2002b].*

According to the classical polymer flow theories [Doi-1986], the flexible polymer becomes oriented and stretched, and may form shish when the Weissenberg number is equal to or larger than 1 ($W_e = \dot{\gamma}\tau \geq 1$; shear rate is high enough to orientate chains, nucleation is increased and crystals' anisotropy grow) [Kumaraswamy-2005]. Keller *et al.* [Keller-1997] distinguished 3 different types of row structures that depend on the magnitude of the applied shear stress. Twisted shish-kebab structures, fibre-aligned shish-kebab structures and high density extended fibril structures may exist, depending on the flow regime intensity, low, medium and high regimes, respectively. In low shear stress regime the lamellae can grow unrestricted due to low density of fibril nucleation centres and they exhibit a twisted structure. For medium shear stress regime they are forced to exhibit fibre-aligned structure due to higher density of nucleating fibres, and for the high shear stress regime the nucleating fibrils are so dense that dominate the morphology [Holt-2002]. Two different kebabs structures, twisted shish-kebab and high density extended fibril structures, depending on shear stress, are presented on Figure 3.21.

There is no doubts that shish are created before kebabs. Somani *et al.* [Somani-2002b] investigated the shish and kebab SAXS intensities variation with time after shear in Ziegler-Natta iPP and showed that I_{shish} rises immediately after shear while I_{kebab} increases after an induction time (inset in Figure 3.22), but its increasing rate is much greater than that of I_{shish}. They also differ in thermal stability. Unoriented iPP crystals melt at about 165 ºC, the kebabs start to melt at about 170-175 ºC, and the shish are completely molten at about 180-185 ºC.

3.6. References

Acierno-2003 — Acierno S, Palomba B, Winter HH, Grizzuti N (2003) *Effect of molecular weight on the flow-induced crystallization of isotactic poly(1-butene)*. Rheol Acta 42:243-250.

Agarwal-2003 — Agarwal PK, Somani RH, Weng W, Mehta A, Yang L, Ran S, Liu L, Hsiao BS (2003) *Shear-Induced crystallization in novel long chain branched polypropylenes by in situ rheo-SAXS and -WAXD*. Macromolecules 36:5226-5235.

Azzurri-2005 — Azzurri F, Alfonso GC (2005) *Lifetime of shear-induced crystal nucleation precursors*. Macromolecules 38:1723-1728.

Ballard-1980 — Ballard DGH, Burgess AN, Nevin A, Cheshire P, Longman GW, Schelten J (1980) *Small Angle Neutron Scattering studies on polypropylene*. Macromolecules 13:677-681.

Bent-2003 Bent J, Hutchings LR, Richards RW, Gough T, Spares R, Coates PD, Grillo I, Harlen OG, Read DJ, Graham RS, Likhtman AE, Groves DJ, Nicholson TM, McLeish TCB (2003) *Neutron-mapping polymer flow: scattering, flow visualization and molecular theory*. Science 301:1691-1695.

Blundell-1996 Blundell DJ, MacKerron DH, Fuller W, Mahendrasingam A, Martin C, Oldman RJ, Rule RJ, Riekel C (1996) *Characterization of strain-induced crystallization of poly(ethylene terephthalate) at fast draw rates using synchrotron radiation*. Polymer 37:3303-3311.

Butler-2002 Butler S, Harrowell P (2002) *Factors determining crystal–liquid coexistence under shear.* Nature 415:1008-1011.

Chai-2003 Chai CK, Auzoux Q, Randrianatoandro H, Navard P, Haudin J-M (2003) *Influence of pre-shearing on the crystallisation of conventional and metallocene polyethylenes*. Polymer 44:773-782.

Doi-1986 Doi M, Edwards SF (1986) *The theory of polymer dynamics*. Clarendon, Oxford.

Duplay-2000 Duplay C, Monasse B, Haudin J-M, Costa J-L (2000) *Shear-induced crystallization of polypropylene: Influence of molecular weight*. J Mater Sci 35:6093-6103.

Earl-1979 Earl WL, VanderHart DL (1979) *Observations in solid polyethylenes by carbon-13 nuclear magnetic resonance with magic angle sample spinning*. Macromolecules 12:762-767.

Eder-1997 Eder G, Janeschitz-Kriegl H (1997) *Crystallization.* Materials Science and Technology. Process Polym 18:269–342, ed. HEH Meijer, Wiley-VCH Weinheim.

Elmoumni-2003 Elmoumni A, Winter HH, Waddon AJ (2003) *Correlation of material and processing time scales with structure development in isotactic polypropylene crystallization*. Macromolecules 36:6453-6461.

de Gennes-1974 de Gennes PG (1974) *Coil-stretch-transition of dilute flexible polymer under ultra-high velocity gradients*. J Chem Phys 60:5030-5042.

Gutiérrez-2004 Gutiérrez M-CG, Alfonso GC, Riekel C, Azzurri F (2004) *Spatially resolved flow-induced crystallization precursors in isotactic polystyrene by simultaneous Small- and Wide-Angle X-ray microdiffraction*. Macromolecules 37:478-485.

Heeley-2002 Heeley EL, Poh CK, Li W, Maidens A, Bras W, Dolbnya IP, Gleeson AJ, Terrill NJ, Fairclough JPA, Olmsted PD, Ristic RI, Hounslow MJ, Ryan AJ (2002) *Are metastable, precrystallisation, density-fluctuations a universal phenomena?* Faraday Discuss 122:343-361.

Hill-1983 Hill MJ, Barham P, Keller A (1983) *Hairdressing shish-kebabs; comprehensive survey and theoretical discussion of overgrowth crystallization.* Colloid Polym Sci 261:721-735.

Holt-2002 Holt J (2002) S*tructure of polethylene materials subjected to shear flow in the melt*. The University of Reading. Whiteknights, United Kingdom.

Hsiao-1995 Hsiao BS, Sauer BB, Verma RK, Zachman HG, Seifert S, Chu B, Harney P (1995) *New insight of isothermal melt crystallization in poly(aryl ether ether ketone) via time-resolved simultaneous Small-Angle X-ray Scattering/Wide-Angle X-ray Diffraction measurements*. Macromolecules 28:6931-6936.

Imai-1992 Imai M, Mori K, miaukami T, Kaji K, Kanya T (1992) *Structural formation of poly (ethylene terephthalate) during the induction period of crystallization: 1. Ordered structure appearing before crystal nucleation*. Polymer 33:4451-4456.

Imai-1994 Imai M, Kaji K, Kanya T (1994) *Structural formation of poly(ethylene terephthalate) during the induction period of crystallization. 3. Evolution of density fluctuations to lamellar crystal*. Macromolecules 27:7103-7108.

Isayev-1995 Isayev AI, Chan TW, Shimojo K, Gmerek M (1995) *Injection-molding of semicrystalline polymers. 1. Material characterization*. J Appl Polym Sci 55:807-819.

Janeschitz-Kriegl-1999 Janeschitz-Kriegl H, Ratajski E, Wippel H (1999) *The physics of athermal nuclei in polymer crystallization*. Colloid Polym Sci 277:217-226.

Janeschitz-Kriegl-2003a Janeschitz-Kriegl H, Ratajski E, Stadlbauer M (2003) *Flow as an effective promotor of nucleation in polymer melts: a quantitative evaluation*. Rheol Acta 42:355–364.

Janeschitz-Kriegl-2003b Janeschitz-Kriegl H (2003) *How to understand nucleation in crystallizing polymer melts under real processing conditions*. Colloid Polym Sci 281:1157-1171.

Janeschitz-Kriegl-2007 Janeschitz-Kriegl H (2007) *An unusual but consistent view on flow induced crystallization of polymers*. Monatshefte für Chemie 138:327-335.

Jerschow-1996 Jerschow P, Janeschitz-Kriegl H (1996) *On the development of oblong particles as precursors for polymer crystallization from shear flow: origin of the so-called fine grained layers*. Rheol Acta 35:127-133.

Jerschow-1997 Jerschow P, Janeschitz-Kriegl H (1997) *The role of long molecules and nucleating agnets in shear induced crystallization of isotactic polypropylenes*. Int Polym Process 12:72-77.

Keller-1997 Keller A, Kolnaar HWH (1997) *Flow induced orientation and structure formation*. Mater Sci and Technol, Processing of Polymers 18:189-268.

Kimata-2007 Kimata S, Sakurai T, Nozue Y, Kasahara T, Yamaguchi N, Karino T, Shibayama M, Kornfield JA (2007) *Molecular basis of the shish-kebab morphology in polymer crystallization*. Science 316:1014-1017.

Kornfield-2002 Kornfield JA, Kumaraswamy G, Issaian AM (2002) *Recent advances in understanding flow effects on polymer crystallization*. Ind Eng Chem Res 41:6383-6392.

Kriste-1975 Kirste RG, Kruse WA, Ibel K (1975) *Determination of the conformation of polymers in the amorphous solid state and in concentrated solution by neutron diffraction*. Polymer 16:120-124.

Kumaraswamy-1999 Kumaraswamy G, Issaian AM, Kornfielfd JA (1999) *Shear-enhanced crystallization in isotactic polypropylene. 1. Correspondence between in situ rheo-optics and ex situ structure determination*. Macromolecules 32:7537-7547.

Kumaraswamy-2000 Kumaraswamy G, Varma RK, Issaian AM, Kornfield JA, Yeh F, Hsiao BS (2000) *Shear-enhanced crystallization in isotactic polypropylene. Part 2. Analysis of the formation of the oriented skin*. Polymer 41:8931-8940.

Kumaraswamy-2002 Kumaraswamy G, Kornfield JA, Yeh F, Hsiao BS (2002) *Shear-enhanced crystallization in isotactic polypropylene. 3. Evidence for a kinetic pathway to nucleation*. Macromolecules 35:1762-1769.

Kumaraswamy-2004 Kumaraswamy G, Verma RK, Kornfield JA, Yeh F, Hsiao BS (2004) *Shear-enhanced crystallization in isotactic polypropylene. In-situ synchrotron SAXS and WAXD*. Macromolecules 37:9005-9017.

Kumaraswamy-2005 Kumaraswamy G (2005) *Crystallization of polymers from stressed melts*. J Macromol Sci, Part C: Polym Rev 45:375–397.

LeDuc-1999 LeDuc P, Haber C, Bao G, Wirtz D (1999) *Dynamics of individual flexible polymers in a shear flow.* Nature 399:564-566.

Li-2005a Li L, De Jeu WH (2005) *Flow-induced mesophases in crystallizable polymers*. Adv Polym Sci 181:75-120.

Li-2005b Li ZM, Li LB, Shen KZ, Yang MB, Huang R (2005) *In situ poly(ethylene terephthalate) microfibers- and shear-induced non-isothermal crystallization of isotactic polypropylene by on-line Small Angle X-ray Scattering*. Polymer 46:5358-5367.

Lieberwirth-2000 Lieberwirth I, Loos J, Petermann J, Keller A (2000) *Observation of shish crystal growth into nondeformed melts*. J Polym Sci, Polym Phys 38:1183-1187.

Liedauer-1993 Liedauer S, Eder G, Janeschitz-Kriegl H, Jerschow P, Geymayer W, Ingolic E (1993) *On the kinetics of shear induced crystallization in polypropylene*. Intern Polym Proc 8:236-244.

Martins-1999 Martins JA, Cruz-Pinto JJC (1999) *The temperature calibration on cooling of differential scanning calorimeters*. Thermochimica Acta 332:179-188.

Martins-2006 Martins JA, Zhang W, Brito AM (2006) *Saturation of shear-induced isothermal crystallization of polymers at the steady state and the entanglement-disentanglement transition*. Macromolecules 39:7626-7634.

Martins-2008 Martins JA, Zhang W (2008) *Effect of melt memory on the shear-induced non-isothermal crystallization of polypropylene and evaluation of the size of precursor structures*. Submitted to Macromolecules.

Mykhaylyk-2008 Mykhaylyk OO, Chambon P, Graham RS, Patrick J, Fairclough A, Olmsted PD, Ryan AJ (2008) *The specific work of flow as a criterion for orientation in polymer crystallization*. Macromolecules 41:1901-1904.

Nagatake-2000 Nagatake W, Takahashi T, Masubuchi Y, Takimoto JI, Koyama K (2000) *Development of sheer flow thermal rheometer for direct measurement of crystallization fraction of polymer melts under shear deformation*. Polymer 41:523-531.

Nogales-2001 Nogales A, Hsiao BS, Somani RH, Srinivas S, Tsou AH, Balta-Calleja FJ, Ezquerra TA (2001) *Shear-induced crystallization of isotactic polypropylene with different molecular weight distributions: in situ Small- and Wide-Angle X-ray Scattering studies*. Polymer 42:5247-5256.

Nogales-2003 Nogales A, Olley RH, Mitchell GR (2003) *Directed crystallisation of synthetic polymers by low-molar-mass self-assembled templates*. Macromol Rapid Commun 24:496-502.

Nowicki-2004 Nowacki R, Monasse B, Piorkowska E, Galeski A, Haudin JM (2004) *Spherulite nucleation in isotactic polypropylene based nanocomposites with montmorillonite under shear*. Polymer 45:4877-4892.

Pennings-1965 Pennings AJ, Kiel AM (1965) *Fractionation of polymers by crystallization from solution. III. The morphology of fibrillar polyethylene crystals grown in solution*. Kolloid Z Z Polymere 205:160-162.

Perkins-1997 Perkins TT, Smith DE, Chu S (1997) *Single polymer dynamics in an elongational flow*. Science 276:2016-2021.

Petermann-1977 Petermann J, Gleiter H (1977) *Electron microscopic observations on the crystallization of row structures in strained melts*. Polym Lett Ed 15:649-654.

Pogodina-2001 Pogodina NV, Lavrenko VP, Srinivas S, Winter HH (2001) *Rheology and structure of isotactic polypropylene near the gel point: quiescent and shear-induced crystallization*. Polymer 42:9031-9043.

Pope-1978 Pope DP, Keller A (1978) *A study of the chain extending effect of elongational flow in polymer solutions*. Colloid Polym Sci 256:751-756.

Pratt-1978 Pratt LR, Hsu CS, Chandler D (1978) *Statistical mechanics of small chain molecules in liquids. I. Effects of liquid packing on conformational structures*. J Chem Phys 68:4202-4212.

Ryan-1999 Ryan AJ, Fairclough JPA, Terrill NJ, Olmsted PD, Poon WCK (1999) *A scattering study of nucleation phenomena in polymer crystallization*. Faraday Discussion 112:13-29.

Seki-2002 Seki M, Thurman DW, Oberhauser JP, Kornfield JA (2002) *Shear-mediated crystallization of isotactic polypropylene: the role of long chain-long chain overlap*. Macromolecules 35:2583-2594.

Smith-1999 Smith DE, Babcock HP, Chu S (1999) *Single-polymer dynamics in steady shear flow*. Science 283:1724-1727.

Somani-2000 Somani RH, Hsiao BS, Nogales A, Srinivas S, Tsou AH, Sics I, Balta-Calleja FJ, Ezquerra TA (2000) *Structure development during shear flow induced crystallization of i-PP: in-situ Small Angle X-ray Scattering study*. Macromolecules 33:9385-9394.

Somani-2002a Somani RH, Yang L, Hsiao BS (2002) *Precursors of primary nucleation induced by flow in isotactic polypropylene*. Physica A 304:145-157.

Somani-2002b Somani RH, Yang L, Hsiao BS, Agarwal PK, Fruitwala HA, Tsou AH (2002) *Shear-induced precursor structures in isotactic polypropylene melt by in-situ rheo-SAXS and rheo-WAXD studies*. Macromolecules 35:9096-9104.

Somani-2005 Somani RH, Yang L, Zhu L, Hsiao BS (2005) *Flow-induced shish-kebab precursor structures in entangled polymer melts*. Polymer 46:8587-8623.

Somani-2006 Somani RH, Yang L, Hsiao BS (2006) *Effects of high molecular weight species on shear-induced orientation and crystallization of isotactic polypropylene*. Polymer 47:5657-5668.

Van der Beck-2006 Van der Beck MHE, Peters GWM, Meijer HEH (2006) *Influence of shear flow on the specific volume and the crystalline morphology of isotactic polypropylene*. Macromolecules 39:1805-1814.

Wang-1997 Wang W, Schultz JM, Hsiao BS (1997) *Dynamic study of crystallization- and melting-induced phase separation in PEEK/PEKK blends*. Macromolecules 30:4544-4550.

Vleeshouwers-1996 Vleeshouwers S, Meijer HEH (1996) *A rheological study of shear induced crystallization*. Rheologica Acta 35:391-399.

Yang-2004 Yang L, Somani RH, Sics I, Hsiao BS, Kolb R, Fruitwala H, Ong C (2004) *Shear-induced crystallization precursor studies in model polyethylene blends by in-situ rheo-SAXS and rheo-WAXD*. Macromolecules 37:4845-4859.

Zhang-2006 Zhang W, Martins JA (2006) *Evaluation of the effect of melt memory on shear-induced crystallization of low-density polyethylene*. Macromol Rapid Commun 27:1067-1072.

Zhang-2007 Zhang W, Martins JA (2007) *Shear-induced non-isothermal crystallization of low-density polyethylene.* Polymer 48:6215-6220.

4. Origin of the melt memory effect during the crystallization of high-density polyethylene with different crosslinking degrees

Abstract

One linear and two slightly crosslinked high-density polyethylenes were used to study the effect of chain interactions resulting from crosslinks on the saturation of crystallization kinetics of melts sheared at temperatures above their equilibrium melting temperature. By shearing the melts at these temperatures and recording further their crystallization kinetics, it was intended to generate the thermal and mechanical history responsible for the melt memory effect. It was found a saturation of crystallization kinetics for melts sheared up to steady state. The excess of the specific free energy of these melts was evaluated, and it was used to predict the precursor structures dimensions at steady state. It was also proposed that erasing the melt memory effect results in the randomization and aggregation of precursor structures existing at steady state. It was predicted that precursor structures of quiescent and relaxed polymer melts should be similar in length, but larger in thickness, when compared with those existing at steady state.

4.1. Introduction

Thermal analysis instruments, among them Differential Scanning Calorimeters, DSC's, are usually used to study the quiescent crystallization of polymer melts. Samples cut from previously extruded polymer pellets are molten in aluminium pans to increase the sample contact area with the pan, the pans crimped, and DSC experiments performed. Further, samples heated above the polymer equilibrium melting temperature are cooled down to the crystallization temperature with a fast cooling rate, and the exothermal peak's evolution is recorded as a function of crystallization time. Because polymers retain the memory of their previous thermal and mechanical history, reproducible crystallization experiments are only obtained when samples are heated at high temperatures for a short time or at lower temperatures for a longer time. This annealing process at temperatures above the polymer equilibrium melting temperature is necessary to erase the "melt memory". This effect was studied, among others, by Ziabicki and Alfonso [Ziabicki-1994, Alfonso-1995].

Because polymer samples were submitted to previous shear deformations during their processing stage, it seems natural to assign the melt memory effect origin to deformations

imposed during that stage, which are frozen during solidification and erased after thermal treatments above the equilibrium melting temperature. It is the purpose of this work to verify this assumption for polyethylene samples with different, small, crosslinking degrees. Therefore, the quiescent (isothermal and non-isothermal) crystallization kinetics of a relaxed melt, with its melt memory erased, is recorded when it is cooled from a specific melt temperature. Controlled shear deformations applied at the same melt temperature should then enhance the crystallization kinetics until its saturation.

One single argument justifies the saturation of crystallization kinetics. It is the finite volume of material and the need of stable nuclei with critical dimensions. It is known from experimental results that the maximum nuclei density in polymer crystallization should be around 10^{19} nuclei/m^3 [Janeschitz-Kriegl-2003]. Three different factors contribute to this value. The most significant contribution results from the supercooling degree, which is around 10^{11} to 10^{12} nuclei/m^3. An additional contribution of around 10^5 up to 10^6 nuclei/m^3 results from deformations applied to the supercooled melt. The contribution studied in this work to the overall nucleation density is no more than 10^2 nuclei/m^3 [Zhang-2007].

Before going on to a detailed description of the experimental procedure and results obtained, and to fundament further the discussion and conclusions made in this work, it is important to make a brief literature review of the effect of shear flow on crystallization kinetics.

It is consensual that shear flow, applied above or below the equilibrium melting temperature, accelerates crystallization kinetics. The acceleration results from an increase of nucleation density. The origin of this increase is assigned to the formation of precursor structures. It is considered that they are induced only by flow deformation of the melt, and therefore inexistent in a quiescent, relaxed melt [Somani-2002a, Somani-2002b, Gutiérrez-2004, Azzuri-2008]. However, the same structures responsible for the acceleration of crystallization from sheared melts should also be at the origin of melt memory effect.

The origin of these structures in unknown and many researchers dedicated efforts to understand their formation and identify their size. Some experimental techniques used for this purpose were birefringence and turbidity measurements [Kornfield-2002, Kumaraswamy-1999], depolarized light spectroscopy, Small and Wide Angle X-ray Scattering that were coupled to shear cells, usually modified Linkam hot-stages [Nogales-2003, Somani-2002a, Somani-2002b, Somani-2005]. Besides rheometers and modified rheometers [Elmoumni-2003, Acierno-2003, Pogodina-2001], other instruments were also used to follow the effect of shear on crystallization. Some experiments carried out with modified instruments can be classified in two types: those making used of the short-term

shearing protocol [Kornfield-2002, Jerschow-1997, Janeschitz-Kriegl-2007] where shear deformation is applied at the nominal crystallization temperature, and "*the melt memory protocol*" where shear deformation is applied above the melting temperature [Martins-2006, Zhang-2006]. Still other experimental setups include the "generation of precursor structures" with extruders. With the extruder working at steady state, the extrudate (iPP) was frozen in liquid nitrogen and the length-scale of precursor structures evaluated by SAXS was between 50 and 200 Å [Ryan-1999].

From these and other experiments, we know that precursor structures do not have crystallographic order, that they are "long-lived" and survive up to two hours after cessation of shear, and that they are characterized by a layer-like superstructure with an average spacing between layers of 400 Å. It is also assumed, *without proof*, that they are formed only after shearing the melt and that they are too tinny and thin to have any influence on the rheology of polymer melts [Janeschitz-Kriegl-1997, Janeschitz-Kriegl-1999].

The results presented in this work allow indentifying the melt state where precursor structures reach their maximum effectiveness, which is also the melt state responsible for the melt memory effect. To our knowledge, this is the first work where the effect of crosslinking degree on the crystallization kinetics of sheared melts is analysed and discussed. Quiescent crystallization studies with crosslinked polyethylene samples showed that crystallization kinetics accelerates by increasing the crosslinking degree, a result ascribed to the increase of gel fraction [Hutzler-2000].

Below, the experimental part of the work describes the material's characterization and equipments used. The experimental protocols followed with thermal analysis equipments (a Differential Scanning Calorimeter and a shear DTA) and rheometers are described with detail. A sample of representative experimental results for the quiescent and shear-induced crystallization kinetics is presented, together with results obtained with a rheometer that were crucial to identify and characterize the melt state responsible for the saturation of crystallization. The discussion also presents predictions for the dimensions of precursor structures at steady state and discusses their validity.

4.2. Experimental

4.2.1. Materials characterization

The material used in this work was a high density polyethylene, grade Stamylan HD 2H280 from DSM, named PEA, with a melt flow index equal to 22 g/10 min (200 ºC with

a load of 2.16 kg, ISO 1133). This material was crosslinked by reactive extrusion with a peroxide concentration of 0.01 % and 0.05 % per weight, yielding samples PEB and PEC, respectively. The polyolefins were tumble mixed with different peroxide concentrations in a laboratory modular Leistritz LSM 30.34 intermeshing co-rotating twin-screw extruder according to a procedure already used for the same material (barrel temperature 200 ºC, screw speed 75 rpm and flow rate 5 kg/h) [Machado-2001]. The corresponding melt flow index for PEB and PEC is 12 g/min and 2.5 g/min, respectively.

Despite the evident differences in the melt flow index, attempts to evaluate the gel content failed. This evaluation followed a procedure already used for the same polymer [Machado-2001]. Samples of around 1.5 g were placed in 120 mesh stainless-steel cages and immersed in boiling toluene. The extractions were carried out under reflux for 24 h with solvent change after 12 h. After removal from the boiling solvent, the samples were dried in a vacuum oven during 5 h at 80 ºC in a nitrogen atmosphere. After weighting the samples of PEA, PEB and PEC, the gel content evaluated did not show differences between them, which allowed us to conclude that it was too small to be detected.

Relevant properties for these materials are in Table 4.1. All samples have similar density measured at 25 ºC. Molecular weights and their distribution were determined at University of Opole (Poland) by Gel Permeation Chromatography, using a Waters 150-C chromatograph with diffractometer detector, at a flow rate of 0.8 ml/min, through PLgel 20 μm MIXED-A (2000-40000000) and PLgel 10 μm MIXED-B (500-10000000) columns, with 1,2,4-trichlorobenzene as eluent at 142 °C (dissolving time of 10 and 24 h). Eluent contained Santanox-R (0.25 g/dm3) was used as stabilizer. Twenty one PE standards with 1320 - 18 × 10^6 g/mol molecular weight range were used for calibration. Each dissolved sample (330 μl) was injected twice. PE chromatograms were obtained by two basic approaches: (***i***) calibration with narrow standards and (***ii***) universal calibration procedure (using calibration with narrow standards different from the polymer investigated). The *K* and α values, the Mark-Houwink constants used for calibration, were taken as 3.95 × 10^{-4} and

Table 4.1. *Molecular characteristics and additional parameters of polyethylene melts, c – peroxide concentration (weight %), ρ – density measured at 25 ºC, t_{In} – induction time.*

PE	*c* (%)	MFI (g/10min)	ρ (g/cm³)	M_n (g/mol)	M_w (g/mol)	M_v (g/mol)	*MWD*	[n] TCB	T_m^0 (ºC)	t_{In} (min)
A	0	22	0.874±0.002	9700	36600	31900	3.8	0.735	148.32±1.05	4.01
B	0.01	12	0.856±0.009	6200	44100	36250	7.1	0.805	144.70±0.77	1.28
C	0.05	2.5	0.866±0.011	7600	54650	43100	7.2	0.91	141.78±1.24	2.06

0.726, respectively.

The branch content was evaluated from NMR ^{13}C experiments performed at the Polish Academy of Sciences (CBMM PAN) in Lodz (Poland). They allowed to conclude that all polymers are nearly linear polymer chains containing short chain branches at the level of 1-2 per 1000 carbons. More information about results of NMR experiments is in Appendix (§A1.3).

Polyethylene radius of gyration decreases with temperature increase. This is easily understandable because of the increase in the population of *gauche* conformational states. For a polyethylene with a molecular weight of 32000 g/mol, similar to the one here used, the temperature coefficient for the unperturbed chain dimensions evaluated by SANS experiments in the temperature range from 100 ºC up to 200 ºC is κ = -1.06 × 10^{-3} K^{-10} [Boothroyd-1991]. The radius of gyration evaluated at 180 ºC was 85 Å. Assuming linear polymer chains, the characteristic ratio is 7.8 and the length of Kuhn monomer at 180 ºC is 14.72 Å.

As discussed in Chapter 2, the plateau modulus value of a specific polymer is an important viscoelastic property. The scattering of data for this value may be very large, and polyethylene is an example of this dispersion. Values estimated for PE vary from 1.0 MPa for a metallocene PE and 2.73 MPa for a HDPE. However, for the same polymers, these values depend on the method used for the plateau modulus evaluation [Liu-2006]. Experimental results for ultra-high molecular weight PE are between 1.92 MPa and 1.95 MPa. The last value was evaluated at 190 ºC and it will be considered in this work. As a result, the molecular weight between entanglements ($M_e = 4\rho RT/5G_N^0$) is calculated to be equal 1199 g/mol. The density of sample A at 190 ºC was obtained from an empirical equation for the temperature variation of density for linear polyethylene [Mark-1996], $\rho = 0.863 - 4.73\times10^{-4}\times T - 0.38\times10^{-6}\times T^2$, which was also used in the evaluation of vertical shift factors of reduced curves (see Appendix, §A1.6.2).

4.2.2. Experimental procedures

4.2.2.1. DSC experiments

A Perkin Elmer DSC7 was used to evaluate the induction time for oxidation, the equilibrium melting temperature and to record the isothermal crystallization kinetics. The purge gas flow rate was 20 cm^3/min for all experiments with the exception of oxygen flow rate in the oxidation induction time experiments.

Oxidation induction time was evaluated at 200 ºC with gas (nitrogen and oxygen) flow rate of 50 cm^3/min and heating rate of 10 ºC/min. It was equal 4.01 min for PEA, 1.28 min for

PEB and 2.06 min for PEC. For this reason, to avoid material degradation, all rheological experiments described below were performed at temperatures lower than 180 ºC. This problem does not exist in DSC and shear DTA experiments for the temperatures tested because the molten polymer is not in direct contact with oxygen, although thermal degradation may also occur at high melt temperatures. Reproducibility of isothermal crystallization experiments obtained in the DSC and shear DTA were crosschecked to ascertain the absence of thermal degradation effects in the shear DTA instrument.

Equilibrium melting temperature was evaluated by the Hoffman and Weeks plot construction, and it is indicated in Table 4.1. The heating rate used for the isothermal experiments was 10 ºC/min. Further details of these experiments are in the Appendix (§A1.2.1).

The quiescent isothermal crystallization experiments were performed after a calibration with indium and lead at 0.1 ºC/min. To evaluate the effect of melt memory, or the reproducibility of isothermal crystallization experiments at a specified temperature (124 ºC), the polymer sample was heated at 200 ºC, kept at this temperature during different times (5, 30 and 60 min), cooled to the crystallization temperature at -60 ºC/min, and the crystallization recorded. All other isothermal crystallization experiments were performed following a similar protocol *i.e.*, after erasing the melt memory. The same sample, with the melt memory erased, was used for all experiments. The waiting time at the melt temperature was 5 min and the crystallization temperatures were between 124 ºC and 127 ºC.

4.2.2.2. Rheometer experiments

Two constant force rheometers were used, a Physica MCR 300 rheometer (Paar Physica) and an AR-G2 rheometer (TA Instruments), with parallel plate configurations (25 mm diameter). A gap size of 0.7 mm was used in all experiments. An important experimental step in the use of these instruments is the correction of their nominal temperature to take into account temperature differences between them and the temperature recorded with the shear DTA instrument. Procedures for doing these calibrations were already described [Martins-2004]. They make use of the same metal standards used for DSC calibrations to correct temperature in the rheometers. Dynamic experiments at different heating rates were performed at a constant stress of 12 kPa and oscillation frequency of 1 Hz over samples of standard metals placed between the rheometer plates. The sudden change of phase angle was taken as the melting onset temperature. The isothermal correction was evaluated by extrapolation to zero heating rate of the melting temperature values measured at different heating rates.

The low thermal conductivity of polymers and the sample's thermal resistance were considered to evaluate the real sample temperature, which was further checked with calibrated external thermocouple's measurements. For both rheometers, it was found that the real polymer sample temperature is 20 ºC below the nominal rheometer temperature. Samples used in the rheometer experiments were prepared by melting polymer pellets in a hot machine at 160 ºC for 1 min (to avoid degradation of the material). Circular discs with thickness of around 2 mm and diameter of 25 mm were obtained. The temperature range of rheometer experiments was between 140 ºC and 180 ºC. The lower test temperature (140 ºC) is below the equilibrium melting temperature of all polymers, but above their nominal melting temperature evaluated with the DSC at the heating rate of 2 ºC/min (see Appendix §A1.2.1).

Additional experiments performed with rheometers were stress sweep experiments, shear stress growth experiments and Controlled Shear Rate experiments (CSR). The first set of experiments allowed evaluating the optimal constant stress used in Small Amplitude Oscillatory Shear experiments carried out at the viscoelastic linear regime. In the second set, the sample viscosity was measured as a function of time while the sample was sheared with constant shear rate. Finally, in the CSR experiments the shear viscosity or shear stress was measured as a function of shear rate. Below is a brief description of these experiments.

A series of stress sweep experiments were performed at 10 and 0.1 Hz to evaluate a constant stress ensuring linear viscoelastic behaviour in the temperature range of interest (140-170 ºC). From the results shown in Appendix (§A1.6.1), the constant stress selected was 70 Pa for PEA, 300 Pa for PEB and 20 Pa for PEC. All experiments performed in the viscoelastic linear regime used this stress value.

4.2.2.3. Shear DTA

The effect of controlled shear deformations on crystallization kinetics was studied with a shear DTA instrument. It contains a cylindrical accumulator with around 200 mm of length and 20 mm of internal diameter, a 20 mm length conical coupling valve and a capillary channel with 60 mm length and 2 mm of diameter. Control valves at the entrance and exit of capillary allow the polymer melt flow from the accumulator to the capillary channel, and from this to the floor, just like in a capillary rheometer. When closed, these valves thermally insulate the accumulator from the capillary channel, where thermal analysis measurements are performed. Controlled melt deformation is therefore generated in the accumulator. For the shear rates used, the flow is perfectly stable after the first 5 mm of the capillary channel length.

A pressure drop of 10 MPa along the accumulator, conical coupling valve and capillary channel was evaluated from polyethylene rheological data (power law exponent $n = 0.622$ and $K = 2840$). According to literature information, the ratio between isothermal compressibility and thermal expansion coefficient of HDPE at 170 ºC is $dT/dp = 154$ ºC/kbar [Zhao-2004]. Therefore, the equilibrium melting temperature of PEA (148.3 ºC), which is the highest value between the three samples analyzed, will be shifted at most up to 163.7 ºC, below the temperatures used for shear DTA experiments.

A detailed description of shear DTA instrument was presented elsewhere [Martins-2005]. The differential thermal analyser setup at the capillary channel allows monitoring the sample temperature variation with respect to a reference, which is recorded as a function of time and temperature. The molten polymer is initially pumped from an accumulator to the capillary channel at a low shear rate (lower than 0.5 s^{-1}). After melt relaxation during 5 min, shear pulses of different duration and intensity are applied at the accumulator, where melt deformations are generated. Then, the sheared melt at the capillary channel is cooled down to the crystallization temperature with constant cooling rate (between 20 ºC/min and 30 ºC/min, depending on the melt and cooling bath temperatures) and crystallization kinetics is recorded.

Shear pulses were applied always at a temperature higher than the equilibrium melting temperature. The apparent shear rate at the wall was corrected with the Rabinowitsch correction for the material's non-Newtonian behaviour. The strain applied to the molten polymer was evaluated from the values of true shear rate at the wall and shearing time. The experimental error of these evaluations is ±10 % around the mean. It results from small differences in the cooling rate used in different experiments and the procedures used to evaluate the true shear rate at the capillary channel wall.

The temperatures used for shear DTA experiments, between 200 ºC and 250 ºC, were higher than those used in the rheometer. Because during these experiments the polymer was not in direct contact with air, it was considered that no oxidative degradation occurred. The validity of this assumption is based on the comparison of isothermal crystallization kinetics in the DSC (where the sample was in direct contact with the purge gas) and in the shear DTA for the same melt and crystallization temperatures.

4.3. Results

Melt memory and quiescent crystallization experiments

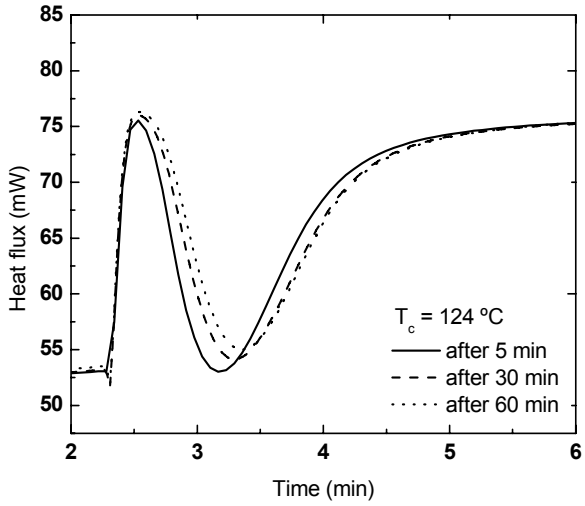

Figure 4.1. *Heat flow variation as a function of time for the isothermal crystallization of PEC at 124 ºC with annealing times of 5 min, 30 min and 60 min.*

Figure 4.1 shows a result similar to others already reported for the melt memory effect in quiescent crystallization. They refer to PEC, the sample with higher crosslinking degree, for which the effect of melt memory should be more visible. As shown below, samples PEA and PEB have shorter reptation time than PEC. Therefore, at the same melt temperature, their melts should attain a relaxed state faster. This effect is observed only in experiments performed with "fresh" (non-annealed) polymer samples because the shape of crystallization curves changes after annealing during different times. Annealing of the PEC sample (weight around 10.684 mg) during 30 min and 60 min at 200 ºC yielded similar curves. We considered therefore that 30 min of annealing erases the melt memory effect. This annealing time is necessary to ensure reproducible crystallization results. All "fresh" samples used in DSC experiments passed through this annealing process prior to further crystallization studies.

Table 4.2 indicates the half-crystallization time results obtained from quiescent isothermal crystallization experiments recorded with the DSC for melts "without memory". The increase of crosslinking degree accelerates crystallization kinetics, shifting

Table 4.2. *Crystallization half-time evaluated from isothermal crystallization experiments performed with a DSC at the indicated temperatures.*

T	A	B	C
(ºC)	$t_{1/2}$ (s)	$t_{1/2}$ (s)	$t_{1/2}$ (s)
124	165.5	97.2	77.4
125	319.2	171.0	126.0
126	631.2	310.8	276.0
127	838.8	945.6	649.2

the half-crystallization time to lower values. The equilibrium melting temperature, evaluated by the Hoffman and Weeks plot construction also decreases from the uncrosslinked sample to crosslinked samples, PEB and PEC, being lowest for the last one, which suggests that crosslinked samples have thinner lamellae. This results was confirmed by SEM scans of different samples after isothermal crystallization at the same temperature T = 127 ºC (see §A1.4 at the Appendix).

Further SEM morphological analysis of the same samples demonstrates that nucleation density increases with the sample's crosslinking degree. The average spherulite diameter estimated from Scanning Electron Microscopy of samples crystallized at 127 ºC is 175 μm, 28 μm and 7.5 μm for PEA, PEB and PEC, respectively (see Figures A1.8 and A1.9 at Appendix). The corresponding nucleation density is 3.57×10^{11} nuclei/m^3, 8.70×10^{13} nuclei/m^3 and 4.53×10^{15} nuclei/m^3 for PEA, PEB and PEC, respectively. We note the particularly large values of nucleation density evaluated for PEB and PEC samples.

Comparison between quiescent DSC and shear DTA experiments

As mentioned at the Introduction, the melt memory effect was assigned to ordered clusters, also called embryos and precursor structures, that exist in deformed melts, being absent in quiescent melts after a long enough annealing time, similar to that used to obtain the results shown in Figure 4.1. The molecular origin of these structures is unknown, but it is assumed that it can be investigated by shear-induced crystallization experiments performed under well-controlled conditions of flow history and temperature. Some of these studies were performed with a shear DTA instrument. Before describing these results, we must ensure the validity of shear DTA experiments by comparing them with results obtained at the same

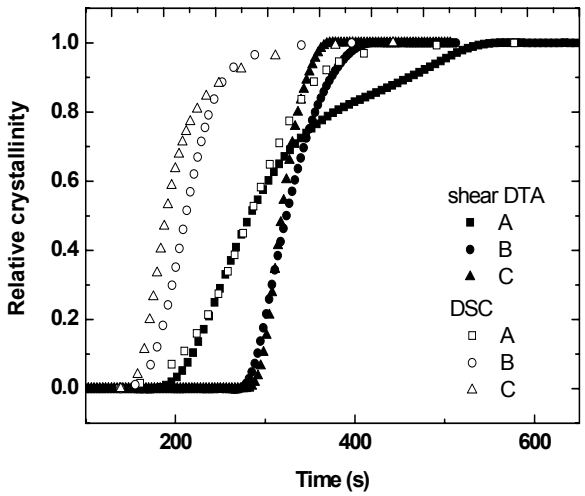

Figure 4.2. *Isothermal crystallization recorded with the DSC (open symbols) and the shear DTA (full symbols) at 125 ºC for polyethylene with different crosslinking degree: A (square), B (circle) and C (triangle).*

crystallization temperature in a DSC.

Figure 4.2 shows quiescent isothermal crystallization curves obtained with the shear DTA and DSC, under the same conditions, after erasing the melt memory effect. The results shown refer to the same crystallization temperature (125 ºC), however the start temperature was different for the DSC and shear DTA experiments. It was 200 ºC for all DSC experiments. For the shear DTA experiments it was 210 ºC for PEA, and 250 ºC for PEB and PEC. Despite the small difference in the start temperature, the results obtained for PEA samples with both instruments are similar. Differences appear for samples PEB and PEC, and they are ascribed to the different initial temperature, which, due to their high viscosity, was a requirement to perform shear DTA experiments with these samples.

Crystallization kinetics after shear

Results of shear shear-induced crystallization experiments performed with the shear DTA instrument, following the procedure described in the experimental part of the work, are presented in Figures 4.3 to 4.6.

Figure 4.3 shows the isothermal crystallization of PEA at 127 ºC after a pre-shearing at 200 ºC. The pre-shearing was applied at constant shearing time (60 s) and increasing shear rate, and constant shear rate (44.9 s^{-1}) and increasing shearing time. As described in the experimental part of the work, after shearing the melt was cooled under controlled conditions to the nominal crystallization temperature. The objective of these experiments was to demonstrate that strain is the factor controlling saturation of crystallization. However, because of the polymer high viscosity and the motor force torque limitations in the shear DTA

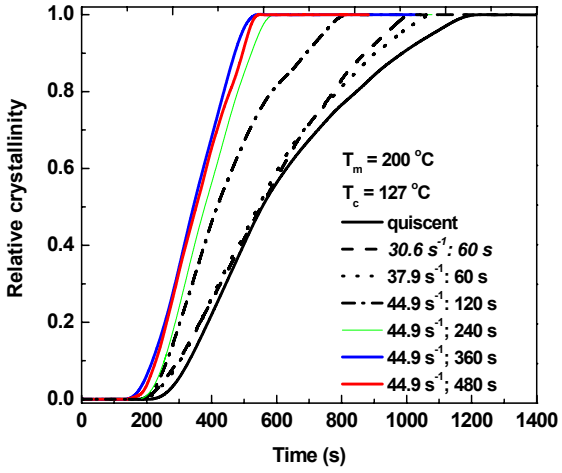

Figure 4.3. *Effect of shear flow on the isothermal crystallization of PEA. The sheared melt temperature is 200 ºC and T_c = 127 ºC. The solid line shows the quiescent crystallization of a melt with its memory erased. The acceleration of crystallization resulting from shear deformations, different shearing times and shear rates, is also indicated. The saturation was observed at $\dot{\gamma}_w$ = 44.9 s^{-1} and 360 s, corresponding to γ_w = 16164 s.u..*

instrument, it was not possible to use larger shear rates values (more than 45 s^{-1}) for the same shearing time (60 s). These experiments would allow comparing critical strain values (those obtained with constant shearing time and different shear rates with others obtained with constant shear rate and different shearing times).

Figure 4.3 shows the extent at which a melt sheared at a high temperature retains the memory of previous deformations, and their effect on crystallization kinetics. An acceleration of crystallization kinetics with shear deformation is observed, and for melts sheared at 200 ºC the saturation of crystallization occurs at a relatively high strain, ≈ 16000 s.u.. Similar results were observed for PEB and PEC (Figure 4.4) where shearing was done at 250 ºC with constant shear rate and different shearing times. As discussed below, the lower strain in this case resulted from the relatively high melt temperature.

Figures 4.5 and 4.6 show the effects of crystallization and melt temperature on the saturation of crystallization kinetics. For the same melt temperature and different crystallization temperatures, the crystallization saturates at the same strain (Figure 4.5). The different half crystallization times at saturation result only from the supercooling degree effect on crystallization kinetics. For the same crystallization temperature and different melt temperatures, the saturation of crystallization occurs at different strains, which decrease with the sheared melt temperature increase (Figure 4.6). These results refer only to PEA, but similar results were also obtained for PEB and PEC and to other polymers used in previous studies [Martins-2006, Zhang-2006, Zhang-2007].

The dependence of crystallization kinetics on the sheared melt temperature explains the differences between results recorded with the shear DTA and DSC for PEB and PEC samples shown in Figure 4.2, and the differences in the critical strain values evaluated for these materials shown in Figure 4.5.

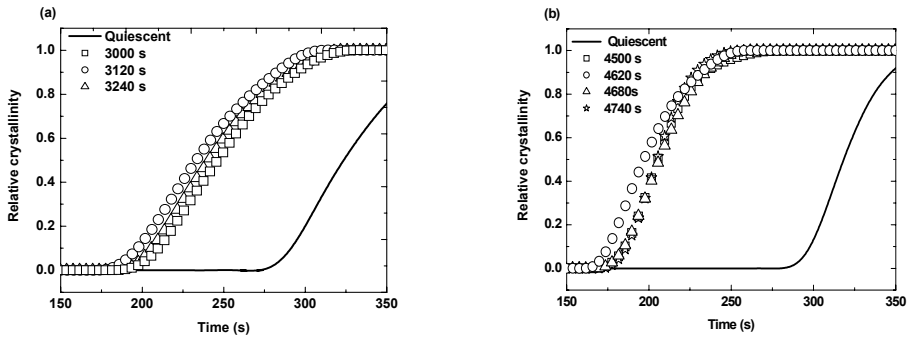

Figure 4.4. *Isothermal crystallization of PEB (a) and PEC (b) recorded with shear DTA for crystallization temperature of 125 ºC, sheared melt temperature of 250 ºC, constant shear rate (2.8 s^{-1} for B and 2.4 s^{-1} for C) and shearing times are indicated. The average critical strain for PEB is 8400 s.u. and for PEC it is 10800 s.u..*

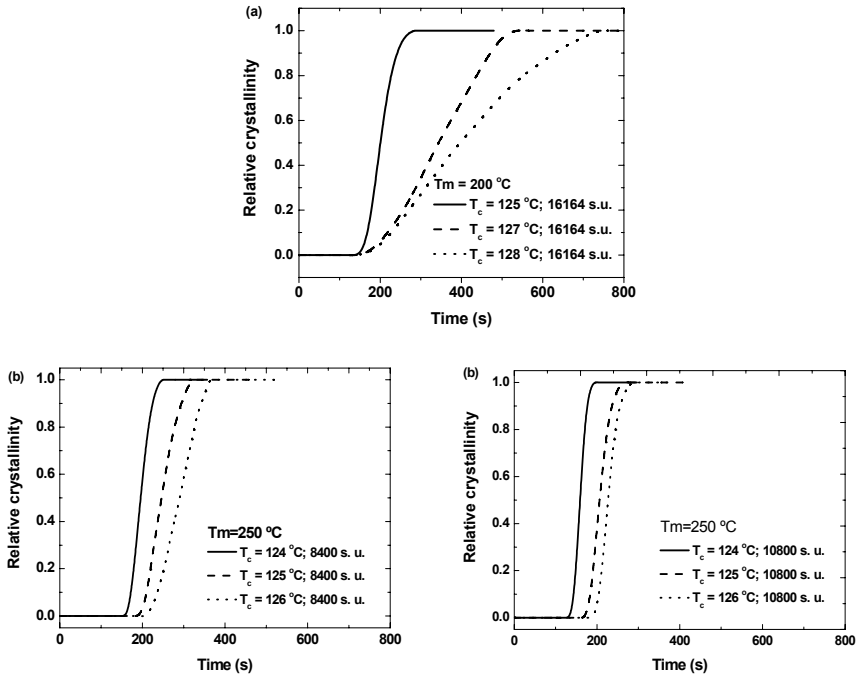

Figure 4.5. *Effects of crystallization temperature on the saturation of crystallization. Constant sheared melt temperatures (200 ºC for PEA and 250 ºC for PEB and PEC) and shear rates (44.9 s^{-1} for A, 2.8 s^{-1} for B, 2.4 s^{-1} for C) were used. The crystallization temperatures for PEA (a), PEB (b) and PEC (c) are indicated. The average critical strain for A is 16164 s.u., for B is 8400 s.u. and for C - 10800 s.u.. The measurement error in the strain values is ±10%.*

The above results indicate that the strain applied to the molten polymer, above its equilibrium melting temperature, is the factor that controls the saturation of crystallization from sheared melts. This strain, defined as critical strain [Martins-2006, Zhang-2006], is considered as the minimum strain value needed to align the maximum number of chain segments with the flow direction. As was also found in previous works, the observed temperature dependence suggests that the attainment of a well-defined melt state should be at

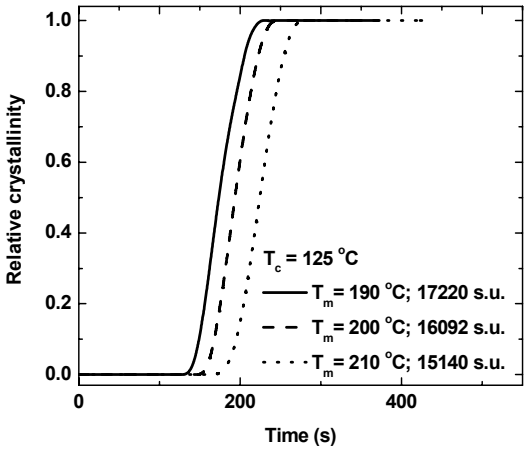

Figure 4.6. *Effect of sheared melt temperature on the saturation of crystallization for PEA for constant crystallization temperature (125 ºC). The average critical strain needed to saturate crystallization at different melt temperatures is indicated.*

the origin of the effects observed. Results presented below confirm the validity of this assessment for slightly crosslinked polymer samples.

Identification of the melt state responsible for the saturation of crystallization

As discussed in previous works [Zhang-2006, Martins-2006], the saturation of crystallization from sheared melts at constant strain, and the temperature dependence of this strain with the melt temperature, decreasing with it, indicates that a well-defined melt state should be responsible for this saturation. The only known well-defined melt state is the steady state. The easiest way to identify the conditions for the attainment of this state is with shear stress growth experiments.

In these experiments a constant shear rate is applied to the molten polymer between parallel plates (or between a cone and a plate [Martins-2006]). The variation of viscosity, or shear stress, is then monitored as a function of shearing time. The viscosity increases initially, passes by a maximum value, then it decreases and reaches a plateau at steady state. The plateau onset is well defined for linear polymer chains, but its definition may be a difficult task for branched polymer chains and polymers where different chains interact via covalent bonds, as it happens for the slightly crosslinked polymers used in this work, or with ionomers.

In these experiments it is evaluated the strain at the onset of steady state for different melt temperatures. Relatively low temperatures were used because of the low polymer thermal stability and the long experimental time needed to detect the attainment of steady

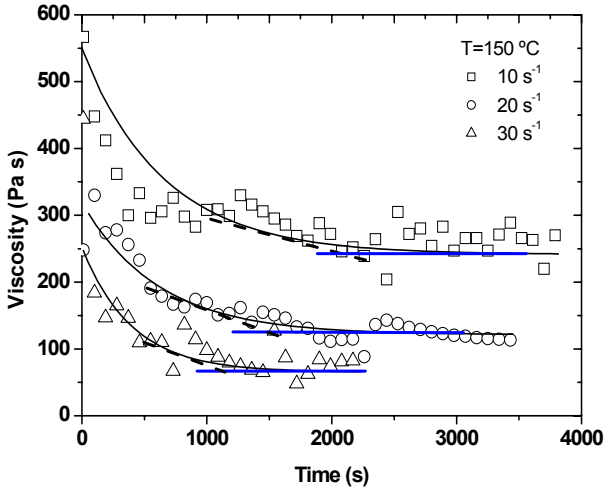

Figure 4.7. *Transient viscosity as a function of time for PEA in shear stress growth experiments performed at 150 ºC. Solid lines show the procedure for evaluating the critical strain at the onset of steady state. The average value evaluated was 28068 s.u. (± 5010 s.u.), corresponding to shear rates of 10 s^{-1} (23050 s.u.), 20 s^{-1} (30600s.u.) and 30 s^{-1} (30540 s.u.). Note, that average critical strain was evaluated from set of experiments and the curves presented here represent the average of the measurements performed.*

state. Results obtained for PEA at 150 ºC are presented in Figure 4.7. The viscosity (or shear stress) stabilizes at a constant strain, which marks the beginning of steady state where the density of entanglements in the sheared melt is constant. The decrease of viscosity from the maximum down to steady state, which may be of several orders of magnitude, is assigned to a loss of entanglements. This assignment resulted from measurements of the longest relaxation time (reptation time) for unsheared melts, with their melt memory erased, and melts sheared up to steady state. The last ones have lower reptation time. For PE the ratio between the reptation time at different melt states ($\tau_{unsheared}/\tau_{critically\ sheared}$) is two, which indicates that 1/2 of the initial entanglements were destroyed during the transition from the maximum viscosity value to the steady state [Zhang-2006].

For a specific melt temperature, the onset of steady state is shear rate independent. It occurs at a constant strain. An accurate evaluation of this strain is difficult because these measurements may be affected by several experimental errors. Besides polymer thermal degradation, mass loss of polymer between plates may also occur. For these reasons, these experiments were repeated several times, at least five times for each shear rate and temperature. The curves indicated in Figure 4.7 represent experiments within the average of the five measurements performed. Despite the relatively small branching content of this polymer, the figure illustrates the difficulty in the definition of the onset of steady state. For this reason, the experimental curves were fitted with a single exponential decay function and the onset of steady state was evaluated at the intersection point between a tangent line to the plateau and another tangent line to the inflection point of the exponential decay function.

The strain values at the onset of steady state (critical strain) for PEA, PEB and PEC obtained at different temperatures with a rheometer in parallel plate configuration and with a shear DTA instrument are in Figure 4.9. The critical strain, either the one measured at the onset of the steady state or that needed to saturate the crystallization from a sheared melt, measured with the shear DTA, showed similar temperature dependence, and both approach a limiting value at high temperatures. The experimental results seem to suggest that this critical strain increases with sample crosslinking degree. However, the reduced number of data points and the experimental error associated does not allow quantifying precisely this type of variation. Therefore, all critical strain data points for the three materials were fitted with a single equation, which is within the experimental error bars for the measurements performed. It was on this basis that was considered the assumption of a similar critical strain at a specific temperature for all polymers tested, regardless their crosslinking degree.

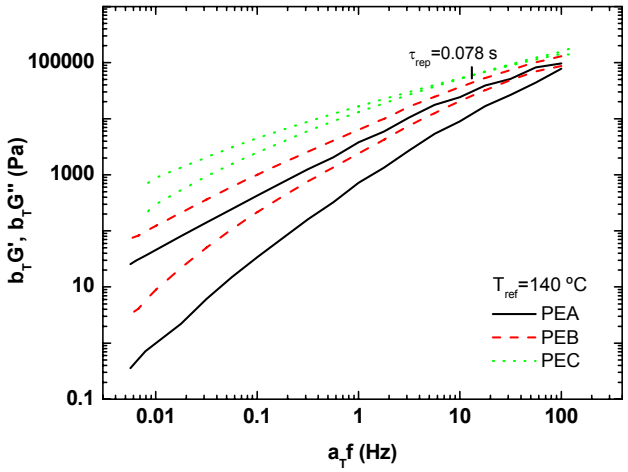

Figure 4.8. *SAOS reduced curves for polyethylene A, B and C at reference temperature of 140 ºC.*

Further rheological characterization of PEA, PEB and PEC samples allowed to get additional information about the dependence of polymer melt morphology on the crosslinking degree. Small Amplitude Oscillatory Shear and Controlled Shear Rate experiments were performed to evaluate and compare flow activation energies. From SAOS experiments the longest relaxation time (reptation time) and its temperature variation was also obtained. This time was evaluated at the crossing-point between the storage and loss modulus curves [Zhang-2006]. Figure 4.8 illustrates the procedure for PEC, and it shows also the reduced curves at 140 ºC for PEA and PEB. For these two samples the crossing point between $G'(\omega)$ and $G''(\omega)$ would occur and a higher frequency (shorter time), which is outside the experimental range available with the instruments used. Therefore, it was concluded that their reptation time was smaller than that of PEC sample, which is an acceptable result

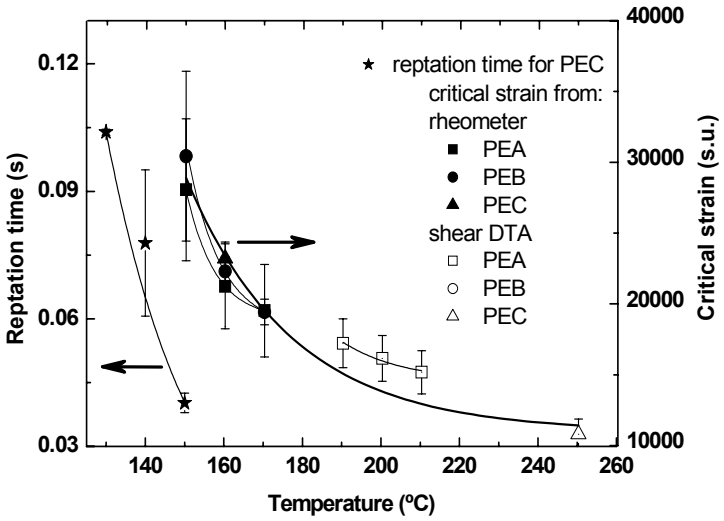

Figure 4.9. *Temperature variation of the reptation time (stars) for polyethylene C and critical strain for polyethylene A, B and C. The critical strain measured with shear DTA (open symbols) and in shear-stress growth experiments with parallel plate (filled symbols) is plotted as a function of sheared melt temperature: squares represent PEA, circles – PEB and triangles – PEC.*

because of the higher peroxide concentration in this sample. Figure 4.9 also shows the reptation time results for this sample evaluated at different temperatures. It is concluded that their temperature variation is similar to that of the critical strain measured with the shear DTA or with the rheometer.

Measurements of reptation time for other polymers indicated similar temperature variation [Martins-2006, Zhang-2006]. Further, reptation time measurements were performed for unsheared (relaxed) melts, and melts sheared up to steady state. Results of these experiments mentioned above allowed identifying the entanglement loss during the transition to steady state. Similar experiments were not performed with these materials due to difficulties in establishing a well-defined steady state.

All these results (the shear DTA and rheometer) suggest that the degree of orientation reached by the chain segments at the steady state should have reached a limiting value. Because the same strain saturates the viscosity at steady state and the crystallization from sheared melts, one must conclude that the attainment of the same melt state must be responsible for these effects. This issue will be discussed below.

The flow activation energies of different samples was evaluated by fitting with an Arrhenius equation the horizontal shift factors used to construct reduced curves similar to those shown in Figure 4.8. These activation energies were evaluated from SAOS and CSR experiments. A detailed description is presented in the Appendix (§1.6.2). Table 4.3 shows the values obtained. As expected, similar values were obtained for SAOS and CSR experiments.

The flow activation energy evaluated for PEA is similar to other literature results of polyethylene, between ~26 and ~33 kJ/mol [Malmberg-1998]. It increases for crosslinked samples, being for PEC almost twice the value obtained for PEA. For SAOS experiments of PEC, the flow activation energy was evaluated from reptation time measurements indicated in Figure 4.8 (see Figure A1.15 at Appendix). The reason for this procedure was the difficulty in obtaining a good superposition in all frequency range of curves obtained at different temperatures.

4.4. Discussion

Quiescent crystallization experiments

Apparently, the effect of crosslinking in the isothermal crystallization kinetics of polymers was not discussed with detail in the literature. Two references were found reporting

Table 4.3. *Activation energies evaluated from SAOS experiments for polyethylene A, B and C.*

PE	E_a (kJ/mol)	
	SAOS	CSR
A	30.70±1.64	34.91±1.53
B	32.55±1.05	36.93±0.97
C	67.05±5.06	69.32±1.85

these studies, one on irradiated polyethylene [Hutzler-2000] and the other on the crystallization kinetics of LLDPE crosslinked with peroxides by reactive extrusion [Ramos-2005], similarly to the materials PEB and PEC used in this work. The reported results are similar to those here presented. However, the analysis of crystallization kinetics was superficial, and no morphological studies were reported.

The results of Table 4.2 indicate that, for the same crystallization temperature, the half-time of crystallization decreases with the increase of crosslinking degree. Also the equilibrium melting temperature decreases with the increase of crosslinking degree. The decrease of the half of crystallization time was explained by a significant increase of nucleation density, from 3.57×10^{11} nuclei/m^3 for the uncrosslinked sample up to 4.53×10^{15} nuclei/m^3 for PEC. The decrease of equilibrium melting temperature was explained by the smaller lamellae thickness of crosslinked samples. A precise quantification of this decrease was not possible to be performed, but SEM results shown in Appendix (§A1.4) suggest this variation.

The puzzling result of these experiments is to figure out the different melt morphology of samples PEA, PEB and PEC, prior to crystallization, and the factor(s) responsible for the relatively high nucleation density of PEC samples. The supercooling degree cannot be considered as the responsible factor because it is lower by around 6.5 ºC for the PEC sample with respect to the supercooling degree of PEA (note that all nucleation densities were estimated for samples crystallized at the same temperature). Since crosslinks are excluded from the folded chain lamellae, one possible explanation seems to be that crosslinking favoured the formation of ordered clusters of chains between croslinking points at the molten state, and that the size of these ordered clusters decreases with the crosslinking degree, providing therefore preferred sites for primary nuclei formation. This point will be discussed further on in this work.

Temperature dependence of critical strain

As mentioned above, it was assumed that the critical strain needed to saturate crystallization kinetics from sheared melts is independent on the polymer crosslinking degree.

Although one could expect that the attainment of steady state should be crosslinking degree dependent, the results shown in Figure 4.9 indicate that, within the experimental measurement errors, the strain needed to establish the steady state might also be considered to be crosslinking degree independent.

Behaviour similar to the one reported here for the crosslinked PE's was also observed for sodium partially neutralized ethylene-methacrylic acid ionomer (Surlyn). The temperature dependence of critical strain (to saturate crystallization and to establish a steady state) was discussed with more detail in a previous work of Zhang *et al.* [Zhang-2008]. Results of shear stress growth experiments obtained in this work are indicated in Figure 4.10. It was found a first transient steady state, which is followed by another steady state at larger strains. The viscosity increase after the initial, transient, steady state was interpreted as the result of reformation of ionic interactions in the melt. It was found that the strain needed to establish the transient steady state was similar to the strain needed to saturate the crystallization kinetics of melts sheared at the same temperature.

In agreement with results obtained for crosslinked polyethylene samples, it was concluded that the strain magnitude needed to saturate crystallization depends on the base polymer chemical structure, and on the chain linearity and branching content, but it is independent on the existence/absence of ionic interactions or crosslinks.

Origin of the melt memory effect

It is generally considered that melt memory effect results from precursor structures for crystallization. However, it is not known how precursor structures are created under shear

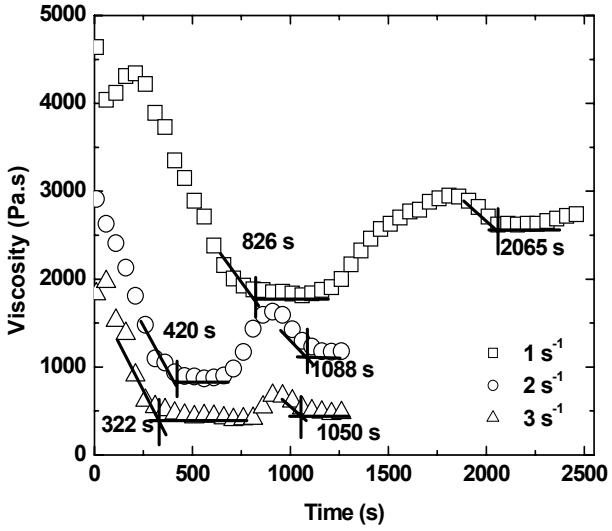

Figure 4.10. *Transient viscosity as a function of time in stress growth experiments performed at 160 ºC with parallel plate configuration for sodium partially neutralized ethylene-methacrylic acid ionomer [Zhang-2008].*

flow, or even if they are created by flow, or if flow just enhances their activity. Also, crystallization enhancement in deformed polymer melts results from the formation of precursor structures, which are at the origin of primary nuclei. According to some investigators, precursors of primary nuclei consist of aggregates of ordered chain segments without crystallographic order [Somani-2002a, Somani-2002b]. Its existence implies the existence of order at the molten state, the enhancement of (positional) order by the action of flow and the coexistence of ordered structures with a dynamic melt. Therefore, understanding and controlling their origin remains still a challenge.

It is also assumed that precursor structures are too tinny and thin to have any influence in the rheology of polymer melts [Janeschitz-Kriegl-1997, Janeschitz-Kriegl-1999]. This explains the low variation of radius of gyration for quiescent and sheared melts. Their size decreases with the melt temperature because higher energy conformational states became more populated.

The results obtained with the shear DTA instrument indicate that the saturation of shear-induced crystallization kinetics can occur when melts, well above their equilibrium melting temperature, are sheared up to a limiting critical strain. This strain decreases with the melt temperature increase. After heating the melt for a time long enough (around 30 min at 200 ºC), crystallization experiments become reproducible, and the memory of deformations applied by shear flow is erased.

Because saturation of crystallization is observed when melts are sheared at relatively high temperatures, it can be concluded that precursor structures for crystallization are active even at high temperatures. These results are not consistent with the explanation of Strobl *et al.* [Häfele-2005] for the formation of precursor structures for crystallization. They considered that at high temperatures, where the melt memory is erased, the precursor structures are objects void from crystallites, being progressively filled with crystallites and increasing in volume during crystallization.

The reason for the inconsistence resides not only on the experimental observation of saturation of crystallization at lower strains for high temperatures, but also in the link that was established between the strains needed to saturate crystallization and the strains needed to establish a steady state. It results then that it is the understanding of melt morphology at steady state the key to explain the origin of precursor structures for crystallization and the melt memory effect.

Results here presented, and others [Zhang-2006, Martins-2006], demonstrate that precursor structures for crystallization are active well above the equilibrium melting temperature and that they reach the maximum effectiveness at steady state. Because precursor

structures must consist of a set of aligned chain segments, without any crystallographic order, they must coexist with a dynamic melt and disentangled melt at steady state. According to previous measurements of reptation time for unsheared melts, with the melt memory induced by flow deformations erased, and the reptation time for melts sheared up to steady-state, the last ones were one-half lower than the former, indicating that one-half of the initial entanglements were destroyed during the transition to steady state [Zhang-2006].

It seems therefore clear, from these and others results [Zhang-2006, Martins-2006, Kumaraswamy-1999], that precursors structures for crystallization are more active at the disentangled steady state. Otherwise, it would be impossible to observe the acceleration of crystallization kinetics and its saturation by shearing a polymer melt at temperatures above its (nominal or equilibrium) melting temperature. However, these results do not imply that precursor structures are absent in melts outside this state and that they are destroyed during the annealing procedures used to erase the melt memory.

Crystallization kinetics in quiescent and sheared melts seems therefore to be correlated. It is usually considered, *without proof*, that precursor structures are formed only after shearing the melt and that they are destroyed by melting the polymer at temperatures above their melting temperatures for long time. This is the current interpretation for the experiments used to erase the melt memory effect in the quiescent crystallization. However, this interpretation still leaves us with an important and answered question, which is how to explain the earlier crystallization stages in a melt absent of precursor structures. How the initial stages of order could be established without any residual stage or order, even though small?

Possible answers to the above questions are provided below, together with the presentation of a different view for melt morphology, evolution of crystallization process, and predictions for the dimensions of precursor structures, which follows a previously unpublished work [Martins-2008].

It is assumed that a quiescent polymer melt contains local ordered regions, with a certain length and thickness, which are composed of small sections of adjacent chain segments with similar conformational states. The size of these ordered regions and their role in the melt morphology will be discussed below. It is assumed further that application of shear will destroy some of these ordered regions (the less stable, containing conformational states sequences of higher energy), while other regions will be fragmented in thinner regions and are orientated with the flow direction. The steady state would represent therefore the state of maximum alignment of oriented (thin) regions with the flow direction, and the critical strain is

the minimum value of strain needed to align the maximum number of chain segments with the flow direction, with a limiting orientation angle.

The crystallization at a constant temperature is accelerated with the increase of shear strain because thinner, and more oriented, regions are generated. These oriented regions are the precursor structures, and they are the origin of primary nuclei. Another aspect of the different view mentioned above is the erasing process of the melt memory and the description of the earlier crystallization stages in quiescent melts.

The erasing process of the melt memory, and the consequent delaying of crystallization kinetics, results from the aggregation of the thinner and fragmented regions previously oriented with flow. The minimization of the free energy of a system as the result of an annealing process, in this case resulting from the entropy increase due to the spatial randomization of previously oriented regions, is well documented for polymers and inorganic materials.

In quiescent melts, when the melt memory effect was completely erased due to the long annealing process at a low temperature or shorter annealing process at a higher temperature, the oriented regions reach their maximum thickness, and the melt has a higher viscosity. In a quiescent melt these structures are distributed isotropically. Since they are thick and smaller in number, in comparison with those existing at steady state, the crystallization kinetics (and also the nucleation density) will be slower because they have to diffuse to the crystalline lamellae growth front. These are the reasons for the crystallization kinetics slowing down in quiescent and relaxed melts. However, even for relaxed melts, crystallization at the same temperature from melts heated up at different temperatures yields a different kinetics. The reason in this case is the length (not the thickness) of the oriented regions that decreases with the temperature increase of the melt [Martins-2008]. Below predictions for the dimensions of these structures are presented.

Predictions of precursor structures' dimensions

To evaluate the dimension of precursor structures the interaction potential energy between parallel chain molecules of length L is evaluated from an equation derived by Salem [Salem-1962]:

$$W = -\frac{3\pi CL}{8\lambda^2 r^5} \quad , \tag{4.1}$$

where r is the shortest separation distance between the chains, λ is effective bong length along the chain axis and C is a constant, which is related to the Hamaker constant A by

$$A = \pi^2 C\rho^2 \quad , \tag{4.2}$$

where ρ is the number density of molecules in each chain. It was evaluated at a specific temperature by dividing the number of atoms in the repeated unit by its van der Waals volume.

The Hamaker constant A is evaluated from the Lifshitz theory of van der Waals interactions, where the interacting forces are derived in terms of dielectric constants and refractive indexes. Considering two identical chains interacting across vacuum (which is usual in these conditions), the total Hamaker constant for the two chains contains an entropic zero-frequency contribution ($A_{\nu=0}$), which includes the Keesom and Debye dipolar contributions to the van der Waals interactions, and a dispersion energy contribution ($A_{\nu>o}$), which includes the London energy contribution. If the interactions are assumed to be non-retarded and additive, the result obtained is

$$A_{total} = A_{\nu=0} + A_{\nu>0} = \frac{3}{4} k_B T \left(\frac{\varepsilon - \varepsilon_o}{\varepsilon + \varepsilon_o} \right)^2 + \frac{3h\nu_e}{16\sqrt{2}} \cdot \frac{\left(n^2 - {n_o}^2\right)^2}{\left(n^2 + {n_o}^2\right)^{3/2}} \quad , \tag{4.3}$$

where ε and ε_o are the static dielectric constants for the polymer and vacuum, n and n_o are the corresponding refractive indexes, h and k_B are the Planck and Boltzmann constants, respectively, T is the absolute temperature and ν_e is the main electronic absorption frequency in the UV ($\cong 3.0 \times 10^{15}$ Hz) [Israelachvili-1992].

Based on the above description of melt morphology and precursor structures formation, a physical meaning was assigned to flow activation energy values evaluated from rheological experiments. The same value for this energy was evaluated from experiments at the viscoelastic linear regime and viscoelastic non-linear regime. It was considered that barriers to flow in polymer melts result from three main contributions [Martins-2008]. The conformational energy barriers, the rigidity of the network, which depends on the existence of crosslinks or ionic interactions between chain segments, and the interactions resulting from regions with aligned chain segments, which are parallel chain segments of the same or adjacent chains in the same conformational state. This last contribution is the one assigned to the W value in eq. (4.1). Contributions resulting from the rigidity of the network are impossible to evaluate, at least at this stage. The relevant contribution from the conformational energy barriers is the height of the energy barrier between *trans* and *gauche* conformations, which, according to literature is between 16 and 22 kJ/mol [Robertson-2001]. A similar value ($\approx$ 15.49 kJ/mol) was also obtained for the internal energy barriers of simple *n-alkanes* and used with rotational isomeric state model [Abe-1966]. The value of 16 kJ/mol was used in the evaluations described below.

Considering the flow activation energy of 30.7 kJ/mol for PEA, it results then that the value evaluated for W is 14.7 kJ/mol. A slightly larger value is obtained when the flow activation energy of 34.91 kJ/mol evaluated from CSR experiments is used: 18.91 kJ/mol. The difference between these two values is similar to the thermal energy at the temperature of the experiments, ≈ 4 kJ/mol.

For the temperature of 473.15 K, which was used in the shear DTA experiments, and the following constants for PE, $\varepsilon = 2.3$ and $n = 1.49$, the value evaluated for the Hamaker constant is $A = 5.51 \times 10^{-20}$ J. Values of one were considered for the static dielectric constant and refractive index of vacuum.

It is known that the refractive index decreases with the temperature increase. Also, the static dielectric constant of PE has similar variation. However, because polyethylene is an apolar polymer these temperature variations (of the refractive index and dielectric constant) may be neglected. Moreover, estimates of the above values for the temperature range used in this work were not found in the literature searched.

The constant C in eq. (4.1) was evaluated from the Hamaker constant and the number density of molecules in each chain. For this evaluation, the temperature variation of van der Waals volume of PE was considered [van Krevelen-1997]. With $\rho = 9.95 \times 10^{28}$ atoms/m^3, the value evaluated for C is 5.64×10^{-79} J/m^6 – Table 4.4. Using values for the other parameters of eq. (4.1) indicated in this table, the predicted length of precursor structures at 473.15 K is in range between 28.8 and 37.1 Å, far below the average lamellae thickness of PE, around 200 Å. The highest value was obtained considering the flow activation energy evaluated from Controlled Shear Rate experiments (see Table 4.3). Therefore, the precursor structures for PE contain around two Kuhn monomers (Kuhn monomer length around 14.72 Å). If instead of the value $r = 3.46$ Å for the minimum separation distance between parallel chains, the value for the b dimension of the ortorrombic unit cell of PE was considered ($b = 4.945$ Å), the predicted length of precursor structures would now be in the range between 172 and 221 Å, around 12-15 Kuhn monomers. These predictions will be discussed further below.

The above predictions refer only to sample A (linear polymer), but the precursor structures' length predictions for samples PEB and PEC should be similar. These evaluations were not performed because for these samples, due to their crosslinking, the precise evaluation of network contribution to the conformational and network energy barrier is unknown.

As discussed above in the origin of melt memory effect, it is assumed that the melt morphology at steady state results from the fragmentation and orientation with the flow

direction of ordered regions existing in the quiescent polymer melt. Therefore, the critically sheared melt has an excess free energy in comparison with the quiescent melt. Following the model presented above, this excess free energy is purely entropic. Assuming then that precursor structures are cylindrical clusters of oriented chain segments without crystalline order, which was demonstrated experimentally, the excess free energy may be related to the dimensions (length and thickness) of precursor structures at steady state [Martins-2008]. For a specific temperature, their dimensions are evaluated from the excess of *specific* free energy,

$$\Delta F_{ex} = \frac{\pi d L \sigma - \pi d^2 \gamma / 2}{\pi d^2 L / 4} = \frac{4\sigma}{d} - \frac{2\gamma}{L} \quad , \tag{4.4}$$

where $\pi d^2 L/4$ is the volume of element of the ordered region, σ is the lateral surface free energy (1.18×10^{-2} J/m^2 for polyethylene) and γ is basal surface free energy evaluated from

$$\gamma = \gamma_0 \left(1 - \frac{T}{T_{crit}} \right)^{1+r} \quad , \tag{4.5}$$

where T_{crit} is a critical temperature and γ_0 is a constant. For PE the critical temperature is equal to 1030 K and $\gamma_0 = 5.37 \times 10^{-2}$ J/m^2 [van Krevelen-1997, Mark-1996]. The basal surface energy evaluated at 473.15 K is 2.53×10^{-2} J/m^2. In eq. (4.4) it was considered a positive contribution to the excess free energy from the lateral surface of ordered regions and that extremities of these regions contribute to decrease the excess free energy. Because there is no volume change on melts during shearing, and also because polymer melts are nearly incompressible, it is irrelevant the use in eq. (4.4) of a free energy at constant volume or at constant pressure. This argument holds also for the evaluation made below.

Values for the excess free energy and precursor structures thickness are unknown in eq. (4.4). The excess free energy can be evaluated from the variation in the excess of Helmoltz specific free energy $\delta(\Delta F_{ex})$, with the assumption that this increase is purely orientational. This variation, as a result of an infinitesimal deformation, is given by $\boldsymbol{\sigma}:\boldsymbol{\delta\varepsilon}$, where $\boldsymbol{\sigma}$ and $\boldsymbol{\delta\varepsilon}$ are the stress and the virtual deformation tensors, respectively. For a single step strain, $\sigma = GC^{-1/2} / tr\left(C^{-1/2}\right)$, $\boldsymbol{C}^{1/2}$ is the square root of the Finger tensor, **tr** is the trace operation and $G = 6G_N^0 = 6\rho RT / M_e$ [Marrucci-2002, Kohler-2005]. From the above equations, the excess of the specific free energy is equal to

$$\delta\left(\Delta F_{ex}\right) = \frac{G}{\lambda_1 + \lambda_2 + \lambda_3} \cdot \left(\lambda_1 \delta\varepsilon_1 + \lambda_2 \delta\varepsilon_2 + \lambda_3 \delta\varepsilon_3 \right) \quad , \tag{4.6}$$

where λ_i^2 are the eigenvalues of the Finger tensor $\boldsymbol{C}^1$. Since at the undeformed state $\lambda_i = 1$, and $\delta\varepsilon_i = \delta\lambda_i / \lambda_i$, the above equation reduces to:

$$\Delta F_{ex} = G \cdot \ln\left[\left(\lambda_1 + \lambda_2 + \lambda_3 \right) / 3 \right] \quad . \tag{4.7}$$

For unidirectional flow it is considered that λ_1 is equal to the strain at the onset of steady state. The incompressibility condition ($\lambda_1\lambda_2\lambda_3 = 1$) may be used to evaluate λ_2 and λ_3: $\lambda_2 = \lambda_3$.

The critical strain value at 200 ºC evaluated from results of Figure 4.9 is 13820 s.u.. The plateau modulus is usually obtained by Small Amplitude Oscillatory Shear experiments but for PEA it was not possible to reach this plateau, and a literature value (G_N^0 = 1.95 MPa) was considered as described above (§4.2). With these two values, the excess specific free energy calculated from eq. (4.7) is 9.9×10^7 J/m^3.

As was shown previously [Martins-2006], the excess specific free energy decreases with temperature increase. For LDPE this decrease is around 10 J/cm^3 for a temperature difference of 30 ºC (from 190 to 220 ºC). The larger length of precursor structures at lower melt temperature explains the larger strains needed to saturate crystallization. The temperature dependence of precursor structure's length is a direct result of eq. (4.1), and it comes from the temperature dependence of Hamaker constant and the temperature variation of van der Waals volume. The accuracy of these evaluations is also dependent on the plateau modulus value used in eq. (4.4).

The calculated value of the excess free energy was later inserted in eq. (4.4) and precursor structures' thickness was calculated. The value estimated at steady state is between 4.82 Å and 4.98 Å for L in range of 28.8 and 37.1 Å (r = 3.46 Å) and 5.51-5.55 Å for L in range of 172 and 221 Å (b = 4.945 Å). It is therefore visible that large deviations in the precursor's length (more that 7 times larger) changes the thickness by only 0.7 Å.

Eq. (4.4) may also be used to estimate directly the thickness of precursor structures in quiescent melts. Making ΔF_{ex} = 0 for a quiescent melt, it results that $d = (2\sigma/\lambda)L$. For L = 30 Å, d ≈28 Å, approximately two times the a dimension of the orthorhombic PE unit cell.

These predictions agree with dimensions of ordered regions in polyethylene melts made by Kavassalis *et al.* [Kavassalis-1993] in their molecular dynamics simulation of polyethylene crystallization. They used three different starting geometries: (***i***) Single polyethylene chains with 500, 750, 1000, or 2000 CH_2 units, with the skeletal bonds initially in all-trans conformation; (***ii***) A single chain of 1000 CH_2 units, with the bonds in

Table 4.4. *The values used to evaluate the dimension of precursor structures of polyethylene A at temperature of 473 K. Explanation of used symbols was made in text above [van Krevelen-1997, Mark-1996].*

C (J·m^6)	r (Å)	λ (Å)	$E_{conf+net}$ (kJ/mol)	G_N^0 (MPa)	γ_c (s.u.)	T_{crit} (K)	γ_0 (J/m^2)	σ (J/m^2)
5.64×10^{-79}	3.46	1.26	16.0	1.95	13820	1030	5.37×10^{-2}	1.18×10^{-2}

conformations corresponding to the rotational isomeric state distribution, and (***iii***) A set of four chains, each with 500 CH_2 units, with the skeletal bonds initially in all-trans conformations and placed in random orientation with respect to one another, but in close contact.

Simulations were made for different times at 300 K. They concluded that chain folding results from attractive van der Waals interactions between chain segments and that a minimum chain length is required for the formation of stable folded chain lamellae. It was found that the average number of methylene units in a run of all-trans sequences is about 30 units, which corresponds to approximately 40-45 Å, nearby the value estimated for the length of precursor structures in PE. For single chains with 500 and 750 CH_2 units, the lamellar thickness varied between 25 and 35 Å while for set of four chains, each with 500 CH_2, it increased after 700 ps at 300 K to 50 Å. For the chains with bonds in conformations corresponding to the rotational isomeric state distribution, a simulation performed at 600 K predicted a lamellar fold length after 1000 ps varying from 23 to 42 Å.

Despite this agreement and the soundness of the predictions here made, it must be stressed that they were based on assumptions clearly presented in this work and on literature results for some relevant and critical parameters used by these predictions. Two of these parameters are the plateau modulus and the value of the energy barrier for the local and correlated conformational energy jumps. An accurate result of this energy should be evaluated for polymer solutions with a concentration below the overlap concentration and under theta conditions.

4.5. Conclusions

The main goal of this work was to establish the origin of melt memory effect observed in the crystallization of polymers in general, and specifically in polyethylene melts with different crosslinking degree. It was observed by experiments performed with a shear DTA instrument that controlled deformations applied above the equilibrium melting temperature saturate crystallization kinetics, and that the strain required for achieving this saturation decreases with the melt temperature increase. The melt state responsible for this saturation was identified as the steady state in shear flow. The strain at the onset of this state was evaluated. Its value is similar to the strain needed to saturate the crystallization of melts sheared at the same temperature.

The excess of the specific free energy of melts sheared up to steady state was evaluated. The evaluation considered that the increase in the free energy of sheared melts is purely entropic. An expression was proposed to relate this excess specific free energy with the dimensions of precursor structures at steady state. It was assumed that precursor structures do not have crystallographic order, that they have cylindrical shape, that lateral surface free energy (surface free energy along the length) of these structures is the same as the lateral surface free energy in primary or secondary surface nucleation processes. The basal surface free energy was evaluated from an empirical relationship, and it was considered further that basal surfaces contribute to decrease the excess of specific free energy. The excess of the specific free energy for melts sheared up to steady state, which was evaluated from the strain values needed to establish that state and the plateau modulus value for the polymer in question, was then expressed as a function of precursor structures surface free energies, their length and thickness.

To evaluate the length of precursor structures a physical meaning was assigned to flow activation energy. It was assumed that the difference between flow activation energy and the energy barrier for local and correlated conformational energy jumps results from ordered regions in the melt. These ordered regions result from van der Waals interactions between aligned chain segments of the same chain, or of adjacent chains.

The predicted dimensions of precursor structures at steady state and 473 K is: length between 28.8 Å and 37.1 Å and thickness between 4.82 Å and 4.98 Å. It was proposed that erasing the melt memory effect in the quiescent crystallization of polymers results in the decrease of the melt excess specific free energy, which is achieved a randomization of the precursor structures existing at steady state. Associated to this randomization process is the association of neighbouring precursor structures, to yield structures with the same length but of larger thickness. Their thickness will be maximum for quiescent melts, with their melt memory erased, where the excess of the specific free energy is zero. The thickness value predicted for these conditions is 28 Å, around two times the *a* dimension of the orthorhombic PE unit cell. The existence of these structures in quiescent polymer melts explains also the granular structure of lamellae in semicrystalline polymers.

4.6. References

Abe-1966 Abe A, Jernigan RL, Flory PJ (1966) *Conformational energies of n-alkanes and the random configuration of higher homologs including polymethylene.* J Am Chem Soc 88:631-639.

Acierno-2003 Acierno S, Grizzuti N (2003) *Measurements of the rheological behavior of a crystallizing polymer by an "inverse quenching" technique*. J Rheol 47:563-576.

Alfonso-1995 Alfonso GC, Ziabicki A (1995) *Memory effects in isothermal crystallization. II. Isotactic polypropylene.* Colloid Polym Sci 273:317-323.

Azzuri-2008 Azurri F, Alfonso GC (2008) *Insights into formation and relaxation of shear-induced nucleation precursors in isotactic polystyrene.* Macromolecules 41:1377-1383.

Boothroyd-1991 Boothroyd AT, Rennie AR, Boothroyd CB (1991) *Direct measurement of the temperature dependence of the unperturbed dimensions of a polymer*. Europhys Lett 15:715-719.

Elmoumni-2003 Elmoumni A, Winter HH, Waddon AJ (2003) *Correlation of material and processing time scales with structure development in isotactic polypropylene crystallization*. Macromolecules 36:6453-6461.

Gutiérrez-2004 Gutiérrez M-CG, Alfonso GC, Riekel C, Azzurri F (2004) *Spatially resolved flow-induced crystallization precursors in isotactic polystyrene by simultaneous Small- and Wide-Angle X-ray microdiffraction*. Macromolecules 37:478-485.

Häfele-2005 Häfele A, Heck B, Hippler T, Kawai T, Kohn P, Strobl G (2005) *Crystallization of poly(ethylene-co-octene). II Melt memory effects on first order kinetics.* Eur Phys J E 16:217-224.

Hutzler-2000 Hutzler BW, Machado LDB, Villavicencio A-LCH, Lugão AB (2000) *Crystallization of irradiated polyethylene.* Rad Phys Chem 57:431-434.

Israelachvili-1992 Israelachvili J (1992) *Intermolecular and surface forces*. Academic Press Limited, London.

Janeschitz-Kriegl-1997 Janeschitz-Kriegl H (1997) *Conditions of nucleation in crystallizable polymers: reconnaissance of positions – a critical evaluation.* Colloid Polym Sci 275:1121-1135.

Janeschitz-Kriegl-1999 Janeschitz-Kriegl H , Ratajski E, Wippel H (1999) *The physics of athermal nuclei in polymer crystallization.* Colloid Polym Sci 277:217-226.

Janeschitz-Kriegl-2003 Janeschitz-Kriegl H (2003) *How to understand nucleation in crystallizing polymer melts under real processing conditions*. Colloid Polym Sci 281:1157-1171.

Janeschitz-Kriegl-2007 Janeschitz-Kriegl H (2007) *An unusual but consistent view on flow induced crystallization of polymers*. Monatshefte für Chemie 138:327-335.

Jerschow-1997 Jerschow P, Janeschitz-Kriegl H (1997) *The role of long molecules and nucleating agents in shear induced crystallization of isotactic polypropylenes*. Int Polym Process 12:72-77.

Kavassalis-1993 Kavassalis TA, Sundararajan PR (1993) *A molecular dynamics study of polyethylene crystallization*. Macromolecules 26:4144-4150.

Kohler-2005 Kohler WH, Shrikhande P, McHugh AJ (2005) *Modeling melt spinning of PLA fibers.* J Macromol Sci Phys 44:185-202.

Kornfield-2002 Kornfield JA, Kumaraswamy G, Issaian AM (2002) *Recent advances in understanding flow effects on polymer crystallization*. Ind Eng Chem Res 41:6383-6392.

van Krevelen-1997 van Krevelen DW (1997) *Properties of polymers, their correlation with chemical structure, their numerical estimation and prediction from additive group contribution.* Elsevier Science Publishers.

Kumaraswamy-1999 Kumaraswamy G, Issaian AM, Kornfielfd JA (1999) *Shear-enhanced crystallization in isotactic polypropylene. 1. Correspondence between in situ rheo-optics and ex situ structure determination*. Macromolecules 32:7537-7547.

Liu-2006 Liu C, He J, van Ruymbeke E, Keunings R, Bailly C (2006) *Evaluation of different methods for the determination of the plateau modulus and the entanglement molecular weight.* Polymer 47:4461-4479.

Machado-2001 Machado AV, Covas JA, Van Duin M (2001) *Monitoring polyolefin modification along the axis of a twin screw extruder. I. Effect of peroxide concentration.* J Appl Polym Sci 81:58-68.

Malmberg-1998 Malmberg A, Kokko E, Lehmus P, Löfgren B, Seppälä JV (1998) *Long-chain branched polyethene polymerized by metallocene catalysts Et[Ind]$_2$ZrCl$_2$/MAO and Et[IndH4]$_2$ZrCl$_2$/MAO*. Macromolecules 31:8448-8454.

Mark-1996 Mark JE (1996) *Physical properties of polymer handbook*. ed. Woodbury, New York.

Marrucci-2002 Marrucci G, Ianniruberto G (2002) *Modelling rheology and free energy of entangled polymers: State of the art.* Macromol Symp 185:199-210.

Martins-2004 Martins JA, Cruz-Pinto JJC (2004) *True sample temperatures in isothermal differential scanning calorimetry scans and their effect on the overall polymer crystallization kinetics.* J Appl Polym Sci 91:125-131.

Martins-2005 Martins JA, Zhang W, Brito AM, Infante U, Romero M, Soares FO (2005) *Isothermal and nonisothermal crystallization of polymers: Analysis with a shear differential thermal analyzer*. Rev Sci Instr 76:105105-105106.

Martins-2006 Martins JA, Zhang W, Brito AM (2006) *Saturation of shear-induced isothermal crystallization of polymers at the steady state and the entanglement-disentanglement transition*. Macromolecules 39:7626-7634

Martins-2008 Martins JA, Zhang (2008) *Effect of melt memory on the shear-induced non-isothermal crystallization of polypropylene and evaluation of the size of precursor structures*. Submitted to Macromolecules.

Nogales-2003 Nogales A, Olley RH, Mitchell GR (2003) *Directed crystallisation of synthetic polymers by low-molar-mass self-assembled templates*. Macromol Rapid Commun 24:496-502.

Pogodina-2001 Pogodina NV, Lavrenko VP, Srinivas S, Winter HH (2001) *Rheology and structure of isotactic polypropylene near the gel point: quiescent and shear-induced crystallization*. Polymer 42:9031-9043.

Ramos-2005 Ramos VD, da Costa HM, Pereira AO, Rocha MCG, de S. Gomes A (2005) *Effect of peroxide concentration on the modification of the LLDPE: statistical experimental design and thermal properties*. Polym Bull 54:117-122.

Robertson-2001 Robertson MB, Klein PG, Ward IM, Packer KJ (2001) *NMR study of the energy difference and population of the gauche and trans conformations in solid polyethylene.* Polymer 42:1261-1264.

Ryan-1999 Ryan AJ, Fairclough JPA, Terrill NJ, Olmsted PD, Poon WCK (1999) *A scattering study of nucleation phenomena in polymer crystallization*. Farad Discus 112:13-29.

Salem-1962 Salem LJ (1962) *Attractive forces between long saturated chains at short distances*. J Chem Phys 37:2100-2112.

Somani-2002a Somani RH, Yang L, Hsiao BS (2002) *Precursors of primary nucleation induced by flow in isotactic polypropylene*. Physica A 304:145-157.

Somani-2002b Somani RH, Yang L, Hsiao BS, Agarwal PK, Fruitwala HA, Tsou AH (2002) *Shear-induced precursor structures in isotactic polypropylene melt by in-situ rheo-SAXS and rheo-WAXD studies*. Macromolecules 35:9096-9104.

Somani-2005 Somani RH, Yang L, Zhu L, Hsiao BS (2005) *Flow-induced shish-kebab precursor structures in entangled polymer melts*. Polymer 46:8587-8623.

Zhang-2006 Zhang W, Martins JA (2006) *Evaluation of the effect of melt memory on shear-induced crystallization of low-density polyethylene*. Macromol Rapid Commun 27:1067-1072.

Zhang-2007 Zhang W, Martins JA (2007) *Shear-induced nonisothermal crystallization of low-density polyethylene*. Polymer 48:6215-6220.

Zhang-2008 Zhang W, Martins JA, *Viscoelastic flow behaviour of sodium partially neutralized ethylene–methacrylic acid ionomer*. to be submitted.

Zhao-2004 Zhao L, Capt L, Kamal MR, Choi P (2004) *On the use of pressure-volume-temperature data of polyethylene liquids for the determination of their solubility and interaction parameters*. Polymer Eng Sci 44, 853-860.

Ziabicki-1994 Ziabicki A, Alfonso GC (1994) *Memory effects in isothermal crystallization. I. Theory*. Colloid Polym Sci 272:1027-1042.

5. Shear-induced crystallization of Ziegler-Natta and metallocene catalyzed polyethylene

Abstract

The motivation behind this work was to verify the impossibility mentioned in literature of saturating the crystallization kinetics and the morphology developed at solid state from pre-sheared melts of metallocene polyethylene. A Ziegler-Natta and a metallocene-based polyethylene, with molecular weight and polydispersity similar to those used in a previous work, were used for these studies. Both polymer melts were pre-sheared at different temperatures, above their equilibrium melting temperature, cooled down to the crystallization temperature and the crystallization kinetics recorded with a shear DTA instrument. Similarly to results reported for other materials, and contrary to other published results, it was found for both materials an acceleration of crystallization kinetics with shear strain and its saturation at large strains. The strain needed to saturate crystallization is similar to that needed to establish a steady state in shear flow, and it decreases with the sheared melt temperature. The metallocene-based polyethylene reaches a steady state at larger strains than those needed to establish the same state for the Ziegler-Natta polyethylene, this probably being the reason for contrary conclusions in previous works. The agreement with results obtained for other polymers is also extended to the relative values of reptation time and their temperature dependence.

5.1. Introduction

The heterogeneous Ziegler-Natta catalyst was developed in the early 1950's [Ziegler-1955a, Ziegler-1955b, Natta-1955a, Natta-1955b]. A material synthesized with these catalysts has polydispersity index higher than 3 and the co-monomer is incorporated heterogeneously along the chain. The homogeneous metallocene type catalyst was developed in the 1980's [Sinn-1980]. They are a combination of a transition metal and two cyclopentadienyl ligands coordinated in a sandwich structure. Because metallocene catalysts are single-site catalysts, they allow obtaining linear polymers with lower polydispersity index (around 2) and well-defined architecture.

The properties of Ziegler-Natta and metallocene catalyzed polymers were previously described by others, however there is only a few publications concerning polyethylene

[Mirabella-2001, Shih-1999, Chiu-2002, Malmberg-2002, Yan-1999] and the main interest of authors is the effect of long or short chain branching on the rheological flow behaviour and crystallization kinetics. Relevant to this work are the effects of branching degree in the morphology development at the solid state and of different catalysts on the rheological behaviour and crystallization kinetics, both quiescent and after shear. The works mentioned below will describe some of the above effects.

The effect of highly short chain branching on the morphology developed at the solid state was studied by Wang *et al.* [Wang-2001] who worked with metallocene-based polyethylene with an ethyl branching content of 10.4 mol%. This kind of polymer has unique molecular architecture, which includes uniform distribution of SCB (Short Chain Branching) and narrow molecular weight distribution. A network structure was found at the solid state where small crystals are "physical crosslinks" and ethylene sequences are connections. Based on the DSC stepwise fractionation method, the length of the crystallisable ethylene sequence was estimated to be too short to develop a fold similar to that observed in the lamellar crystals. Wang *et al.* named those structures fringed-micelle-like crystals. The thickness of fringed-micelle-like crystal was determined by Small Angle X-ray Scattering to be 26 Å.

The rheological behaviour at the molten state and in the vicinity of liquid-to-solid transition (gel point) was studied by Winter *et al.* [Gelfer-2003]. They investigated the viscoelastic properties of ethylene-hexene copolymers of metallocene and Ziegler-Natta linear low density polyethylenes differing in branching degree. ZN-LLDPE contains a bimodal intermolecular branching distribution with relatively high fractions of both low-branched chains (branching content $x < 1$ mol%) and highly branched chains ($5 < x < 12$mol%). The branching distribution of M-LLDPE is unimodal, with an average branching of 2.61 mol%. For reference materials they used un-branched polyetyhlenes, ZN-HDPE and M-HDPE. They found that the rheological behaviour in the vicinity of liquid-solid transition is determined by content of linear molecules rather than by the overall branching. To reach this conclusion, they made experiments with blends of different content of two polymers, one un-branched (ZN-HDPE) and the other branched (M-LLDPE). It was found that for ZN-HDPE/M-LLDPE blends the increase of ZN-HDPE content from 10 to 50 [w/w%] enhances the overall composition heterogeneity and causes the narrowing of solidification interval when compared with the solidification interval width of M-LLDPE or ZN-LLDPE. It was also found that polymers synthesized with Ziegler-Natta catalysts have lower flow activation energy than metallocene-based polymers, and that the onset of shear thinning occurs earlier for ZNPE. These results are understandable because usually ZN polyethylenes have higher branching degree.

The effect of catalyst type on the development of melt morphology was studied by Rastogi *et al.* [Rastogi-2005, Lippits-2007]. They used two different ultra-high molecular weight polyethylenes (UHMW-PE). One was obtained from highly active heterogeneous Ziegler-Natta catalysts and high polymerization temperatures. The other was obtained from single site catalysts and low polymerization temperatures. Because of the high catalytic activity and high polymerization temperature, the crystalline lamellae and the amorphous regions of the ZNPE are composed of different chains, while for metallocene samples the whole crystal is made up of a single chain. It was found that different melt states are obtained for these two PE's. For the ZNPE, regardless the heating mode used, a homogeneous melt is always obtained. By homogeneous, it is meant a melt with regular distribution of entanglements along the chain. On the other hand, fast melting of MPE yields also a homogeneous melt, but melting with a slow heating rate yields a heterogeneous melt. In this case, the homogeneous melt state is reached after long heating time.

Description of the influence of pre-shear history on the crystallization of two copolymers, a Ziegler–Natta catalyzed linear low density polyethylene (LLDPE), hexane-copolymer, and a linear metallocene, hexane-copolymer, of similar melt flow index, density and molecular weight (~10^5 g/mol), but of different molecular weight distributions (3.4 and 2.1, respectively) was made by Chai *et al.* [Chai-2003]. They used a Linkam shearing cell with quartz windows in close thermal contact with the silver block heaters. The polymer sample was sheared at the test temperature (T_s = 190, 170 and 150 ºC) with a given shear rate (from 1 to 18 s^{-1}) during a shearing time t_s, left there for a waiting time in range of 0-10 min, and cooled down to 90 ºC at a controlled cooling rate of 20 ºC/min. Small Angle Light Scattering patterns were recorded during the whole process. For ZNPE the spherulite radius was found to decrease with pre-shear and saturated at a strain of ~10^3 s.u. with a value of ½ the spherulite radius without shear ($R_0 \approx 12\ \mu m$ for ZNPE). For the linear metallocene PE no spherulite radius variation with pre-shear was observed ($R_0 \approx 3\ \mu m$ for MPE). It was also found that the ZNPE's spherulite radius decreases with the increase of waiting time at the test temperature, until a limiting value of waiting time, above which the shperulite size doesn't change. According to Chai *et al.*, this limiting waiting time value represents the largest relaxation time of ZNPE, which however is 20 times the longest relaxation time evaluated by Small Amplitude Oscillatory Shear experiments. It was also concluded that the consequence of shear was giving ellipsoidally deformed spherulites, elongated in the flow gradient direction. The authors found also surprising that chain orientation for the ZNPE sample requires a large amount of shear deformation, around 1000 s.u., to reach a steady state while for the metallocene PE all shear effects described above were not observed.

The different results obtained by Chai *et al.* for Ziegler-Natta and metallocene-based polyethylenes were the motivation for the experiments described below. It is known that linear polymer chains, regardless the catalyst type used in their synthesis, can reach in shear flows a well defined steady state. Because is was demonstrated in previous works that steady state is the melt state responsible for the saturation of crystallization of polymers sheared above their equilibrium melting temperature, it was a surprise to find the conclusion that the crystallization kinetics of pre-sheared metallocene-based polyetheylenes cannot saturate. Experimental results presented below aim to demonstrate the invalidity of this conclusion and that metallocene-based PE's behaves in a way similar as any other linear polymer chain.

5.2. Experimental

5.2.1. Materials characterization

Two different polyethylenes were used in this work: Ziegler–Natta catalyzed polyethylene (ZNPE) and metallocene polyethylene (MPE). Some materials properties are summarized in Table 5.1. Both polymers have similar density measured at 25 ºC. ZNPE has an average molecular weight (M_w) of ~114650 g/mol and a molecular weight distribution (*MWD*) of 3.7 and MPE has M_w of ~106100 g/mol and molecular weight distribution of ~2.3. The equilibrium melting temperature was evaluated according to procedure described in Chapter 4 (§4.2.2.1.) and it is shown in Table 5.1 to be higher for the Ziegler-Natta polyethylene. Oxidation induction time evaluated by DSC (T = 200 ºC, gas-nitrogen and oxygen, flow rate of 50 ml/min, heating rate 10 ºC/min) is equal to 2.13 min for ZNPE and 30.19 min for MPE.

^{13}C NMR experiments performed in the Polish Academy of Sciences (Lodz, Poland) allowed to conclude, that ZNPE is a copolymer of ethylene and octene with 3.03 molar % of octene and has 88.84 wt% of carbon atoms in ethylene sequences and 11.16 wt% of carbon atoms in octene, while the MPE is a copolymer of ethylene and hexene with 2.6 molar % of

Table 5.1. *Density, average molecular weights, polydispersity, equilibrium melting temperature, and oxidation induction time for ZNPE and MPE. The density ρ was measured at 25 ºC.*

Polymer	ρ (g/cm³)	M_n (g/mol)	M_w (g/mol)	M_z (g/mol)	*MWD*	T_m^o (ºC)	$t_{\ln}$ (min)
ZNPE	0.8389±0.003752	30700	114650	438200	3.7	127,660	2.13
MPE	0.8358±0.001952	46100	106100	185000	2.3	125,485	30.19

hexene and has 92.6 wt% of carbon atoms in ethylene sequences and 7.4 wt% of carbon atoms in hexene. More information about NMR results is presented at Appendix (§A1.3).

5.2.2. Crystallization kinetics and rheological experiments

The experimental protocols used for DSC, rheometer and shear DTA experiments were described in Chapter 4 (§4.2.2). Additional information concerning temperature ranges used in rheometer experiments is presented below. Controlled Shear Rate experiments (CSR) were performed between 140 ºC and 170 ºC for ZNPE and between 140 ºC and 180 ºC for MPE. The constant stress used for experiments in the viscoelastic linear regime evaluated in the above temperature range was 1000 Pa for both polymers. Small Amplitude Oscillatory Shear experiments were performed between 130 ºC and 170 ºC for ZNPE and between 140 ºC and 170 ºC for MPE. Shear stress growth experiments were performed between 150 and 170 ºC for ZNPE and between 180 and 200 ºC for MPE. The reason of this high temperature range for shear stress growth experiments results from the need to detect the attainment of steady state, which occurs after shearing the melt after a relatively long time that decreases with the sheared melt temperature increase.

5.3. Results

Melt memory and quiescent crystallization experiments

Figure 5.1 shows the effect of melt memory on the quiescent crystallization of these two polymers. These results are similar to others already reported in the literature and presented in Chapter 4. Two samples weighting 11.329 mg and 11.104 mg, for ZNPE and

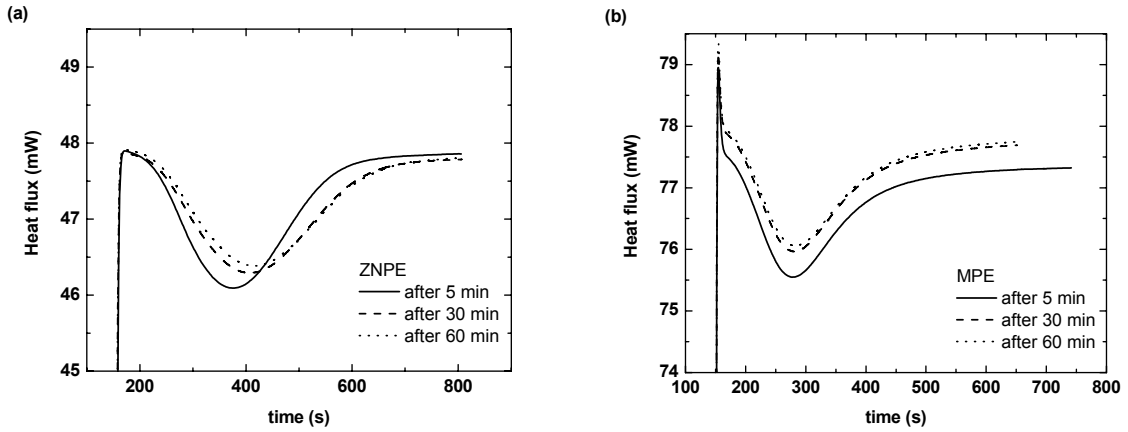

Figure 5.1. *Heat flow variation as a function of time for the isothermal crystallization of Ziegler-Natta (a) and metallocene (b) polyethylene at 112 ºC after annealing at 200 ºC during 5 min, 30 min and 60 min.*

Table 5.2. *Half-time of crystallization obtained from isothermal experiments performed by DSC.*

T (ºC)	$t_{1/2}$ (s)	
	ZNPE	**MPE**
110		151.8
111	63.0	221.4
112	87.6	348.0
113	127.8	511.2
114	193.2	
115	343.2	
116	512.4	
117	843.0	

MPE, respectively, were heated up to 200 ºC, and cooled with a rate of -60 ºC/min to the crystallization temperature (112 ºC). Results of crystallization after annealing with different times at the melt temperature are in Figure 5.1. The shape of crystallization curves after annealing during 30 and 60 min is similar. It was concluded that 30 min of annealing erases the melt memory effect. Therefore, all "fresh" samples used in DSC crystallization experiments passed through this annealing process prior to further crystallization studies.

The half-crystallization time results obtained from quiescent isothermal crystallization experiments recorded in the DSC for melts "without memory" are in Table 5.2. It is visible that ZNPE crystallizes faster than MPE.

Further SEM morphological analysis of crystallized samples demonstrated that ZNPE has lower nucleation density. The average spherulite diameter evaluated from Scanning Electron Microscopy of samples crystallized at 117 ºC was around 70 μm for ZNPE and 8 μm for MPE (see Figures A1.8 and A1.9 at Appendix) corresponding to a nucleation density of 5.57×10^{12} nuclei/m^3 and 3.73×10^{15} nuclei/m^3 for ZNPE and MPE, respectively.

The value obtained for the spherulite radius of MPE (R_0 = 4 μm) agrees with the value obtained by Chai *et al.* [Chai-2003] (R_0 = 3 μm), which is not surprising since the molecular weight and molecular weight distribution are similar for both samples. The relatively different values obtained for the spherulite radius of the ZNPE used in this work (R_0 = 35 μm) and that of Chai *et al.* (R_0 = 12 μm) may be explained by difference in the molecular weight distribution of both samples (3.7 and 3.1 for the ZNPE used in this work and by Chai, respectively). It must be noted however, that Chai's results refer to the non-isothermal crystallization of melts sheared above their equilibrium melting temperature. Also, the final spherulite radius depends on the crystallization temperature. Since the applied deformation and cooling rate used by Chai *et al.* are similar for metallocene and Ziegler-Natta polyethylenes, the relative difference in their corresponding final spherulite sizes may be

comparable with the relative difference in the spherulite radius for the polyethylene samples used in this work.

The surprising results of these experiments are the faster crystallization kinetics of ZNPE and the factor(s) responsible for its lower nucleation density when compared with MPE sample's results. In principle, one would expect an opposite behaviour to the one here reported, namely that crystallization kinetics would be fastest for the polymer with higher nucleation density. One factor responsible for the faster crystallization kinetics in ZNPE may be the supercooling degree. Because nucleation densities were estimated for samples crystallized at the same temperature (112 ºC), the supercooling degree is around 2.2 ºC higher for ZNPE sample (see Table 5.1). A possible explanation for the lower nucleation density of ZNPE, when compared with that evaluated for MPE, is its higher branching content. NMR results yielded for ZNPE higher molar % of octene branches and more wt% of carbon atoms in octene branches than MPE has in the corresponding hexene branches. However, the results of Winter *et al.* [Gelfer-2003] mentioned at the introduction for the addition of un-branched ZN-HDPE with M-LLDPE indicate that the content of linear molecules, rather than the overall branching, controls the steepness of the transition from the liquid to the solid phase. These conflicting conclusions will be discussed further.

Crystallization kinetics after shear

Results of experiments obtained with the shear DTA instrument following the protocol described in §4.2.2.3 are presented in Figures 5.2, 5.3 and 5.4.

Figure 5.2 shows the isothermal crystallization at 115 ºC after shearing at 240 ºC with constant shear rate and increasing shearing times. As shown in Chapter 4, the crystallization

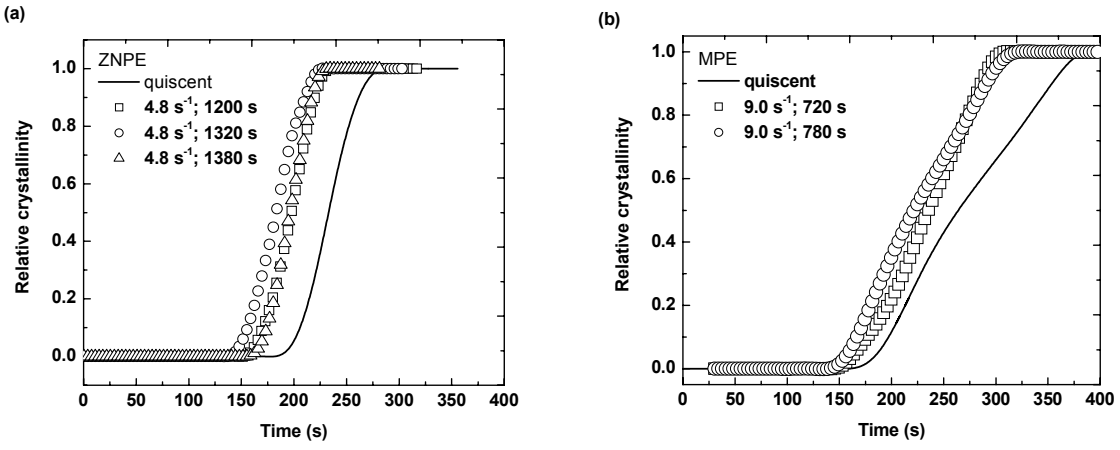

Figure 5.2. *Isothermal crystallization of polyethylene Ziegler-Natta (a) and metallocene (b) recorded with shear DTA: T_c =115 ºC, T_m = 240 ºC, constant shear rate of 4.8 s^{-1} for ZNPE and 9.0 s^{-1} for MPE, shearing times indicated. The average critical strain for ZNPE is 5760 s.u. and for MPE – 6480 s.u..*

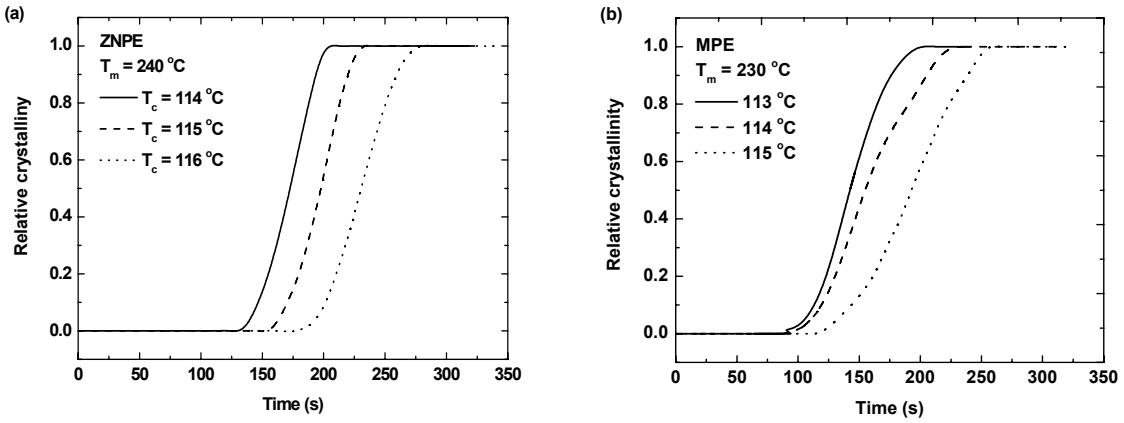

Figure 5.3. *Effect of crystallization temperature on saturation of crystallization. Constant shearing temperatures (240 ºC for ZNPE and 230 ºC for MPE) and shear rate (4.8 s^{-1} for ZNPE and 7.6 s^{-1} for MPE) at different crystallization temperatures for ZNPE (a) and MPE (b). The average critical strain for ZNPE is 5760 s.u. and for MPE - 6840 s.u.. The measurement error in the strain values is ±10% around the mean and it results from small variations of cooling rate to the crystallization temperature.*

kinetics is accelerated with the increase of shearing time until saturation takes places. The calculated value of strain for this melt temperature was around 5760 s.u. for ZNPE and 6480 s.u. for MPE. Further increase of shearing time doesn't accelerate crystallization.

Figures 5.3 and 5.4 show the effects of crystallization and melt temperatures on the saturation of crystallization kinetics. For the same melt temperature and different crystallization temperatures, crystallization kinetics saturates at the same strain (Figure 5.3). For the same crystallization temperature and different melt temperatures, saturation occurs at lower strains for higher melt temperatures (Figure 5.4). As shown in Chapter 4 and in other works [Martins-2006, Zhang-2007], the saturation of crystallization kinetics depends only on the sheared melt temperature, being crystallization temperature independent. This limiting

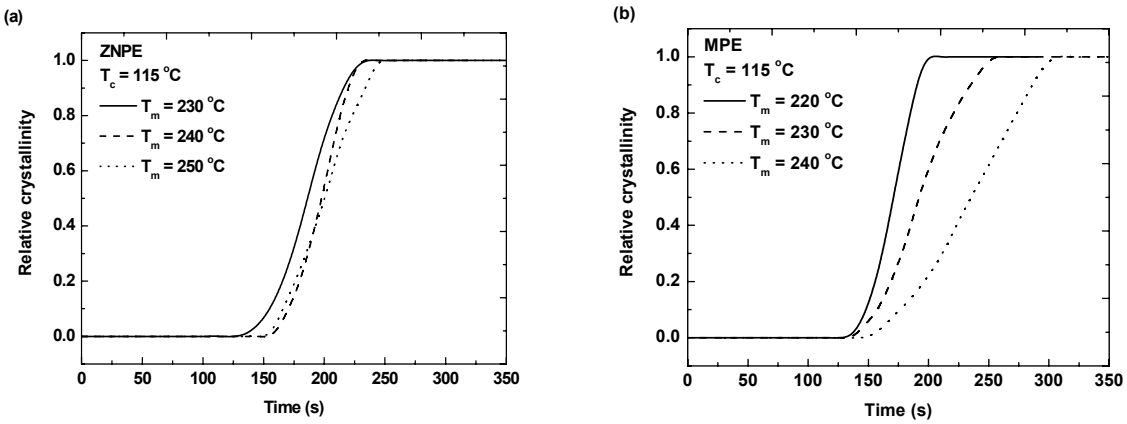

Figure 5.4. *Effect of shearing temperature on saturation of crystallization. Constant crystallization temperature (115 ºC) and shear rate (4.8 s^{-1} for ZNPE and 7.6 s^{-1} for MPE) at different shearing temperatures for ZNPE (a) and MPE (b). The average critical strain for ZNPE at melt temperature 230 ºC is equal to 5929 s.u., for 240 ºC - 5760 s.u. and for 250 ºC - 5508 s.u. and for MPE at melt temperature 220 ºC it is 7776 s.u., for 230 ºC – 6840 s.u. and for 240 ºC – 6480 s.u.. The measurement error in the strain values is ±10% and results from small variations on the cooling rate.*

strain value needed to saturate crystallization kinetics from sheared melts was already defined in Chapter 4 as the *critical strain*. It is the minimum value of strain needed to align the maximum number of chain segments with the flow direction. As will be also shown below, the same critical strain is required for reaching a steady state in steady shear experiments. Contrary to the results obtained by Chai *et al.* [Chai-2003], it is reported here that crystallization kinetics of pre-sheared melts saturates also in metallocene based polyethylenes.

Identification of the melt state responsible for the saturation of crystallization

Figure 5.5 shows results of shear stress growth experiments obtained in a rheometer with parallel plate configuration at 190 ºC and 170 ºC for MPE and ZPE, respectively. The full set of results obtained for these two polymers at different melt temperatures is in Figure 5.6. From these experiments the strain at the onset of steady state, the critical stain, is evaluated. As shown in Figure 5.6, it agrees with the strain values that saturate crystallization, allowing therefore identifying the melt state responsible for the saturation of crystallization [Martins-2006]. The variation of viscosity (or shear stress) with time, at constant shear rate, increases initially, passes through a maximum, decreases and stabilizes at a constant value. The onset of this stabilization defines the steady state, where the density of entanglements in the sheared melt is constant.

Figure 5.5 shows how difficult is the definition of the onset of steady state. As discussed in Chapter 4, the difficulty arises from polymer thermal degradation, which is a problem to be considered at high melt temperatures, the mass loss of polymer between plates, among other effects, that affect the accuracy with which strain values at the onset of

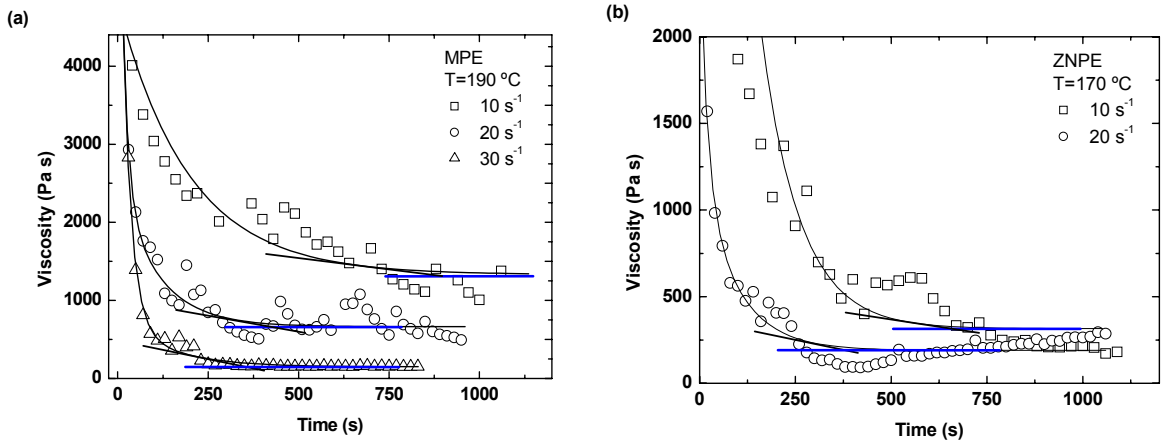

Figure 5.5. *Transient viscosity as a function of time in stress growth experiments performed at 190 ºC for MPE (a) and at 170 ºC for ZNPE (b). The solid lines show the procedure for evaluating the critical strain at the onset of the steady state. For metallocene polyethylene an average critical strain of 9330 s.u. (± 1364) at the onset of the transient steady state is evaluated from the experimental results, part of which is presented on this figure, for shear rates of 10 s^{-1} (9070 s.u.), 20 s^{-1} (8300 s.u) and 30 s^{-1} (10620 s.u.). For Ziegler-Natta polyethylene an average critical strain of 7230 s.u. (± 562) was evaluated from shear rates of 10 s^{-1} (6700 s.u.) and 20 s^{-1} (7760 s.u).*

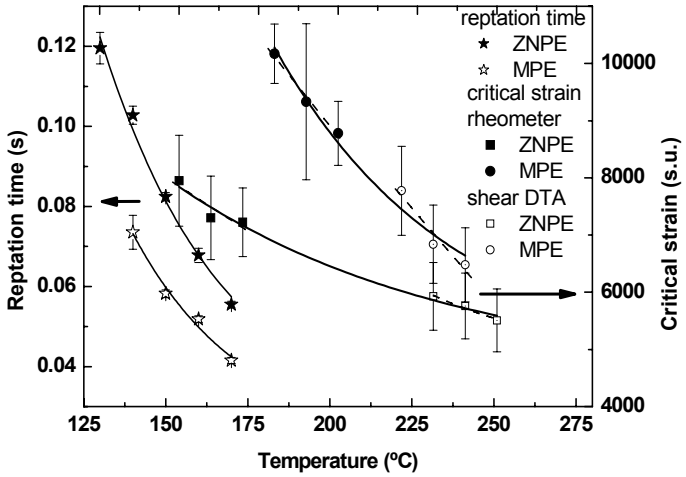

Figure 5.6. *Temperature variation of the reptation time (stars) and critical strain for polyethylene ZN and M. The critical strain measured with shear DTA (open symbols) and in shear stress growth experiments with parallel plate (filled symbols) is plotted as a function of sheared melt temperature: squares represent ZNPE and circles - MPE.*

steady state are evaluated. For these reasons, these experiments were repeated several times (at least three times for each temperature at given shear rate) and the strain values indicated in the Figure 5.5 correspond to an experiment within the average of the measurements performed.

Due to difficulties mentioned above, the experimental curves were fitted with a single exponential decay function, and the onset of steady state was evaluated at the intersection point between a tangent line to the plateau and another tangent line to the inflection point of the exponential decay function. The critical strain necessary to stabilize the viscosity in shear flows at constant shear rate evaluated with the rheometer is similar to that obtained with the shear DTA at the same melt temperature. Figure 5.6 shows the values of critical strain evaluated from results obtained with both instruments at different melt temperatures. The critical strain, either the one measured at the onset of the steady state or that needed to saturate the crystallization from a sheared melt, measured with the shear DTA, showed similar temperature dependence, and both approach a limiting value at high temperatures. Therefore, the critical strain data points obtained by two different instruments for both polymers were fitted with a single equation shown in Figure 5.6.

Figure 5.6 shows also the temperature variation of reptation time evaluated by SAOS experiments performed with a constant stress of 1000 Pa for both polymers in the viscoelastic linear regime. This temperature dependence is similar to that described in previous works [Martins-2006, Zhang-2006]. An example of SAOS experiments is illustrated in Figure 5.7, where the reduced curves of $G'(\omega)$ and $G''(\omega)$ at 160 ºC are indicated. From these experiments the flow activation energies were also evaluated and compared with values of

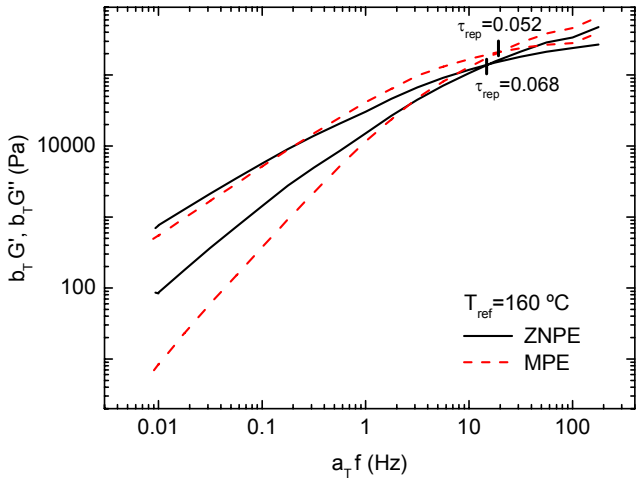

Figure 5.7. *Reduced curves of Small Amplitude Oscillatory Shear experiments for Ziegler-Natta and metallocene polyethylene at the reference temperature of 160 ºC.*

flow activation energy obtained from Controlled Shear Rate experiments (see Figure A1.13 at Appendix). These activation energies were evaluated by fitting with an Arrhenius equation the horizontal shift factors used to construct reduced curves similar to those shown in Figure 5.7. A detailed description of the procedure is presented in Appendix (§1.6.2), and the values obtained are in Table 5.3. As expected, similar values were obtained for SAOS and CSR experiments. Also, flow activation energies evaluated from reptation times of SAOS experiments (see Figure A1.15 at Appendix) agree with values shown in Table 5.3. Due to the reduced number of data points obtained for ZNPE in CSR experiments values of this flow activation energy are lacking in Table 5.3. These data points were not obtained due to the lower thermal stability of ZNPE at higher temperatures. The above values agree with literature results. Similarly to Winter *et al.* [Gelfer-2003] it was found that flow activation energy of MPE is higher than that of ZNPE.

5.4. Discussion

As mentioned in the results presentation, the fast crystallization kinetics and the lower nucleation density of the ZNPE when compared with that obtained for MPE, contrast with

Table 5.3. *Flow activation energies evaluated by Small Amplitude Oscillatory Shear and Controlled Shear Rate experiments for the Ziegler-Natta and metallocene polyethylenes.*

PE	E_a (kJ/mol)	
	SAOS	CSR
ZN	24.46±1.53	-
M	29.93±1.21	26.38±3.00

the conclusion of Winter *et al*. [Gelfer-2003] that the content of linear molecules, rather than the overall branching, controls the steepness of the transition from the liquid to the solid phase. One important aspect in polymer crystallization was neglected in the Winter *et al.* analysis, namely the different polymer molecular weight and the sample's polydispersity. For polymers with similar molecular weight but different molecular weight distribution, the crystallization kinetics is faster for the sample of higher polydispersity. This results from the competing effects of diffusion of chain molecules to the lamellae growth front and from the surface nucleation. While it is known that high molecular weight polymer chains promote nucleation, and that atactic polymer chains are segregated from the lamellae growth front, it appears that crystallisable polymer chains of lower molecular weight are more readily incorporated in the crystalline lamellae than longer polymer chains, which face higher energy barriers to diffuse to the lamellae growth front. However, Keith and Padden [Keith-1963] stated that very low molecular weight components are also rejected by growing crystals and higher concentration of those components, treated as impurities, can slow down the spherulite growth rate. The rate of advance of a crystallization front depends then rather upon the interplay of the heat transport and diffusion of impurities. The effect of molecular weight on nucleation rate described by Mandelkern *et al.* [Ergoz-1972] was already mentioned in Chapter 2 (see Figure 1.25, it is double logarithmic plot of the time required for 1% of the absolute amount of crystallinity to develop as a function of molecular weight). For lower molecular weight range, the crystallization kinetics decrease with the molecular weight increase, until a maximum in the crystallization rate is obtained, which is crystallization temperature dependent. Then, further increase of molecular weight delays crystallization kinetics, until a plateau is reached at very high molecular weight. This behaviour is more pronounced for higher crystallization temperature.

The shear stress growth results shown in Figure 5.5 indicate that, despite the difficulties in obtaining a well defined steady state for the metallocene polyethylene, especially evident for the experiments performed at low shear rates, this state can be defined. This definition is more evident for the experiment performed at 30 s^{-1}. At lower shear rates a set of oscillations occur, with increase and decrease of viscosity. The difficulty observed for experiments carried out at low shear rates may result from two combined effects: the rotational component of shear flow and the low polydispersity of polymer chains. Therefore, a possible explanation for the oscillations in viscosity is the following. Because in shear flows around 50% of the contour chain length may be aligned with the flow direction, and because of the relatively narrow molecular weight distribution of this polymer, the chain alignment with the flow direction will be, in principle, more homogeneous than in a polymer of higher

polydispersity. From this chain alignment physical interactions between adjacent chain segments may occur, contributing to the transient viscosity increase. The decrease will occur afterwards resulting from the rotational component of shear flow. At high shear rates, the stronger rotational component of shear flow inhibits efficient chain alignments, this being probably the reason for not detecting any viscosity increase at 30 s^{-1}. However, to fully clarify this aspect future work will be needed with samples of different molecular weights and narrow molecular weight distribution.

As shown in Figure 5.6 the reptation time of Ziegler-Natta polyethylene is longer than that of metallocene polyethylene. The question arises if longer reptation time of Ziegler-Natta polyethylene results from the differences between their masses or tube diameters (because of the higher branching content of ZNPE). From NMR results it is known that ZNPE is more branched, has higher M_w and *MWD* than MPE.

To evaluate the tube diameter it is necessary the evaluation of molecular weight between entanglements, M_e, which is done from plateau modulus value by

$$G_N^0 = \frac{4}{5}\frac{\rho RT}{M_e} \quad , \tag{5.1}$$

where G_N^0 is plateau modulus, R is ideal gas constant, T is the absolute temperature and ρ is the polymer density at temperature T. The following values of plateau modulus were used: 1.97 MPa for metallocene polyethylene (according to results of Wood-Adams *et al.* [Wood-Adams-2000]) and 2.0 MPa for Ziegler-Natta polyethylene [Rastogi-2005]. Since the values of plateau modulus are identical for both polymers, and they have similar density (see Table 5.1), similar molecular weight between entanglements, and tube diameters, are obtained. It can be therefore concluded that the main influence on the different reptation time values results from the different molecular weight of two polymers. Also proportionality between reptation times (Figure 5.6) and molecular weights of ZNPE and MPE (Table 5.1)

$$\frac{\tau_{ZN}}{\tau_M} \propto \frac{\left(M_{w,ZN}\right)^{3.4}}{\left(M_{w,M}\right)^{3.4}} \tag{5.2}$$

confirms that this increment results only from differences of their masses. The ratio between the reptation time of ZNPE and MPE at 170 ºC is equal to 1.335 and the ratio between the masses 1.301.

Similar calculation may be made with results of Chai *et al.* [Chai-2003]. Since the procedure used to evaluate the longest relaxation time indicated in Table 1 of this work is unknown, for this evaluation it was used the procedure used above and the SAOS data shown in Figure 3a, which was obtained at 190 ºC. The reptation time evaluated for ZNPE at 190 ºC is then equal to 0.088 s and for MPE is 0.069 s. The ratio between reptation times is equal to

1.268, and the ratio between masses is 1.191. The larger difference in this case may be ascribed to the large error in the evaluation of reptation time for MPE from data of Figure 3a in ref. [Chai-2003]. Another source for this difference may be the polymer thermal degradation during the rheological experiment, a fact that was not considered in the work of Chai *et al.*

Based on the above results, a conclusion similar to that already presented in Chapter 4 may be obtained for the morphology of critically sheared melts, which is at the origin of melt memory effect. Because crystallization from critically sheared melts saturates and, as shown in another works [Martins-2006, Zhang-2006], critically sheared melts have low number of entanglements, around 1/2 the initial number of entanglements for PE, we must conclude that precursor structures for crystallization are active at temperatures above the polymer equilibrium melting temperature, that they reach maximum effectiveness at steady state, that they cannot be considered as conceptual objects void from crystallites [Häfele-2005], but instead they must be considered as real objects, because they accelerate crystallization when sheared, and retard crystallization after annealing. Because it is known that precursor structures are long-lived [Azzurri-2005], and they do not have crystalline order [Somani-2002], we must envisage now the coexistence of these oriented structures without crystalline order with a dynamic disentangled melt. According to the standard model, the morphology of this melt is described by the random coiled model, in which it is known from experiments that the radius of gyration of polymer chains in shear flow increases only by 1.73 times the chain radius of gyration in a quiescent melt [Bent-2003]. It is this conception of melt morphology that is questioned by these results and those of Chapter 4.

Since precursor structures do not have crystallographic order, they must consist of a set of aligned chain segments, which implies the existence of a physical interaction between them. The only possible interaction results from van der Waals forces. The interaction potential energy between parallel chain segments, resulting from van der Waals forces, was evaluated by Salem [Salem-1962]. The final equation was presented in Chapter 4 - eq. (4.1). It expresses the interaction potential energy as a function of Hamaker constant, which depends on the polymer refractive index and its dielectric constant, the polymer charge density, the average separation distance between chains and the length of interacting regions. Therefore, the parameters in Salem's equation may be evaluated from polymer chemical structure, and the knowledge of interaction potential energy allows the evaluation of the precursor structures' length.

To carry on this evaluation, we must consider the effect of these ordered regions with aligned chain segments, interacting with van der Waals forces, in the flow activation energy.

Clearly, the value measured from experiments of flow activation energy must have a physical meaning. This physical meaning was already discussed in Chapter 4, and it will be complemented with further discussion below.

According to the model proposed in Chapter 4 for the quiescent and critically sheared polymer melt morphology, polymer chains interact, and the results of these interactions are the formation of ordered regions in the melt. Therefore, as in the tube model, a test chain is selected randomly. We consider now the barriers to the flow of this test chain with respect to the neighbouring chain segments. At least two energy barriers must be considered. One results from the *trans-gauche* conformational transitions and the other results from the interaction potential energy between aligned chain segments. Because the flow of a specific segment of the test chain must involve movements of all other segments in the same chain, conformational transitions can only occur if chain segments in the ordered regions are released of their interactions. These two energy barriers must be evaluated separately, and flow activation energy is the sum of these two energy barriers. An additional contribution to flow activation energy is the contribution resulting from the network [Martins-2008a], which includes the effects of ionic interactions, crosslinks (as shown in Chapter 4), and eventually the polymer molecular weight.

The key problem appears then to be the evaluation of the *trans-gauche* conformational energy barrier. Accurate values of this energy barrier may be evaluated from NMR experiments with polymer solutions or polymer melts of un-entangled polymer chains. In fact it was found that the energy barrier for "conformational transitions" in entangled iPP polymer melts is similar to that of viscosity [Moe-2000], which led the authors to the wrong conclusion that "*rearrangement of chain conformation required for flow is simply the result of many independent conformational transitions*". Results by the same authors of un-entangled polyethylene melts led them to the conclusion that "*the activation energy for conformational dynamics was 16.592 kJ/mol, significantly less than flow activation energy for polyethylene melts*" [Qiu-2000].

It seems clear that conformational transitions cannot be the unique effect for resistance to flow in entangled melts, playing much less significant role in un-entangled melts. Therefore, the increment from 16 kJ/mol to the measured value of flow activation energy

Table 5.4. *The values used to evaluate the dimension of precursor structures of Ziegler-Natta and metallocene polyethylene at temperature of 473 K. Explanation of used symbols was made in Chapter 4 and in the text above [van Krevelen-1997, Mark-1996].*

C ($J \cdot m^6$)	r (Å)	λ (Å)	$E_{conf+net}$ (kJ/mol)	T_{crit} (K)	γ_0 (J/m^2)	σ (J/m^2)
5.64×10^{-79}	3.46	1.26	16.0	1030	5.37×10^{-2}	1.18×10^{-2}

must result from ordered regions in the melt. It was demonstrated that topological constraints to the chains motion cannot be responsible for this increment [Martins-2008b]. The interaction potential energy of topological constraints is similar to the thermal energy of the melt (or lower).

The procedure used for evaluating the dimensions of precursor structures of ZNPE and MPE is similar to that used in Chapter 4 (§4.4). To evaluate their length eq. (4.1) was used. The parameters used by this equation are repeated here in Table 5.4. Following the previous discussion, the values of W (interaction potential energy of aligned chain segments in the ordered regions) was evaluated from the difference between flow activation energy (Table 5.3) and the energy barrier for *trans-gauche* conformational transitions evaluated for un-entangled PE melts (or PE solutions under ideal conditions), the 16 kJ/mol [Qiu-2000]. The results are in Table 5.5.

The values predicted for the precursor structure's length, obtained by application of eq. (4.1), with the parameters of Table 5.4, are indicated in Table 5.5. One parameter of difficult choice is the average separation distance between chain segments. Two values were considered. One is the minimum separation distance between chain segments – 3.43 Å (it may be evaluated by considering bond lengths and angles, and that the minimum separation distance between two atoms of different chains is equal to two times the van der Waals radius of hydrogen, or by evaluating the attractive and repulsive interaction potential energy and the minimum of this function). The other is the b dimension of the orthorhombic unit cell of polypropylene – 4.945 Å. Values of L obtained for these two separation distances are also in Table 5.5. All evaluations were made for T = 473 K and the range in the precursor structures' length for MPE results from the different flow activation energy evaluated by SAOS and CSR experiments (see Table 5.3). One can see that the length of precursor structures goes from around 20 Å up to around 100 Å, below the typical lamellae thickness of polyethylene melts, which is around 200 Å.

The precursor structures thickness is evaluated with eq. (4.4), with the surface energy values given in this chapter. The results obtained are also in Table 5.5. The difference with respect to values evaluated in Chapter 4 results from the different values of critical strain evaluated for the ZNPE and MPE indicated in Figure 5.6. The excess free energy was evaluated with eq. (4.7), already discussed in Chapter 4 [Marrucci-2002]. Besides the critical strain values, eq. (4.7) requires also knowledge of plateau modulus.

The critical strain for ZNPE at 473 K was obtained by extrapolation of experimental rheometer and shear DTA results shown in Figure 5.6. The value obtained was 6400 s.u.. Similarly, for MPE at 473 K the critical strain was 8780 s.u.. Literature values were used for

Table 5.5. *Interaction potential energy of aligned chain segments (difference between average flow activation energy and 16 kJ/mol), length and thickness of precursor structures at steady state evaluated using r = 3.46 Å ($L_{ss,r}$ and $d_{ss,r}$) or b = 4.945 Å ($L_{ss,b}$ and $d_{ss,b}$) and for quiescent melts (L_q and d_q).*

	W (kJ/mol)	$L_{ss,r}$ (Å)	$L_{ss,b}$ (Å)	L_q (Å)	$d_{ss,r}$ (Å)	$d_{ss,b}$ (Å)	d_q (Å)
ZNPE	8.46	16.6	99	~17	4.57	5.77	16
MPE	10.38-13.93	20.3-27.3	121-163	~25	4.7-4.96	5.68-5.75	23

the plateau modulus: 2.0 MPa for Ziegler-Natta polyethylene [Rastogi-2005], and 1.97 MPa for the metallocene polyethylene [Wood-Adams-2000].

As shown in Chapter 4, the values evaluated for the thickness depend on those used for length, which depends on the value considered for the separation distance between chains. The values obtained for *d* are also in Table 5.5. The values obtained are around 5 Å, the *b* dimension of the orthorhombic unit cell. Increasing the length of precursor structures almost 6 times, increases the thickness by 0.8 Å. Similar dependence was also found in Chapter 4 (§4.4).

The thickness of precursor structures in a quiescent melt can be estimated from eq. (4.4), with $\Delta F_{ex} = 0$. The values obtained are also shown in Table 5.5. They are between four times and three times the *a* dimension of the orthorhombic PE unit cell MPE and ZNPE, respectively. A more detailed justification of these values and of their agreement with simulation results was made in Chapter 4.

5.5. Conclusions

The main goal of this work was to verify the impossibility of enhancement and saturation the crystallization kinetics of metallocene-based polyethylene presented in literature and to establish the origin of melt memory effect observed in the crystallization of polymers obtained with different catalysts. Based on results obtained, it is concluded that metallocene-based polyethylene behaves in a way similar as any other linear polymer chain. Controlled shear deformations applied above the equilibrium melting temperature enhances crystallization kinetics until saturation, and the strain required for achieving this saturation decreases with the melt temperature increase. This saturation was found to occur at higher critical strains for metallocene polyethylene comparing to Ziegler-Natta polyethylene.

In agreement with results obtained in Chapter 4, it is concluded here that at the origin of melt memory effect are precursor structures, which do not have crystallographic order and consist of a set of aligned chain segments. The interaction between them results from van der

Waals forces. Assuming that the difference between flow activation energy and the energy barrier for local and correlated conformational energy jumps results from ordered regions in the melt, a physical meaning was assigned to flow activation energy and the dimension of precursor structures evaluated. For Ziegler-Natta polyethylene the length of precursor structures is around 16.6 Å, while for metallocene PE it varies between 20.3 and 27.3 Å. The thickness of precursor structures is around 4.57 Å for ZNPE and 4.70-4.96 Å for MPE. Precursor structures in quiescent melts are thicker, between 16 Å and 23 Å. The effect of shear flow is the fragmentation of precursor structures existing in quiescent melts and their orientation with flow direction.

5.6. References

Azzurri-2005 — Azzurri F, Alfonso GC (2005) *Lifetime of shear-induced crystal nucleation precursors*. Macromolecules 38:1723-1728.

Bent-2003 — Bent J, Hutchings LR, Richards RW, Gough T, Spares R, Coates PD, Grillo I, Harlen OG, Read DJ, Graham RS, Likhtman AE, Groves DJ, Nicholson TM, McLeish TCB (2003) *Neutron-mapping polymer flow: scattering, flow visualisation and molecular theory*. Science 301:1691-1695.

Chai-2003 — Chai CK, Auzoux Q, Randrianatoandro H, Navard P, Haudin J-M (2003) *Influence of pre-shearing on the crystallisation of conventional and metallocene polyethylenes*. Polymer 44:773-782.

Chiu-2002 — Chiu F-C, Fu Q, Peng Y, Shih H-H (2002) *Crystallization kinetics and melting behavior of metallocene short-chain branched polyethylene fractions*. J Polym Sci. Polym Phys 40:325-337.

Ergoz-1972 — Ergoz E, Fatou JC, Mandelkern L (1972) *Molecular weight dependence of the crystallization kinetics of linear polyethylene: I. Experimental results*. Macromolecules 5:147-157.

Gelfer-2003 — Gelfer M, Horst RH, Winter HH, Heintz AM, Hsu SL (2003) *Physical gelation of crystallizing metallocene and Ziegler-Natta ethylene–hexene copolymers*. Polymer 44:2363-2371.

Häfele-2005 — Häfele A, Heck B, Hippler T, Kawai T, Kohn P, Strobl G (2005) *Crystallization of poly(ethylene-co-octene). II Melt memory effects on first order kinetics*. Eur Phys J E 16:217-224.

Keith-1963 — Keith HD, Padden FJ (1963) *A phenomenological theory of spherulitic crystallization.* J App Phys 34:2409-2421.

van Krevelen-1997 — van Krevelen DW (1997) *Properties of polymers, their correlation with chemical structure, their numerical estimation and prediction from additive group contribution*. Elsevier.

Lippits-2007 Lippits DR, Rastogi S, Höhne GWH, Mezari B, Magusin PCMM (2007) *Heterogeneous distribution of entanglements in the polymer melt and its influence on crystallization*. Macromolecules 40:1004-1010.

Malmberg-2002 Malmberg A, Gabriel C, Steffl T, Münstedt H, Löfgren B (2002) *Long-chain branching in metallocene-catalyzed polyethylenes investigated by low oscillatory shear and uniaxial extensional rheometry.* Macromolecules 35:1038-1048.

Mark-1996 Mark JE (1996) *Physical properties of polymer handbook*. ed. Woodbury, New York.

Marrucci-2002 Marrucci G, Ianniruberto G (2002) *Modelling rheology and free energy of entangled polymers: State of the art.* Macromol Symp 185:199-210.

Martins-2006 Martins JA, Zhang W, Brito AM (2006) *Saturation of shear-induced isothermal crystallization of polymers at the steady state and the entanglement-disentanglement transition*. Macromolecules 39:7626-7634.

Martins-2008b Martins JA (2008) *Entanglements, the ether of polymer physics*. To be submitted.

Martins-2008a Martins JA, Zhang, W (2008) *Physical meaning of flow activation energy*. To be submitted.

Mirabella-2001 Miravella FM (2001) *Correlation of the melting behavior and copolymer composition distribution of Ziegler-Natta-catalyst and single-site-catalyst polyethylene copolymers*. J Polym Sci. Polym Phys 39:2800-2818.

Moe-2000 Moe NE, Qiu XH, Ediger MD (2000) *^{13}C NMR study of segmental dynamics of atactic polypropylene melts.* Macromolecules 33:2145-2152.

Natta-1955a Natta G, Pino P, Corradini P, Danusso F, Mantica E, Mazzanti G, Moraglio G (1955) *Crystalline high polymers of α-olefins*. J Am Chem Soc 77:1708-1710.

Natta-1955b Natta G (1955) *A new class of polymers from α-olefins having exceptional structural regularity*. J Polym Sci 16:143-154.

Qiu-2000 Qiu XH, Ediger MD (2000) *Local and global dynamics of unentangled polyethylene melts by ^{13}C NMR*. Macromolecules 33:490-498.

Rastogi-2005 Rastogi S, Lippits DR, Peters GWM, Graf R, Yao Y, Spiess HW (2005) *Heterogeneity in polymer melts from melting of polymer crystals.* Nat Mater 4:635-641.

Salem-1962 Salem LJ (1962) *Attractive forces between long saturated chains at short distances*. J Chem Phys 37:2100-2112.

Shih-1999 Shih H-H, Wong C-M, Wang Y-C, Huang C-J, Wu C-C (1999) *Hot tack of metallocene catalyzed polyethylene and low-density polyethylene blend.* J Appl Polymer Sci 73:1769-1773.

Sinn-1980 Sinn H, Kaminsky W (1980) *Ziegler-Natta Catalysis*. Adv Organomet Chem 18:99-149.

Somani-2002 Somani RH, Yang L, Hsiao BS (2002) *Precursors of primary nucleation induced by flow in isotactic polypropylene*. Physica A 304:145-157.

Wang-2001 Wang C, Chu M-C, Lin T-L, Lai S-M, Shih H-H, Yang J-C (2001) *Microstructures of highly short-chain branched polyethylene*. Polymer 42:1733-1741.

Wood-Adams-2000 Wood-Adams PM, Dealy JM, deGroot AW, Redwine OD (2000) *Effect of molecular structure on the linear viscoelastic behavior of polyethylene*. Macromolecules 33:7489-7499.

Yan-1999 Yan D, Wang W-J, Zhu S (1999) *Effect of long chain branching on rheological properties of metallocene polyethylene.* Polymer 40:1737-1744.

Zhang-2006 Zhang W, Martins JA (2006) *Evaluation of the effect of melt memory on shear-induced crystallization of low-density polyethylene*. Macromol Rapid Commun 27:1067-1072.

Ziegler-1955a Ziegler K, Holzkamp E, Breil H, Martin H (1955) *Das Mülheimer Normaldruck-Polyäthylen-Verfahren.* Angew Chem 67:541-547.

Ziegler-1955b Ziegler K, Gellert HG, Zosel K, Lehmkuhl W, Pfohl W (1955) *Herstellung von Aluminiumalkylen und Dialkylaluminiumhydriden*. Angew Chem 67:424.

Appendix

To illustrate the problems presented and discussed in this work, and also results obtained for the quiescent crystallization of polymers and their morphology, polyethylene was used as model polymer. Much information about polymer morphology was obtained with this polymer. As will be shown below, its chain is highly flexible, it can be linear or branched, the polymer may be slightly crosslinked by reactive processing in an extruder, its molecular weight can vary from 500-60000 g/mol for an LDPE up to 3000000-6000000 g/mol for UHMWPE, the glass transition temperature is low (≈ -80 ºC), the melting temperature may change from 105 ºC up to 135 ºC, and the degree of crystallinity can vary between 40 and 100 %. Polyethylene has the simplest chemical structure of all polymers. The basic unit CH_2 is repeated along the chain. Because of the linear sequence of methylene units and chain flexibility, polyethylene is able to crystallize very fast and may exhibit a high degree of crystallinity. Below, a brief summary of some PE physical properties relevant to this work will be presented. In addition, further details of experiments used to support results and conclusions in Chapters 4 and 5 will also be presented.

1.1. Conformational energy barriers, crystalline structure and chain flexibility of polyethylene

Polyethylene chain segments may adopt three different low energy conformations: *gauche* (*g*+ and *g*-) and *trans* (*t*). Conformation *trans* have lower energy than *gauche* (see Figure A1.1). The differences between those conformations for polyethylene were presented by many authors [Robertson-2001, Sundararajan-1995]. Robertson *et al.* [Robertson-2001] found that in crystallized parts polymer chains can have only *trans* conformation while in amorphous phase there is fast exchange between *trans* and *gauche* energy states. The *g* and *t* states are populated according to a Boltzmann distribution:

$$\frac{n_g}{n_t} = A\exp\left(-\Delta E / RT\right) \quad , \tag{A1.1}$$

where ΔE is the energy difference between *gauche* and *trans* states, $n_{g,t}$ is the number of *gauche* and *trans* conformations and A is a pre-exponential factor. It is possible to determine A and E values for the PE amorphous phase. It was found that *gauche* population increases with temperature and barrier height between *trans* and *gauche* conformations is in the range 16 - 22 kJ/mol for T between 20 ºC and 100 ºC, while for lowest temperature (20 ºC) thermal energy RT is only 2.4 kJ/mol. The calculated energy difference between *g* and *t* conformations

evaluated from NMR results for the amorphous phase of semicrystalline polyethylene sample was found to be ΔE = 6.4 ± 0.5 kJ/mol and A value is higher than 5.7 [Robertson-2001]. For melts and solutions the accepted value ΔE is between 2 and 4 kJ/mol, and A = 2 [Smith-1996, Karpfen-1984, Colombo-1980]. Because of degeneracy of *gauche* states, the value of A is equal to 2 for the molten phase, but for the amorphous phase in crystallized samples it can vary between 2 and 6 depending on the morphology. The highest value of A means highest number of folds (higher number of *gauche* states) for a sample with high crystallinity and small lamellar thickness (total lamellar surface area is maximized).

Under normal conditions (1 atm = 101325 Pa) polyethylene crystallizes in the orthorhombic structure with a unit cell dimensions of: a = 7.40 Å, b = 4.93 Å, c = 2.53 Å; the C - C bond length is 1.53 Å [Caminiti-2000, Lavine-2003, Ko-2004]. The structure of PE unit cell is in Figure A1.2. For high pressure the unit cell is hexagonal with $a = b \neq c$ and $\alpha = \beta = 90^{o}$, $\gamma = 120^{o}$.

In each chain, the sp^3 carbon backbones are fully hydrogen saturated [Serra-2000]. Chains are kept together by van der Waals forces, and the same forces causes chains to fold.

Sundararajan and Kavassalis [Sundararajan-1995] made molecular dynamic simulations for polyethylene models at 300 K where the all-*trans* conformation was used as starting geometry of chains with different amount of CH_2 units, from 30 to 1000. Changes in the chains configurations were followed as a function of residence time at 300 K. Particularly, the change in radius of gyration and energy interactions between segments, assigned to van der Waals energy were investigated as a function of time for chain folding due to fluctuations in the conformation of some of the bonds. For folded chains the radius of gyration decreases

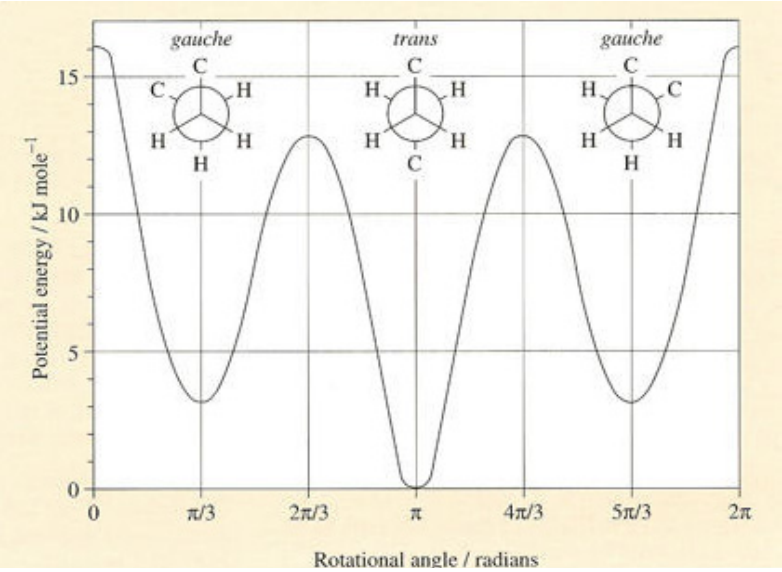

Figure A1.1. *The energy profile dependent on different rotation angles for polyethylene.*

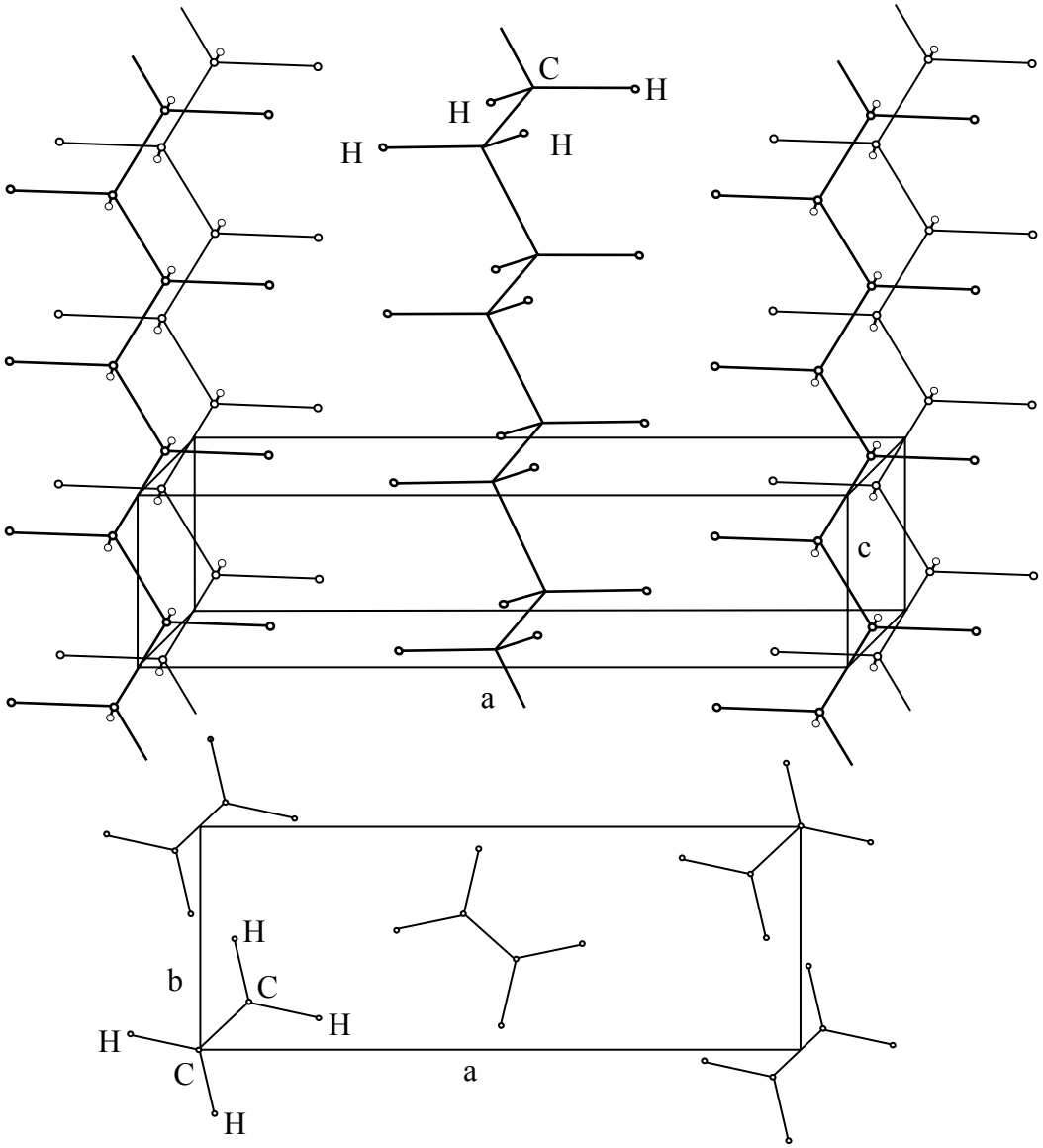

Figure A1.2. *The arrangement of molecular chains in a unit cell of polyethylene.*

when compared with the starting conformation, and the energy of interaction, of van der Waals type, between parallel chain stems increases. It is observed that some critical chain length is required for folds to be stabilized into lamella. For formation of stable folds, the van der Waals interaction energy between parallel chain stems has to be large enough to overcome the energy barriers due to torsion and bond-angle deformation. If this interaction energy is too low, the process of folding is reversible. Different values for the torsional energy barrier were used in this study. For an energy barrier of 2 kcal/mol multi-stem lamella of low thickness (around 25-30 Å) were formed. For higher values of torsional energy barrier, the time required for chain folding increases and the lamellar thickness increases. It is around 100 Å for and energy barrier of 3 kcal/mol and around 250 Å for an energy barrier of 6 kcal/mol.

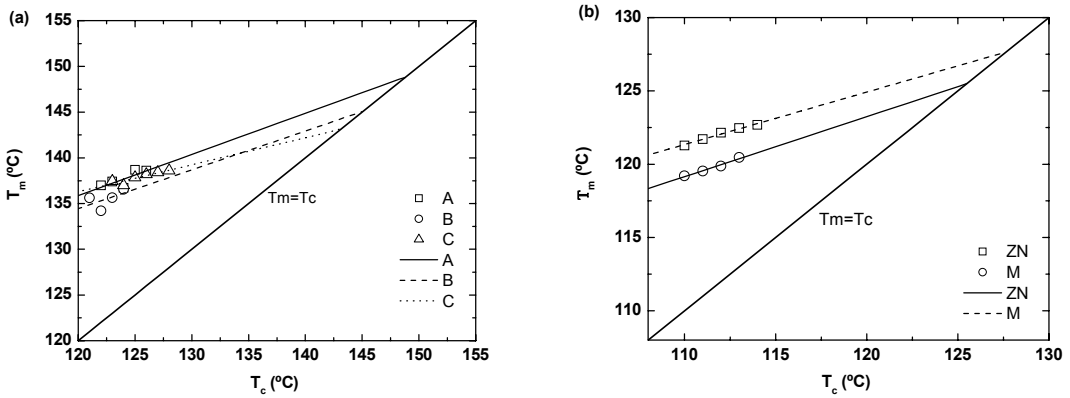

Figure A1.3. *The Hoffman-Weeks plots, it is the relationship between melting and crystallization temperatures for A, B and C (a) and ZN and M (b) polyethylenes for cooling rate of 10 ºC/min.*

1.2. DSC results

1.2.1. Evaluation of the thermodynamic (equilibrium) melting temperature

The equilibrium melting temperature was evaluated with a Perkin Elmer DSC-7 using the Hoffman-Weeks plot construction. The polymer sample was annealed at 200 ºC for 30 min to erase the melt memory effect, cooled to different crystallization temperatures (T_c) with a cooling rate of -60 ºC/min, and left at T_c for the time necessary to complete the crystallization process. The crystallized sample was then heated to 200 ºC with a heating rate of 10 ºC/min. The melting temperature was assigned to the peak value.

The Hoffman and Weeks plot construction starts from the assumption that when melt occurs, the lamellae thickness is a factor γ larger than the critical lamellae thickness, $l = \gamma l^*$, where l^* is the critical lamellae thickness. Replacing the above equation in the Thomson-Gibbs equation, it results then

$$T_m = T_m^o(1 - 1/\gamma) + T_c/\gamma \quad . \tag{A1.2}$$

Plotting the melting temperature against the corresponding crystallization temperature allows

Table A1.1. *The evaluated values of thermodynamic melting temperature for polyethylene A, B, C, ZN and M for cooling rate of 10 ºC/min.*

PE	Tm^0 (ºC)
A	148.32±1.05
B	144.70±0.77
C	141.78±1.24
ZN	127.66
M	125.48

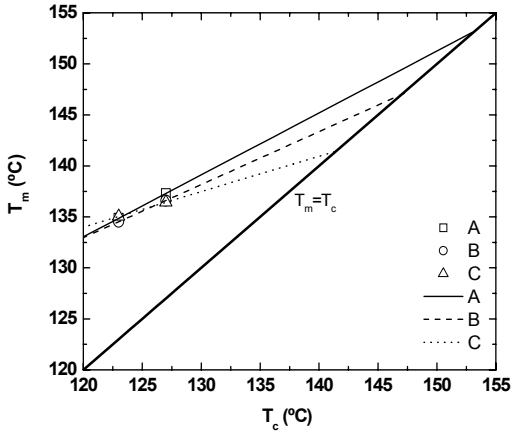

Figure A1.4. *Evaluation of equilibrium melting temperature of polyethylene A, B and C using the Hoffman-Weeks plot for cooling rate of 2 ºC/min.*

to evaluate the factor γ. The intercept of this line with the line corresponding to $T_m = T_c$ yields the equilibrium melting temperature T_m^o .

Values of this temperature for polyethylenes A, B, C, ZN and M obtained from Figure A1.3 are presented in Table A1.1. Additional set of experiments similar to those described above were performed with a lower cooling rate of 2 ºC/min (Figure A1.4 and Table A1.2). In principle, within the experimental measurement errors, the same value should have been obtained for both heating rates. We may consider that the differences observed result from the small number of data points used in this evaluation.

1.2.2. Sample thermal resistance evaluation

As demonstrated in previous works [Martins-2003, Martins-2004, Zhang-2004], accounting for the polymer sample thermal resistance is imperative to precisely evaluate the true sample temperature both for DSC, shear-DTA and rheometer experiments. Previous experiments allowed concluding that, due to the relatively small diameter of capillary channel in the shear-DTA, thermal lag corrections due to the sample thermal resistance in this instrument are small, within the instrument experimental error (≈ 1ºC), and may be neglected [Martins-2005]. However, precise evaluations of equilibrium melting temperature and true sample temperature in rheometers require the evaluation of sample thermal resistance.

Table A1.2. *Equilibrium melting temperature of polyethylene A, B and C evaluated from heating experiments at 2 ºC/min.*

PE	Tm^o (ºC)
A	153.125
B	147.00
C	141.44

Table A1.3. *Weight and dimension of samples used in the thermal resistances' evaluations.*

	Weight (mg)	Thickness (mm)	Length×width (mm^2)
Indium	4.154	-	-
Indium	3.477	-	-
PE A	11.103	0.6325	4.17×4.43
Indium	4.085	-	-
PE B	11.24	0.602	4.36×4.83
Indium	7.175	-	-
PE C	11.10	0.7675	4.24×4.04

For rheometers the evaluation performed in previous works was used in the experiments here described [Martins-2003, Zhang-2004]. The reason for adopting this procedure resulted from the similarity of thermal resistances evaluated here and in previous works.

The procedure presented below, used to evaluate the sample thermal resistance, was applied to estimate the polymer melting temperature at a specific heating rate, which was used latter on to evaluate the equilibrium melting temperature described above. The sample thermal resistance evaluation was made by making the difference in the reciprocal of the ascending slope of indium peak and of another indium sample with similar weight, but now placed over a polymer sample with known area and thickness (see Figure A1.5). The experiments were performed in a temperature range between 70 ºC and 180 ºC with a heating rate of 10 ºC/min. All samples have cuboid shape. The weights and dimensions of samples used in these experiments are presented in Table A1.3 and the values of thermal resistance are shown in Table A1.4.

The corrected sample's temperature can be then calculated using following equations:

$$R_{In} = \frac{\Delta T_{In}}{\Delta\left(\Delta \dot{Q}_{In}\right)} \quad , \tag{A1.3}$$

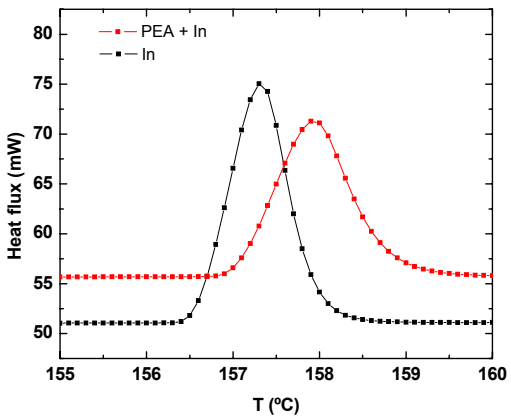

Figure A1.5. *DSC plots for indium alone and indium over PE used to evaluate the thermal resistance.*

Table A1.4. *Thermal resistance values for polyethylene A, B and C.*

PE	R_{sample} (K/W)
A	22.659
B	15.391
C	10.258

$$R_{PE+In} = \frac{\Delta T_{sample+In}}{\Delta\left(\Delta \dot{Q}_{sample+In}\right)} \quad , \tag{A1.4}$$

$$R_{sample} = R_{sample+In} - R_{In} \quad , \tag{A1.5}$$

$$T_{corrected} = T_{sample} - R_{sample} \cdot \Delta \dot{Q}_{subtracted} \quad , \tag{A1.6}$$

where:

$$\Delta \dot{Q}_{subtracted} = \Delta \dot{Q}_{sample} - \Delta \dot{Q}_{blank} \quad . \tag{A1.7}$$

In Figure A1.6 there are plotted two lines of the heat flux versus temperature, one obtained from DSC (black) and second obtained from eq. (A1.6) (red). The differences between melting temperatures obtained experimentally and from eq. (A1.6) are equal to: 1.43 ºC for PEA, 0.48 ºC for PEB and 0.95 ºC for PEC.

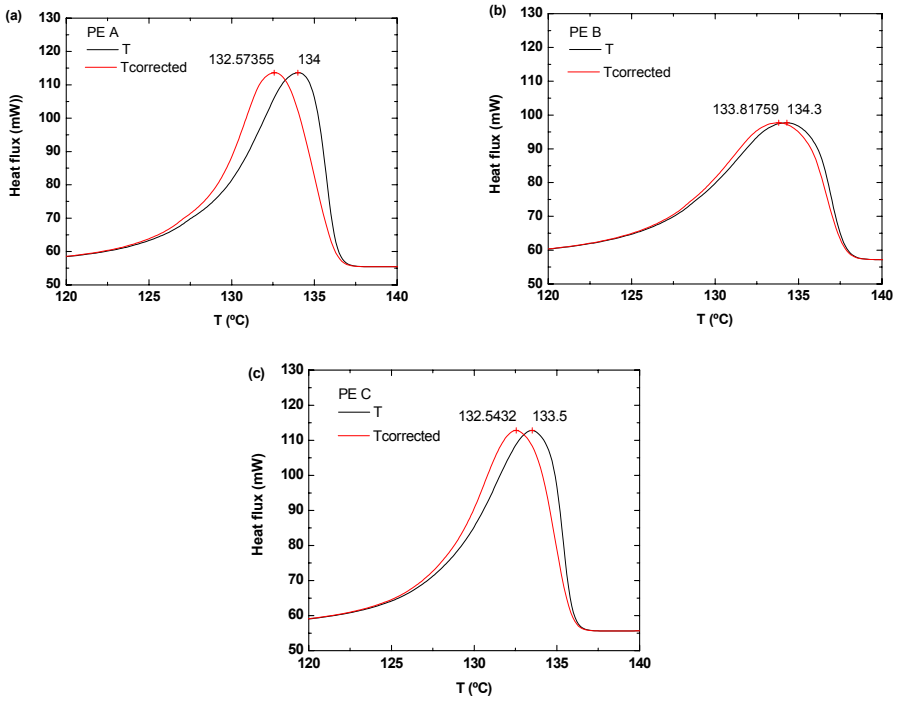

Figure A1.6. *The plots of heat flux as a function of temperature obtained from DSC (black line) and corrected by thermal resistance (red line) for polyethylene A (a), B (b) and C (c).*

Table A1.5. *The shift values and corresponding codes obtained from NMR experiment performed for A, B, C, ZN and M polyethylenes.*

A		B		C		ZN		M	
Shift (ppm)	code	Shift (ppm)	code	Shift (ppm)	code	Shift (ppm)	code	Shift (ppm)	code
31.66	A3	32.15	A1	31.63	A1	39.01	A1''	39.04	A1''
29.47	A4	29.97	A4	29.45	A4	35.40	E1 or A2'	35.39	E1 or A2'
13.46	A1	29.54	A5	29.01	A5	34.99	D1	32.96	E4
		28.79	A3	22.29	A2	31.22	A4	31.25	A4
		22.79	A2			30.73	A5	30.75	A5 or E3
						30.32	D2	28.10	A3 or E2
						28.08	A3 or E2	23.63	E5
						24.10	D3	14.77	E6
						14.79	D4		

1.3. NMR results

Polymer testing by NMR (Nuclear Magnetic Resonance Spectroscopy) provides detailed structural information on chain architecture. Polymer characteristics obtained from NMR analysis provides an extensive range of useful data that allows the evaluation of branching degree extend in polymer chains. NMR spectra are plotted as absorption versus chemical shift, *d*. The chemical shift for proton NMR is the difference between the frequency of absorption of the sample and a standard, normalized by the standard absorption frequency.

As mentioned in Chapters 4 and 5, the ^{13}C NMR test was performed with an NMR

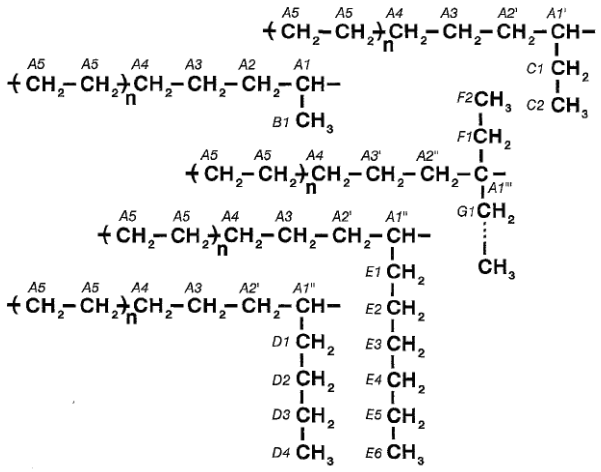

Code	Shift (ppm)
A1	32.8
A1′	39.8
A1″	38.2
A1‴	39.2
A2	37.4
A2′	34.6
A2″	37.4
A3	27.2
A3′	25.9
A4	30.6
A5	30.0
B1	20.1
C1	27.0
C2	10.9
D1	34.3
D2	27.3
D3	23.3
D4	14.0
E1	34.6
E2	27.2
E3	30.0
E4	32.3
E5	22.8
E6	14.0
F1	29.5
F2	8.1
G1	36.0

Figure A1.7. *Examples of different chain architectures and corresponding shifts values obtained from NMR results according to ref. [Randall-1973].*

Spectrometer DSX 300 (Bruker) in the Polish Academy of Science (CBMM PAN, Lodz, Poland), at 398 K, sample's weight of 140 mg and solvent - TCB/C_6D_6. The shift values obtained from NMR spectra of different samples (Table A1.5) were ascribed to codes of methylene group according to their sequences in the polyethylene chain (see Figure A1.7 [Randall-1973]). The conclusions concerning the chain architecture were already described in Chapter 4 (for PE A, B and C) and 5 (for ZN and MPE).

1.4. SEM results

The morphology of polyethylene samples after quiescent crystallization was examined with a Scanning Electron Microscopy (Polish Academy of Science CBMM Lodz, Poland). The polymer samples were annealed previously in DSC during 30 min at 200 ºC (to erase the melt memory effect), cooled down to crystallization temperature (127 ºC for PEA, B and C, and 117 ºC for ZN and MPE) with cooling rate of -60 ºC/min and crystallization was recorded. From samples crystallized at chosen crystallization temperatures the specimens were cut off at room temperature using sharp blade and etched in mixture of H_2SO_4 : H_3PO_4 : $KMnO_4$ (1vol : 1vol : 2% of total weight) for 30 minutes. After that they were submerged in a cold solution of H_2SO_4 (2 volumes H_2SO_4 : 7 volumes of H_2O) and four ultrasonic baths (1 - diluted H_2SO_4 – composition as above, 2 – 30 % H_2O_2 from the fridge, 3 – H_2O, 4 - acetone) during at least 2 minutes for each tube. The etched specimens were fixed to microscopic stages, sputtered with gold and observed using SEM Jeol 5500LV instrument working in high vacuum and with accelerating voltage of 10 kV.

Figure A1.8 presents some SEM scans obtained. The magnification was selected to show one spherulite in each scan. For PEA, PEB and PEC it is clear that the first has largest spherulites while spherulites of PEC have the smallest size. Similar trend is observed for lamellae thickness, although their precise value was not evaluated. PEA has the thickest lamellae and lamellae of PEC are the thinner. This conclusion was also inferred from equilibrium melting temperature evaluations. For comparison, SEM images of Ziegler-Natta and metallocene polyethylene are also shown. Ziegler-Natta spherulites are larger than those of metallocene polyethylene.

In the Figure A1.9 the additional scans are shown. The purpose of this figure was to compare the density of spherulites (note different magnification used: 250 for polyethylene A, B and C and 1000 for Ziegler-Natta and metallocene). It is visible that from PEA, PEB and PEC, density of spherulites is the highest for PEC and smallest for PEA, while from ZNPE and MPE it is higher for MPE.

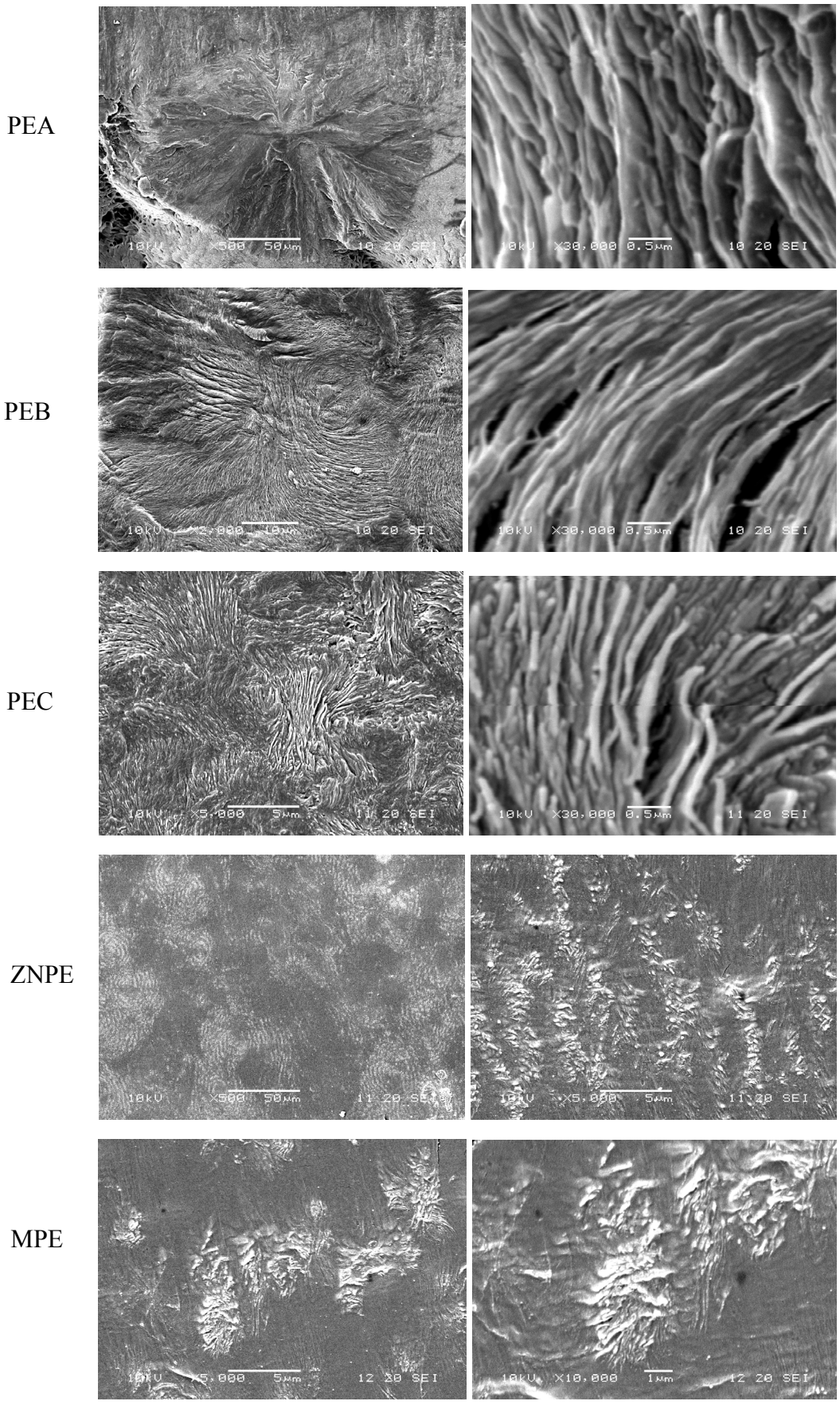

Figure A1.8. *SEM scans for samples crystallized at 127 ºC (PEA, B and C) and 117 ºC (ZN and MPE). Magnifications are indicated in the pictures.*

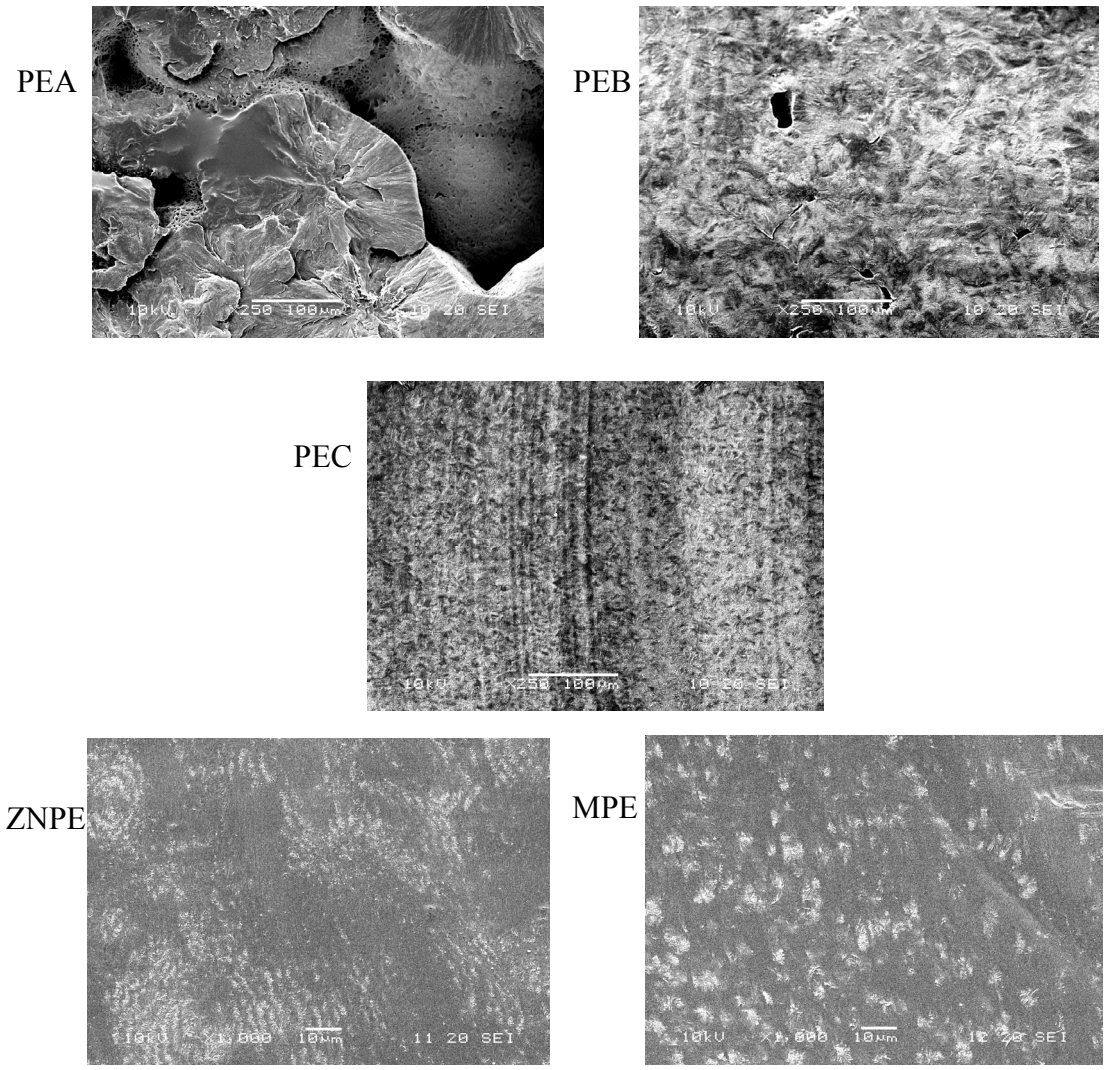

Figure A1.9. *SEM scans different polyethylene samples studied at the same magnification, showing the nucleation density in different polymers.*

1.5. WAXS results

Computer controlled X-ray diffractometer (Phillips), coupled to a sealed-tube source of filtered CuK_α radiation $\lambda = 0.1541$ nm, operating at 50 kV and 30 mA, filtered by Ni filter and electronically, was used for X-ray measurements. The divergence slit opening was 0.05^o.

The conclusion of WAXS results shown in Figure A1.10 is that the unit cell in all samples is orthorhombic and that crosslinking did not affect the crystalline structure.

1.6. Rheometer results

1.6.1. Evaluation the constant strain from stress sweeps experiments

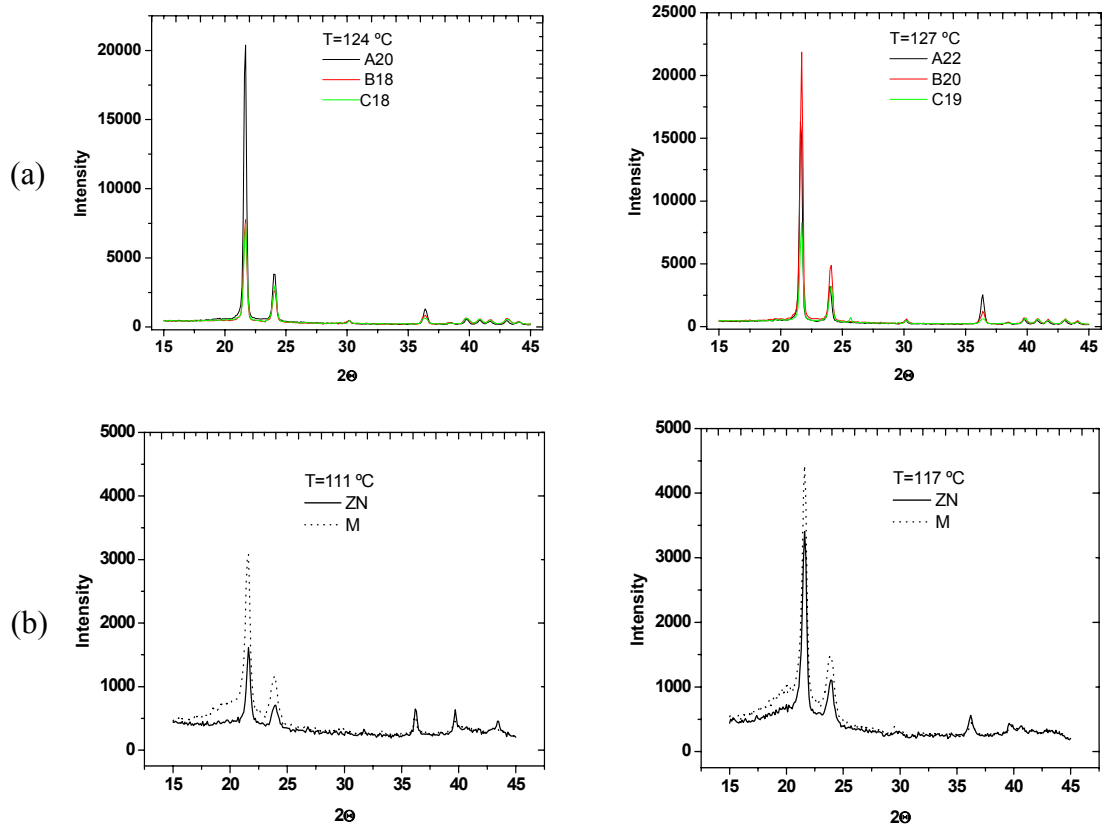

Figure A1.10. *WAXS patterns for polyethylene A, B and C (a) and ZN and M (b) at indicated temperatures.*

Stress sweep experiments are crucial rheological experiments in constant force rheometers to establish the optimal stress for ensuring viscoelastic linear behaviour in the experimental temperature and frequency range. These experiments shown below were performed with an AR-G2 rheometer (TA Instruments).

Two different values of frequency sweeps were used: 10 Hz and 0.1 Hz. From the plot of storage modulus versus shear stress, the optimal stress value for a given polymer was selected under the condition of a constant modulus value for all frequencies and temperatures

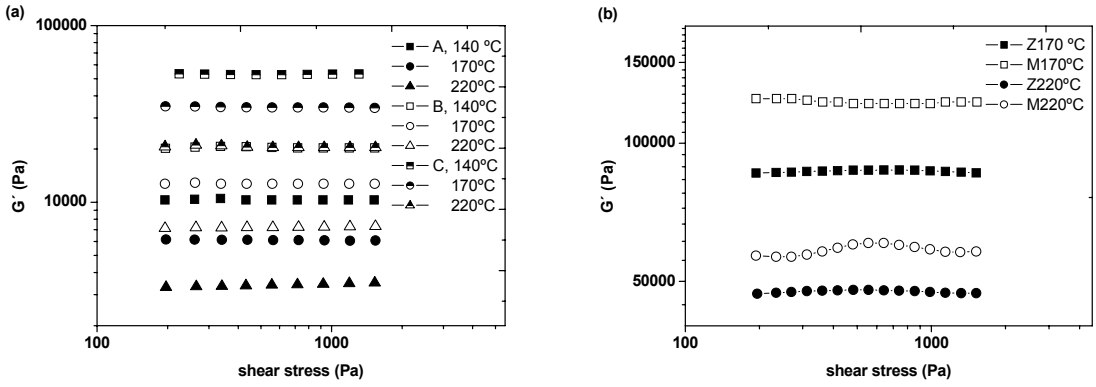

Figure A1.11. *The storage modulus as a function of shear stress for A, B and C (a) and ZN and M (b) polyethylenes, ω=10 Hz, shear stress in range of 200 - 1500 Pa, at temperatures indicated.*

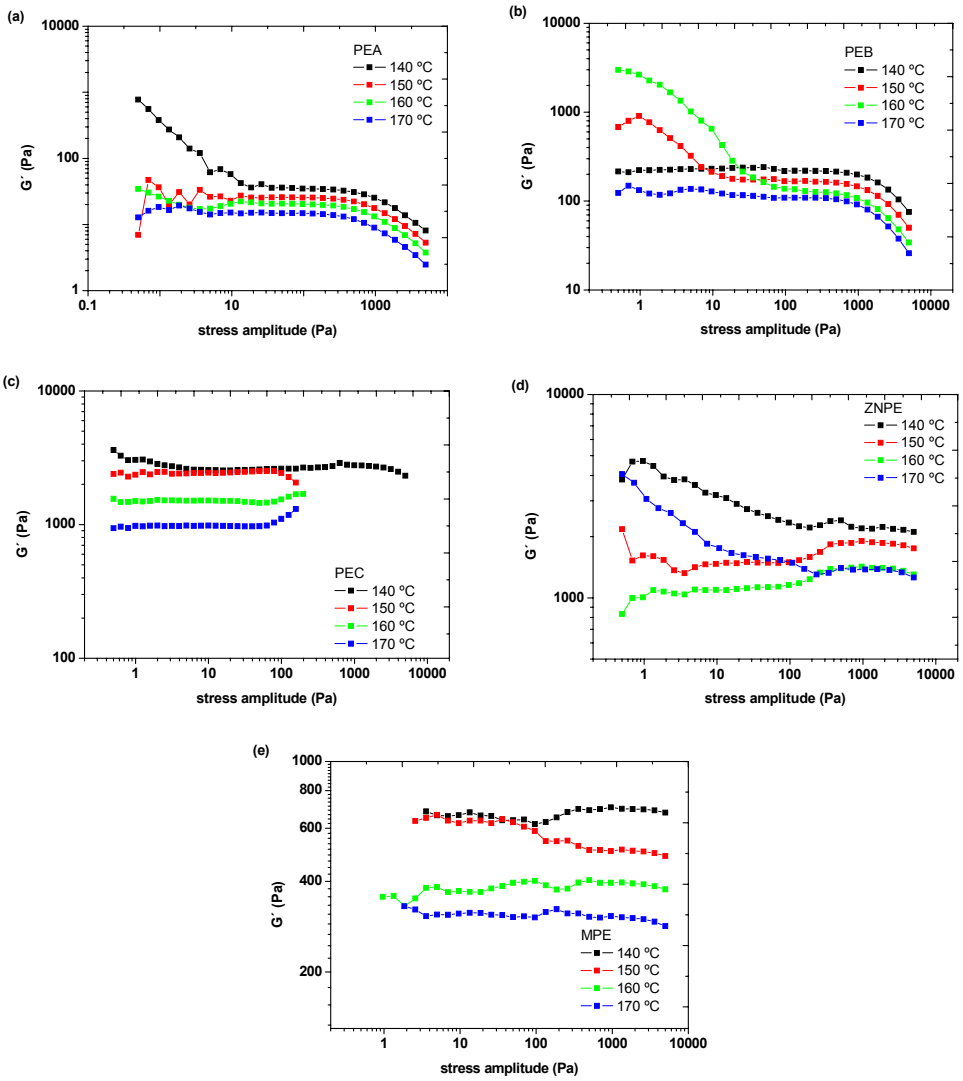

Figure A1.12. *The results of stress sweep experiments for polyethylene A (a), B (b), C (c), ZN (d) and M (e) performed at ω=0.1 Hz and temperature range of 140-170 °C.*

tested. As shown in Figure A1.11, for all polymers at frequency sweep of 10 Hz, the elastic modulus *G*' is almost constant over the entire range of applied stresses.

For stress scans at 0.1 Hz (Figure A1.12), the optimal stress value was selected among the lowest possible values of *G*'. This selection was made for shifting the reptation time value to lower values of frequency. The values of stress for A, B, C, ZN and M polyethylene

Table A1.6. *The values of stress extracted from Figures A1.11 and A1.12 for polyethylene A, B, C, ZN and M for two different frequencies used.*

PE	τ (Pa)
A	70
B	300
C	20
ZN	1000
M	1000

extracted from the Figures A1.11 and A1.12 are presented in Table A1.6.

It is important to note that the different trend in the plot of *G'* versus shear stress for Ziegler-Natta polyethylene at 170 ºC is caused by polymer degradation. For this reason, the maximum temperature of 160 ºC was used in the rheometer to obtain reproducible results for this polymer.

1.6.2. Flow activation energy

The procedure for the evaluation of flow activation energy from SAOS experiments was already described in Chapter 4. Curves of storage and loss modulus versus frequency obtained for different temperatures were shifted vertically and horizontally in such a way that any overlapping regions of the curve at the reference temperature and curves at other temperatures are superimposed. The amount by which a given curve was vertically shifted to superimpose with a curve at the reference temperature is b_T. The horizontal shift is a_{T/T_0}. The temperature dependence of horizontal shift factors a_{T/T_0} follows the Arrhenius equation $\ln a_{T/T_0} = \frac{\Delta E}{R}\left(\frac{1}{T_0} - \frac{1}{T}\right)$, while the vertical shift factor b_T results from the modulus variation with density and temperature: $b_T = \frac{\rho \cdot T}{\rho_0 \cdot T_0}$ [Aklonis-1983]. The density correction was made using an empirical relationship for the viscosity variation with temperature: $\rho = 0.863\text{-}4.73\times10^{-4}\times T\text{-}0.38\times10^{-6}\times T^2$ for linear polymers (used to correct the density of A, B and C polyethylene), and $\rho = 0.882\text{-}7.97\times10^{-4}\times T\text{+}0.74\times10^{-6}\times T^2$ for branched polymers (used to correct the density of ZN and M polyethylene) [Mark-1996].

Flow activation energy was then calculated from the slope of a plot of the horizontal shift factors ($\log a_{T/T_0}$) against the reciprocal of the absolute melt temperature (*1/T*). Similar

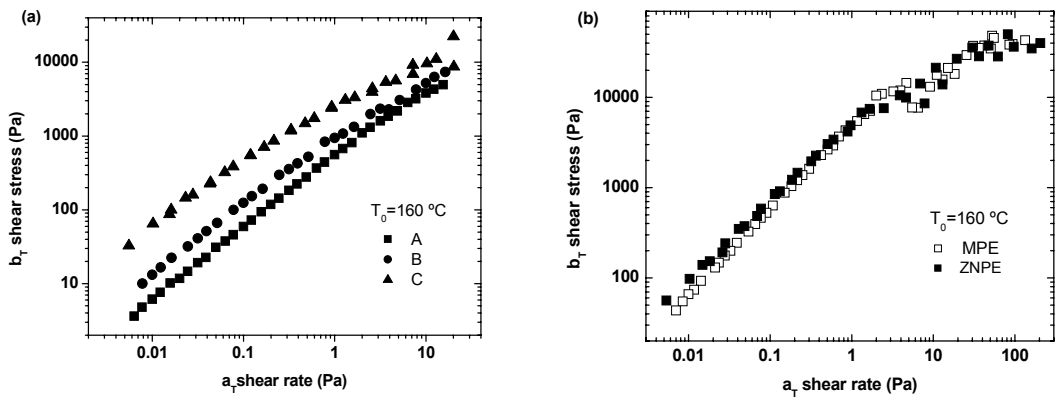

Figure A1.13. *Reduced curves of Controlled Shear Rate experiments for polyethylene A, B and C (a) and ZN and M (b) at reference temperature of 160 ºC.*

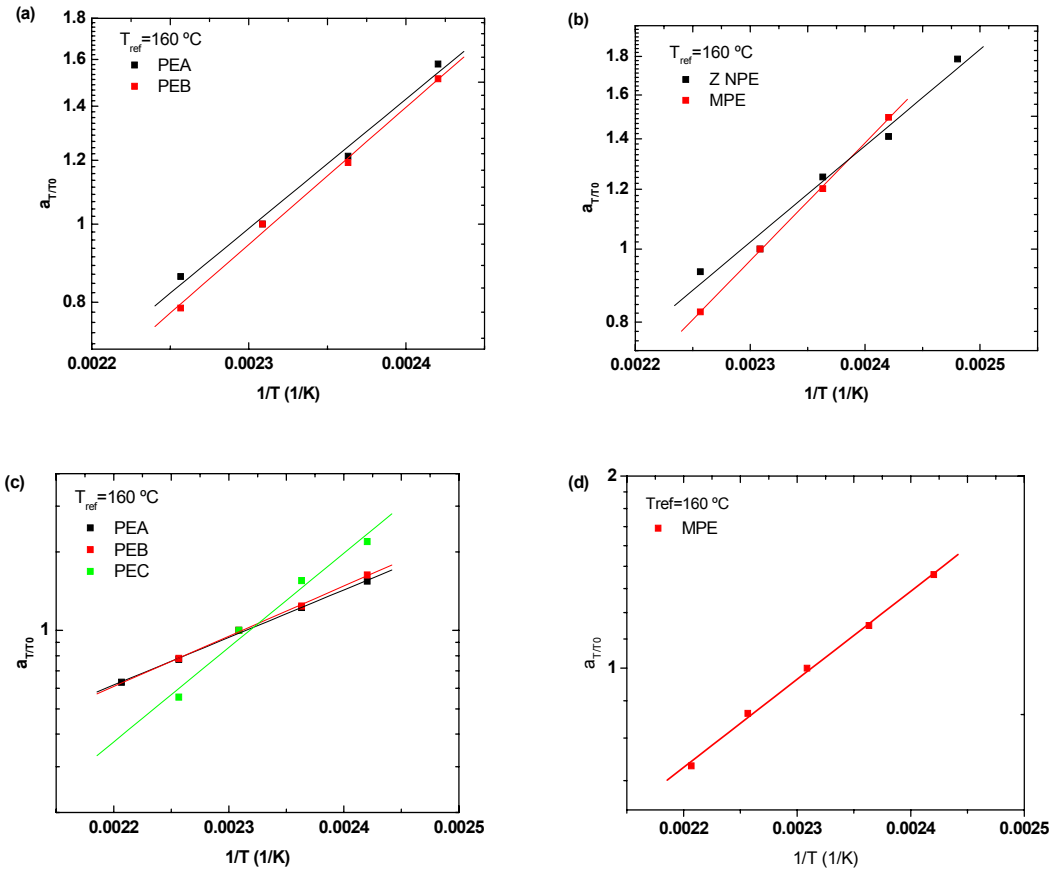

Figure A1.14. *The plots of shift factor as a function of reciprocal of temperature for reference temperature of 160 ºC; (a) from SAOS experiment for A and B (b) from SAOS experiment for ZN and M, (c) from CSR experiment for A, B and C (d) from CSR experiment for M.*

procedure was used for evaluating the activation energy from Controlled Shear Rate experiments. The reduced curves obtained from SAOS experiments were presented in Chapters 4 (PEA, B and C at reference temperature of T_0=140 ºC) and 5 (ZN and MPE at reference temperature of T_0=160 ºC), and reduced curves obtained from CSR experiments at reference temperature of T_0=160 ºC for all polymers are plotted in Figure A1.13.

The values of activation energies obtained from slope of shift factor against

Table A1.7. *The activation energies obtained from Small Amplitude Oscillatory and Controlled Shear Rate experiments for polyethylene A, B, C, ZN and M.*

PE	E_a (kJ/mol)	
	SAOS	CSR
A	30.70±1.64	34.91±1.53
B	32.55±1.05	36.93±0.97
C	*67.06±5.06*	69.32±1.85
ZN	24.46±1.53	-
M	29.93±1.21	26.38±3.00

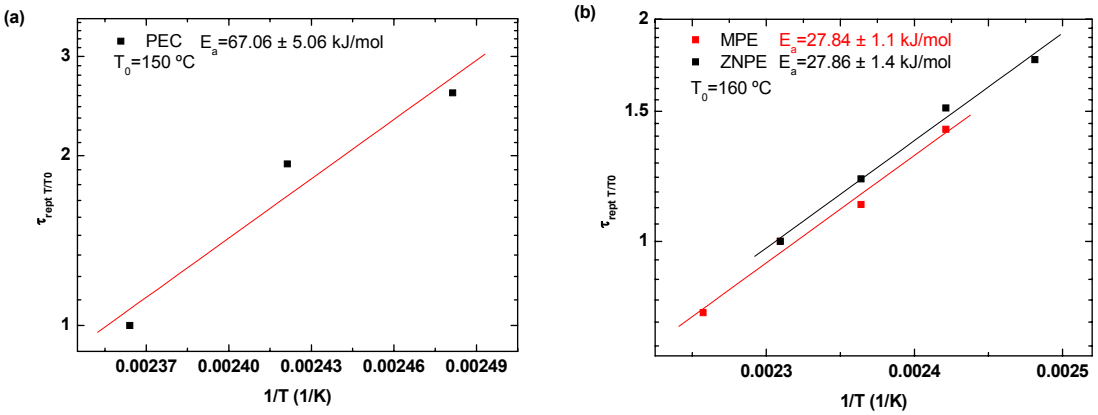

Figure A1.15. *The plot of shift factor of reptation times as a function of reciprocal of temperature obtained from SAOS experiments for polyethylene C (a) and Ziegler-Natta and metallocene polyethylene (b).*

the reciprocal of temperature (Figure A1.14) are presented in Table A1.7. It is visible that for given polymer the values obtained from SAOS and CSR experiments are similar and for polyethylene A, B and C the activation energy increase with the crosslinking degree. The value of activation energy for PEC obtained from SAOS experiments (italic font in Table A1.7) was obtained using the values of reptation times, instead of shifting the curves of *G'* and *G''*, and result agrees with that of CSR experiments. The plot of shift factor of reptation times against reciprocal of temperature is shown in Figure A1.15.

It is expected that the activation energy of Ziegler-Natta polyethylene will be lower than that of metallocene polyethylene since ZN polyethylene has higher branching degree (see NMR results in §5.2.1). This trend is observed for activation energies obtained from SAOS experiments and evaluated by *G'* and *G''* curves. The values obtained from SAOS experiments but evaluated by reptation times are almost the same for both polymers, the only difference is larger error for Ziegler-Natta polyethylene. The lack of value of activation energy for ZNPE from CSR experiments is caused by small amount of experimental points which make the value of E_a not trustable. More points could not be obtained because of high degradability of this polymer.

After comparison the values of activation energy of linear polyethylene melts (A, ZN, M) obtained at this work with those presented in literature, good agreement is found. The range of the activation energy for linear polyethylene melts given by Malmberg *et al.* [Malmberg-1998] is between ~26 and ~33 kJ/mol.

1.7. References

Aklonis-1983 Aklonis JJ, MacKnight WJ (1983) *Introduction to polymer viscoelasticity*. 2nd ed, Wiley-Interscience, New York.

Caminiti-2000 Caminiti R, Pandolfi L, Ballirano P (2000) *Structure of polyethylene from X-ray powder diffraction: influence of the amorphous fraction on data analysis.* J Macromol Sci, Phys B39 4:481-491.

Colombo-1980 Colombo L, Zerbi G (1980) *Enthalpy difference of rotational isomers in liquid butane and pentane from infrared spectra*. J Chem Phys 73:2013.

Karpfen-1984 Karpfen A, Berger A (1984) *Ab initio studies on polymers. VI. Torsional potential in regular polyethylene chains.* J Comput Chem 5:11-18.

Ko-2004 Ko MJ, Waheed N, Lavine MS, Rutledge GC (2004) *Characterization of polyethylene crystallization from an oriented melt by molecular dynamics simulation.* J Chem Phys 6:2823-2832.

Lavine-2003 Lavine MS, Waheed N, Rutledge GC (2003) *Molecular dynamics simulation of orientation and crystallization of polyethylene during uniaxial extension.* Polymer 44:1771-1779.

Malmberg-2002 Malmberg A, Gabriel C, Steffl T, Münstedt H, Löfgren B (2002) *Long-chain branching in metallocene-catalyzed polyethylenes investigated by low oscillatory shear and uniaxial extensional rheometry.* Macromolecules 35:1038-1048.

Mark-1996 Mark JE (1996) *Physical properties of polymer handbook*. ed. Woodbury, NY.

Martins-2003 Martins JA, Zhang W, Carvalho V, Brito AM, Soares FO (2003) *Evaluation of the sample temperature increase during the quiescent and shear-induced isothermal crystallization of polyethylene.* Polymer 44:8071-8079.

Martins-2004 Martins JA, Cruz Pinto JJC (2004) *True sample temperatures in isothermal Differential Scanning Calorimetry scans and their effect on the overall polymer crystallization kinetics.* J Appl Polymer Sci 91:125-131.

Martins-2005 Martins JA, Zhang W, Brito AM, Infante U, Romero M, Soares FO (2005) *Isothermal and nonisothermal crystallization of polymers: analysis with a shear differential thermal analyzer.* Rev Sci Instrum 76:105105.

Randall-1973 Randall JC (1973) *Carbon-13 NMR of ethylene-1-olefin copolymers: Extension to the short-chain branch distribution in a low-density polyethylene.* J Polym Sci Polym Phys Ed 11:275-287.

Robertson-2001 Robertson MB, Klein PG, Ward IM, Packer KJ (2001) *NMR study of the energy difference and population of the gauche and trans conformations in solid polyethylene.* Polymer 42:1261-1264.

Serra-2000 Serra S, Iarlori S, Tosatti E, Scandolo S, Santoro G (2000) *Dynamic and thermal properties of polyethylene by ab initio simulation.* Chem Phys Lett 31:339-345.

Smith-1996 Smith GD, Jaffe RL (1996) *Quantum chemistry study of conformational energies and rotational energy barriers in n-alkanes.* J Phys Chem 100:18718-18724.

Sundararajan-1995 Sundararajan PR, Kavassalis TA (1995) *Molecular dynamics study of polyethylene chain folding: the effects of chain length and the torsional barrier*. J Chem Soc Faraday Trans 91:2541-2549.

Zhang-2004 Zhang W, Martins JA (2004) *The temperature calibration of a parallel plate rheometer and evaluation of the thermal lags during polymer solidification.* Thermochim Acta 413:101-110.

Future works

In scope of the thesis some additional aspects deserve further attention:
-In the Chapter 4 the effect of crosslinking degree on critical strain value was investigated. Due to the reduced number of data points, large experimental error and high degradability of polymers used, it was not possible to evaluate this effect properly, therefore it was assumed that for given melt temperature the critical strain is similar for chosen polymers, A, B and C, regardless their crosslinking degree. It is suggested that this type of variation should be quantified precisely.

- For polymers similar to those studied in this work it is suggested to measure the reptation time for unsheared (relaxed) melts and for melts sheared up to steady state, to identify the entanglement loss during the transition to steady state.

- According to ref. [Zhang-2008] for sodium partially neutralized ethylene-methacrylic acid ionomer (Surlyn), there exist more than one steady state. The first one called “transient steady state” is followed by the second, at larger strains. For the sample similar to those used at this work but with smaller degradability it should be checked if similar behaviour can bed found, together with the magnitude of second strain.

- The prediction of precursor structures was not done for crosslinked samples, it B and C polyethylene, because network contribution to the conformational and network energy barrier is unknown. An accurate value of the energy barrier for the local and correlated conformational energy jumps should be evaluated for polymer solutions with a concentration below the overlap concentration and under theta conditions. The evaluation of this contribution would give possibility to predict the size of precursor structures for polymers with different crosslinking degree. Also the plateau modulus values for all polyethylene samples should be evaluated from SAOS experiments.

- As was mentioned in Chapter 5 (page 172) a well defined steady state for metallocene polyethylene can be defined, however some difficulties at low shear rates are observed, a set of oscillations occurs, what is ascribed to two combined effects: the rotational component of shear flow and the low polydispersity of polymer chains. Additional work should be done to clarify this asspect with samples of different molecular weights and narrow molecular weight distribution.

- Since due to small amount of experimental data the activation energy for Ziegler-Natta polyethylene from CSR experiments was not possible to obtained, it is suggested to perform this kind of experiment once again but with sample of smaller degradability. The obtained value of activation energy should be then compared with the value obtained for ZNPE from SAOS experiments and MPE obtained from both kinds of experiment.